pif

NASA TECHNICAL TRANSLATION

NASA TT F-809

NASA TT F-809



# AEROSPACE VEHICLES AS OBJECTS OF CONTROL

*by A. S. Shatalov, Yu. I. Topcheyev, and V. S. Kondrat'yev*



*"Mashinostroyeniye" Press*
*Moscow,* 1972

NATIONAL AERONAUTICS AND SPACE ADMINISTRATION • WASHINGTON, D. C. • MAY 1974

| 1. Report No. NASA TT F-809 | 2. Government Accession No. | 3. Recipient's Catalog No. |
|---|---|---|
| 4. Title and Subtitle<br>AEROSPACE VEHICLES AS OBJECTS OF CONTROL | | 5. Report Date<br>May 1974<br>6. Performing Organization Code |
| 7. Author(s)<br>A.S. Shatalov, Yu.I. Topcheyev, and V.S. Kondrat'yev | | 8. Performing Organization Report No.<br>10. Work Unit No. |
| 9. Performing Organization Name and Address<br>Scripta Technica, Inc.<br>1511 K Street, N.W.<br>Washington, D.C. 20005 | | 11. Contract or Grant No.<br>NASw-2484<br>13. Type of Report and Period Covered<br>Translation |
| 12. Sponsoring Agency Name and Address<br>National Aeronautics and Space Administration<br>Washington, D.C. 20546 | | 14. Sponsoring Agency Code |

15. Supplementary Notes

Translation of "Letatel'nyye Apparaty kak Ob'yekty Upravleniya", Moscow "Mashinostroyeniye" Press, 1972, 240 pp. In the Series "Spravochnaya Biblioteka Inzhenera-Konstruktora. Osnovy Proyektirovaniya Sistem Upravleniya Letatel'nymi Apparatami" (Design Engineer's Reference Library. Design Fundamentals of Aerospace Vehicle Control Systems)

16. Abstract

The book discusses equations of motion of aerospace vehicles with various arrangements of wings and control surfaces. The equation devised are complete descritpions of the systems and can therefore be reduced to a system of transfer functions and control diagrams that take account of interactions of the various parts of the vehicle.

The dynamic characteristics of the vehicles are presented for standard input disturbances, which are represented in the form of Laplace and z-transforms. A matrix form of descritpion of the vehicle is proposed as a means of taking account of the nonstationary nature of the controlled object. These characteristics make it possible to identify the object on the basis of experimental data.

| 17. Key Words (Selected by Author(s)) | 18. Distribution Statement<br>Unclassified-Unlimited<br>Cat. 01 | | |
|---|---|---|---|
| 19. Security Classif. (of this report)<br>Unclassified | 20. Security Classif. (of this page)<br>Unclassified | 21. No. of Pages<br>208 | 22. Price*<br>$5.75 |

*For sale by the National Technical Information Service, Springfield, Virginia 22151

UDC 629.7.05.001.2(083)

## ANNOTATION

/4*

**Aerospace Vehicles as Objects of Control.** Shatalov, A.S., Topcheyev, Yu.I. and Kondrat'yev, V.S. Mashinostroyeniye, 1972, 240 pp.

This book examines the dynamic equations of motion of various types of aerospace vehicles with two-and three-dimensional arrangements of the wings and control surfaces and of types with pivoting wings and gasdynamic controls. The equation systems are presented for a complete dynamic scheme that takes account of the motion of the center of mass, rotation about the center of mass, structural elasticity, and motions of liquids in tanks. The equations are linearized to simplify the equation system. This has made it possible to convert to the transfer functions and control structural diagrams of the vehicles, so that reciprocal effects between channels could be taken into account in lucid presentation.

The dynamic characteristics of the vehicles are presented for standard input disturbances, which are represented in the form of Laplace and z-transforms. A matrix form of description of the vehicle is proposed as a means of taking account of the nonstationary nature of the controlled object. These characteristics make it possible to identify the object on the basis of experimental data.

The book is intended for design engineers engaged in the design of aerospace-vehicle control systems. It will also be useful to college graduate and undergraduate students in the corresponding specialties.

PRECEDING PAGE BLANK NOT FILMED

*Numbers in the margin indicate pagination in the foreign text.

# FOREWORD

/5

Control of the flight of an aerospace vehicle consists in maintaining the desired trajectory of its center of mass and orientation and stabilization with respect to the center of mass. These functions are performed by an automatic or semi-automatic control system in which the aerospace vehicle is the object of control.

The dynamic characteristics of an aerospace vehicle as a controlled object depend on a number of parameters: mass, moments of inertia, aerodynamic coefficients, and so forth. These parameters are the initial basis for writing the differential equations that describe the dynamics of the vehicle's motion or its dynamic characteristics as functions of time. Together with these primary characteristics, there are also so-called secondary (derived) characteristics, an example of which is found in the gain and phase frequency characteristics, which establish relationships between harmonic signals at the output and input of the aerospace vehicle [4, 5]. In these characteristics, the angles or angular velocities of deflection of the controls and the variation of engine thrust are treated as input signals. The output signals are the angle and angular velocity of rotation of the vehicle's axes, g-force, the linear displacement of the center of mass, and the changes in the altitude and direction of flight. All of these signals are presented in the form of vectors or vector projections. In writing the dynamic equations of aerospace vehicles, therefore, considerable attention is given to selection of the coordinate system in which the motion of the vehicles is examined.

The book discusses four types of coordinate systems (earth-based, body, drag, and semiattached body), use of which makes it possible to write systems of dynamic equations of motion for aerospace vehicles under various conditions of use. The resulting system of differential equations is nonlinear; considerable mathematical difficulty is encountered in its solution or analysis. To surmount them, the systems of nonlinear differential equations are linearized with respect to reference trajectories by the method of small increments, so that the motion of the vehicle can be resolved into short-period and long-period motions. If it is assumed that the coefficients of the equation system vary little in time, and if the "frozen"-coefficient method is used, this method makes it possible to apply the direct Laplace transform to the equation system and to reduce the system of differential equations to algebraic equations, with the result that easily inspected stationary structural diagrams of the vehicle can be constructed and the dynamics of their motion analyzed for individual channels on the basis of the transfer functions tabulated in the present book.

/6

However, reciprocal effects between channels are observed as a result of the "crossflow" effect at large angles of attack for cruciform-wing aerospace vehicles, which are symmetrical about the longitudinal axis. The effect on the dynamics of the vehicle's motion in three dimensions is taken into account by one of the various possible methods.

So that the characteristics of the stationary object can be obtained for various inputs, the book presents a compact mathematical description of the standard responses that can be used for conversion back to the transfer-function coefficients.

Along with stationary objects, nonstationary objects with variable parameters are also treated in matrix form, and the conditions under which this representation is necessary are stated.

Chapters III, IV, and V, Sec. 4 of Chapter II, and Appendix IV were writen by A.S. Shatalov and Chapters I and II and Appendixes I, II and III by Yu. I. Topcheyev and V.S. Kondrat'yev.

All comments and suggestions regarding the book should be sent to "Mashinostroeniye" Press at Moscow, B-66, 1-y Basmannyy Per., d. 3.

TABLE OF CONTENTS /238

# CHAPTER I

/7

# TYPES OF AEROSPACE VEHICLES AND THE CONFIGURATIONS OF THEIR CONTROLS

## 1.1. AEROSPACE VEHICLE CLASSIFICATION PRINCIPLES

Aerospace vehicles of various classes now have great flight altitude and speed ranges. The shaded area in Fig. 1.1 indicates the flightperformance zone of aerospace vehicles in terms of altitudes and speeds (Mach numbers). The lower boundary of the zone is characterized by the temperature strength characteristics of both the vehicle itself and its engines. The upper boundary is determined by the controllability and flightstability potential of the vehicle [30, 31].

/8

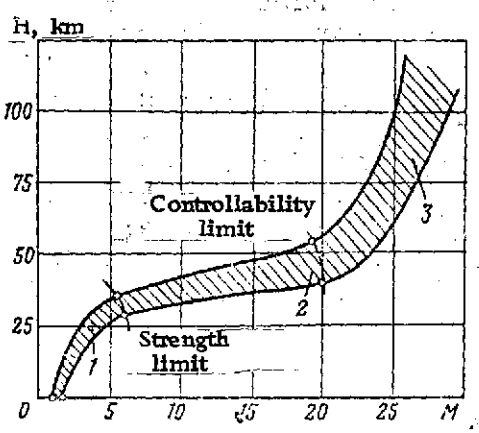


Figure 1.1. Maximum Altitude and Speed Performance Limits of Aerospace Vehicles. 1) Airplanes; 2) hypersonic aerospace vehicles (ASV); 3) rocket boosters and space vehicles of various types.

All aerospace vehicles can be classified into three groups on the basis of flight speeds and altitudes: conventional vehicles, hypersonic vehicles, and vehicles that fly on circular or ballistic trajectories.

At the same time, they can also be classified on the basis of the type of controls used. Here again there are three quite distinct groups: aerospace vehicles with aerodynamic controls, vehicles with gasdynamic controls, and vehicles with combination controls (combinations of aerodynamic and gasdynamic controls).

Airplanes and antiaircraft, air-to-air, and air-to-surface missiles are usually clasified in the first group.

The second group (vehicles with combination controls) usually includes hypersonic airplanes, the last stages of antiaircraft missiles, rocket airplanes, and many other vehicle types. Their altitude limits range from 30 to 50 km and sometimes even higher [30].

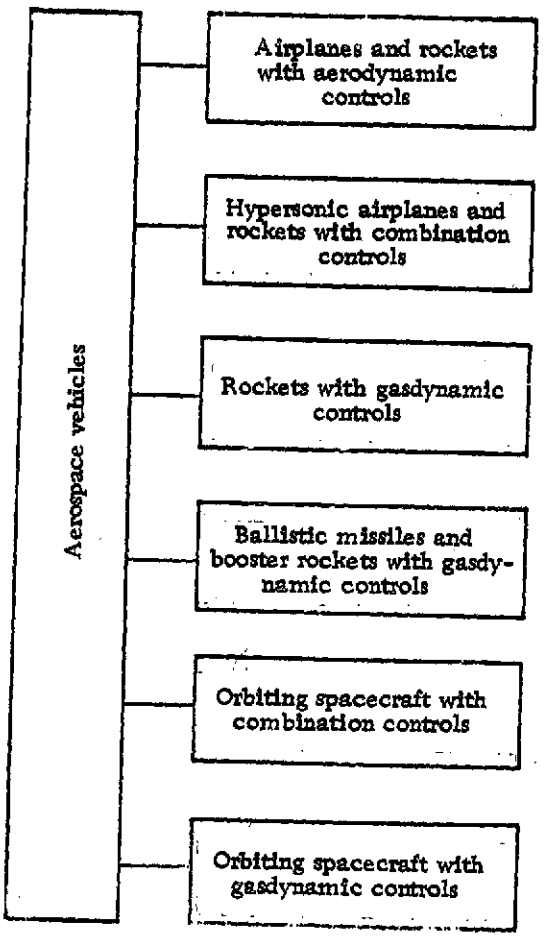


Figure 1.2. Unified Aerospace-Vehicle Classification Scheme.

Hypersonic airplanes and long-range winged rockets, rocket boosters, and their last stages can usually be classified as aerospace vehicles of the third group. The lower boundary for this group of ASV's is approximately 50-80 km. There is no upper limit [30].

We should note that the above classification of aerospace vehicles is not quite definitive. Certain foreign antitank devices fly at low heights and use gasdynamic controls. Short-range ballistic missiles may also have gasdynamic controls only. Orbiting near-earth space vehicles of the rocket-airplane type have aerodynamic and gasdynamic controls, etc.

The two aerospace-vehicle classifications that we have con-

sidered can be combined into a single system. This unified classification makes it possible to infer the purpose of the ASV, and the principle embodied in its mode of flight and in the control of the vehicle proper. /9

Figure 1.2 presents a unified ASV classification scheme. In this classification, each aerospace vehicle falls into one of six classes: airplanes and rockets with aerodynamic controls; hypersonic airplanes and rockets with combined controls; /10 rockets with gasdynamic controls; ballistic missiles and rocket boosters with gasdynamic controls; orbiting space vehicles with combination controls; orbiting space vehicles with gasdynamic controls.* We shall use this classification in Chapters I and II.

## 1.2. AIRPLANES AND ROCKETS WITH VARIOUS SCHEMES FOR DEVELOPING LIFT AND CONTROL MOMENTS

Airplanes and rockets with aerodynamic controls also include vehicles in which the forces required to develop the controlling moments are created by control surfaces. Airplanes and rockets of this group can be classified into several subgroups depending on the positions of the wings and the control surfaces. If the wing is placed toward the bottom of /11 the fuselage, we have a low-wing configuration; if the wing is at mid-height, we have a mid-wing vehicle, and, finally, if the wing is at the top of the fuselage, we have a high-wing type. The wing may be fixed or hinged, as indicated in Fig. 1.3, a,b, and c. In the last case, we say that the airplane has a variable-geometry wing.

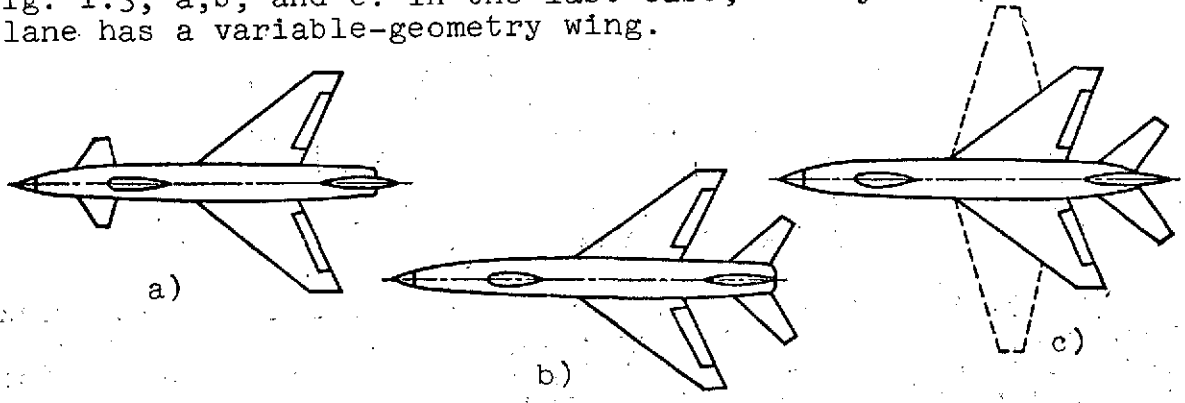


Figure 1.3. Aerodynamic Configurations of Airplanes. a) With control surfaces in "Canard" configuration; b) with normal control-surface placement; c) with variable-geometry wing.

*The last two classes are not considered here, since a separate book will be devoted to them.

The relative positions of the wings and horizontal tail surfaces have a strong influence on the layout of an airplane. When the tail surfaces are placed ahead of the wings, it is said that the airplane has a "canard" aerodynamic layout (see Fig. 1.3a). At positive angles of attack $\alpha$, the airplane is balanced by deflection of the elevators through a positive angle, i.e, when

$$\left(\frac{\alpha}{\delta_e}\right)_{bal} > 0. \tag{1.1}$$

If the control surfaces are aft of the wings, the airplane is said to have the normal configuration (Fig. 1.3b). In this scheme, the elevators must be deflected through a negative angle to obtain a positive angle of attack, i.e.,

$$\left(\frac{\alpha}{\delta_e}\right)_{bal} < 0. \tag{1.2}$$

If the elevators are placed near the trailing edge of the wing, the airplane is said to be laid out in a "tailess" configuration. The balance relation (1.2) is obviously retained in this case. The vertical tailplane is at the rear of the fuselage in all configurations. The ailerons of airplanes are situated on the trailing or lateral edges of its wings and develop rolling moments or assist in countering them.

An airplane is made to climb or descend by changing the elevator deflection angle $\delta_e$ and, consequently, the amount of lift.

A rotor deflection $\delta_r$ results in a flat turn. Aerospace vehicles having the airplane configuration with two-dimensional wing arrangement can execute coordinated turns by simultaneous deflections of the ailerons ($\delta_a$) and elevators ($\delta_e$). /12

The lift Y of an airplane with two-dimensional wing arrangement can be varied by varying the fuselage angle of attack $\alpha$. Lift is increased simultaneously by a component of the engine's thrust T, i.e.,

$$Y = P \sin(\alpha + \varphi_e), \tag{1.3}$$

where $\phi_e$ is the engine setting angle on the airplane.

We should note that the sum of the two angles $\alpha + \phi_e \leq 20°$. This indicates a small increase in the lift of the airplane due to the normal component of engine thrust. /13

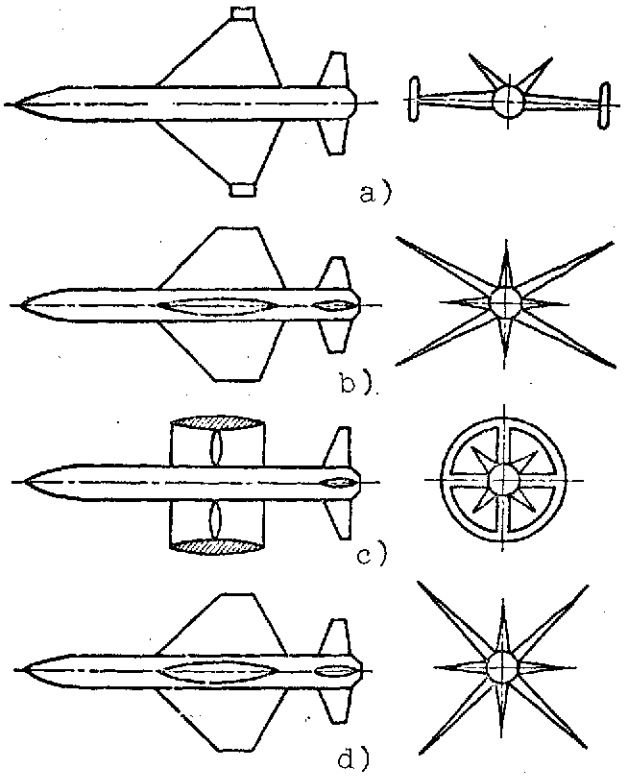


Figure 1.4. Configurations of Rockets with Aerodynamic Controls and Various Types of Wings. a) With two-dimensional wing; b, d) with three-dimensional wing arrangement; c) with annular wing.

Aerodynamically controlled rockets have a wider range of possible configurations than airplanes, since they make use of various wing forms (airplane configuration) and three-dimensional wing arrangements (cruciform wings). Diagrams of possible aerodynamic configurations for rockets with various types of wings are shown in Fig. 1.4.

Rocket configurations are also classified as normal, "canard," and "tailless" depending on the relative positions of the control surfaces and wings along the body of the rocket. The rocket configurations shown in Fig. 1.4 are normal in regard to the placement of the control surfaces and wings.

The relative positions of the control surfaces and wings along the body of a rocket strongly influence its configuration. Several /1 variations are possible here. Figure 1.5 illustrates the placement of control surfaces and wings at a 45° angle to the axis (the so-called X-X configuration). In Fig. 1.5b, the wings have the X configuration and the control surfaces the + configuration; this scheme is usually designated as X-+. Two other schemes are also

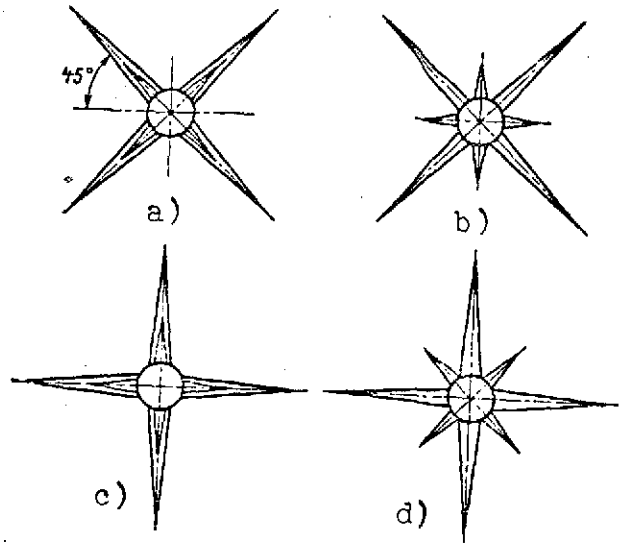


Figure 1.5. Diagrams Showing Relative Positions of Control Surfaces and Wings on Cross Sections Through Bodies of Rockets. a) Scheme X-X; b) scheme +X; c) scheme ++; d) scheme X+.

conceivable: +-+ (Fig. 1.5c) and +-X (Fig. 1.5b).

Rollerons or spoilers can be used on rockets to stabilize them with respect to the $Ox_1$ axis. A rolleron is a heavy rotor that twists the slipstream at speeds up to several thousand revolutions per minute. Figure 1.6a shows rollerons at the wingtips of a rocket. As the rocket rolls at angular velocity $\omega_x$, a gyroscopic moment appears and causes the ailerons (see Fig. 1.6a) to deflect. The rolling motion of the rocket is countered by this moment. With increasing flight speed of the rocket, the angular velocity of the rotors also increases, and, accordingly, so do the aileron deflections. Figure 1.6 shows spoilers arranged perpendicular to the flow along the trailing edge of a wing. Spoilers require small control moments, and this is an advantage of this system, although excessive drag is created when they are extended into the stream at a 90° angle. They can therefore be used on rockets designed for flight at high altitudes.

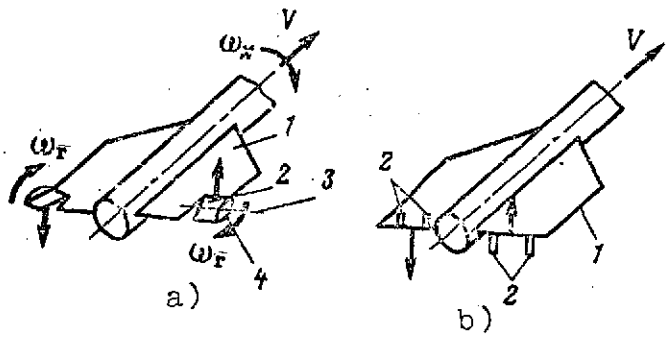


Figure 1.6. Diagrams Showing Arrangement of Rollerons and Spoilers on Rocket Wings. a) For Rollerons; 1) wing; 2) elevon; 3) elevon axis; 4) rotor; b) for spoilers: 1) wing; 2) spoilers.

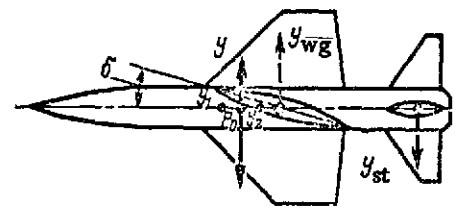


Figure 1.7. General Appearance of Rocket with Pivoting Wings.

One variety of the "canard" configuration is the pivoting-wing vehicle. It acquires its lift by pivoting /1

the wing, and its body is set practically in line with the free stream. In this configuration, the wings are located at the center of gravity and also act as control devices, while the non-moving rear surfaces serve as the vehicle's stabilizer (Fig. 1.7). The rocket can also be rolled if differential control is provided for the wings.

Let us write the balance condition for the rocket in the form

$$M_z^{\alpha}\alpha + M_z^{\delta}\delta = 0, \tag{1.4}$$

where $M_z^{\alpha}$ is the static derivative of the rocket's moment with respect to the angle $\alpha$ and $M_z^{\delta}$ is the static derivative of the rocket's moment with respect to the angle $\delta$. We find from (1.4)

$$\left(\frac{\alpha}{\delta}\right)_{bal} = -\frac{M_z^{\delta}}{M_z^{\alpha}}. \tag{1.5}$$

When $M_z^{\alpha}$ is negative, the sign of $(\alpha/\delta)_{bal}$ is the same as that of the derivative $M_z^{\delta}$. This indicates that when the wing is deflected through $+\delta$, the body of the vehicle also assumes a positive angle of attack $\alpha$.

We should note that the sign of $M_z^{\delta}$ depends on the trim of the rocket and the dimensions of the stabilizers. Figure 1.7 indicates the wing lift $Y_{wg}$ (applied at the wing aerodynamic center $F_{wg}$) and the stabilizer lift $Y_{st}$ due to wing downwash (applied at the stabilizer aerodynamic center $F_{st}$). The resultant lift Y associated with the wing deflection angle is applied at the aerodynamic center $F_0$ of the rocket (see Fig. 1.7). If the center of mass is located at the same point, we have /16

$$x_T - x_{F_0} = 0. \tag{1.6}$$

Here $M_z^{\delta} = 0$ and $(\alpha/\delta)_{bal} = 0$.

In this case, the angle of attack of the rocket body is zero at all control-surface deflection angles $\delta$.

If the center of mass is shifted to a point $Y_1$ forward of the aerodynamic center $F_0$, i.e.,

$$x_T - x_{F_0} < 0, \tag{1.7}$$

we have $M_z^\delta < 0$ and $(\alpha/\delta)_{bal} < 0$, and the angle of attack of the rocket body is set at a small negative value. On displacement of the center of mass to $Y_2$ aft of center, we have

$$x_T - x_{F_0} > 0 \tag{1.8}$$

and $M_z^\delta > 0$, so that $(\alpha/\delta)_{bal} > 0$.

In this case, the body will have a small positive angle of attack.

We see from the above that a rocket with a pivoting-wing configuration responds quickly, since its lift changes immediately with the pivot angle $\delta$. The small-rocket body angles of attack of this configuration ensure good operating conditions for ramjet engines, preventing flow detachment at the diffuser.

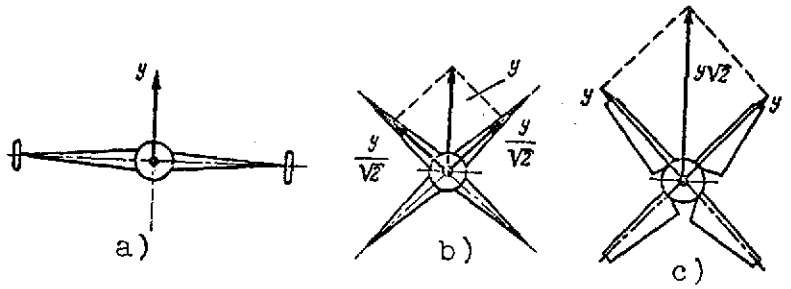


Figure 1.8. Lift-Developing Schemes for Rockets with Various Configurations. a) With Two-dimensional wing; b) with cruciform wings; c) with pivoting wings.

Let us compare three schemes for the development of lift for rockets having the same given wing area. The first rocket, a flat-winged type, has a lift Y (Fig. 1.8a); the second, with fixed cruciform wings, will also create the resultant lift Y if each wing has a lift equal to $\frac{Y}{\sqrt{2}}$ (Fig. 1.8b); the third, pivoting-wing configuration (Fig. 1.8c) has a resultant lift $Y\sqrt{2}$. Thus, the lift of pivoting wings in the plane of the bisector is 1.41 times the lift in the planes of fixed wings. /17

Fixed cruciform wings provide for turning the rocket without roll, thus improving its speed of response. For this reason, the

three-dimensional wing arrangements are usually used in piloteless vehicles of the air-to-air and surface-to-air classes, which are designed for use against aerial targets, where fast response is necessary [28]. Pivoting wings in a three-dimensional arrangement are used in ramjet-engined air-to-surface vehicles, since this eliminates flow detachment at the diffuser, an effect associated with large angles of attack [28].

The demand for increased altitude capability in aircraft has led to the development of vehicles of a new type: hypersonic airplanes with combination controls.

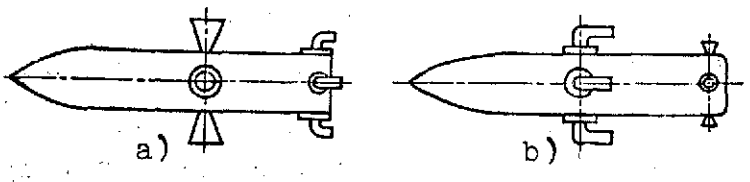


Figure 1.9. Diagrams of Rockets with Gasdynamic Lift-Generating Devices and Gasdynamic Controls. a) With fixed nozzles at center of gravity; b) with moving nozzles at center of gravity.

Hypersonic airplanes fly at high altitudes [30] and also use fixed wings to generate lift. However, the substantial decrease in the effectiveness of aerodynamic controls has made it necessary to use gasdynamic controls on hypersonic airplanes. Pivoting engines and pivoting nozzles are used in this case [10].

Let us now consider several different schemes for gasdynamic control of the last stages of rockets (Fig. 1.9). Let us place two nozzles at the rocket's center of mass (see Fig. 1.9a). These nozzles have a control system that directs the stream of gas into the required nozzle. This develops a reaction force that results in application of an additional g-force to the rocket stage. Pivoting nozzles have been used as devices developing controlling moments on rockets. /18

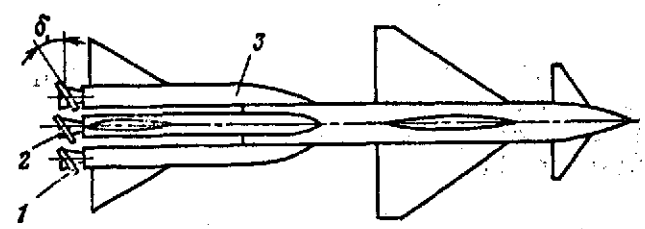


Figure 1.10. Diagrams of Rockets with Gasdynamic Controls.

Figure 1.9b presents a diagram of a rocket with lateral pivoting nozzles that are used to develop secondary g-forces. As in the first scheme, the control moments are produced by nozzles mounted at the end of the body.

The last stages of surface-to-air and air-to-air rockets designed for effectiveness at high altitudes are provided with gasdynamic control devices. Here the controlling forces are created not by turning the body of the rocket, but by means of jet nozzles [28].

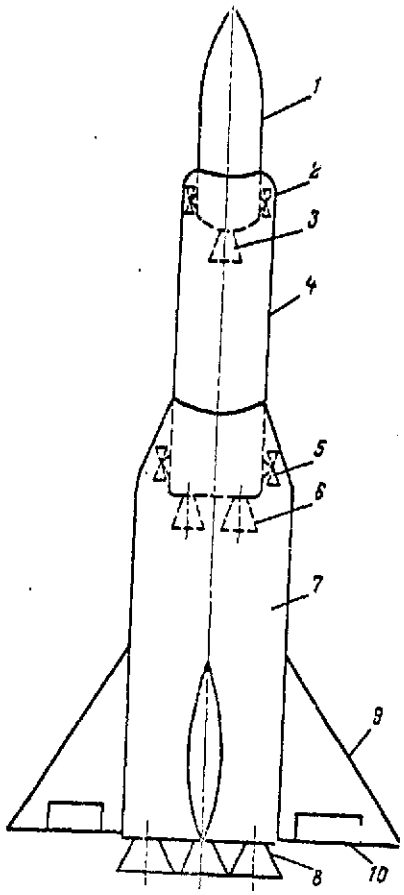


Figure 1.11. Diagram of Three-Stage Rocket Booster for Space Vehicle. 1) Third stage of rocket; 2) third-stage stabilizing engines; 3) sustainer engine; 4) second stage of rocket; 5) second-stage stabilizing engines; 6) sustainer engines; 7) first stage of rocket; 8) first-stage sustainer engines; 9) nonmoving stabilizer; 10) aerodynamic control surfaces.

Surface-to-surface missiles can also be made with two stages. The first stage consists of several groups of launch boosters 3, with deflector rings 1 mounted on nozzles 2 (Fig. 1.10). Rotation of the deflector through an angle $\delta$ deflects the launch-booster engine jet. Nozzle extensions may also be used together with the deflectors [29]. /2

These devices give rise to lateral forces that act on the

vehicle, and a rolling moment is also generated when a differential control system is used. It is obvious in this case that the gasdynamic controls will be used when the rocket is climbing slowly during the beginning phase of its flight. At this time, the aerodynamic controls are not effective enough to produce the required flight trajectory or to counter roll disturbances. For this reason, gasdynamic control devices are also used here (in the form of deflectors, extensions, or pivoting nozzles).

Booster rockets are single-use multistage vehicles. Figure 1.11 diagrams the layout of a 3-stage spacecraft booster rocket. The first stage 7 has a stabilizer 9 with aerodynamic control surfaces 10 and pivoting engine chambers 8. We see from this that the first stage has combined controls – aerodynamic and gasdynamic. The second stage 4 is fitted only with pivoting engine chambers 6. Finally, the third stage 1 is provided with a single pivoting chamber 3. The pivoting chambers are used to create lateral forces that guide the stages of the rocket onto the desired ballistic trajectories. Stabilizing engines – 5 for the second stage and 2 for the third stage – are used to counter rolling moments. Engines 8, which have a differential control system, are used to stabilize the rolling moment of the first stage at high altitudes. The aerodynamic control surfaces 10 are used at low altitudes [2].

# CHAPTER II

/2

# EQUATIONS OF MOTION AND TRANSFER FUNCTIONS OF AEROSPACE VEHICLES

In the design of control systems for aerospace vehicles, the latter can be regarded, depending on their purpose and geometrical dimensions, as rigid or elastically deformable structures. Most airplanes and rockets (of the air-to-surface, air-to-air, and surface-to-air types) are regarded as absolutely rigid bodies, since their frames deform little in practice. Booster rockets and strategic bombers are subject to considerable structural deformation, and this strongly influences the design of the stabilization systems and control loops for vehicles of these classes. Nevertheless, even these vehicles are regarded as rigid material structures during the first design stage. During this stage, the layout chosen for the vehicle is evaluated, the effectiveness of controls is investigated, and the stabilization and control system takes form. The effects of vibration of the whole of the rocket and motions of its liquid fuel during stabilization and control are taken into account in the following design stage. Below we present the dynamic equations of the vehicle and its transfer functions, which do not, as a rule, take these factors into account. Consideration of elastic hull vibrations is discussed in Chapter IV and in detail in the book [15].

## 2.1. FORMALIZATION CONDITIONS FOR VEHICLE EQUATIONS OF MOTION

As we know, a mathematical model of any aerospace vehicle can be assembled to represent the real picture of the physical processes that take place during flight with varying degrees of accuracy. /2
The completeness of a model is rather hard to define, depending primarily on the nature of the problem to be solved, the type of vehicle, and the extent and reliability of our knowledge of the initial characteristics.

The type of problem to be solved determines the basic flight regimes, analysis of which makes possible correct selection of the reference system.

It will be recalled that inertial and noninertial reference frames are distinguished in mechanics. Thus, the earth-based coordinate system is a noninertial system, since it describes a curvilinear motion in "immobile" space. However, it is possible in certain problems of the dynamics of motion, e.g., for flight within the atmosphere at velocities far below circular ($V_c$ = 8.1 km/sec), to neglect the earth's diurnal motion and curvature and to assume that the center of the earth is fixed in space. In this case, the earth-based coordinate system can be regarded as in-

ertial. But the use of this coordinate system in study of the motion of space vehicles results in substantial calculating errors. Thus, knowing the type of aerospace vehicle on the basis of its application, we can simplify the notation of its equations of motion by taking the coordinate system into account.

## Coordinate Systems

Let us examine the coordinate systems that have been used most widely in determining the characteristics of aerospace vehicles as objects of control.

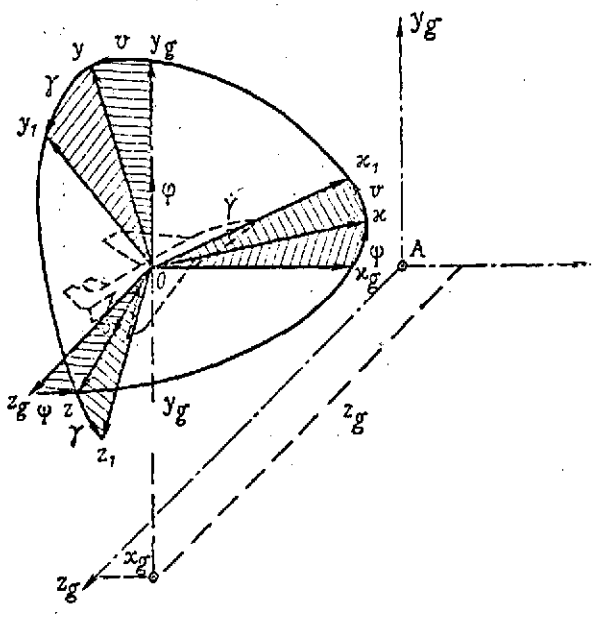


Figure 2.1. Determination of Position of Airplane (Rocket) in Earth-Based Coordinate Axes.

The earth-based coordinate system. The origin of the earth-based coordinate system is placed at the center of mass of the ASV (Fig. 2.1). The axis $Ox_g$ lies in the plane parallel to the local horizon and is directed along the tangent to the meridian in the direction of the North Pole. The axis $Oy_g$ is directed upward along the local vertical. This axis lies in the plane of the axis $Ox_g$ and is so directed as to form a right-hand (left-hand) coordinate system. There are also other variants of the earth coordinate system, but they differ from one another only in the position of the origin (moving or fixed on the earth's surface) and in the orientation of the $Ox_g$ axis in the plane of the local horizon. /23

Body coordinate system. This system (see Fig. 2.1) is used to determine the position of an ASV with respect to an earth coordinate system. Its origin is placed at the center of mass of the ASV. The axes $Ox_1$ and $Oy_1$ are placed in the vertical plane of symmetry of the vehicle and directed along its principal axes of inertia. Since the directions of the principal axes of inertia differ little in most cases from those of the vehicle's geometrical axes, it can be assumed that the axis $Ox_1$ is directed along the axis of the body (or parallel to the wing chord), that the axis $Oy_1$ is perpendicular

to $Ox_1$, and that $Oz_1$ is perpendicular to the ASV's plane of symmetry and points in the direction of the starboard wing.

Written in this coordinate system, the equations of motion of the ASV are simplified in certain respects as result of elimination of terms containing centrifugal moments.

The position of the body system relative to the earth system is determined by three angles: the angle of pitch $\vartheta$, angle of yaw $\psi$, and the angle of roll $\gamma$ (see Fig. 2.1). The angle of pitch $\vartheta$ is the angle between the axis $Ox_1$ and the local horizontal plane. The angle of roll $\gamma$ is the angle between the axis $Oy_1$ and the vertical plane passing through the axis $Ox_1$. The angle of yaw $\psi$ is the angle between the earth axis $Ox_g$ and the projection of the axis $Ox_1$ onto the local horizontal plane.

The relation between the angles of pitch, roll, and yaw on the one hand and the projections $\omega_{x1}, \omega_{y1}, \omega_{z1}$ of the angular-velocity vector $\bar{\omega}$ onto the axes of the body coordinate system on the other are found by successive rotations of the body axes with respect to the earth axes and is given by the formulas

$$\left.\begin{aligned}\omega_{x_1}&=\dot{\gamma}+\dot{\psi}\sin\vartheta;\\ \omega_{y_1}&=\dot{\psi}\cos\vartheta\cos\gamma+\dot{\vartheta}\sin\vartheta;\\ \omega_{z_1}&=\dot{\vartheta}\cos\gamma-\dot{\psi}\cos\vartheta\sin\gamma,\end{aligned}\right\} \tag{2.1}$$

or, with respect to $\dot{\vartheta}, \dot{\gamma}, \dot{\psi}$

$$\left.\begin{aligned}\dot{\vartheta}&=\omega_{y_1}\sin\gamma+\omega_{z_1}\cos\gamma;\\ \dot{\gamma}&=\omega_{x_1}-\operatorname{tg}\vartheta(\omega_{y_1}\cos\gamma-\omega_{z_1}\sin\gamma);\\ \dot{\psi}&=\sec\vartheta\,(\omega_{y_1}\cos\gamma-\omega_{z_1}\sin\gamma).\end{aligned}\right\} \tag{2.2}$$

Semiattached body coordinate system. In this coordinate system, the Ox axis is directed along the projection of the flight-speed vector onto the plane of symmetry of the aircraft, the Oy axis along the perpendicular to the Ox axis in the aircraft's plane of symmetry, and the Oz axis along the span of the starboard wing, i.e., it coincides with $Oz_1$. Aerodynamic forces and moments are usually measured in the semiattached body coordinate system in wind-tunnel studies. This is dictated by the design features of aerodynamic balances.

A vehicle is oriented with respect to the free-steam velocity vector by two angles: $\alpha$ and $\beta$ (see Fig. 2.2a). The angle of attack is the angle between the projection of the velocity vector onto the vertical plane of symmetry of the vehicle and the body axis $Ox_1$, and the angle of slip $\beta$ is the angle between the veloc-

ity vector and the ASV's vertical plane of symmetry.

Drag and wind coordinate systems. In studying the motion of a vehicle's center of gravity, it is convenient to use a moving coordinate system in which the Ox axis is directed along the velocity vector V of the vehicle's center of mass with respect to the air; if the Oy axis is then directed along the perpendicular to the Ox axis, which lies in the local vertical plane containing the vector V, and the Oz axis is directed perpendicular to the plane xOy, the result is a drag coordinate system, whose position with respect to the earth system is determined by two angles: 1) the angle $\psi_V$ between the projection of the velocity vector V onto the local horizontal plane and the axis $Ox_g$, and 2) the angle $\theta$ between the velocity vector V and the local horizontal plane. The angle $\theta$ is usually called the slope or flightpath angle, and the angle $\Psi$ the heading angle of the trajectory. If the axis Oy is placed in the ASV's vertical plane of symmetry perpendicular to Ox, and Oz is perpendicular to the plane xOy, the result is the wind coordinate system, whose position relative to the drag system is determined only by the angle $\gamma_V$. When $\gamma_V = 0$, the two coordinate systems coincide. Let us write the kinematic relationships describing the variation of the angular coordinates $\Psi$, $\theta$, and $\gamma_V$.

For the wind coordinate system

$$\left.\begin{aligned}\omega_x &= \dot{\gamma}_v + \dot{\psi}_v \sin\theta;\\ \omega_y &= \dot{\Psi}_v \cos\theta\cos\gamma_v + \dot{\theta}\sin\gamma_v;\\ \omega_z &= -\dot{\Psi}_v \cos\theta\sin\gamma_v + \dot{\theta}\cos\gamma_v.\end{aligned}\right\} \qquad (2.3)$$

For the drag coordinate system

$$\left.\begin{aligned}\omega_x &= \dot{\Psi}_v \sin\theta;\\ \omega_y &= \dot{\Psi}_v \cos\theta;\\ \omega_z &= \dot{\theta},\end{aligned}\right\} \qquad (2.4)$$

where $\omega_x$, $\omega_y$, $\omega_z$ are the projections of the angular-velocity vector of the rotation of the drag (wind) coordinate system with respect to the earth onto the drag (wind) axes.

## 2.2. GENERAL EQUATIONS OF MOTION OF AEROSPACE VEHICLES /26

As we noted above, the earth's superficial rectangular coordinate system can be regarded as inertial for vehicles designed for flight within the atmosphere at velocities substantially lower than circular. The motion of a "rigid" ASV in an arbitrarily choosen moving rectangular coordinate system with its origin at the center of inertia is described by a system of six scalar differential equations, three of which reflect the condition of force

equilibrium in the projections onto the coordinate axes, while three reflect equilibrium of the moments about these coordinate axes [10, 20].

Airplanes and Rockets with Aerodynamic and Combined Systems for Development of Controlling and Stabilizing Forces

The three force equations and the three moment equations take the form

$$\left.\begin{aligned}
&m(\dot{V}_x+V_z\omega_y-V_y\omega_z)=F_x;\\
&m(\dot{V}_y+V_x\omega_z-V_z\omega_x)=F_y;\\
&m(\dot{V}_z+V_y\omega_x-V_x\omega_y)=F_z;\\
&J_x\dot{\omega}_x+(J_z-J_y)\omega_y\omega_z-J_{xy}(\omega_x\omega_z-\dot{\omega}_y)-\\
&\quad-J_{xz}(\dot{\omega}_z+\omega_x\omega_y)+J_{yz}(\omega_z^2-\omega_y^2)=M_x;\\
&J_y\dot{\omega}_y+(J_x-J_z)\omega_x\omega_z+J_{yz}(\omega_x\omega_y-\dot{\omega}_z)-\\
&\quad-J_{xy}(\dot{\omega}_x+\omega_z\omega_y)+J_{xz}(\omega_x^2-\omega_z^2)=M_y;\\
&J_z\dot{\omega}_z+(J_y-J_x)\omega_x\omega_y+J_{xz}(\omega_y\omega_z-\dot{\omega}_x)-\\
&\quad-J_{zy}(\dot{\omega}_y+\omega_x\omega_z)+J_{xy}(\omega^2-\omega_x^2)=M_z.
\end{aligned}\right\} \qquad (2.5)$$

where $V_x$, $V_y$, $V_z$ are the projections of the velocity vector of the ASV's center of inertia onto the axes of the chosen coordinate system, $\omega_x$, $\omega_y$, $\omega_z$ are the projections of the angular-velocity vector of this system relative to the fixed system onto the axes of the chosen coordinate system, $F_x$, $F_y$, $F_z$ are the projections of the resultant of all external forces acting on the vehicle, $M_x$, $M_y$, $M_z$ are the moments of all external forces about the corresponding axes, and $J_x$, $J_y$, $J_z$, $J_{xy}$, $J_{xz}$, $J_{yz}$ are the axial and centrifugal moments of inertia of the vehicle. Let us examine the composition of the external forces and moments acting on the ASV and the basic relationships used in aerodynamics to describe them. /2

The resultant external-force vector can be written (Fig. 2.2 a)

$$F=P+F_a+G+F_c+F_d, \qquad (2.6)$$

where P is the thrust of the engine, $F_a$ is the vector of the aerodynamic force that arises as the vehicle moves relative to the air, G is the force of gravity, $F_c$ are the controlling forces created by the controls (deflection of control surfaces, change

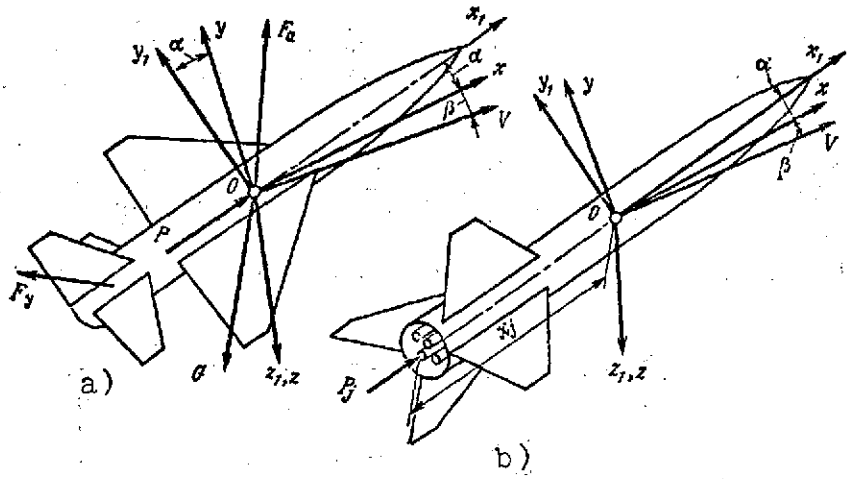


Figure 2.2. Nomenclature of Angles of Attack, Slip, and Roll. a) For airplane; b) ballistic missile.

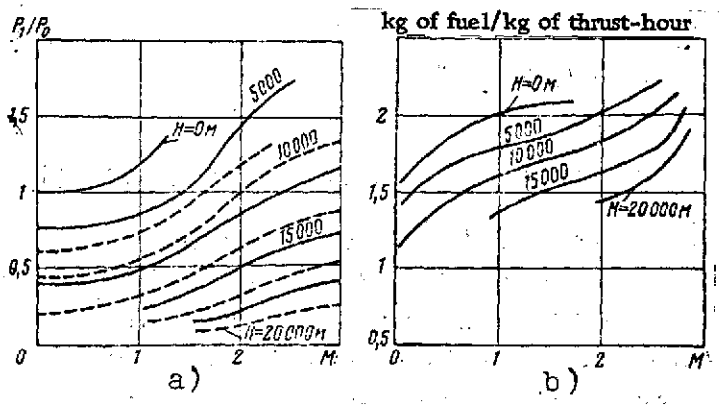


Figure 2.3. Characteristics of Airplane Engines. a) Altitude-Speed Curves of turbojet engine with afterburner in terms of thrust ratio ($P_1$ is the thrust at altitude H and $P_0$ the thrust at H = 0); b) specific fuel consumption curves of fully thrust-augmented turbojet engine.

in direction of thrust vector, etc.), and $F_d$ are the disturbing forces due to wind, blast-wave, or other action [12]. Resolving the vector F into components along the coordinate axes, we obtain

$$\left.\begin{aligned} F_x &= P_x + X + G_x + F_{cx} + F_{dx}; \\ F_y &= P_y + Y + G_y + F_{cy} + F_{dy}; \\ F_z &= P_z + Z + G_z + F_{cz} + F_{dz}. \end{aligned}\right\} \quad (2.7)$$

The basic characteristics of a powerplant are its thrust and specific fuel consumption. The thrust function P = f(V, H) for a fixed engine setting is called the altitude-speed characteristic and is usually stated graphically (Fig. 2.3a) [10, 28]. The fuel-consumption curve for a given engine is similar in shape to the thrust curve and determines the time variation of the mass and moments of inertia of the vehicle (see Fig. 2.3b) [10, 28]. The direction of the thrust force is stated in the body coordinate system. As we know from our course in aircraft aerodynamics [19], /29

it is customary to express the force $F_a$ in terms of the dimensionless coefficient $c_R$:

$$F_a = c_R \frac{S\rho V^2}{2}, \tag{2.8}$$

where ρ is the mass density of the air, V is the flight speed, and S is a characteristic with the dimensions of area. When the aerodynamic force $F_a$ is projected onto the axes of a system bound to the vehicle, the forces usually distinguished are the frontal drag X, the lift Y, and the lateral force Z; they are expressed in terms of the respective dimensionless coefficients $c_x$, $c_y$, and $c_z$:

$$X = c_x \frac{S\rho V^2}{2}; \quad Y = c_y \frac{S\rho V^2}{2}; \quad Z = c_z \frac{S\rho V^2}{2}. \tag{2.9}$$

As a rule, these forces are stated in the semiattached body coordinate system. The dimensionless coefficients are, in general, complicated functions of both the geometry of the vehicle and the kinematic parameters of its motion. Their expressions are usually limited with accuracy sufficient for practice to the linear terms of the Taylor-series expansions

$$\begin{aligned} c_y &= c_{y_0}(M) + c_y^{\alpha}(M)\alpha + c_y^{\delta}(M)\delta + \ldots; \\ c_z &= c_{z_0}(M) + c_z^{\beta}\beta + c_z^{\delta}\delta + \ldots, \end{aligned} \tag{2.10}$$

/3

where M is the Mach number.

The frontal drag coefficient is presented in the form

$$c_x = c_{x_0}(M) + A(M)c_y^2 + c_x(H). \tag{2.11}$$

The dimensionless coefficients $c_y^{\delta}$, $c_z^{\delta}$ appear in the expressions for the aerodynamic control forces $F_{cy}$ and $F_{cz}$. Controlling forces from the powerplant are created either by changing engine setting or by changing the direction of the thrust vector (see Chapter I). In studying the moments on the ASV, it is more convenient to use the body coordinate system. We shall therefore consider all moments with respect to these axes from now on. The principal moment of the forces can be written

$$M = M_a + M_{dp} + M_c + M_d, \tag{2.12}$$

where $M_a$ is the static aerodynamic moment, which depends on the

position of the Ox axis, with respect to the velocity vector (angles $\alpha$, $\beta$), $M_{dp}$ is the aerodynamic damping moment, which depends on the angular velocity of rotation of the vehicle $(\omega_x, \omega_y, \omega_z, \dot{\alpha}, \dot{\beta})$, $M_c$ is the controlling moment developed by the controls ($\delta_a$, $\delta_r$, $\delta_e$,...), and $M_d$ is the disturbing moment due to thrust eccentricity, asymmetry of the tailplane, and the effects of wind and other factors not taken into account in the preceding terms in equation system (2.5). In addition, all of the above moments depend on flight regime (H, V). Projecting the principal moment M onto the body coordinate axes, we obtain $M_x$, $M_y$, and $M_z$. In aerodynamics, moments, like the aerodynamic forces, are written in terms of dimensionless moment coefficients:

$$M_x = m_x \frac{lSQV^2}{2}; \quad M_y = m_y \frac{lSQV^2}{2}; \quad M_z = m_z \frac{bSQV^2}{2}, \tag{2.13}$$

where $l$ is the half-span of the wing and b is its aerodynamic chord. In the general case, expressions for the dimensionless moment coefficients are usually terminated after the second-order Taylor-series terms. As a rule, only linear terms of the expansion are taken into account for ASV with airplane configurations. For vehicles with small-aspect-ratio wings, and especially for "canards," the rolling-moment coefficient $m_x$ is strongly influenced by asymmetry of the flow at nonzero angles of slip; consequently, it is often necessary to include terms with second derivatives. /31

Confining the Taylor-series expansion to linear terms, we can write the coefficients $m_x$, $m_y$, and $m_z$ in the following forms:

$$\left.\begin{aligned} m_x &= m_x^{\omega_x}\omega_x + m_x^{\omega_y}\omega_y + m_x^{\delta_e}\delta_e + m_x^{\delta_r}\delta_r + \\ &\quad + m_x^{\beta}\beta + \ldots; \\ m_y &= m_y^{\omega_y}\omega_y + m_y^{\omega_x}\omega_x + m_y^{\delta_e}\delta_e + m_y^{\delta_r}\delta_r + \\ &\quad + m_y^{\beta}\beta + \ldots; \\ m_z &= m_z^{\alpha}\alpha + m_z^{\dot{\alpha}}\dot{\alpha} + m_z^{\omega_z}\omega_z + m_z^{\delta_a}\delta_a + \ldots. \end{aligned}\right\} \tag{2.14}$$

The quantities $m_x^{\omega_x}$, $m_y^{\omega_x}$, etc. are the partial derivatives of the aerodynamic-moment coefficients $m_x$, $m_y$, and $m_z$ with respect to the parameter indicated by the superscript and are, in turn, functions of Mach number. Using relations (2.5)-(2.13), we write the dynamic equations of motion for airplanes and rockets with respect to their axes in the form

$$
\left.
\begin{aligned}
&m(\dot{V}_x+V_z\omega_y-V_y\omega_z)=P_x+\\
&\quad+c_x\frac{SQV^2}{2}+mg_x+F_{c\,x}+F_{d\,x}\\
&m(\dot{V}_y+V_x\omega_z-V_z\omega_x)=P_y+\\
&\quad+c_y\frac{SQV^2}{2}+mg_y+F_{c\,y}+F_{d\,y};\\
&m(\dot{V}_z+V_y\omega_x-V_x\omega_y)=P_z+c_z\frac{SQV^2}{2}+mg_z+\\
&\quad+F_{c\,z}+F_{d\,z};\\
&J_x\dot{\omega}_x+(J_z-J_y)\omega_y\omega_z+J_{xy}(\omega_x\omega_z-\dot{\omega}_y)-\\
&\quad-J_{xz}(\dot{\omega}_z+\omega_x\omega_y)+J_{yz}(\omega_z^2-\omega_y^2)=\\
&\quad=m_x\frac{lSQV^2}{2}+M_{c\,x}+M_{d\,x};\\
&J_y\dot{\omega}_y+(J_x-J_z)\omega_x\omega_z+J_{yz}(\omega_x\omega_y-\dot{\omega}_z)-\\
&\quad-J_{xy}(\dot{\omega}_x-\omega_z\omega_y)+J_{xz}(\omega_x^2-\omega_z^2)=\\
&\quad=m_y\frac{lSQV^2}{2}+M_{c\,y}+M_{d\,y};\\
&J_z\dot{\omega}_z+(J_y-J_x)\omega_x\omega_y+J_{xz}(\omega_y\omega_z-\dot{\omega}_x)-\\
&\quad-J_{zy}(\dot{\omega}_y+\omega_x\omega_y)+J_{xy}(\omega_y^2-\omega_x^2)=\\
&\quad=m_z\frac{bSQV^2}{2}+M_{c\,z}+M_{d\,z}.
\end{aligned}
\right\}
\qquad (2.15)
$$

/3

This equation system will be linearized later and brought to a form convenient for determination of transfer functions for airplanes and rockets.

The expressions considered above for the aerodynamic forces and moments acting on ASV's are conventional and are widely used in practical calculations to determine the characteristics of the vehicles as controlled objects. The expressions given for the dimensionless coefficients [(2.10), (2.14)] are used in linearizing the equations of motion (2.15) and can, if it is necessary to obtain high accuracy in the solution, be supplemented by nonlinear terms of the expansions.*

Supplemented by the kinematic relations (see Sec. 2.1) and by the laws of variation of the mass and moments of inertia, the equations of motion (2.15) describe the motion of the vehicle in three dimensions and form a system of nonlinear differential equations. As we know, it is generally not possible to find solu- /3

*It is assumed that the aerodynamic characteristics of many vehicles are linear over the entire in-flight ranges of the angles of attack $\alpha$ and slip $\beta$ and the angular velocities.

tions for such equations in elementary functions or quadratures. Subsequent work with the equations can therefore take at least two directions.

1. Use of digital computers for analysis of the equation systems. Computers can be used for numerical integration of differential equations of practically any complexity and with the desired accuracy. In this case, an attempt is made to take account of complicated nonlinear relationships in which the aerodynamic forces and moments depend on the parameters of the vehicle's motion, to introduce various refinements into the equation system to interrelate the control channels, etc. The result is a unified interrelated equation system that gives a rather complete picture of the vehicle's complex multidimensional motion.

2. Simplification of the system of equations of motion of the ASV for preliminary selection of the parameters of the automatic devices used in the stabilization and control systems. In this case, the three-dimensional motion is resolved into longitudinal and lateral motions of the center of mass and a motion about the center of mass. The vehicle's equations of motion are linearized with allocation of the motion among the control channels.

The first direction requires detailed study of the specific vehicles and control systems for them. The results obtained can be used for analysis or synthesis of the automatic system as a whole. The second trend, on the other hand, brings out the basic properties of the vehicle itself as an object of automatic control, and this is the purpose of the present book.

Liquid-Propellant Rockets and Rocket Boosters

A distinctive property of vehicles of this type is the presence of substantial liquid masses on board. Movement of liquids through pipelines and in the propellant tanks of the rocket results in the appearance of additional forces exerted on the body of the rocket by the liquids. Most significant among these are the Coriolis and inertia forces, which must be taken into account in Eqs. (2.5). The Coriolis forces are much larger for rockets of the present class than for airplanes and winged rockets, since the lift of large rockets is produced only by engine thrust, and this requires high per-second fuel and oxidizer flowrates. The Coriolis force and moment exerted on the body by the liquid flowing in a j-th pipeline at velocity $v_r$ relative to the body can be found from the relations /34

$$F_{cj}=-\int_{l_j} 2\omega\times v_r\,dm;\quad M_{cj}=\int_{l_j} 2r'\times\omega\times v_r\,dm, \tag{2.16}$$

where $\omega$ is the angular velocity of rotation of the rocket.

The total Coriolis force and the corresponding moment are

$$F_{\text{ic}} = \sum_{j=1}^{N} F_{\text{c}j}, \qquad M_{\text{c}} = \sum_{j=1}^{N} M_{\text{c}j}. \tag{2.17}$$

Inertial forces arise as a result of the mobility of liquids in propellant tanks. The free surfaces of the liquids are deflected from their undisturbed positions in the presence of accelerations and angular velocities that arise under the action of external forces and moments. In turn, the sloshing liquids give rise to forces and moments that act on the body of the rocket.

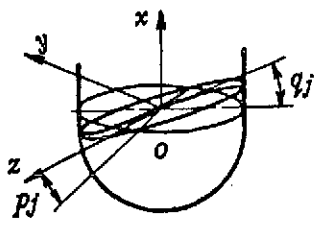


Figure 2.4. Positions of Liquid Surface in Rocket Tank.

Writing the equations of motion of a body with cavities that are partly filled by liquids is a complex task that has been studied in a number of works [1, 17]. Let us describe the basic premises and results of solution of this problem. The liquids are regarded as ideal and incompressible, and their motion as nonvortical, so that it can be described with the aid of the velocity potential. On the assumption that the deflections of the free surface from its undisturbed position are small, a partial differential equation is written for this potential. Investigation of this equation, together with the system of ordinary differential equations describing the motion of the rocket's body, involves major difficulties and can be completed only when the fuel tanks are positioned symmetrically and have simple shapes, e.g., those of the cylinder or sphere. It is possible in these cases to introduce /3 generalized coordinates that satisfy the ordinary differential equations, which is equivalent to replacement of a system with an infinite number of degrees of freedom by a system with a finite number. We might, for example, choose as these generalized coordinates the angular inclination of the free liquid surface near the line at which it intersects the plane of the undisturbed level and the angular rotation of this line relative to the Oz axis (Fig. 2.4). It can be shown [1] that these coordinates (we shall denote them by $q_\nu$ and $p_\nu$) satisfy the equations

$$\left.\begin{aligned} &\ddot{q}_\nu + \varepsilon_\nu \dot{q}_\nu + \Omega_\nu^2 q_\nu = (R_{\nu y}\dot{V}_y + R_{\nu\vartheta}\ddot{\vartheta} + R_{\nu\vartheta}\vartheta)\cos p_\nu + \\ &\quad + (R_{\nu z}\dot{V}_z + R_{\nu\psi}\ddot{\psi})\sin p_\nu; \\ &\ddot{p}_\nu + \mu_\nu \dot{p}_\nu + \Omega_\nu^2 p_\nu = R_{\nu\gamma}\ddot{\gamma}. \end{aligned}\right\} \tag{2.18}$$

(here $\nu$ is the number of the fuel tank).

These equations are similar to the equations of pendulums with natural frequency $\Omega_\nu$ and damping $\varepsilon_\nu$ and $\mu_\nu$, respectively. The right-hand side expresses the forces exerted on the liquid by the solid body of the rocket. Theoretical calculation of the

coefficients $R_{\nu\eta}$, $R_{\nu\vartheta}$, $R_{\nu\gamma}$ and $\Omega_\nu$ is possible only in simple cases, and the damping can be determined only by experiment. It is usually very small, and this gives rise to substantial difficulties in the design of automatic stabilization systems and makes it necessary to introduce mechanical dampers, perforated partitions, etc., thus increasing design weight. Great importance attaches to the natural frequency, which is determined by the relation

$$\Omega_\nu = \sqrt{\lambda_\nu V_{x0} - g_x}, \tag{2.19}$$

where $\lambda_\nu$ is a certain constant and $g_x$ is the projection of the acceleration of gravity onto the same axis. This relation is physically lucid.

A simple interpretation can also be found for the expression for the force exerted on the body by the moving liquid:

$$F_{l\,y} = -\sum_{\nu=1}^{N} \tilde{R}_{\nu y} \ddot{q}_\nu \cos p_\nu. \tag{2.20}$$

We see that it is proportional to the generalized accelerations, and that the coefficient $\tilde{R}_{\nu y}$ plays the part of a mass associated with the coordinate $q_{\nu y}$. /36

Similarly, we have for motion in the yaw plane

$$F_{l\,z} = -\sum_{\nu=1}^{N} \tilde{R}_{\nu z} \ddot{q}_\nu \sin p_\nu. \tag{2.21}$$

The component acting on the body along axis Ox is, as we should expect, equal to zero:

$$F_{l\,x} = 0.$$

The expressions for the moments take the form

$$\left.\begin{aligned} M_{l\,x} &= -\sum_{\nu=1}^{N} \tilde{R}_{\nu\eta} \ddot{p}_\nu; \\ M_{l\,y} &= -\left[\sum_{\nu=1}^{N} \tilde{R}_{\nu\eta} \ddot{q}_\nu + (\dot{V}_{x0} - g_x) \sum_{\nu=1}^{N} \tilde{R}_{\nu z} q_\nu\right] \sin p_\nu; \\ M_{l\,z} &= -\left[\sum_{\nu=1}^{N} \tilde{R}_{\nu\vartheta} \ddot{q}_\nu + (\dot{V}_{x0} - g_x) \sum_{\nu=1}^{N} \tilde{R}_{\nu y} q_\nu\right] \cos p_\nu. \end{aligned}\right\} \tag{2.22}$$

We note that only the fundamental vibration frequency is taken into account in each tank in the above description of liquid sloshing. Consideration of higher harmonics results in only minor corrections because of the rapid decrease in the coefficients $R^{(n)}_{\nu\vartheta}, R^{(n)}_{\nu\psi}, \ldots, \tilde{R}^{(n)}_{\nu\gamma}$ with increasing harmonic number n. Let us now turn to description of the motion of the rocket's body with consideration of the Coriolis $F_C$ and liquid $F_l$ forces and the corresponding moments $M_C$ and $M_l$.

We write the equations of the forces and moments in the projections onto the body coordinate system on the basis of Fig. 2.2b and Eqs. (2.5) with consideration of the symmetry of the ballistic missile with respect to the Ox axis. We shall assume that there is little change in the directions of the principal axes of inertia during flight. In writing the equations, we assume that the directions of the principal axes of inertia coincide with the axes of the rocket and do not change during flight; the result is the system

$$
\left.
\begin{aligned}
&m(\dot V_x + V_z\omega_y - V_y\omega_z) = P_x + c_x\frac{S_\rho V^2}{2} + \\
&\quad + mg_x + F_{cx} + F_{cx} + F_{dx} + F_{lx};\\
&m(\dot V_y + V_x\omega_z - V_z\omega_x) = P_y + c_y\frac{S_\rho V^2}{2} + \\
&\quad mg_y + F_{cy} + F_{cy} + F_{dy} + F_{ly};\\
&m(\dot V_z + V_y\omega_x - V_x\omega_y) = P_z + c_z\frac{S_\rho V^2}{2} = \\
&\quad + mg_z + F_{cz} + F_{cz} + F_{dz} + F_{lz};\\
&J_x\dot\omega_x + (J_z - J_y)\omega_y\omega_z = m_x\frac{lS_\rho V^2}{2} + \\
&\quad + M_{px} + M_{cx} + M_{cx} + M_{dx} + M_{lx};\\
&J_y\dot\omega_y (J_x - J_z)\omega_z\omega_x = m_y\frac{lS_\rho V^2}{2} + \\
&\quad + M_{py} + M_{cy} + M_{cy} + M_{dy} + M_{ly};\\
&J_z\dot\omega_z + (J_y - J_x)\omega_x\omega_y = m_z\frac{bS_\rho V^2}{2} + \\
&\quad + M_{pz} + M_{cz} + M_{cy} + M_{dy} + M_{lz};\\
&\ddot q_\nu + \varepsilon_\nu\dot q_\nu + \Omega_\nu^2 q_\nu = (R_{\nu y}\dot V_y + R_{\nu\vartheta}\ddot\vartheta + \\
&\quad + R_{\nu\vartheta}\vartheta)\cos p_\nu + (R_{\nu z}\dot V_z + R_{\nu\psi}\ddot\psi)\sin p_\nu;\\
&\ddot p_\nu + \mu_\nu\dot p_\nu + \Omega_\nu^2 p_\nu = R_{\nu\gamma}\ddot\gamma;\\
&\qquad\qquad \nu = 1, 2, \ldots, N,
\end{aligned}
\right\} \qquad (2.23)
$$

where

$$
\begin{aligned}
F_{cx} &= 2m(V_z\omega_y - V_y\omega_z)\\
F_{cy} &= 2m(V_x\omega_z - V_z\omega_x)\\
F_{cz} &= 2m(V_y\omega_x - V_x\omega_y)
\end{aligned}
$$

are the Coriolis forces; $M_{Cx}$, $M_{Cy}$, and $M_{Cz}$ are the moments of these forces, $P_x$, $P_y$, and $P_z$ are the total thrust forces from the rocket's engines; and $M_{px}$, $M_{py}$, and $M_{pz}$ are the total moments of the rocket's engine-thrust forces. We shall assume that the flow of the gases and liquids within the body of the rocket is axially symmetrical; then the Coriolis force and its moment have the components /38

$$\left.\begin{aligned} &F_{cx}=0;\quad F_{cy}=F_{cy}^{\omega_z};\quad F_{cz}=F_{cz}^{\omega_y}\omega_y;\\ &M_{cx}=0;\quad M_{cy}=M_{cy}^{\omega_y}\omega_y;\quad M_{cz}=M_{cz}^{\omega_z}\omega_z. \end{aligned}\right\} \qquad (2.24)$$

The Coriolis moments have various effects on the rocket. If the engines are aft of the center of mass, the damping moments are larger than the driving moments, i.e.,

$$\left.\begin{aligned} &M_{cy}^{\omega_y}<0;\\ &M_{cz}^{\omega_z}<0. \end{aligned}\right\} \qquad (2.25)$$

We shall assume that the air in which the vehicle is flying has a velocity $V_a$ and also consider N engines. We denote the projections of engine thrust onto the axes by $P_{jx}, P_{jy}, P_{jz}$, and the angles beteen the thrust vectors and the y and z axes by $\phi_j$ and $\lambda_j$. Then, considering the smallness of the angle between Ox and the engine-thrust vectors, we can write

$$\left.\begin{aligned} &P_x\simeq\sum_j P_j;\\ &P_y\simeq\sum_j P_j\varphi_j;\\ &P_z\simeq\sum_j P_j\lambda_j. \end{aligned}\right\} \qquad (2.26)$$

Denoting by $x_j$, $y_j$, and $z_j$ the corresponding distances from the point of application of vector P on the nozzle exit section to the center of mass of the rocket, we obtain

$$\left.\begin{aligned} &M_{P_x}=\sum_j(y_j\lambda_j-z_j\varphi_j)P_j;\\ &M_{P_y}=\sum_j(z_j-x_j\lambda_j)P_j;\\ &M_{P_z}=\sum_j(x_j\varphi_j-y_j)P_j. \end{aligned}\right\} \qquad (2.27)$$

Equation system (2.23) can be brought to the following form on the basis of expressions (2.24-2.27):

$$
\begin{aligned}
&m(\dot V_x+V_z\omega_y-V_y\omega_z)=\sum_j P_j+\frac{c_xS_0}{2}(V_x-\\
&\quad -V_{\bar d x})^2+mg_x+F_{c x}+F_{d x}+F_{\bar l x};\\
&m(\dot V_y+V_x\omega_z-V_z\omega_x)=\sum_j P_j\varphi_j=\frac{(c_{x_0}+c_y^\alpha)S_0}{2}\times\\
&\quad \times(V_x-V_{\bar d x})(V_y-V_{\bar d y})+mg_y+F_{c y}^{\omega_z}\omega_z+\\
&\quad +F_{c y}+F_{d y}+F_{\bar l y};\\
&m(\dot V_z+V_y\omega_x-V_x\omega_y)=\sum_j P_j\lambda_j+\frac{(c_{x_0}+c_z^\beta)S_0}{2}\times\\
&\quad \times(V_x-V_{\bar d x})(V_z-V_{\bar d z})+mg_z+F_{c z}^{\omega_y}\omega_y+\\
&\quad +F_{c x}+F_{d x}+F_{\bar l z};\\
&J_x\dot\omega_x+(J_z-J_y)\omega_y\omega_z=\frac{m_x lS_0}{2}V^2+\\
&\quad +\sum_j(y_j\lambda_j-z_j\varphi_j)P_j+M_{\bar c x}+M_{\bar d x}+M_{\bar l x};\\
&J_y\dot\omega_y+(J_x-J_z)\omega_z\omega_x=m_y\frac{lS_0V^2}{2}+\\
&\quad +\sum_j(z_j-x_j\lambda_j)+P_j+M_{\bar c y}^{\omega_y}\omega_y+\\
&\quad +M_{\bar{dp}y}+M_{\bar d y}+M_{\bar l y};\\
&J_z\dot\omega_z+(J_y-J_x)\omega_x\omega_y=m_z\frac{bS_0V^2}{2}+\\
&\quad +\sum_j(x_j\varphi_j-y_j)P_j+M_{\bar c z}^{\omega_z}\omega_z+\\
&\quad +M_{\bar c z}+M_{\bar d z}+M_{\bar l z};\\
&\ddot q_\nu+\varepsilon_\nu\dot q_\nu+\Omega_\nu^2q_\nu=(R_{\nu y}\dot V_y+R_{\nu\ddot\vartheta}\ddot\vartheta+R_{\nu\vartheta}\vartheta)\cos p_\nu+\\
&\quad +(R_{\nu z}\dot V_z+R_{\nu\ddot\psi}\ddot\psi)\sin p_\nu;\\
&\ddot p_\nu+\mu_\nu\dot p_\nu+\Omega_\nu^2p_\nu=R_{\nu\dot\omega_x}\dot\omega_x.\\
&\qquad\qquad \nu=1,2,\ldots,N_\nu
\end{aligned}
\tag{2.28}
$$

The resulting equation system (2.28) is then linearized, and the linearized equations are used to determine the transfer functions of the ballistic missiles and rocket boosters.

## 2.3. LINEARIZATION AND BASIC METHODS OF SIMPLIFICATION OF AEROSPACE-VEHICLE EQUATIONS OF MOTION

The methodological aspect of linearization of the system of differential equations describing the motion of an aerospace ve-

hicle is illuminated quite fully in a number of works on flight dynamics [18, 21]. We recall that the method for linearization of the equations is essentially based on the assumption that the parameters of the disturbed motion ($V$, $\alpha$, $\beta$, $\gamma$, $\vartheta$, $\psi$,... and their derivatives) differ little from the parameters of the initial motion at the same time. Terms containing the deviations of the disturbed-motion parameters from the parameters of the initial motion in powers higher than the first can then be neglected in the equations of motion as small quantities of higher order. It is more convenient to linearize the equations of ASV motion after first dividing them into two independent systems, one of which describes the longitudinal motion and the other the lateral motion. The fundamental possibility of this separation results from the symmetry of the vehicle about the longitudinal plane $Ox_1y_1$. If flight takes place in a certain vertical plane and the plane of symmetry of the vehicle coincides at all times with the flight plane (as is possible, for example, with ideal roll stabilization), then the kinematic parameters $\beta$, $\gamma$, $\omega_x$, $\omega_y$ will at all times equal zero. In this case, the vehicle's motion will consist of a progressive motion of its center of mass along the axes $Ox_1$ and $Oy_1$ and a rotational motion around the axis $Oz_1$. This is known as the longitudinal motion, and is characterized by the parameters $V$, $\theta$, $\vartheta$, $\alpha$, $\omega_z$, $H$, $x$. Accordingly, the lateral motion consists of progressive motion of the center of mass along the axis $Ox_1$ and rotational motions around the axes $Ox_1$ and $Oy_1$. We should note at once that no matter how we simplify the equations of the lateral motion, we shall never be able to exclude from them such longitudinal parameters as V and H. This means that to investigate the lateral motion independently, it is first necessary to determine the manner in which these parameters vary as time functions, i.e., the differential equations obtained for the lateral motion will be equations with variable coefficients. The possibility of resolving the controlled motion of the ASV into longitudinal and lateral motions also hinges on the operating characteristics of the flight-control system. If the deflection of the pitch controls depends only on the longitudinal parameters, and the deflections of the yaw and roll controls only on the lateral parameters, it is possible to break down the over-all motion in this way. The resulting simplification of the equations of guided motion of the ASV makes it possible to lower the order of the equation system by half and is used extensively in analysis of ASV flight. To determine the characteristics of the longitudinal motion, it is more convenient to write the equations of the forces acting on the ASV in the directions of the Ox and the Oy axes in the wind coordinate system and the equation of moments in the body system. In the wind system, $V_x=V$, $V_z=V_y=0$, $\omega_z=\dot{\theta}$, and the equations of system (2.5), which describe the dynamics of the longitudinal motion,

/41

assume the form

$$\left.\begin{aligned} m\dot{V} &= F_x; \\ mV\dot{\theta} &= F_y; \\ J_z\ddot{\vartheta} &= M_z. \end{aligned}\right\} \tag{2.29}$$

Equation system (2.29) must be supplemented with the geometrical relation between angles

$$\vartheta = \theta + \alpha. \tag{2.30}$$

The projections of the forces onto Ox and Oy are determined by the expressions (provided that the direction of the thrust force coincides with that of the wing chord)

$$\left.\begin{aligned} F_x &= R\cos\alpha - X - G\sin\theta + F_{d\,x}; \\ F_y &= Y + P\sin\alpha - G\cos\theta + F_{d\,y}, \end{aligned}\right\} \tag{2.31}$$

where P is the thrust of the engine, X is the frontal drag, Y is the lift, and G is the weight of the vehicle. The manner in which the mass and moments of inertia of the vehicle vary is usually known, and is determined in terms of the specific propellent-consumption curve and the depletion-sequence program: /4

$$m(t) = m_0 - \int_0^t \dot{C}\,dt, \quad J(t) = f(C, t). \tag{2.32}$$

Further simplification of equation system (2.29) is based on the possibility of resolving the longitudinal disturbed motion into two different types of motion: short-period and long-period. The physical factors responsible for this character of the disturbed motion are the same for all ASV's. The vehicle can change its angle of attack very quickly by rotating about its center of mass. At the same time, the flight speed of the vehicle varies comparatively slowly. The period of the long-period oscillations is usually several tens of seconds (30-100 sec), while the period of the short-period oscillations is a few seconds (1-4 sec). In considering the short-period motion, therefore, we may neglect the velocity deviation $\Delta V$ and assume that the velocity is a known function of time. With this assumption, we may take, instead of the complete system of differential equations of motion (2.29), only the second and third equations, which determine the response of the vehicle to deflection of the controls and to disturbances that offset the equilibrium of the moments and forces with respect to the Oz and Oy axes, respectively. The characteristics of the short-period motion are basic to the preliminary mathematical design of flight-control systems in the longitudinal plane, and we shall devote most of our attention to them below. For example, it is necessary in a number of cases to consider the dynamics of

speed and altitude variation in investigating systems for flight speed and altitude control. The first two equations of system (2.29)

$$\left.\begin{aligned} m\dot{V} &= F_x, \\ mV\dot{\theta} &= F_y, \end{aligned}\right\} \tag{2.33}$$

are usually considered in these problems, supplemented by the moment-equilibrium equation

$$M_z(V, H, \alpha, \delta_e) = 0$$

(the degenerate third equation of system (2.29)) and by the kinematic relation

$$\dot{H} = V \sin\theta. \tag{2.34}$$

Physically, this means that when the controls are deflected, the angle of attack assumes its balanced value instantaneously, with the result that the condition $M_z = 0$ is satisfied throughout the entire flight. Let us linearize equation system (2.29) separately for each form of ASV motion. We shall consider the short-period motion, the approximate equations of which are obtained by dropping the first equation in system (2.29). In the remaining equations, velocity and altitude are assumed to be known time functions. In accordance with the conventional procedure for linearization of the equations, we assign small increments to the parameters of the vehicle's motion, expand the aerodynamic forces and moments in Taylor series in these increments, cut this expansion off at the linear terms, exclude terms of the second order of smallness from consideration, and replace the sines and cosines of the angle of attack by the approximate expressions

$$\sin\alpha \approx \alpha, \quad \cos\alpha \approx 1. \tag{2.35}$$

As a result, we obtain the equations of the short-period motion in the form

$$\left.\begin{aligned} mV\Delta\dot{\theta} &= F_y^{\alpha}\Delta\alpha + F_y^{\vartheta}\Delta\theta + F_y^{\delta_e}\delta_e; \\ J_z\Delta\ddot{\vartheta} &= M_z^{\alpha}\Delta\alpha + M_z^{\dot{\alpha}}\Delta\dot{\alpha} + M_z^{\bar{\omega}_z}\Delta\dot{\vartheta} + M_z^{\delta_e}\delta_e; \\ \Delta\vartheta &= \Delta\theta + \Delta\alpha, \end{aligned}\right\} \tag{2.36}$$

where $F_y^{\alpha}, M_z^{\alpha}, \ldots$ are the partial derivatives of the forces and moments with respect to the parameters indicated by the superior indices.

Using the conventional notation of aerodynamics for the

forces and moments (see Sec. 2.2), we can write the coefficients of the equations in the form

$$\left.\begin{aligned} F_y^{\alpha} &= \frac{c_y^{\alpha} S\varrho V^2}{2} + P; \qquad F_y^{\vartheta} = G\sin\vartheta_0; \\ F_y^{\delta_e} &= \frac{c_y^{\delta_e} S\varrho V^2}{2}; \qquad M_z^{\alpha} = \frac{m_z^{\alpha} bS\varrho V^2}{2}; \\ M_z^{\bar{\omega}_z} &= \frac{m_z^{\bar{\omega}_z} b^2 S\varrho V}{2}; \qquad M_z^{\dot{\bar{\alpha}}} = \frac{m_z^{\dot{\bar{\alpha}}} b^2 S\varrho V}{2}; \\ M_z^{\delta_e} &= \frac{m_z^{\delta_e} bS\varrho V^2}{2}, \end{aligned}\right\} \qquad (2.37)$$

where the coefficients $\overline{m_z^{\omega_z}}$ and $\overline{m_z^{\dot{\alpha}}}$ are brought to dimensionless form with the relations

$$m_z^{\omega_z} = m_z^{\bar{\omega}_z}\frac{b}{V} \text{ and } m_z^{\dot{\alpha}} = m_z^{\dot{\alpha}}\frac{b}{V}.$$

Thus, we have arrived at a system of linear differential equations with variable coefficients whose law of variation is asigned as a function of time and determined by the flight trajectory chosen for the ASV. Let us write equation system (2.37) in the form

$$\left.\begin{aligned} &\dot{\alpha} + z_{\alpha}\alpha - \dot{\vartheta} + z_{\vartheta}\vartheta = -z_{\delta_e}\delta_e; \\ &n_{\dot{\alpha}}\dot{\alpha} + n_{\alpha}\alpha + \dot{\vartheta} + n_{\tau}\dot{\vartheta} = n_{\delta_e}\delta_e, \end{aligned}\right\} \qquad (2.37')$$

where

$$z_{\alpha} = \frac{F_y^{\alpha} - F_y^{\vartheta}}{mV}; \quad z_{\vartheta} = \frac{F_y^{\vartheta}}{mV}; \quad n_{\dot{\alpha}} = -\frac{\overline{M_z^{\dot{\alpha}}}}{J_z}; \quad n_{\alpha} = -\frac{M_z^{\alpha}}{J_z};$$

$$n_{\tau} = -\frac{M_z^{\bar{\omega}_z}}{J_z}; \quad z_{\delta_e} = \frac{F_y^{\delta_e}}{mV}; \quad n_{\delta_e} = \frac{M_z^{\delta_e}}{J_z}.$$

Here and below, the sign of the increment $\Delta$ is omitted to abreviate the notation. If level flight is taken as the initial motion, the coefficient $z_{\vartheta}$ will vanish. Substituting $\omega_{z_1}$ for $\dot{\vartheta}$ in the equations, we obtain

$$\left.\begin{aligned} &\dot{\alpha} + z_{\alpha}\alpha - \omega_{z_1} = -z_{\delta_e}\delta_e; \\ &n_{\dot{\alpha}}\dot{\alpha} + n_{\alpha}\alpha + \dot{\omega}_z + n_{\tau}\omega_{z_1} = n_{\delta_e}\delta_e. \end{aligned}\right\} \qquad (2.38)$$

These equations are usually used to study the short-period component of the motion when it is important to evaluate the frequency and degree of damping of the oscillations. The coefficients of equation system (2.38) for the F-101 aircraft are given in Ap-

pendix 1 [27].

Consideration of the gravity component $Z \neq 0$ (for $\theta_0 \neq 0$) has little effect on the nature of the short-period oscillations defined by Eqs. (2.38), adding only an aperiodic component of the motion with a large time constant. In the design of automatic pilots for longitudinal stabilization of ASV's, therefore, the rule is to use equation system (2.38) with the angle of pitch $\vartheta$ obtained by simple integration

$$\vartheta = \int_0^t \omega_{z_1}\, dt.$$

Let us consider the characteristics of the ASV's long-period motion. In the linearization of Eqs. (2.29), which describe the long-period motion, account is also taken of the dependence of the aerodynamic forces and moments on the velocity and altitude increments u and h:

$$\begin{aligned}
\Delta F_x &= F_x^{\alpha}\alpha + F_x^{\theta}\theta + F_x^{V}u + F_x^{H}h + F_x^{\delta_t}\delta_t;\\
\Delta F_y &= F_y^{\alpha}\alpha + F_y^{\theta}\theta + F_y^{V}u + F_y^{H}h + F_y^{\delta_e}\delta_e + F_y^{\delta_t}\delta_t;\\
M_z &= M_z^{V}u + M_z^{\alpha}\alpha + M_z^{\delta_e}\delta_e,
\end{aligned}$$

where $\delta_t$ is the throttle deflection angle.

Linearizing Eqs. (2.33) and (2.34), we obtain a system of linear differential equations:

$$\left.\begin{aligned}
\dot{u} &= c_{11}u + c_{12}\alpha + c_{13}\theta + c_{14}h + a_t\delta_t;\\
\dot{\theta} &= c_{21}u + c_{22}\alpha + c_{23}\theta + c_{24}h + z_{\delta_e}\delta_e + z_{\delta_t}\delta_t;\\
\dot{h} &= c_{31}u + c_{33}\theta;\\
0 &= c_{41}u + c_{42}\alpha + c_{44}h + m_z^{\delta_e}\delta_e,
\end{aligned}\right\} \qquad (2.39)$$

where

$$c_{11} = \frac{P^V}{m} - \frac{S\varrho_0 V_0}{m}\left(c_x + c_x^M \frac{M_0}{2}\right),$$

$$c_{12} = -\left(c_x^{\alpha}\frac{S\varrho_0 V_0^2}{2m} + \frac{P}{m}\alpha_0\right); \qquad /46$$

$$c_{13} = -g\cos\theta_0;$$

$$c_{14} = \frac{1}{m}\left(P^H - \frac{c_x S V_0^2}{2}\frac{\partial \varrho}{\partial H}\right); \qquad a_t = \frac{P_t^{\delta}}{m};$$

$$c_{21}=\frac{SQ_0}{2M}\left(c_y+c_y^M\frac{M_0}{2}\right)+\frac{P^M M_0}{mV_0^2}\alpha_0;$$

$$c_{22}=c_y^\alpha\frac{SQ_0V_0}{2m}+\frac{P}{mV_0};\quad c_{23}=\frac{g}{V_0}\sin\theta_0;$$

$$c_{24}=\frac{c_ySV_0}{2m}\frac{\partial Q}{\partial H}+\frac{P^H}{mV_0}\alpha_0;\ z_{\delta_{ie}}=\frac{Y_{ie}^\delta}{mV};\ z_{\delta_{it}}=\frac{P_t^\delta}{mV}\alpha_0;$$

$$c_{31}=\theta_0;\quad c_{32}=0;\quad c_{33}=V_0;$$

$$c_{41}=\frac{(m_{z_0})^M+\alpha_0(m_z^\alpha)^M+(m_z^\delta)^M\delta_{e_0}}{a};$$

$$c_{42}=m_z^\alpha;\quad c_{44}=0;$$

$V_0$ and $\theta_0$ are the values of the initial-motion parameters. Let us elaborate on the method of evaluating certain coefficients, e.g.,

$$c_{41}=\frac{\partial M_z}{\partial V}=M_z^V=\frac{\partial M_{z0}}{\partial V}+\left(\frac{\partial M_z^\alpha}{\partial V}\right)\alpha_0+\left(\frac{\partial M_z^\delta}{\partial V}\right)\delta_{e_0},$$

where

$$\frac{\partial M_{z_0}}{\partial V}=\frac{bSQ_0V_0}{J_z}\left[m_{z_0}+\frac{V}{2a}(m_{z_0})^M\right];$$

$$\frac{\partial M_z^\alpha}{\partial V}=\frac{bSQ_0V_0}{J_z}\left[m_z^\alpha+\frac{V}{2a}(m_z^\alpha)^M\right],$$

$$\frac{\partial M_z^\delta}{\partial V}=\frac{bSQ_0V_0}{J_z}\left[m_z^\delta+\frac{V}{2a}(m_z^\delta)^M\right],$$

where $\alpha_0$ is the balanced value of the angle of attack (in undisturbed motion), $\delta_{e0}$ is the balanced value of the control deflection, and a is the velocity of sound. Summing, we obtain /4

$$M_z^V=\frac{bSQ_0V_0}{J_z}\left[m_{z_0}+m_z^\alpha\alpha_0+m_z^\delta\delta_0+\right.$$
$$\left.+\frac{V}{2a}\left\{(m_{z_0})^H+(m_z^\alpha)_{\alpha_0}^M+(m_z^\delta)_{\delta_0}^M\right\}\right],$$

where the sum of the first three terms expresses the balance condition and equals zero. We then determine

$$M_z^\alpha=\frac{m_z^\alpha bSQV^2}{2J_z},\quad M_z^\delta=\frac{m_z^\delta bSQV^2}{2J_z}.$$

It can also be shown that the partial derivative $\frac{\partial M_z}{\partial H}$ equals zero.

thus, the static moment-equilibrium equation is written

$$\frac{1}{a}\left[(m_{z_0})^M+(m_z^a)^M\alpha_0+(m_z^{\delta_e})^M\delta_{e_0}\right]u+m_z^a\alpha+m_z^{\delta_e}\delta_e=0.$$

Using the balance equation for the moments, we eliminate the variable α from system (2.39). We then have

$$\left.\begin{aligned}&\dot{u}=c_{11}^*u-c_{13}\theta-c_{14}^*h=a_{\delta_t}\delta_t+a_{\delta_e}\delta_e;\\&-c_{21}^*u+\dot{\theta}-c_{23}\theta-c_{24}^*h=z_{\delta_t}\delta_t+z_{\delta_e}\delta_e;\\&-c_{31}u-c_{33}\theta+h=0,\end{aligned}\right\}\qquad(2.40)$$

where

$$c_{11}^*=c_{11}-\frac{c_{41}c_{12}}{c_{42}},\quad c_{14}^*=c_{14}-\frac{c_{12}c_{44}}{c_{42}},\quad a_{\delta_e}=-\frac{c_{12}m_z^{\delta_e}}{c_{42}},$$

$$c_{21}^*=c_{21}-\frac{c_{22}c_{41}}{c_{42}},\quad c_{24}^*=c_{24}-\frac{c_{22}c_{44}}{c_{42}},\quad z_{\delta_e}^*=z_{\delta_e}-\frac{c_{22}m_z^{\delta_e}}{c_{42}}.$$

Depending on flight regime, the coefficients of system (2.40) are either constants or functions of time. The differential equation system (2.40) investigated in problems of stabilization of ASV altitude and speed has constant coefficients. For such flight conditions as programmed climbing, acceleration, and deceleration, we obtain an equation system with strongly variable coefficients, since the rates of change of the coefficients are comparable to the rates of change of the flight parameters. /48

As we noted above, the lateral motion of the ASV consists of a progressive motion of the center of mass along Oz and rotational motions around the axes Ox and Oy. This motion is described by the 3rd, 4th, and 5th equations of system (2.5). Let us write these equations in the body coordinate system, which is the most convenient in this case. We note beforehand that in virtue of the vehicle's symmetry about the xOy plane, the centrifugal moments $J_{xz}$ and $J_{yz}$ are small and can be excluded from the analysis. We have

$$\left.\begin{aligned}&m(\dot{V}_z+V_y\omega_{x_1}-V_x\omega_{y_1})=F_{z_1};\\&J_y\dot{\omega}_{y_1}+(J_x-J_z)\omega_{x_1}\omega_{z_1}-\\&\quad-J_{xy}(\dot{\omega}_{x_1}+\omega_{z_1}\omega_{y_1})=M_{y_1};\\&J_x\dot{\omega}_{x_1}+(J_z-J_y)\omega_{y_1}\omega_{z_1}-\\&\quad-J_{xy}(\dot{\omega}_{y_1}-\omega_{x_1}\omega_{z_1})=M_{x_1}.\end{aligned}\right\}\qquad(2.41)$$

We supplement the system with the relations

$$V_x = V\cos\beta\cos\alpha;$$
$$V_y = -V\cos\beta\sin\alpha; \quad \dot{\psi} = \frac{\omega_{y_1}\cos\gamma}{\cos\vartheta};$$
$$V_z = V\sin\beta; \quad \dot{\gamma} = \omega_{x_1} - \omega_{y_1}\cos\gamma\,\mathrm{tg}\,\vartheta.$$

Considering the actual ranges of variation of $\alpha$ and $\beta$, we replace the expressions for $V_x$, $V_y$, and $V_z$ by their approximate values

$$V_x \approx V; \quad V_y \approx -\alpha V; \quad V_z \approx \beta V.$$

From now on, the products of small quantities $\omega_x\omega_z$ and $\omega_y\omega_z$ can be neglected in accordance with the method of small perturbations used in linearization of the equations. In a number of cases, however, as in investigation of the influence of inertial cross couplings on the lateral motion, these terms can be taken into account by programming the variation of $(J_x - J_z)\omega_{z_1}$, $(J_z - J_y)\omega_{z_1}$, $J_{xy}\omega_{z_1}$ as time functions. Having made the substitutions indicated, we reduce Eqs. (2.41) to the form

$$\left.\begin{aligned}
&mV(\dot{\beta} - \alpha\omega_{z_1} - \omega_{y_1}) = F_{z_1};\\
&J_y\dot{\omega}_{y_1} - J_{xy}\dot{\omega}_{x_1} = M_{y_1};\\
&J_x\dot{\omega}_{x_1} - J_{xy}\dot{\omega}_{y_1} = M_{x_1};\\
&\dot{\psi} = \frac{\omega_{y_1}\cos\gamma}{\cos\vartheta};\\
&\dot{\gamma} = \omega_{x_1} - \omega_{y_1}\cos\gamma\,\mathrm{tg}\,\vartheta.
\end{aligned}\right\} \qquad (2.42)$$

The projection of the forces onto Oz is formed as follows:

$$F_{z_1} = c_z\frac{S_0V^2}{2} + c_\delta\frac{S_0V^2}{2} + G\cos\vartheta\sin\gamma,$$

where the first term is due to the presence of the angle of slip, the second to deflection of the controls, and the third to variation of the gravitational-force component. On the assumption that the initial roll equals zero ($\gamma_0 = 0$), the linear lateral-force increment is usually written

$$F_{\Delta z_1} = c_z^\beta\frac{S_0V^2}{2}\beta + c_z^\delta\frac{S_0V^2}{2}\delta + G\cos\vartheta_0\gamma.$$

As a rule, the moments are asigned in the semiattached body coordinate system. Then the projections of these moments in the lateral motion onto the body axes are written

$$M_{x_1}=M_x+M_y\sin\alpha\approx M_x+M_y\alpha;$$
$$M_{y_1}=M_y-M_x\sin\alpha\approx M_y-M_x\alpha.$$

Representing the deviations of the moments in the form of expansions in the increments of the variables $\beta$, $\omega_x$, $\omega_y$, $\delta$, we obtain

$$M_{x_1}=\frac{lS_0V^2}{2}\left(m_x^{\beta}\beta+m_x^{\delta_a}\delta_a+m_x^{\delta_r}\right)+$$
$$+\frac{l^2S_0V}{4}\left(m_x^{\bar{\omega}_x}\omega_{x_1}+m_x^{\bar{\omega}_y}\omega_{y_1}\right);$$
$$M_{y_1}=\frac{lS_0V^2}{2}\left(m_y^{\beta}\beta+m_y^{\delta_r}\delta_r+m_y^{\delta_a}\right)+$$
$$+\frac{l^2S_0V}{2}\left(m_y^{\bar{\omega}_y}\omega_{y_1}+m_y^{\dot{\beta}}\dot{\beta}+m_y^{\bar{\omega}_x}\omega_{x_1}\right),$$

/50

where the partial derivatives of the moment coefficients with respect to the variables of the motion $m_z^{\beta}$, ... have been converted to the body coordinate system and are functions of the Mach number and the angle of attack $\alpha$ (the "half-span" $l$ of the wing is taken as the arm), while the derivatives $m_x^{\bar{\omega}_x}$, $m_y^{\bar{\omega}_y}$, $m_x^{\bar{\omega}_y}$, $m_y^{\bar{\omega}_x}$ are reduced to dimensionless form according to

$$m_x^{\omega_x}=m_x^{\bar{\omega}_x}\frac{l}{2V},\quad m_y^{\omega_y}=m_y^{\bar{\omega}_y}\frac{l}{2V},\ \text{etc.}$$

Substituting the expressions for the forces and moments into Eqs. (2.42) and introducing the new nomenclature for the coefficients, we write system (2.42) in the form

$$\left.\begin{aligned}
&\dot{\beta}=\alpha_0\omega_{x_1}+\omega_{y_1}-z_{\beta}\beta+z_{\gamma}\gamma+z_{\delta_r}\delta_r;\\
&\dot{\omega}_{x_1}=\frac{J_{xy}}{J_x}\dot{\omega}_{y_1}+l_{\beta}^{*}\beta-l_{\omega_x}^{*}\omega_{x_1}+l_{\omega_y}^{*}\omega_{y_1}+l_{\delta_r}^{*}\delta_r+l_{\delta_a}\delta_a;\\
&\dot{\omega}_y=\frac{J_{xy}}{J_y}\dot{\omega}_{x_1}-n_{\beta}^{*}\beta-n_{\dot{\beta}}^{*}\dot{\beta}+n_{\omega_x}^{*}\omega_{x_1}-n_{\omega_y}^{*}\omega_{y_1}+\\
&\quad+n_{\delta_r}^{*}\delta_r+n\delta_a^{*}\delta_a;\\
&\psi=\frac{\omega_{y_1}}{\cos\vartheta_0};\\
&\dot{\gamma}=\omega_{x_1}-\omega_{y_1}\operatorname{tg}\vartheta,
\end{aligned}\right\}\qquad(2.43)$$

where

$$z_{\beta}=\frac{-C_z^{\beta}S_0V}{2m};\qquad z_{\gamma}=\frac{g}{V}\cos\vartheta_0;\qquad z_{\delta_r}=\frac{c_z^{\delta_r}S_0V}{2m};$$

$$l_\beta^* = \frac{m_x^\beta l S_Q V^2}{2J_x}; \qquad l_{\bar{\omega}_x}^* = \frac{m_x^{\bar{\omega}_x} l^2 S_Q V}{4J_x};$$

$$l_r^* = \frac{m_x^{\bar{\omega}_y} l^2 S_Q V}{4J_x}; \qquad l_{\delta_a}^* = \frac{m_x^{\delta_a} l S_Q V^2}{2J_x};$$

$$l_{\delta_r}^* = \frac{m_x^{\delta_r} l S_Q V}{2J_x}; \qquad n_\beta^* = \frac{-m_y^\beta l S_Q V^2}{2J_y};$$

$$n_{\bar{\omega}_y}^* = \frac{m_y^{\bar{\omega}_x} l^2 S_Q V}{4J_y}; \qquad n_r^* = \frac{-m_y^{\bar{\omega}_y} l^2 S_Q V}{4J_y};$$

$$n_{\delta_r}^* = \frac{m_y^{\delta_r} l S_Q V^2}{2J_y}; \qquad n_{\delta_a}^* = \frac{m_y^{\delta_a} l S_Q V^2}{2J_y}; \qquad n_{\dot{\beta}}^* = \frac{-m_y^{\dot{\beta}} l^2 S_Q V}{4J_y};$$

$\alpha_0, \vartheta_0$ are the programmed values of the parameters of the vehicle's longitudinal motion.

To convert to the Cauchy notation of the equations, we eliminate the terms $\frac{J_{xy}}{J_x}\dot{\omega}_{y_1}$ and $\frac{J_{xy}}{J_y}\dot{\omega}_{x_1}$ from the second and third equations of system (2.43) by substitution. As a result of the linearization of system (2.41), we have

$$\left.\begin{aligned}
&\dot{\beta} = \alpha_0\omega_{x_1} + \omega_{y_1} - z_\beta\beta + z_\gamma\gamma + z_{\delta_r}\delta_r;\\
&\dot{\omega}_{x_1} = l_\beta\beta - l_{\bar{\omega}_x}\omega_{x_1} + l_r\omega_{y_1} + l_{\delta_r}\delta_r + l_{\delta_a}\delta_a;\\
&\dot{\omega}_{y_1} = -n_\beta\beta - n_{\dot{\beta}}\dot{\beta} + n_\gamma\omega_{x_1} - n_r\omega_{y_1} + n_{\delta_r}\delta_r +\\
&\quad + n_{\delta_a}\delta_a;\\
&\dot{\gamma} = \omega_{x_1} - \omega_{y_1}\operatorname{tg}\vartheta_0; \quad \dot{\psi} = \frac{\omega_{y_1}}{\cos\vartheta_0}.
\end{aligned}\right\} \qquad (2.44)$$

The procedure for obtaining the coefficients of Eqs. (2.44) is obvious and requires no explanation.

Thus, we have arrived at a system of linear differential equations with variable coefficients whose law of variation is determined by the nature of the vehicle's motion in the longitudinal plane. These equations are usually used to investigate the stabilization of airplane-configurated vehicles, since such vechicles are characterized by strong reciprocal effects between yawing (rotation around $Oy_1$) and rolling (rotation around $Ox_1$) motions and, strictly speaking, one motion cannot be separated from the other).

However, these reciprocal effects are small for axisymmetric ASV's, and the separation into yawing and rolling motions is legitimate. In addition, a similar division is often used for airplane-configurated vehicles in preliminary studies of their characteristics, with subsequent conversion back to the more complete equations.

Bearing these remarks in mind, we proceed with further simplification of the mathematical model of the ASV. We shall assume initially that the angle of pitch $\vartheta$ and the angle of attack $\alpha$ are small and that the centrifugal moment of inertia $J_{xy} = 0$. Discarding the products of small quantities, e.g., $\omega_{y1} \tan \vartheta$, we arrive at the following equation system: /52

$$\left.\begin{aligned}
\dot{\beta} &= +\omega_{y_1} - z_\beta \beta + \frac{g}{V}\gamma + z_{\delta_r}\delta_r;\\
\dot{\omega}_{y_1} &= -n_\beta \beta - n_{\dot\beta}\dot\beta + n_\gamma \omega_{x_1} - n_r \omega_{y_1} + n_{\delta_r}\delta_r + \\
&\quad + n_{\delta_a}\delta_a;\\
\dot{\omega}_{x_1} &= l_\beta \beta - l_{\dot\gamma}\omega_{x_1} + l_r \omega_{y_1} + l_{\delta_r}\delta_r + l_{\delta_a}\delta_a;\\
\dot{\gamma} &= \omega_{x_1},\\
\dot{\psi} &= \omega_{y_1}.
\end{aligned}\right\} \qquad (2.45)$$

As in the case of the longitudinal channel, the lateral motion can, with certain assumptions, also be broken up into separate components: yawing motion, rolling motion, and spiral motion. We obtain the characteristics of the first two motions by assuming straight-line plane motion of the vehicle in which it describes oscillations about the velocity vector, whose rotation is not taken into account. This assumption is based on consideration of the large inertia of center-of-mass motion under the action of lateral forces. In this case, the first equation of system (2.45) is excluded from consideration. Applying the relations $\psi \approx \beta$ and $\omega_{y_1} \approx \dot\psi$, which are valid for this motion, we rewrite the equations in the form

$$\left.\begin{aligned}
\ddot{\psi} + n_{\dot\psi}\dot\psi + n_\beta \psi &= n_\gamma \omega_{x_1} + n_{\delta_r}\delta_r + n_{\delta_a}\delta_a;\\
\dot{\omega}_{x_1} + l_{\dot\gamma}\omega_{x_1} &= l_\beta \psi + l_r \dot\psi + l_{\delta_a}\delta_a + l_{\delta_r}\delta_r;\\
\dot{\gamma} &= \omega_{x_1},
\end{aligned}\right\} \qquad (2.46)$$

where $n_{\dot\psi} = n_{\dot\beta} + n_r$.

This equation system is used when there is a strong cross-coupling between the roll and yaw channels via the coefficients $n_y$ and $l_r$. Further simplication is possible only after prelim- /53

inary studies of the solutions of this system. For axisymmetric ASV's, for which the coefficients $n_y$ and $l_r$ are small, and for airplane-configurated vehicles with roll stabilization, the equations can be further separated by channels:

$$\left.\begin{aligned} &\ddot{\psi}-n_{\dot{\psi}}\dot{\psi}-n_{\psi}\psi=n_{\delta_r}\delta_r;\\ &\dot{\omega}_x-l_{\omega_{x_1}}\omega_{x_1}=l_{\delta_a}\delta_a;\\ &\dot{\gamma}=\omega_{x_1}. \end{aligned}\right\} \qquad (2.47)$$

The first equation of (2.47) describes the yawing motion and serves for determination of the basic characteristics of the vehicle's response to both control and disturbance inputs. The second equation describes the isolated motion in roll and is used for the same purpose as the first.

The spiral motion is a slow motion with a large time constant. A small spiral instability is permitted most ASV's so that it will be possible to obtain the desired values of more important flight-performance parameters, such as the relative damping factor for yawing motion. Spiral instability is not usually regarded as an undesirable effect because (owing to the slowness of the motion) it can easily be eliminated by the pilot or by the control system. In the absence of control, the angles of yaw and roll increase and the airplane gradually builds up a motion with high velocity along a descending spiral.

The characteristics of the spiral motion can be obtained from Eqs. (2.45) by considering rolling motion without slip and without consideration of the yawing moment:

$$\left.\begin{aligned} &\dot{\omega}_y=-\frac{g}{V}\gamma;\\ &\dot{\omega}_{x_1}=l_{\omega_{x_1}}\omega_{x_1}+l_{\omega_{y_1}}+l_{\delta_a}\delta_a; \end{aligned}\right\} \qquad (2.48)$$

or

$$\ddot{\gamma}=l_{\omega_{x_1}}\dot{\gamma}_x-\frac{g}{V}l_{\gamma}\gamma+l_{\delta_a}\delta_a. \qquad (2.49)$$

Often, in an analogy with the short-period motion in the longitudinal plane, yawing motion is studied with consideration of the equation of the lateral forces on the Oz axis. Applying the relations $\Psi_V \approx \phi - \beta$, $\dot{\Psi} \approx \dot{\psi} - \dot{\beta}$, and $\omega_y \approx \dot{\psi}_7$, we obtain from the first two equations of system (2.45) /5

$$\left.\begin{aligned} &\dot{\Psi}+z_{\beta}\Psi=-z_{\beta}\psi-z_{\delta_r}\delta_r;\\ &\ddot{\psi}+n_{\dot{\psi}}\dot{\psi}+n_{\beta}\psi=+n_{\beta}\Psi+n_{\dot{\beta}}\dot{\Psi}+n_{\delta_r}\delta_r. \end{aligned}\right\} \qquad (2.50)$$

This separation of the vehicle's motion by channels usually makes it possible to establish the vehicle's basic dynamic properties. For rockets with aerodynamic controls and for a number of airplane flight modes, however, this simplification may lead to substantial errors in estimates of the vehicle's local stability. In these cases, it becomes necessary to take account of cross-coupling between the individual forms of motion without greatly complicating the mathematical model of the vehicle.

As we know [7, 22], the relation between the longitudinal and lateral motion is mediated by the aerodynamic, kinematic, and inertial interactions, and by the gyroscopic moment of the engine, and the terms of the equations that describe these couplings are nonlinear. The aerodynamic effect is taken into account with longitudinal aerodynamic-force and moment coefficients of the second and higher orders, e.g., $m_x^{\alpha\beta}$, $m_x^{\alpha^2\beta}$, $m_x^{\alpha\omega_y}$, $m_y^{\alpha^2\delta}$, $m_y^{\alpha\omega_x}$, $c_z^{\gamma\beta}$, etc.

By kinematic interaction, we refer to the simultaneous change in the angles of attack and slip when the vehicle is thrown sharply into a roll. This interaction is taken into account in the equations of motion through the terms $\alpha\omega_x$ and $\beta\omega_x$, and strongly influences the dynamics of the motion in flight at large angles of attack and slip. We shall henceforth discuss only these two types of interaction as being the most important ones. It is known from practice [16, 19] that the dynamics of the vehicle's motion are subject to the widest variations in the roll channel (equation of moments about the longitudinal axis of the vehicle).

For airplane-configurated vehicles with a single plane of vertical symmetry, the nature of the longitudinal motion is generally rather insensitive to changes in the steady angle of attack (in the range of subcritical angles of attack). Further, when we recognize that the angles of slip are small in most flight modes (except when complicated three-dimensional maneuvers are being executed), we may neglect the influence of lateral motion on the latter. The simplified equations of lateral motion can therefore be written as follows with consideration of a number of aerodynamic and inertial interactions: /55

$$\left.\begin{aligned}
\dot{\beta} &= -z_\beta(\alpha)\beta + \omega_y + \alpha\omega_x - z_{\delta_\gamma}\delta_\gamma;\\
\dot{\omega}_y &= -n_\beta\beta - n_r\omega_y - n_\gamma(\alpha)\omega_x - n_{\delta_\gamma}\delta_\gamma;\\
\dot{\omega}_x &= -l_\beta(\alpha, \delta_\Sigma)\beta - l_r(\alpha)\omega_y - l_\gamma\omega_x - l_{\delta_\Sigma}\delta_\Sigma - l_{\delta_\gamma}(\alpha)\delta_\gamma.
\end{aligned}\right\} \qquad (2.51)$$

Several coefficients of this system are nonlinear functions of the longitudinal-motion parameters and reflect the change in the conditions of flow past the aerodynamic surfaces on variation of $\alpha$ and $\delta_e$. One of the possible simplified methods of investigating lateral-motion dynamics consists in "freezing" the angle of attack at various levels and using equation system (2.51) as a basis for determining a series of transfer functions with coefficients that depend on the parameters $\alpha_0$ and $\delta_{e_0}$. Assigning various values to $\alpha_0$ and $\delta_{e_0}$, we can use the method of small perturbations to take account of the effects of the longitudinal channels on lateral-motion dynamics.

For rockets with axisymmetric wing designs, the longitudinal and lateral planes of the motion are equivalent in regard to the development of normal forces, i.e., the angles of attack and slip have identical ranges of variation. A normal force can be developed in any direction by assigning specific combinations of angles $\alpha$ and $\beta$. In this case, the additional moment that arises around the vehicle's longitudinal axis due to the "crossflow" effect can be taken into account with sufficient accuracy by the relation [22]

$$\overline{L_x^{cf}} = m_1 \alpha\beta(\beta^2 - \alpha^2) + m_2(\alpha\delta_a - \beta\delta_a), \tag{2.52}$$

where $m_1$ and $m_2$ are constants.

Considering the aerodynamic symmetry of the rockets and the most significant couplings, we write the equations of three-dimensional motion in the form

$$\left.\begin{aligned}
\dot{\alpha} &= -z_\alpha\alpha + \omega_z - \beta\omega_x;\\
\dot{\omega}_z &= -n_\alpha\alpha - n_{\dot{\alpha}}\omega_z - n_{\delta_e}\delta_e;\\
\dot{\beta} &= -z_\beta\beta + \omega_y + \alpha\omega_x;\\
\dot{\omega}_y &= -n_\beta\beta - n_{\dot{\beta}}\omega_y - n_{\delta_r}\delta_r;\\
\dot{\omega}_x &= -l_{\omega_x}\omega_x - l_{\delta_a}\delta_a - L_x^{k_0}.
\end{aligned}\right\} \tag{2.53}$$

/56

Preliminary investigation of system-stability problems requires conversion to a linear model by the method of small perturbations. It is generally necessary to carry out the analysis for various combinations of angles of attack and slip and control-surface deflections.

We shall consider the most typical operational flight modes, from which inferences may be drawn as to the nature of the three-dimensional motion as a whole:

a) longitudinal channel with "frozen" lateral channel ($\beta_0 = \delta_{r_0} = 0$);

b) lateral channel with "frozen" longitudinal channel ($\alpha_0 = \delta_{e_0} = 0$);

c) $\alpha_0 = \beta_0$ and $\delta_{e_0} = \delta_{r_0}$.

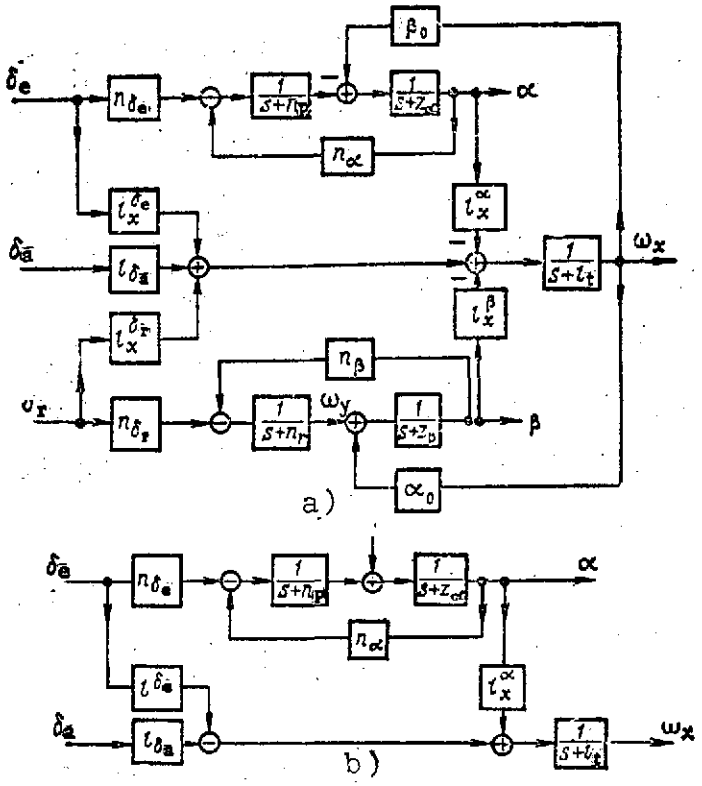


Figure 2.5. Structural Diagrams of Vehicle With Consideration of Cross Coupling Between Channels Due to Large Angles of Attack and Slip.

In these cases, the static value of the moment $L_x^{cf}$ equals zero. Applying increments to the variables $\alpha$, $\beta$, $\omega_x$, $\omega_y$, $\delta_e$, $\delta_r$, and $\delta_a$ and following the usual procedure for linearization of equations, we obtain the system

$$\begin{aligned}
\dot{\alpha} &= -z_\alpha\alpha + \omega_z - \beta_0\omega_x; & \dot{\beta} &= -z_\beta\beta + \omega_y + \alpha_0\omega_x;\\
\dot{\omega}_z &= -n_\alpha\alpha - n_r\omega_z - n_{\delta_e}\delta_e; & \dot{\omega}_y &= -n_\beta\beta - n_r\omega_y - n_{\delta_r}\delta_r;\\
& & \dot{\omega}_x &= -l_t\omega_x - l_{\delta_a}\delta_a - l_x^\alpha\alpha - l_x^\beta\beta - l_x^{\delta_e}\delta_e - l_x^{\delta_r}\delta_r,
\end{aligned} \tag{2.54}$$

where

$$l_x^{\alpha} = m_1\beta_0(\beta_0^2 - 3\alpha_0^2) + m_2\delta_{z_0};$$

$$l_x^{\beta} = m_1\alpha_0(3\beta_0^2 - \alpha_0^2) - m_2\delta_{e_0};$$

$$l_x^{\dot{\alpha}} = m_2\alpha_0; \qquad /57$$

$$l_x^{\dot{\beta}} = -m_2\beta_0.$$

(the increment symbol before the variables is omitted for brevity).

Figure 2.5, a and b, presents structural diagrams of the equation system (2.54) for the basic operating modes after Laplace transformation with zero initial conditions (see Sec. 2.4). Thus, using equation system (2.54), we can obtain various transfer functions with consideration of cross-couplings between channels for use in study of the closed-loop control systems. /5
Other approaches to evaluation of the effects of cross-coupling on the dynamics of vehicle motion are also possible within the framework of the linear theory. For example, conversion to cylindrical coordinates is recommended in [22], since their use makes it possible in many cases to take account of the basic couplings in the vehicle's three-dimensional motion in quite simple form ("crossflow" and kinematic and inertial couplings).

Let us turn to linearization of the equations of motion for ballistic missiles and rocket boosters. As we noted in Sec. 2.2, the Coriolis force and moment $F_C$ and $M_C$ and the force and moment that arise as a result of the mobility of the liquid in tanks, $F_l$ and $M_l$ must be introduced into the dynamic equations of an ASV regarded as a rigid body (2.5). In addition, Eqs. (2.18) for the generalized coordinates $q_\nu$ and $p_\nu$, which characterize the position of the free surface in the $\nu$-th tank, must be attached to system (2.5).

Everything that has been said concerning separation of the vehicle's motion into lateral and longitudinal motion and of the latter, in turn, into long-period and short-period motions, also applies in the case of ballistic missiles.

Using the procedure for obtaining the linearized equations (2.36) for a rigid vehicle, we obtain a system of linearized equations of short-period motion for ballistic missiles and rocket boosters in the following form:

$$mV_{\Delta}\dot{\theta} = F_y^{\alpha}\Delta\alpha + F_y^{\theta}\Delta\theta + F_y^{\delta}\delta + F_{ky}^{\omega_z}\Delta\dot{\theta} - \sum_{\nu=1}^{N}\tilde{R}_{\nu y}\ddot{q}_{\nu}; \qquad (2.55)$$

$$
\begin{aligned}
&J_z\Delta\ddot{\vartheta}=M_z^{\alpha}\Delta\alpha+M_z^{\dot{\alpha}}\Delta\dot{\alpha}+M_z^{\delta_e}\delta_e+M_z^{\omega_z}\Delta\dot{\vartheta}-\\
&\quad-\sum_{\nu=1}^{N}\tilde{R}_{\nu\vartheta}^{\cdot\cdot}\ddot{q}_\nu-\sum_{\nu=1}^{N}\tilde{R}_{\nu y}q_\nu;\\
&\ddot{q}_\nu+\varepsilon_\nu\dot{q}_\nu+\Omega_\nu^2q_\nu=R_{\nu y}V\Delta\dot{\vartheta}+R_{\nu\dot{\vartheta}}\Delta\ddot{\vartheta}-\\
&\quad-R_{\nu\vartheta}\Delta\vartheta.
\end{aligned}
\tag{2.55}
$$

From this system, we exclude the angle $\theta$; neglecting the small quantity $F_{k_y}^{\omega_z}\Delta\dot{\vartheta}$ and omitting the symbol $\Delta$ for simplicity of notation and using the nomenclature presented previously, we obtain a system analogous to (2.38) in the form /59

$$
\left.
\begin{aligned}
&\dot{\alpha}+z_\alpha\alpha-\omega_z+\sum_{\nu=1}^{N}\tilde{R}'_{\nu y}\ddot{q}_\nu=-z_{\delta_e}\delta_e;\\
&\dot{\omega}_z+n_{\dot{\alpha}}\dot{\alpha}+n_\alpha\alpha+\sum_{\nu=1}^{N}\tilde{R}'_{\nu\dot{\vartheta}}\ddot{q}_\nu=n_{\delta_e}\delta_e;\\
&\ddot{q}_\nu+\varepsilon_\nu\dot{q}_\nu+\Omega_\nu^2q_\nu=-R_{\nu y}V_x\dot{\alpha}+(R_{\nu\dot{\vartheta}}+R_{\nu y}V_x)\dot{\omega}_z-\\
&\quad-R_{\nu y}(\dot{V}_{0x}-g_x)\vartheta.
\end{aligned}
\right\}
\tag{2.56}
$$

As we noted above, the lateral motion is described in the case of axisymmetric vehicles by a system consisting of two independent equation systems — in the yaw plane by a system analogous to (2.45), i.e.,

$$
\left.
\begin{aligned}
&\dot{\beta}-\omega_{y_1}-z_\beta\beta+\sum_{\nu=1}^{N}\tilde{R}'_{\nu z}\ddot{q}_\nu=z_{\delta_r}\delta_r;\\
&\dot{\omega}_{y_1}+n_{\dot{\beta}}\dot{\beta}+n_\beta\beta+n_r\omega_{y_1}+\sum_{\nu=1}^{N}R'_{\nu\dot{\psi}}\ddot{q}_\nu=n_{\delta_r}\delta_r;\\
&\ddot{q}_\nu+\varepsilon_\nu\dot{q}_\nu+\Omega_\nu^2q_\nu=-R_{\nu z}V_{x\beta}+R_{\nu\dot{\psi}}\dot{\omega}_{y_1}-\\
&\quad-R_{\nu z}(\dot{V}_{0x}-g_x)\psi,
\end{aligned}
\right\}
\tag{2.57}
$$

where $\dot{\psi}=\omega_{y_1}$

and a system describing the motion in roll:

$$\left.\begin{aligned}\dot{\omega}_{x_1}+\sum_{\nu=1}^{N}\tilde{R}'_{\nu\bar{1}}\ddot{p}_\nu&=l_{\delta_a}\delta_a;\\ \ddot{p}_\nu+\mu_\nu\dot{p}_\nu+\Omega_\nu^2 p_\nu&=R_{\nu\bar{1}}\omega_{x_1}.\end{aligned}\right\}\qquad(2.58)$$

## 2.4. TRANSFER FUNCTIONS OF THE AEROSPACE VEHICLE AS A STATIONARY OBJECT OF CONTROL

/6

### 2.4.A. Comparison of Solutions of Stationary and Nonstationary Equations. The Principle of "Frozen" Coefficients

In the general case, the solutions of the stationary and nonstationary equations can be compared, because of the complexity of the latter, only with digital computers. We shall therefore confine ourselves to a partial analysis with reference to the case of the rather simple second-order equations to which, as we noted above, the angular motion of the vehicle and certain other dynamic relations in the longitudinal motion can be reduced.

Let the second-order differential equation be written in the form

$$T\ddot{y}+2\eta T\dot{y}+(\eta^2+\omega^2)Ty(t)=x(t)\qquad(2.59)$$

and let it reflect, for example, the equation of angular motion of a vehicle in which y is the angular coordinate and x = M is the disturbance moment. If the coefficients of Eq. (2.59) are independent of time, i.e., constant, the equation is said to be stationary. When a unit-pulse disturbance is applied at the input of the system described by Eq. (2.59) at time $t_0$, i.e.,

$$x=\delta[t-t_0],\qquad(2.60)$$

it triggers a response known as the stationary weighting function

$$y=g[t-t_0].\qquad(2.61)$$

It is convenient to introduce the biased argument $\tau = t-t_0$ with the origin at $t = t_0$ as the time reference, since then the stationary weighting function $g(\tau)$ will be a solution of the equation

$$\ddot{g}(\tau)+2\eta\dot{g}(\tau)+(\eta^2+\omega^2)g(\tau)=\frac{1}{T}\delta[\tau].\qquad(2.62)$$

This solution is easily obtained by known methods in the form

$$g[\tau]=\frac{1}{\omega T}e^{-\eta\tau}\sin\omega\tau. \qquad (2.63)$$ /61

In a somewhat different notation for the coefficients of Eq. (2.62), namely:

$$T\ddot{g}(\tau)+2(1+\sigma T)\dot{g}(\tau)+[(\sigma^2+\Omega^2)T+2\sigma]g(\tau)=\delta[\tau], \qquad (2.64)$$

where

$$\eta=\frac{1}{T}+\sigma; \qquad (2.65)$$

$$\omega=\frac{1}{T}\sqrt{\Omega^2T^2-1} \qquad (2.66)$$

the notation for the solution is modified accordingly:

$$g[\tau]=\frac{1}{\sqrt{\Omega^2T^2-1}}e^{-\left(\frac{1}{T}+\sigma\right)\tau}\sin\frac{\tau}{T}\sqrt{\Omega^2T^2-1}, \qquad (2.67)$$

but it remains stationary because it depends only on the one biased argument $\tau$ and does not depend on the time $t_0$ of pulsing.

Let us now compare the stationary weighting function $g[\tau)$ written in the form of Eqs. (2.63) or (2.67) with a nonstationary weighting function of the form

$$g[\tau,t_0)=\frac{e^{-\sigma\tau}}{\Omega(t_0+\tau)}\sin\Omega\tau. \qquad (2.68)$$

Here the criterion of nonstationarity is the dependence on two arguments – $\tau$ and $t_0$.

Let us establish the form of the differential equation whose solution for a unit input pulse will be the nonstationary weighting function (2.68). For this purpose, we rewrite (2.68) in the form

$$(t_0+\tau)g=\frac{1}{\Omega}e^{-\sigma\tau}\sin\Omega\tau, \qquad (2.69)$$

differentiate once with respect to $\tau$:

$$g+(t_0+\tau)\dot{g}=-\sigma(t_0+\tau)g+e^{-\sigma\tau}\cos\Omega\tau \qquad (2.70)$$

and differentiate again:

$$(t_0+\tau)\ddot{g}+2\dot{g}=-\sigma[g+(t_0+\tau)\dot{g}]-\sigma g-\sigma e^{-\sigma\tau}\cos\Omega\tau+\delta[\tau]. \qquad (2.71)$$ /62

The pulse appeared in the right member of Eq. (2.71) on differentiation of the function $f[\tau]=e^{-\sigma\tau}\cos\Omega\tau$, which equals zero when $\tau < 0$ and has a unit jump at $\tau = 0$. Let us express $f(\tau)$ as a funtion of the other terms in (2.70) and substitute it into (2.71). We then obtain

$$(t_0+\tau)\ddot{g}+2[1+\sigma(t_0+\tau)]\dot{g}+[(\sigma^2+\Omega^2)(t_0+\tau)+2\sigma]g=\delta[\tau]. \qquad (2.72)$$

This equation has variable coefficients that depend on the time $t_0 + \tau = t$, and is therefore said to be nonstationary.

Its solution (2.68) was used to write the equations, but the converse problem, with which it is generally necessary to deal, is immeasurably more complex. Recourse is therefore taken to approximate solution of the nonstationary equation on relatively short intervals of variation of the biased agreement $\tau$, substituting the equivalent stationary equation for it. One of the most common substitutions consists in "freezing" of the variable coefficients, i.e., fixing their values at the beginning of the interval at $\tau = 0$ and extending these values over the entire interval from $\tau = 0$ to $\tau = \tau_{max}$.

Applied to the nonstationary equation (2.72), the stationary equivalent will take the form

$$t_0\ddot{g}_э[\tau]+2(1+\sigma t_0)\dot{g}_э[\tau]+[(\sigma^2+\Omega^2)t_0+2\sigma]g_э[\tau]=\delta[\tau]. \qquad (2.73)$$

The analogous equation (2.64) has already been prepared, so that its solution (2.65) can be used as the answer in finding the pulse response of the equivalent system given by Eq. (2.73):

$$g_э[\tau]=\frac{1}{\sqrt{\Omega^2t_0^2-1}}e^{-\left(\frac{1}{t_0}+\sigma\right)\tau}\sin\frac{\tau}{t_0}\sqrt{\Omega^2t_0^2-1}. \qquad (2.74)$$

Let us now compare the exact and equivalent solutions described by (2.68) and (2.74).

Initial values

$$g[0,t_0)=\frac{1}{\Omega t_0};\ g_э[0]=\frac{1}{\sqrt{\Omega^2t_0^2-1}}=$$

$$=g[0,t_0)\cdot\frac{1}{\sqrt{1-\left(\frac{1}{\Omega t_0}\right)^2}};$$

Characteristic frequencies

$$\Omega;\quad \frac{1}{t_0}\sqrt{\Omega^2t_0^2-1}=\Omega\sqrt{1-\left(\frac{1}{\Omega t_0}\right)^2};$$

Damping conditions

/63

$$e^{-\sigma\tau}\frac{1}{t_0+\tau}\ ;\quad \frac{e^{-\left(\sigma+\frac{1}{t_0}\right)\tau}}{t_0}=\frac{e^{-\sigma\tau}}{t_0}\,e^{-\frac{\tau}{t_0}}. \tag{2.75}$$

We see from the comparison that the initial values and the frequencies move closer together at values of the product $\Omega t_0$ that are sufficiently large compared to unity. The damping conditions are described by functions that have the fundamentally different cofactors $\frac{1}{t_0+\tau}$ and $\frac{1}{t}e^{-\frac{\tau}{t_0}}$, but the additional damping introduced by the varying denominator in the solution of the nonstationary equation is offset to some degree by the increase in the damping decrement in the stationary equivalent, as can be seen on expansion of the two solutions in series:

$$\frac{1}{t_0+\tau}=\frac{1}{t_0}-\frac{\tau}{t_0^2}+\frac{\tau^2}{t_0^3}-\frac{\tau^3}{t_0^4}+\ldots;$$

$$\frac{1}{t_0}e^{-\frac{\tau}{t_0}}=\frac{1}{t_0}-\frac{\tau}{t_0^2}+\frac{\tau^2}{2!\,t_0^3}-\frac{\tau^3}{3!\,t_0^4}+\ldots,$$

with attention to the first terms.

The convergence of the nonstationary and equivalent stationary weighting functions also ensures similarity of other response forms, since the weighting function serves as the kernel in the equation of convolution with any input disturbance.

Thus, a harmonic disturbance causes a response whose steady part is proportional to the frequency response and an important index to the dynamic properties of the vehicle, including its stability. /64

If the variable parameters change only slightly during one (or a few) oscillations, it is admissible to substitute the stationary equivalent for the nonstationary object. With time, however, an increment that must be taken into account may accumulate, even if the parameter variation is slow. In this case, several stationary frequency responses must be asigned for the nonstationary object, each of them equivalent on a certain time interval. In more general description of stationary systems with the aid of transfer functions – just as in the case of the frequency-response curves – equivalence to the nonstationary object with a given tolerance can be obtained only on a limited time interval. If the tolerance is exceeded, it is necessary to assign several transfer functions – each for a definite time interval.

## 2.4.B. Conversion to Transfer Functions

Transfer functions can serve as exhaustive characteristics of an aerospace vehicle as an object of control if the principle of linearization of the initial equations and conversion from the nonstationary system to the stationary equivalent are possible. These conditions are valid for the angular motion of the vehicle. Let us consider the angular motion in the form given by (2.59), but endow the input and output coordinates with more general connotations. Let the disturbance be given by an original function; then the response of the previously undisturbed system would also be an original function, and they can be written as the respective Laplace transforms:

$$x[t]=M[t]\doteq X(s); \tag{2.76}$$

$$y[t]=\psi[t]\doteq Y(s). \tag{2.77}$$

For the above transforms, Eq. (2.59) becomes the operator equation

$$(a_2s^2+a_1s+a_0)Y(s)=X(s), \tag{2.78}$$

whence the solution is to be sought in operator form /65

$$Y(s)=W(s)X(s), \tag{2.79}$$

where the transfer function is

$$W(s)=\frac{1}{a_2s^2+a_1s+a_0}. \tag{2.80}$$

It will be more convenient to write it in the standard form used for the linear elements of automatic control systems. Here we can convert from the transfer function in the notation of (2.80) to one or two different types of elements, depending on the signs and relative magnitudes of the coefficients $a_0$, $a_1$, and $a_2$, which determine the nature of the transfer-function poles.

If all coefficients $a_i$ (i = 0, 1, 2) are positive and

$$\frac{a_1}{2\sqrt{a_0}}<1,$$

the transfer function has complex conjugate poles and corresponds to the standard oscillatory element

$$W(s)=\frac{k}{T^2s^2+2\xi Ts+1}, \tag{2.81}$$

where $k=\frac{1}{a_0}$ is the gain (transfer constant) of the element,

$T=\sqrt{\frac{a_2}{a_0}}$ is a relative time constant, and $\xi=\frac{a_1}{2\sqrt{a_0}}<1$ is the relative damping factor. The poles of transfer function (2.81) can be stated in terms of the coefficients introduced above:

$$\beta_1=\beta=-\frac{\xi}{T}+j\frac{\sqrt{1-\xi^2}}{T};\ \beta_2=\beta^*=-\frac{\xi}{T}-j\frac{\sqrt{1-\xi^2}}{T}. \qquad (2.82)$$

When $\xi > 1$, the function (2.81) will have two real poles:

/66

$$\left.\begin{aligned}\beta_1&=\frac{-a_1+\sqrt{a_1^2-4a_0a_2}}{2a_2}=\frac{-\xi+\sqrt{\xi^2-1}}{T};\\ \beta_2&=\frac{-a_1-\sqrt{a_1^2-4a_0a_2}}{2a_2}=\frac{-\xi-\sqrt{\xi^2-1}}{T}\end{aligned}\right\} \qquad (2.83)$$

and can be written in one of the following forms:

$$W(s)=\frac{k/T^2}{\left(s+\frac{\xi}{T}-\frac{\sqrt{\xi^2-1}}{T}\right)\left(s+\frac{\xi}{T}+\frac{\sqrt{\xi^2-1}}{T}\right)}=\frac{k}{T^2(s-\beta_1)(s-\beta_2)}; \qquad (2.84)$$

$$W(s)=\frac{\frac{k}{2T\sqrt{\xi^2-1}}}{s+\frac{\xi-\sqrt{\xi^2-1}}{T}}-\frac{\frac{k}{2T\sqrt{\xi^2-1}}}{s+\frac{\xi+\sqrt{\xi^2-1}}{T}}. \qquad (2.85)$$

The first form (2.84) corresponds to cascaded (series) connection of two aperiodic elements; the second form (2.85) represents the equivalent parallel connection of two aperiodic elements having the time constants

$$T_1=\frac{T}{\xi+\sqrt{\xi^2-1}} \text{ and } T_2=\frac{T}{\xi-\sqrt{\xi^2-1}}$$

and the gains

$$k_1=\frac{k}{2\left[\xi\sqrt{\xi^2-1}-(\xi^2-1)\right]},$$

$$k_2=\frac{k}{2\left[\xi\sqrt{\xi^2-1}+(\xi^2-1)\right]}.$$

With the above nomenclature, Fig. 2.6, a-c, shows various

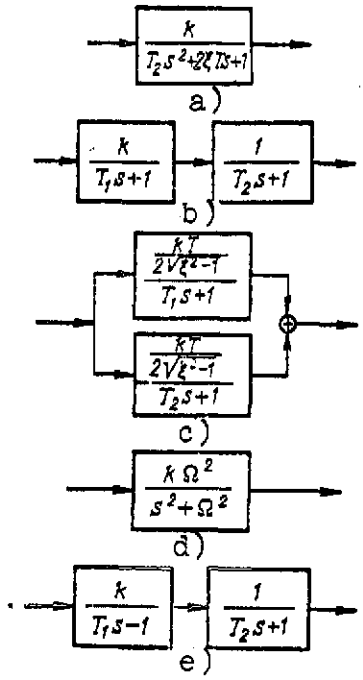


Figure 2.6. Transfer Function of Vehicle's Angular-Motion Loop Represented as Combinations of Standard Elements. a) Oscillatory element; b) two aperiodic elements in series; c) same in parallel; d) conservative element; e) stable and unstable aperiodic elements in series.

structural diagrams for a vehicle in angular motion in accordance with (2.81), (2.84), and (2.85). Different values of the relative damping factor correspond to changes in the aerodynamic configuration of the vehicle and flight conditions. At high flight speeds in dense layers of the atmosphere, the dynamics of a vehicle with developed tail surfaces in the yaw and pitch channels is described by the transfer function of two aperiodic elements (2.84) or (2.85), i.e., the condition $\xi > 1$ is satisfied. In the rarefied atmosphere at greater heights, the damping factor decreases and the vehicle in angular motion at $\xi < 1$ is described by the transfer function of an oscillatory element (2.81). Under the conditions of flight in space, or in the atmosphere when the vehicle has weakly developed tail planes, there is practically no damping ($\xi = 0$). The dynamics of the vehicle's motion is then described by a transfer function of the conservative-element type:

/67 /68

$$W(s)=\frac{k}{T^2s^2+1}=\frac{k\Omega^2}{s^2+\Omega^2}, \qquad (2.86)$$

where $\Omega = 1/T$ is the natural frequency of the undamped oscillations in the angular motion of the vehicle (see Fig. 2.6d).

If the aerodynamic layout of the vehicle places the center of pressure forward of the center of mass, as is characteristic for designs with vestigial tail planes, the coefficient $a_0$ in Eq. (2.78) becomes negative and the transfer function assumes the form

$$W(s)=\frac{1}{a_2s^2+a_1s-a_0}=\frac{k}{T^2s^2+2\xi Ts-1}. \qquad (2.87)$$

Then one of the transfer-function poles

$$\left.\begin{aligned}\beta_1&=\frac{-\xi+\sqrt{\xi^2+1}}{T};\\ \beta_2&=\frac{-\xi-\sqrt{\xi^2+1}}{T}\end{aligned}\right\} \qquad (2.88)$$

(the first one) is positive, so that the transfer function can be represented in the form of the product of transfer functions of stable and unstable aperiodic elements:

/69

$$W(s)=\frac{\frac{k}{T^2}}{\left(s+\frac{\xi+\sqrt{\xi^2+1}}{T}\right)\left(s-\frac{\sqrt{\xi^2+1}-\xi}{T}\right)} \qquad (2.89)$$

or in the form of the algebraic sum of the transfer functions of the same elements with appropriate gains:

$$W(s)=\frac{\frac{k}{2T\sqrt{\xi^2+1}}}{s+\frac{\xi+\sqrt{\xi^2+1}}{T}}-\frac{\frac{k}{2T\sqrt{\xi^2+1}}}{s-\frac{\sqrt{\xi^2+1}-\xi}{T}}. \qquad (2.90)$$

Figure 2.6e shows a cascaded combination of the two elements whose transfer functions appear in (2.89). The conversion to the parallel scheme can be made by analogy with the schemes shown in Fig. 2.6, b and c.

## 2.5. TRANSFER FUNCTIONS AND STRUCTURAL DIAGRAMS OF AEROSPACE VEHICLES

Here we shall examine more complete structural diagrams of various classes of aerospace vehicles, using the "frozen coefficient" principle and the Laplace transform. We apply the Laplace transformation to the linearized equations (2.38), which describe the longitudinal motion of a winged vehicle, so that we obtain the structural diagram of Fig. 2.7a). We determine the transfer functions with the aid of structural transformations of this diagram [25, 26], combining several elements into generalized elements (Fig. 2.7b), from which we obtain

$$\left.\begin{aligned}W^{\omega_{z_1}}_{\delta_e}&=\frac{\omega_{z_1}(s)}{\delta_e(s)}=\frac{k_1(T_1s+1)}{T_2^2s^2+2\xi_2T_2s+1};\\ W^{\alpha}_{\omega_{z_1}}&=\frac{\alpha(s)}{\omega_{z_1}(s)}=\frac{k_3(T_3s+1)}{T_1s+1},\end{aligned}\right\} \qquad (2.91)$$

where

$$k_1=\frac{n_{\delta_e}z_\alpha-n_\alpha z_{\delta_e}}{n_\alpha+n_\tau z_\alpha};\quad T_1=\frac{n_{\delta_e}-n_\alpha z_{\delta_e}}{n_{\delta_e}z_\alpha-n_\alpha z_{\delta_e}};$$
$$T_2=\frac{1}{\sqrt{n_\alpha+n_\tau z_\alpha}};\quad \xi_2=\frac{n_\tau+n_{\dot\alpha}+z_\alpha}{2\sqrt{n_\alpha+n_\tau z_\alpha}};$$
$$k_3=\frac{n_{\delta_e}+n_\tau z_{\delta_e}}{n_\alpha+z_\alpha z_{\delta_e}};\quad T_3=\frac{z_{\delta_e}}{n_{\delta_e}+n_\tau z_{\delta_e}}. \qquad (2.92)$$

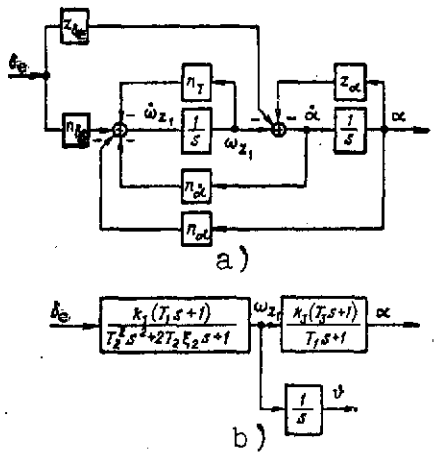


Figure 2.7. Structural Diagrams of Winged Vehicle in Longitudinal Channel. a) Original; b) transformed.

The numerical values of these coefficients for the F-101 airplane are given in Appendix I ( Figs. I.1 and I.2). /70

Flight-vehicle transfer functions in the longitudinal plane for long-period and short-period motions (complete functions with consideration of the gravity component and simplified functions without this component) are given in Appendix III (see Table III.1).

Applying the Laplace transformation to the linearized dynamic equations of the vehicle's lateral motion with zero initial conditions (2.46), we obtain the structural diagram shown in Fig. 2.8a. With structural transformations, we obtain the transformed systems of /71

Fig. 2.8, b and c, in which the series of elements forms transfer functions of the type

$$W^{\dot\psi}_{\delta_\Sigma}=\frac{s\psi(s)}{\delta_\Sigma(s)}=\frac{k_1(T_1s+1)}{T_2^2s^2+2\xi_2T_2s+1};$$
$$W^{\omega_x}_{\psi}=\frac{\omega_x(s)}{\psi(s)}=k_3\frac{T_3s+1}{T_1s+1}, \qquad (2.93)$$

where

$$k_1=\frac{n_{\delta_\Sigma}l_t}{n_\beta+n_{\dot\psi}l_t};\quad T_1=\frac{1}{l_t};$$
$$T_2=\frac{1}{\sqrt{n_\beta+n_{\dot\psi}l_t}};\quad \xi_2=\frac{n_{\dot\psi}+l_t}{2\sqrt{n_\beta+n_{\dot\psi}l_t}}; \qquad /72$$
$$k_3=\frac{n_{\delta_\Sigma}l_\beta}{n_\beta+n_{\dot\psi}l_t};\quad T_3=\frac{l_r}{l_\beta}.$$

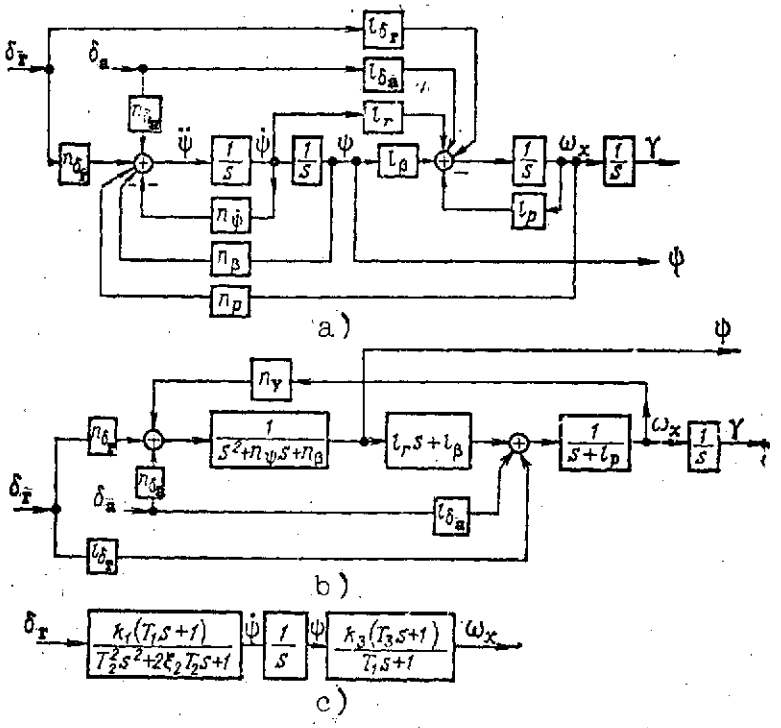


Figure 2.8. Structural Diagrams of Winged Vehicle in Lateral Channel: a) Original; b) and c) transformed.

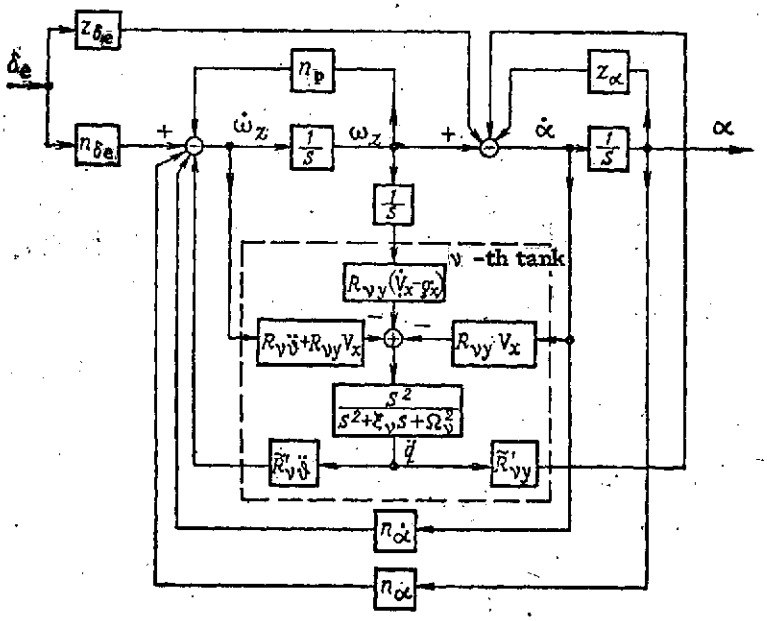


Figure 2.9. Structural Diagram of Ballistic Missile With Consideration of Sloshing of Liquid in ν-th Tank.

Appendix III (see Tables III.2 and III.3) indicates lateral-motion transfer functions.

The transfer functions of a ballistic missile can be obtained from the system of linear differential equations (2.56), (2.57), and (2.58). We apply the Laplace transformation to (2.56) and build the structural diagram for the motion of the missile in the longitudinal plane (Fig. 2.9).

We see from this structural diagram that it incorporates internal loops that take account of liquid sloshing in the tanks (for the $\nu$-th tank in the diagram). In Fig. 2.9, these loops are enclosed in the dashed rectangle. Structural diagrams for lateral motion and roll can be obtained in similar fashion. /7

If liquid sloshing can be neglected in the dynamic processes, the following ballistic-missile transfer function can be derived from Fig. 2.7:

$$W_{\delta_e}^{\vartheta}(s)=\frac{\vartheta(s)}{\delta_e(s)}=\frac{k_1(T_1s+1)}{s\left(T_2^2s^2+2\xi_2T_2s+1\right)}. \qquad (2.94)$$

The relations for calculating the parameters of a ballistic missile are identical to (2.92).

If the effect of gravity is taken into account, the ballistic-missile transfer function assumes the form

$$W_{\delta_e}^{\vartheta}(s)=\frac{\vartheta(s)}{\delta_e(s)}=\frac{k_1(T_1s+1)}{s\left(T_2^2s^2+2\xi_2T_2s+1\right)(T_3s+1)}. \qquad (2.95)$$

The numerical values of these ballistic-missile parameters are presented in the form of plots against time of flight t (see Appendix II, Fig. II.1, a and b). It is seen from Fig. II.1b that the constant $T_3$ is negative. This is explained by the influence of the force of gravity, which tends, as the missile ascends, to increase its deviation from the original trajectory. The presence of the unstable element with time constant $T_3$ indicates the instability of the motion of an unguided ballistic missile on its trajectory.*

*See A.A. Lebedev and V.A. Karabanov, Dinamika System Upravleniya Bespilotnymi Apparatami (The Dynamics of Pilotless-Aircraft Control Systems). Mashinostroyeniye, Moscow, 1965.

# CHAPTER III

/74

# ANGULAR-MOTION CHARACTERISTICS OF THE AEROSPACE VEHICLE AS A STATIONARY LINEAR OBJECT OF CONTROL IN RESPONSE TO STANDARD INPUTS

## 3.1. RESPONSE OF UNGUIDED AEROSPACE VEHICLE TO STANDARD INPUTS APPLIED IN ANALOG FORM

### 3.1.A. Case of Strongly Damped Motion

We stated in Sec. 2.4.B that the relative damping factor $\xi$ exceeds unity in the case of a developed tailplane design, high speed, and high atmospheric density. In this case, the transfer function of the vehicle in angular motion can have two real poles [expression (2.83)] and can be assigned with (2.81).

Let us rewrite it in the form

$$W(s)=\left(\frac{1}{s-\beta_1}-\frac{1}{s-\beta_2}\right)\frac{k}{T^2(\beta_1-\beta_2)}. \qquad (3.1)$$

For an input disturbance given in the operator form X(s), the transform of the reaction is

$$Y(s)=\left[\frac{X(s)}{s-\beta_1}-\frac{X(s)}{s-\beta_2}\right]\frac{k}{T^2(\beta_1-\beta_2)}. \qquad (3.2)$$

We take the quite general rational-fraction form for the transform of the input process:

$$X(s)=\frac{U(s)}{V(s)}=\frac{U(s)}{\nu_n(s-\alpha_1)(s-\alpha_2)\ldots(s-\alpha_m)}, \qquad (3.3)$$

which covers most input-disturbance types encountered in practice. The poles $\alpha_l$ ($l$ = 1, 2,... m) of the input disturbance may be /75 real, complex conjugate, simple, and multiple. For our initial analysis, we introduce a natural limitation, assuming that the poles $\beta_1$ and $\beta_2$ of the transfer function do not coincide with any of the poles $\alpha_l$ of the input disturbance.

Using the general notation X(s) for the transform of the input disturbance and the detailed representation of this disturbance in the form of (3.3), we convert on the basis of the expansion theorem (using the method set forth in [26]) from (3.2) to the expanded transform of the response:

$$Y(s)=\frac{k}{T^2(\beta_1-\beta_2)}\left[\frac{X(\beta_1)}{s-\beta_1}-\frac{X(\beta_2)}{s-\beta_2}\right]+\sum_{i=1}^{j}\frac{W(\alpha_i)\overline{X}^{(i)}(\alpha_i)}{s-\alpha_i}+$$

$$+\sum_{k=j+1}^{\mu}\frac{1}{r_k}\left\{\frac{\partial^r}{\partial\alpha^r}\left[\frac{W(\alpha)\overline{X}^{(k)}(\alpha)}{s-\alpha}\right|_{\substack{\alpha=\alpha_c\\ r=r_c}}\right\}. \qquad (3.4)$$

The first group of terms on the right in (3.4) contains the poles $\beta_1$ and $\beta_2$ of the vehicle's transfer function and the numerical coefficients $X(\beta_1)$ and $X(\beta_2)$ obtained on substitution of concrete values of the poles $\beta_1$, $\beta_2$ into the input-process transform in place of the argument s; it reflects the vehicle's natural motion $Y_{nat}(s)$:

$$Y_{nat}(s)=\frac{k}{T^2(\beta_1-\beta_2)}\left[\frac{X(\beta_1)}{s-\beta_1}-\frac{X(\beta_2)}{s-\beta_2}\right]. \qquad (3.5)$$

Converting back to the originals from the transforms on the basis of the inverse Laplace transformation, we obtain the general form of notation for the natural motion, which is valid for any type of input disturbance:

$$Y_{nat}(t)=k\frac{X(\beta_1)\exp\beta_1 t-X(\beta_2)\exp\beta_2 t}{T^2(\beta_1-\beta_2)}. \qquad (3.6)$$

The second group of terms on the right in (3.4) contains the poles $\alpha_l$ of the input-disturbance transform and reflects the forced motion $Y_{for}(s)$. Among the total of m poles of the input disturbance X(s), we distinguish multiple poles $\alpha_k$, which form /76
$\kappa$ groups with order of multiplicity $r_k + 1$ in each group and nonmultiple poles $\alpha_i$ ($i=1, 2, 3, \ldots, j$), for which $r_i = 0$, so that

$$m=j+\sum_{j+1}^{\mu}(r_k+1)=\mu+\sum_{k=j+1}^{\mu}r_k, \qquad (3.7)$$

where j is the number of nonmultiple poles and $\mu$ is the number of different poles ($\mu = \leq m$).

The coefficients of the expansion $\overline{X}^{(i)}(\alpha_i), \overline{X}^{(k)}(\alpha_k)$ are obtained from the transform (3.3) by striking out the respective polynomials $s - \alpha_i$ and $s - \alpha_k$ in the denominator, i.e.,

$$\overline{\overline{X}}^{i}(\alpha_i)=\frac{U(\alpha_i)}{v_n\dots(s-\alpha_{i-1})(s-\alpha_{i+1})\dots(s-\alpha_j)\prod\limits_{(k)}(s-\alpha_k)^{r_k+1}}=$$

$$=\frac{U(\alpha_i)}{V'(\alpha_i)}, \tag{3.8a}$$

$$\overline{\overline{X}}^{k}(\alpha_k)=\frac{U(\alpha_k)}{v_n\prod\limits_{(i)}(s-\alpha_1)\dots(s-\alpha_{k-1})^{r_{k-1}+1}\times}=$$

$$\times(s-\alpha_{k+1})^{r_{k+1}+1}\dots(s-\alpha_\mu)^{r_\mu+1}$$

$$=\frac{r_k!\,U(\alpha_k)}{\left[\dfrac{\partial^r}{\partial\alpha^r}V(\alpha)\right]_{\substack{r=r_k\\ \alpha=\alpha_k}}}. \tag{3.8b}$$

It is shown in the right-hand sides of (3.8a) and (3.8b) how the operation of canceling polynomials is replaced by the equivalent operation of differentiation of the denominator V(s).

We write out separately the second group of transforms in (3.4):

$$Y_{\overline{\text{for}}}(s)=\sum_{(i)}\frac{W(\alpha_i)\overline{\overline{X}}^{i}(\alpha_i)}{s-\alpha_i}+$$

$$+\sum_{(k)}\left\{\frac{1}{r!}\left[\frac{\partial^r}{\partial\alpha^r}\,\frac{W(\alpha)\overline{\overline{X}}^{k}(\alpha)}{s-\alpha}\right]_{\substack{\alpha=\alpha_k\\ r=r_k}}\right\}, \tag{3.9a}$$

/77

$$Y_{\text{for}}(s)=\frac{k}{T^2}\left\{\sum_{(i)}\frac{\overline{\overline{X}}^{i}(\alpha_i)}{(\alpha_i-\beta_1)(\alpha_i-\beta_2)(s-\alpha_i)}+\right.$$

$$\left.+\sum_{(k)}\left\{\left[\frac{1}{r!}\,\frac{\partial^r}{\partial\alpha^r}\,\frac{\overline{\overline{X}}^{k}(\alpha)}{(\alpha-\beta_1)(\alpha-\beta_2)(s-\alpha)}\right]_{\substack{\alpha=\alpha_k\\ r=r_k}}\right\}\right\} \tag{3.9b}$$

We now convert to the original of the forced motion:

$$y_{\overline{\text{for}}}(t)=\sum_{(i)}W(\alpha_i)\overline{\overline{X}}^{i}(\alpha_i)\exp(\alpha_i t)+$$

$$+\sum_{(k)}\left\{\frac{1}{r!}\,\frac{\partial^r}{\partial\alpha^r}\left[W(\alpha)\overline{\overline{X}}^{k}(\alpha)\exp(\alpha t)\right]\right\}_{\substack{r=r_k\\ \alpha=\alpha_k}}, \tag{3.10a}$$

or

$$Y_{\text{for}}[t]=\frac{k}{T^2}\left\{\sum_{(l)}\frac{\overline{X(\alpha_l)}}{(\alpha_l-\beta_1)(\alpha_l-\beta_2)}\exp(\alpha_l t)+\right.$$

$$\left.+\sum_{(k)}\left\{\frac{1}{r!}\frac{\partial^r}{\partial\alpha^r}\left[\frac{\overline{X(\alpha)}}{(\alpha-\beta_1)(\alpha-\beta_2)}\exp(\alpha t)\right]\right\}_{\substack{r=r_k\\ \alpha=\alpha_k}}\right. \tag{3.10b}$$

It is seen from (3.10, a and b) that the partial processes $\exp(\alpha_i t)$ in the input disturbance also remain in the vehicle's response, and that the transfer function of the vehicle affects only the partial scales. Moreover, in the multiple-pole case, when the parameter $\alpha_k$ is differentiated to separate the cofactor $t^l(l=1, 2 \ldots r_k)$, functions $t^l \exp(\alpha_k t)$ with exponents $l < r_k$ that were not present in the input may appear in the response. Let us give a detailed illustration of the application of (3.6) and (3.9) to specific examples that are important for aerospace vehicles.

Vehicle weighting function

Since the input-disturbance poles $\alpha_i$ and $\alpha_k$ are absent for $X(s) = 1$, the second group of terms in (3.4) vanishes and (3.6) can be used directly; hence /78

$$g[t]=\frac{k}{T^2(\beta_1-\beta_2)}[\exp\beta_1 t-\exp\beta_2 t]. \tag{3.11}$$

The transforms and original of the weighting function for the expanded expressions for the poles in (3.5b) will be

$$G(s)=\frac{k}{2T\sqrt{\xi^2-1}}\left(\frac{1}{s+\frac{\xi+\sqrt{\xi^2-1}}{T}}-\right.$$

$$\left.-\frac{1}{s+\frac{\xi-\sqrt{\xi^2-1}}{T}}\right), \tag{3.12}$$

$$g[t]=\frac{k}{2T\sqrt{\xi^2-1}}\left[\exp\left(-\xi+\sqrt{\xi^2-1}\right)\frac{t}{T}-\right.$$

$$\left.-\exp\left(-\xi-\sqrt{\xi^2-1}\right)\frac{t}{T}\right]. \tag{3.13}$$

With the poles given by (2.88), among which there is one positive pole, the analogous solutions will be written

$$G(s)=\frac{k}{2T\sqrt{\xi^2+1}}\left(\frac{1}{s+\frac{\xi+\sqrt{\xi^2+1}}{T}}-\right.$$

$$\left.-\frac{1}{s-\frac{\sqrt{\xi^2+1}-\xi}{T}}\right), \qquad (3.14)$$

$$g[t]=\frac{k}{2T\sqrt{\xi^2+1}}\left[\exp\left(\sqrt{\xi^2+1}-\xi\right)\frac{t}{T}-\right.$$

$$\left.-\exp\left(-\xi-\sqrt{\xi^2+1}\right)\frac{t}{T}\right]. \qquad (3.15)$$

In Table IV.1, the first line contains the expressions derived for the transfer and weighting functions. Also indicated are certain supplementary forms of notation using the time-constant nomenclature $T_1=\frac{1}{\beta_1}$ and $T_2=\frac{1}{\beta_2}$. /79

## Transient response

The transient response h[t) is the response to a unit step input 1[t) that is constant in the interval from t = $0_+$ to t = ∞. As the vehicle moves, a constant disturbing moment may arise as a result of warping of the tailplanes, other constant structural-shape distortions, and thrust imbalance. If at the same time speed, thrust, and air density remain constant, the moment that arises from these causes will also be constant. Variations of speed, density, and thrust will, even if the structural deflections remain constant, cause an increase or decrease in the disturbing moment. /80

It is convenient to convert to the step function from the exponential function

$$e(t)=e^{\eta t}=\exp\eta t, \qquad (3.16)$$

by putting η = 0; then

$$1[t)=\lim_{\eta\to 0}e^{\eta t}. \qquad (3.17)$$

If η > 0, relation (3.16) takes account of the moment increase; if η < 0, its damping is as indicated in Fig. 3.1a.

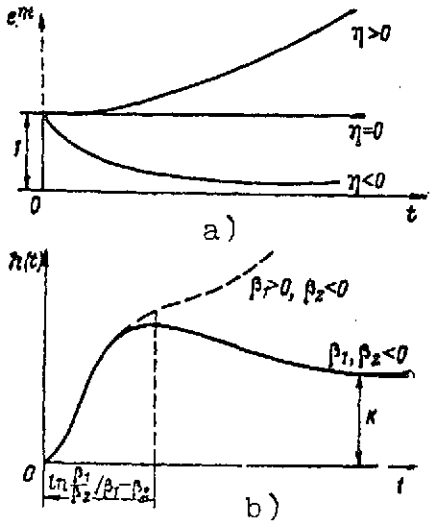


Figure 3.1. Conditions of Transient-Response Excitation. a) Exponential and step inputs; b) transient responses for negative and one positive poles of vehicle transfer function.

The transform for the input (3.16) will be

$$X(s)=E(s)\frac{1}{s-\eta}. \qquad (3.18)$$

We prepare terms for substitution into (3.5a):

$$X(\beta_1)=\frac{1}{\beta_1-\eta},\quad X(\beta_2)=\frac{1}{\beta_2-\eta}.$$

For substitution into (3.10b), we find

$$\overline{X}^{-i-}(\alpha)=\overline{X}^{-i-}(\eta)=1,$$

where i = 1 and $\alpha_i = \alpha_1 = \eta$. Combining the results obtained after substitution of the elements into relations (3.5) and (3.9), we obtain

$$H_E(s)=\frac{k}{T^2(\beta_1-\beta_2)}\left[\frac{1}{(\beta_1-\eta)(s-\beta_1)}-\right.$$
$$\left.-\frac{1}{(\beta_2-\eta)(s-\beta_2)}\right]+\frac{k}{T^2}\frac{1}{(\eta-\beta_1)(\eta-\beta_2)(s-\eta)}. \qquad (3.19)$$

It is easy to convert to the original from the transform $H_E(s)$:

$$h_E(t)=\frac{k}{T^2(\beta_1-\beta_2)}\left[\frac{\exp\beta_1 t}{\beta_1-\eta}-\frac{\exp\beta_2 t}{\beta_2-\eta}+\frac{\beta_1-\beta_2}{(\eta-\beta_1)(\eta-\beta_2)}\exp\eta t\right]. \qquad (3.20)$$

If $\eta = 0$, the original will be the transient response /81

$$h(t)=\frac{k}{T^2(\beta_1-\beta_2)}\left(\frac{1-\exp\beta_2 t}{\beta_2}-\frac{1-\exp\beta_1 t}{\beta_1}\right). \qquad (3.21)$$

We write the transient-response transform in greater detail for negative poles $\beta_1$, $\beta_2$ assigned by relations (2.82):

$$H(s)=\frac{k}{2\sqrt{\xi^2-1}}\left[\frac{\frac{1}{s}-\frac{1}{s+\frac{1}{T}(\xi+\sqrt{\xi^2-1})}}{-\xi-\sqrt{\xi^2-1}}-\right.$$
$$\left.-\frac{\frac{1}{s}-\frac{1}{s+\frac{1}{T}(\xi-\sqrt{\xi^2-1})}}{-\xi+\sqrt{\xi^2-1}}\right] \qquad (3.22)$$

and the corresponding original

$$h(t)=\frac{k}{2\sqrt{\xi^2-1}}\left[\frac{1-\exp\left(-\xi-\sqrt{\xi^2-1}\right)\frac{t}{T}}{-\xi-\sqrt{\xi^2-1}}-\right.$$
$$\left.-\frac{1-\exp\left(-\xi+\sqrt{\xi^2-1}\,\frac{t}{T}\right.}{-\xi+\sqrt{\xi^2-1}}\right]. \qquad (3.23)$$

In the case of unlike signs of the poles, $\beta_1>0$, $\beta_2<0$, the transform of the transient response and its original take the respective forms

$$H(s)=\frac{k}{2\sqrt{\xi^2+1}}\left[\frac{\dfrac{1}{s-\frac{1}{T}\left(\sqrt{\xi^2+1}-\xi\right)}-\dfrac{1}{s}}{\sqrt{\xi^2+1}-\xi}+\right.$$
$$\left.+\frac{\dfrac{1}{s}-\dfrac{1}{s+\frac{1}{T}\left(\sqrt{\xi^2+1}+\xi\right)}}{\sqrt{\xi^2+1}+\xi}\right] \qquad (3.24)$$

/82

$$h(t)=\frac{k}{2\sqrt{\xi^2+1}}\left[\frac{\exp\left(\sqrt{\xi^2+1}-\xi\right)\frac{t}{T}-1}{\sqrt{\xi^2+1}-\xi}+\right.$$
$$\left.+\frac{1-\exp\left(-\sqrt{\xi^2+1}-\xi\right)\frac{t}{T}}{\sqrt{\xi^2+1}+\xi}\right]. \qquad (3.25)$$

Standard transient-response plots appear in Fig. 3.1b.

Response to linear and power-law variation of moment in time

The power-law dependence on the time $t^{\nu}$ has the transform

$$X(s)=\frac{\nu!}{s^{\nu+1}}\dot{\div}t^{\nu}. \qquad (3.26)$$

It will be convenient at first to consider the more general function

$$X(s)=\frac{\nu!}{(s-\eta)^{\nu+1}}\dot{\div}t^{\nu}e^{\eta t}, \qquad (3.27)$$

from which the conversion to the power-law function is made by substituting $\eta = 0$.

To determine the response to the input of (3.27), we shall use relation (3.4), into which the following series coefficients must be substituted:

$$\left.\begin{aligned} X(\beta_1)&=\frac{\nu!}{(\beta_1-\eta)^{\nu+1}};\\ X(\beta_2)&=\frac{\nu!}{(\beta_2-\eta)^{\nu+1}};\\ \overset{-k-}{X}(\alpha_k)&=\overset{-1-}{X}(\eta)=\nu!, \end{aligned}\right\} \tag{3.28}$$

where $k=1$, $\alpha_k=\eta$, $r_k=\nu$.

The response transform for the transfer function

$$W(\alpha_k)=\frac{k}{T^2\eta^2+2\xi T\eta+1}$$

is obtained after substitution in the form

$$\Pi_E(s)=\frac{k\nu!}{T^2(\beta_1-\beta_2)}\left[\frac{1}{(\beta_1-\eta)^{\nu+1}(s-\beta_1)}-\right.$$
$$\left.-\frac{1}{(\beta_2-\eta)^{\nu+1}(s-\beta_2)}+\frac{\partial^\nu}{\partial\eta^\nu}\left[\frac{k}{T^2\eta^2+2\xi T\eta+1}\,\frac{1}{s-\eta}\right]\right], \tag{3.29}$$

whence follows the original

$$\Pi_E[t]=\frac{k\nu!}{T^2(\beta_1-\beta_2)}\left[\frac{\exp\beta_1 t}{(\beta_1-\eta)^{\nu+1}}-\frac{\exp\beta_2 t}{(\beta_2-\eta)^{\nu+1}}\right]+$$
$$+k\frac{\partial^\nu}{\partial\eta^\nu}\left(\frac{\exp\eta t}{T^2\eta^2+2\xi T\eta+1}\right). \tag{3.30}$$

The second term in (3.30) reflects the forced motion $\Pi_{E_{for}}$. We write it in expanded form, using Leibniz' theorem for differentiation of the product:

$$\Pi_{E_{for}}[t]=e^{\eta t}\left[t^\nu W(\eta)+\nu t^{\nu-1}W'(\eta)+\right.$$
$$\left.+\frac{\nu(\nu-1)}{2!}t^{\nu-2}W''(\eta)+\ldots+W^{(\nu)}(\eta)\right]. \tag{3.31}$$

In the case of a power-law input disturbance (3.26), relation (3.29) yields the transform of the function with $\eta = 0$:

$$\Pi(s)=\frac{k\nu!}{T^2(\beta_1-\beta_2)}\left[\frac{1}{\beta_1^{\nu+1}(s-\beta_1)}-\frac{1}{\beta_2^{\nu+1}(s-\beta_2)}\right]+$$
$$+\left[\frac{\partial^\nu}{\partial\eta^\nu}\left(\frac{k}{T^2\eta^2+2\xi T\eta+1}\cdot\frac{1}{s-\eta}\right)\right]_{\eta=0}, \tag{3.32}$$

while (3.30) yields the original

$$\Pi[t]=\frac{kv!}{T^2(\beta_1-\beta_2)}\left[\frac{\exp\beta_1 t}{\beta_1^{v+1}}-\frac{\exp\beta_2 t}{\beta_2^{v+1}}\right]+$$
$$+k\left[\frac{\partial^v}{\partial\eta^v}\left(\frac{\exp\eta t}{T^2\eta^2+2\xi T\eta+1}\right)\right]_{\eta=0} \qquad (3.33)$$

and (3.31) the forced motion

$$\Pi_{for}[t]=t^vW(0)+vt^{v-1}W'(0)+\frac{v(v-1)}{1\cdot 2}W''(0)+\ldots \qquad /84$$
$$\ldots+W^{(v)}(0). \qquad (3.34)$$

We determine the derivatives of the transfer function W(η) with η = 0 by continuous division of the numerator of W(η), i.e., k, by its inverted denominator, which gives

$$\begin{array}{l|l}\dfrac{k}{(-2\xi T\eta-T^2\eta^2)k}\ldots. & \dfrac{1+2\xi T\eta+T^2\eta^2}{[1-2\xi T\eta+4(\xi^2-1)T^2\eta^2-}\\ \dfrac{[(4\xi^2-1)T^2\eta^2+2\xi T^3\eta^3]k}{[-4\xi(2\xi^2-1)T^3\eta^3-} & -4\xi(2\xi^2-1)T^3\eta^3+\\ -(4\xi^2-1)T^4\eta^4]k & +(16\xi^4-12\xi^2+1)T^4\eta^4\ldots]k.\end{array}$$

Since the quotient must be identically equal to the Maclaurin's series

$$W(\eta)=W(0)+W'(0)\eta+\frac{W''(0)\eta^2}{2!}+\ldots, \qquad (3.35)$$

we obtain on equating the coefficients at like powers of η

$$W(0)=k;$$
$$W'(0)=-2k\xi T;$$
$$\frac{W''(0)}{2!}=4k(\xi^2-1)T^2,$$
$$\frac{W'''(0)}{3!}=-4k\xi(2\xi^2-1)T^3;$$
$$\frac{W''''(0)}{4!}=-k(16\xi^4-12\xi^2+1)T^4.$$

After substituting the calculated values of the derivatives into (3.32), the latter assumes the form

$$\Pi_{\text{for}}[t]=k[t^{\nu}-2\xi T\nu t^{\nu-1}+4(\xi^2-1)T^2\times \times\nu(\nu+1)t^{\nu-2}+\ldots]. \tag{3.36}$$

Relation (3.34) can be rewritten

$$\Pi_{\text{for}}[t]=W(0)x(t)+W'(0)\dot{x}(t)+\frac{W''(0)}{2!}\ddot{x}(t)+\ldots \tag{3.37}$$

The form of (3.37) is retained irrespective of the number of terms in the description (3.27) of the input disturbance.

Various forms of representation of the natural and forced motions are given in Table IV (p.190) for the power-law input function. Regardless of the nature of the transfer-function poles (pp.190-195), the formulas for calculating the forced motion are identical and we may use any of them at will or the universal forced-motion formula (3.37), which is valid for all columns and lines of the table.

Response to harmonically varying moment

Let us consider a sine-wave input of frequency $\omega$ and unit amplitude, i.e.,

$$X(s)=\frac{\omega}{s^2+\omega^2}=\frac{\omega}{(s-j\omega)(s+j\omega)}\dot{\div}\sin\omega t, \tag{3.38}$$

and substitute it into (3.4). For this purpose, we first evaluate the coefficients of the expansion in the natural motion

$$X(\beta_1)=\frac{\omega}{\beta_1^2+\omega^2};\quad X(\beta_2)=\frac{\omega}{\beta_2^2+\omega^2}$$

and the forced motion

$$\overset{-1-}{X}(\alpha_1)=\overset{-1-}{X}(j\omega)=\frac{\omega}{\alpha_1+j\omega}=\frac{\omega}{j2\omega}=\frac{1}{2j};$$

$$\overset{-2-}{X}(\alpha_2)=\overset{-2-}{X}(-j\omega)=\frac{\omega}{\alpha_2-j\omega}=\frac{\omega}{-j2\omega}=-\frac{1}{2j},$$

where $\alpha_1=j\omega$, $\alpha_2=-j\omega$ are the poles of the transform of the input disturbance (3.38).

Using these coefficients, we obtain

$$\Gamma(s)=\frac{k}{T^2(\beta_1-\beta_2)}\left(\frac{\omega}{\beta_1^2+\omega^2}\frac{1}{s-\beta_1}-\frac{\omega}{\beta_2^2+\omega^2}\frac{1}{s-\beta_2}\right)+ +\frac{1}{2j}\left[\frac{W(j\omega)}{s-j\omega}-\frac{W(-j\omega)}{s+j\omega}\right]. \tag{3.39}$$

We operate with the transform of the forced motion separately: /86

$$\Gamma_{\text{for}}(s)=\frac{s[W(j\omega)-W(-j\omega)]+j\omega[W(j\omega)+W(-j\omega)]}{2j(s^2+\omega^2)}=$$
$$=\frac{s\,\mathrm{Im}\,W(j\omega)+\omega\,\mathrm{Re}\,W(j\omega)}{s^2+\omega^2}, \qquad (3.40)$$

where we have separated the real and imaginary parts of the complex transfer function

$$W(j\omega)=\mathrm{Re}\,W(j\omega)+j\,\mathrm{Im}\,W(j\omega). \qquad (3.41)$$

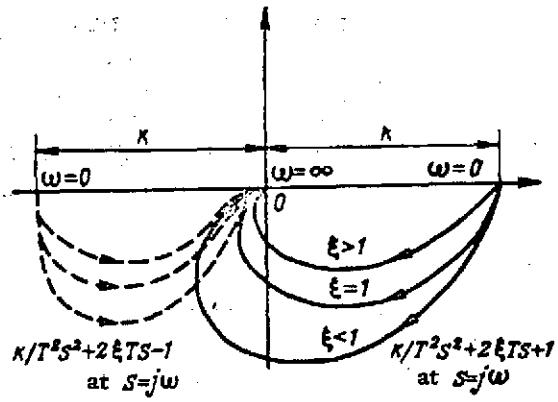


Figure 3.2. Gain-Phase Frequency Characteristics Corresponding to Second-Order Transfer Function With Various Values of the Parameters.

/87

Simplifying (3.40), we obtain

$$\Gamma_{\text{for}}(s)=|W(j\omega)|\frac{s\sin\varphi+\omega\cos\varphi}{s^2+\omega^2}, \qquad (3.42)$$

where $\varphi=\operatorname{arctg}\frac{\mathrm{Im}\,W(j\omega)}{\mathrm{Re}\,W(j\omega)}$. (3.43)

We now convert from the transform (3.39) to the original:

$$r[t]=\frac{k\omega}{T^2(\beta_1-\beta_2)}\left(\frac{\exp\beta_1 t}{\beta_1^2+\omega^2}-\frac{\exp\beta_2 t}{\beta_2^2+\omega^2}\right)+$$
$$+|W(j\omega)|\sin(\omega t+\varphi). \qquad (3.44)$$

The first group of terms determining the natural motion has already been analyzed in the preceding examples, but with a different scale.

The second term characterizes the forced motion, which is a harmonic oscillation of the same frequency as the driving moment, but with a different amplitude and a different phase. These parameters of the oscillations are fully determined by the gain-phase frequency characteristic

$$W(j\omega)=\frac{k}{j2\xi T\omega-\omega^2T^2\pm1}. \qquad (3.45)$$

Figure 3.2 presents hodographs of the functions W(jω) on the complex plane as the frequency varies from ω = 0 to ω = ∞ for positive and negative values of the last term ±1 in the denominator of (3.45).

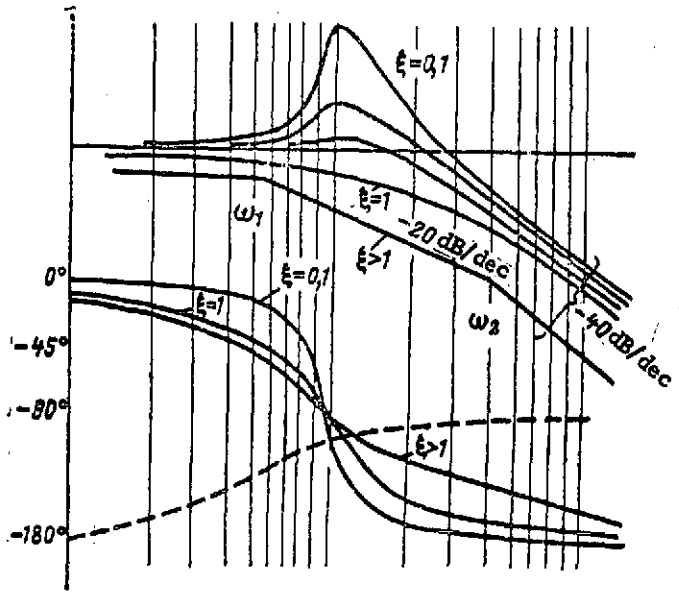


Figure 3.3. Logarithmic Frequency Characteristics Corresponding to Second-Order Transfer Function.

The variations of amplitude and phase as functions of frequency are indicated separately on logarithmic frequency characteristics (Fig. 3.3). /88

The inflections of the asymptotic logarithmic frequency characteristics occur at the conjugate frequencies

$$\left.\begin{aligned}\omega_1&=\frac{\xi-\sqrt{\xi^2-1}}{T};\\ \omega_2&=\frac{\xi+\sqrt{\xi^2-1}}{T},\end{aligned}\right\} \tag{3.46}$$

for two negative transfer-function poles and at the frequencies

$$\left.\begin{aligned}-\omega_1&=\frac{\xi-\sqrt{\xi^2+1}}{T};\\ \omega_2&=\frac{\xi+\sqrt{\xi^2+1}}{T}\end{aligned}\right\} \tag{3.47}$$

for poles of unlike sign. Formulas for calculation of responses to harmonic input disturbances appear on p. 191 in Table IV.1. The last line on p. 195 contains the same formulas but with a different symbol for the frequency, $\omega = \Omega$.

Response to oscillating moment pulse

Figure 3.4 shows a form of pressure variation that is encountered in practice in the combustion chambers of vehicle reaction engines, in the form of brief oscillations that build up initially in uneven running and then damp out. If, in addition, there is a thrust imbalance, the disturbing moment acting on the vehicle will also vary in proportion to this curve. /89

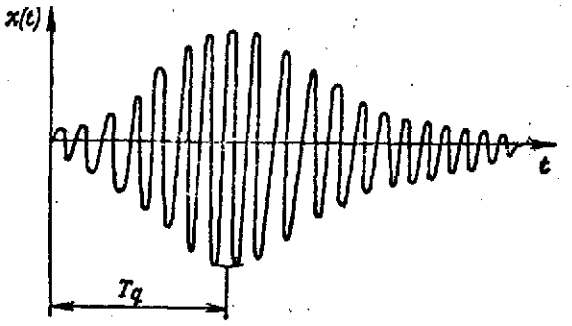


Figure 3.4. Oscillating Moment Pulse.

This curve is approximated rather closely by the function

$$x(t)=t^{\nu}e^{-\sigma t}\sin\omega t, \qquad (3.48)$$

which we shall call an oscillating pulse. In choosing the approximating function, it is recommended that the exponent $\sigma$ be matched to the descending branch of the curve, and that the cofactor exponent be obtained from the formula given in [25]:

$$\nu=\sigma T_q-1,$$

where $T_q$ is the abscissa of the center of gravity of the oscillating-pulse envelope.

The transform of the complex function (3.48) can be obtained from the known transform of the sine wave (3.38) by the following operations in the transform region:

$$X(s)=(-1)^{\nu}\frac{\partial^{\nu}}{\partial\sigma^{\nu}}\left[\frac{\omega}{(s+\sigma)^2+\omega^2}\right]=\frac{\omega U_{\nu}(s)}{[(s+\sigma)^2+\omega^2]^{\nu+1}}. \qquad (3.49)$$

Differentiation has been carried out in the right side of (3.49), with the result that it has been possible to write its denominator in general form and the following functions have been obtained for the numerator, depending on the multiplicity of differentiation $\nu$:

$$\left.\begin{aligned}&\nu=0,\ U_0(s)=1;\\&\nu=1,\ U_1(s)=2(s+\sigma);\\&\nu=2,\ U_2(s)=2[3(s+\sigma)^2-\omega^2];\\&\nu=3,\ U_3(s)=24(s+\sigma)[(s+\sigma)^2-\omega^2]\ \ldots\ \text{etc.}\end{aligned}\right\} \qquad (3.50)$$

To use (3.4) to calculate the response to the input given by

the transform (3.49), it is necessary to prepare the coefficients of the expansion first for the natural-motion components:

$$X(\beta_1)=\frac{\omega U_\nu(\beta_1)}{[(\beta_1+\sigma)^2+\omega^2]^{\nu+1}};\quad X(\beta_2)=\frac{\omega U_\nu(\beta_2)}{[(\beta_2+\sigma)^2+\omega^2]^{\nu+1}};$$

then the transform of the natural motion will be

$$Q_{\text{nat}}(s)\frac{\omega}{T^2(\beta_1-\beta_2)}\left[\frac{U_\nu(\beta_1)}{[(\beta_1+\sigma)^2+\omega^2]^{\nu+1}}\frac{1}{s-\beta_1}-\right.$$
$$\left.-\frac{U_\nu(\beta_2)}{[(\beta_2+\sigma)^2+\omega^2]^{\nu+1}}\frac{1}{s-\beta_2}\right]. \qquad (3.51)$$

From this we obtain the original written in the form investigated previously, but with more complex coefficients in the partial functions (exponents):

$$q_{\text{nat}}[t]=\frac{\omega}{T^2(\beta_1-\beta_2)}\left\{\frac{U_\nu(\beta_1)\exp\beta_1 t}{[(\beta_1+\sigma)^2+\omega^2]^{\nu+1}}-\right.$$
$$\left.-\frac{U_\nu(\beta_2)\exp\beta_2 t}{[(\beta_2+\sigma)^2+\omega^2]^{\nu+1}}\right\}. \qquad (3.52)$$

In calculating the forced motion, it must be remembered that the transform of input (3.49) contains two different roots:

$$\alpha_3=\alpha=-\sigma+j\omega,\ \alpha^*=-\sigma-j\omega=\alpha_4$$

and can be written in the form of the product

$$X(s)=\frac{\omega U_\nu(s)}{[(s-\alpha)(s-\alpha^*)]^{\nu+1}}=\frac{\omega U_\nu(s)}{(s+\sigma-j\omega)^{\nu+1}(s+\sigma+j\omega)^{\nu+1}}. \qquad (3.53)$$

Thus we have for k = 3 and 4, $\alpha_k = \alpha$, and $r_k = \nu$

$$\overset{-3-}{X}(\alpha_3)=\frac{\omega U_\nu(\alpha)}{(\alpha-\alpha^*)^{\nu+1}};$$

$$\overset{-4-}{X}(\alpha_4)=\frac{\omega U_\nu(\alpha^*)}{(\alpha^*-\alpha)^{\nu+1}}.$$

Then the transform of the forced motion, which contains two terms (k = 3, 4) will be presented in the form

$$Q_{\text{for}}(s)=\frac{\omega}{\nu!}\left[\frac{\partial^{\nu}}{\partial\alpha^{\nu}}\ \frac{U_{\nu}(\alpha)\,W(\alpha)}{(\alpha-\alpha^{*})^{\nu+1}(s-\alpha)}+\right.$$

/91

$$\left.+\frac{\partial^{\nu}}{\partial\alpha^{*\nu}}\ \frac{U_{\nu}(\alpha^{*})\,W(\alpha^{*})}{(\alpha^{*}-\alpha)^{\nu+1}(s-\alpha^{*})}\right]. \qquad (3.54)$$

Since the poles $\alpha$ and $\alpha^*$ are mutually conjugate, so are both terms in (3.54), and their sum equals twice the real part of the first term or twice the imaginary part of the first term multiplied by j, i.e.,

$$Q_{\overline{\text{for}}}(s)=\frac{2\omega}{\nu!}\ \text{Im}\left\{\frac{\partial^{\nu}}{\partial\alpha^{\nu}}\left[\frac{jU_{\nu}(\alpha)\,W(\alpha)}{(\alpha-\alpha^{*})^{\nu+1}(s-\alpha)}\right]\right\} \qquad (3.55)$$

In differentiating, it is helpful to use Leibniz' theorem for the product of the two functions $\frac{1}{(\alpha-\alpha^{*})^{\nu+1}}$ and $\frac{U_{\nu}(\alpha)\,W(\alpha)}{s-\alpha}$.

To separate the differentiation sign from the functions, we introduce intermediate nomenclature for the first function

$$\frac{1}{(\alpha-\alpha^{*})^{\nu+1}}=\frac{1}{\gamma^{\nu+1}}, \qquad (3.56a)$$

where

$$\gamma=\alpha-\alpha^{*}=j2\omega. \qquad (3.56b)$$

We can then substitute in (3.55)

$$\frac{\partial^{\nu}}{\partial\alpha^{\nu}}=\left(\frac{\partial}{\partial\alpha}+\frac{\partial}{\partial\gamma}\right)^{\nu} \qquad (3.56c)$$

and rewrite it in the form

$$Q_{\text{for}}(s)=\frac{2\omega}{\nu!}\ \text{Im}\left\{\left(\frac{\partial}{\partial\alpha}+\frac{\partial}{\partial\gamma}\right)^{\nu}\times\right.$$
$$\left.\times\left[\frac{jU_{\nu}(\alpha)\,W(\alpha)}{(s-\alpha)}\ \frac{1}{\gamma^{\nu+1}}\right]_{\substack{\alpha=-\sigma+j\omega\\ \gamma=j2\omega}}\right\}. \qquad (3.57)$$

Converting to the originals, we obtain

$$\frac{U_\nu(\alpha)W(\alpha)}{s-\alpha} \div U_\nu(\alpha)W(\alpha)\exp \alpha t,$$

and write the derivatives of this function with respect to α as follows: /92

$$\frac{\partial^k}{\partial \alpha^k}[U_\nu(\alpha)W(\alpha)\exp \alpha t] = \exp \alpha t\left(t+\frac{\partial}{\partial \alpha}\right)^k U_\nu(\alpha)W(\alpha).$$

Consequently,

$$q_{for}[t] = \frac{2\omega \exp(-\sigma t)}{\nu!} \operatorname{Im}\left\{\left[\exp(j\omega t)\left(t+\frac{\partial}{\partial \alpha}+\right.\right.\right.$$
$$\left.\left.\left.+\frac{\partial}{\partial \gamma}\right)^\nu \frac{jU_\nu(\alpha)W(\alpha)}{\gamma^{\nu+1}}\right]_{\substack{\alpha=-\sigma+j\omega \\ \gamma=j2\omega}}\right\}. \qquad (3.58)$$

We then write the forced response in the form of a polynomial:

$$q_{for}[t] = \frac{2\omega \exp(-\sigma t)}{\nu!}[t^\nu F_\nu + t^{\nu-1}F_{\nu-1} + \ldots + tF_1 + F_0]. \qquad (3.59)$$

We determine the function $F_\nu$ from (3.58)

$$F_\nu = \operatorname{Im}\left[\frac{\exp(j\omega t)U_\nu(-\sigma+j\omega)W(-\sigma+j\omega)}{2^{\nu+1}\omega^{\nu+1}(j)^\nu}\right] =$$
$$= \frac{1}{2^{\nu+1}\omega^{\nu+1}}|U_\nu(-\sigma+j\omega)W(-\sigma+$$
$$+j\omega)|\sin\left(\Omega t+\varphi-\frac{\nu\pi}{2}\right),$$

where

$$\varphi = \arctan\frac{\operatorname{Im}[U_\nu(-\sigma+j\omega)W(-\sigma+j\omega)]}{\operatorname{Re}[U_\nu[-\sigma+j\omega)W(-\sigma+j\omega)]}.$$

In its entirety, the first term of polynomial (3.59) will be

$$q_\nu[t] = \frac{|U_\nu(-\sigma+j\omega)W(-\sigma+j\omega)|}{(2\omega)^\nu \nu!} \times$$
$$\times t^\nu e^{-\sigma t}\sin\left(\omega t+\varphi-\frac{\nu\pi}{2}\right). \qquad (3.60)$$

Thus, the forced component of the response will contain the input-disturbance function with different amplitude and phase and, in addition, $\nu$ additional terms with exponents t from $\nu - 1$ to 0, but with the same frequency and damping coefficient as the exponential function. Each of these terms has its own scale (amplitude) and the corresponding phase.

Table IV.1 (p. 191) gives the components of the natural response to the oscillating pulse separately for each type of transfer-function pole, and the forced part of the response is shown in the form common to columns 2 and 3. /93

3.1.B. The Case of Medium- and Weakly-Damped Motion

The damping factor is characterized quantitatively by the parameter $\xi$. The present case corresponds to values of $\xi$ in the range $0 < \xi < 1$, which results in the appearance of complex conjugate poles $\beta$, $\beta^*$, which are defined by (2.82), in the vehicle's operator transfer function. Since relation (3.4) takes account of all types of poles, all of the solutions obtained for the preceding case remain valid for the forced motion, so that it was possible in IV.1 to display the forced solutions in a notation common to both columns in most cases. In specific cases, it is not difficult to convert from this common notation to specific transfer functions.

Let us now discuss certain aspects of calculation of the natural motion.

We rewrite the first term of (3.4) in the form

$$Y_{\text{nat}}(s) = \frac{k}{T^2(\beta - \beta^*)}\left[\frac{X(\beta)}{s-\beta} - \frac{X(\beta^*)}{s-\beta^*}\right] = \frac{k}{T\sqrt{1-\xi^2}} \operatorname{Im}\frac{X(\beta)}{s-\beta}. \tag{3.61}$$

From this it is easy to obtain the original reflecting the part of the response corresponding to the vehicle's natural motion for any type of input disturbance:

$$y_{\text{nat}}(t) = \frac{k\exp\left(-\xi\frac{t}{T}\right)}{T\sqrt{1-\xi^2}}\left|X\left(-\frac{\xi}{T} + j\frac{\sqrt{1-\xi^2}}{T}\right)\right| \times \sin\left(\frac{t}{T}\sqrt{1-\xi^2} + \varphi\right); \tag{3.62}$$

where

/94

$$\varphi = \arctan \frac{\operatorname{Im} X\left(-\frac{\xi}{T} + j\frac{\sqrt{1-\xi^2}}{T}\right)}{\operatorname{Re} X\left(-\frac{\xi}{T} + j\frac{\sqrt{1-\xi^2}}{T}\right)} \qquad (3.63)$$

Here the nature of the input influences only the scale and phase of the oscillations.

When the vehicle's transfer function is defined by (2.86), its natural motion in the absence of damping is obtained from (3.62) on substitution of $\xi = 0$, which gives

$$Y_{\text{nat}}[t] = k\Omega |X(j\Omega)| \sin\left[\Omega t + \arctan \frac{\operatorname{Im} X(j\Omega)}{\operatorname{Re} X(j\Omega)}\right], \qquad (3.64)$$

where

$$\Omega = \frac{1}{T}. \qquad (3.65)$$

Having the general formulas (3.61)-(3.65) for the natural motion and (3.10a) for the forced motion, we proceed to determination of standard responses for the same specific inputs that were considered in the first case of Sec. 3.1A.

Vehicle weighting function

Instead of relations (3.12) and (3.13) with $0<\xi<1$, we have the following relations on the basis of (3.61):

$$G(s) = \frac{k}{T\sqrt{1-\xi^2}} \operatorname{Im} \frac{1}{s + \frac{\xi}{T} - j\frac{\sqrt{1-\xi^2}}{T}}, \qquad (3.66)$$

$$g[t] = \frac{k \exp\left(-\xi \frac{t}{T}\right)}{T\sqrt{1-\xi^2}} \sin \frac{t}{T}\sqrt{1-\xi^2}. \qquad (3.67)$$

In the absence of damping, i.e., for $\xi = 0$, we have

$$g[t] = \frac{k}{T} \sin \frac{t}{T} = k\Omega \sin \Omega t. \qquad (3.68)$$

Transient response

Instead of (3.22) for $0<\xi<1$ we obtain a new expression, for which we prepare intermediate quantities.

Firstly, we denote by $H_{\text{nat}}(s)$ the transform of the natural motion determined according to (3.62) for $X(s) = 1/s$. We then calculate the coefficient $X(\beta)$ for it: /95

$$X(\beta)=\frac{1}{s}\Big|_{s=\beta}=\frac{T}{-\xi+j\sqrt{1-\xi^2}}=T\exp[j(\pi+\arccos\xi)].$$

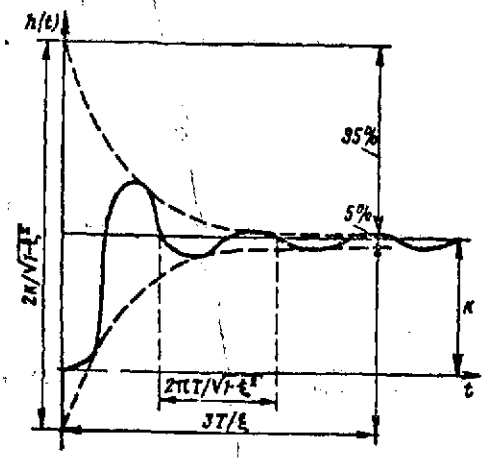


Figure 3.5. Transient Response of Stable Oscillatory Element.

Then

$$H_{\text{nat}}(s)=\frac{k}{\sqrt{1-\xi^2}}\operatorname{Im}\frac{\exp[j(\pi+\arccos\xi)}{s-\beta}=$$
$$=-\frac{k}{\sqrt{1-\xi^2}}\operatorname{Im}\frac{\exp(j\arccos\xi)}{s-\beta}. \quad (3.69)$$

The transform $H_{for}(s)$ of the forced component is found from (3.9a), which is strongly simplified and brought in the present case to the form

$$H_{\text{for}}(s)=W(\alpha)|_{\alpha=0}=W(0)=k.$$

The general sum of the natural and forced components is written

$$H(s)=k\left[1-\frac{1}{\sqrt{1-\xi^2}}\operatorname{Im}\frac{\exp(j\arccos\xi)}{s-\beta}\right]. \quad (3.70)$$

To convert to the original, we transform separately the complex function

$$L^{-1}\left\{\frac{\exp(j\arccos\xi)}{s-\beta}\right\}=$$
$$=\exp\left[-\xi\frac{t}{T}+j\left(\arccos\xi+\frac{t}{T}\sqrt{1-\xi^2}\right)\right]$$

and separate its imaginary part

$$\exp\left(-\xi\frac{t}{T}\right)\sin\left(\frac{t}{T}\sqrt{1-\xi^2}+\arccos\xi\right).$$

Then the transient response assumes the form

$$H(t)=k\left[1-\frac{\exp\left(-\xi\frac{t}{T}\right)}{\sqrt{1-\xi^2}}\sin\left(\frac{t}{T}\sqrt{1-\xi^2}+\arccos\xi\right)\right]. \quad (3.71)$$

For t = 0 we have $\sin(\arccos\xi)=-\sqrt{1-\xi^2}$ and H(0) = 0.

/96

Figure 3.5 shows the transient response of a stable oscillatory element and indicates the period of the oscillations and the damping conditions.

For $\xi = 0$, we obtain from the above formulas

$$H(s)=k\left(1-\operatorname{Im}\frac{\exp j\pi/2}{s-\beta}\right)=k\left(1-\operatorname{Im}\frac{j}{s-j\Omega}\right), \tag{3.72}$$

$$H[t]=k\left(1-\cos\frac{t}{T}\right)=k(1-\cos\Omega t). \tag{3.73}$$

Response to linear and power-law moment functions

We leave the forced response component in the form of (3.37), and use (3.61), in which the value of the coefficient $X(\beta)$ must be determined, for the natural component. Since $X(s)=\frac{\nu!}{s^{\nu+1}}$, we have

$$X(\beta)=\frac{\nu!\,T^{\nu+1}}{(-\xi+j\sqrt{1-\xi^2})^{\nu+1}}=$$
$$=\nu!\,T^{\nu+1}\exp[j(\pi+\arccos\xi)(\nu+1)].$$

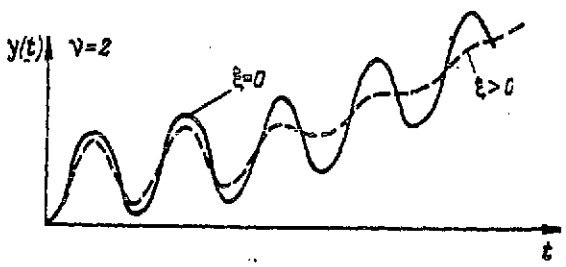


Figure 3.6. Response of ASV Having an Oscillatory-Element Type of Transfer Function to an Input Signal Assigned in the Form of a Quadratic Function.

For the natural-motion component, this yields the transform $\Pi_{nat}(s)$ = /9

$$=\frac{k\nu!\,T^{\nu}}{\sqrt{1-\xi^2}}\operatorname{Im}\frac{\exp[j(\pi+\arccos\xi)(\nu+1)]}{s+\frac{\xi}{T}-j\frac{\sqrt{1-\xi^2}}{T}}, \tag{3.74}$$

from which it is easy to convert to the original

$$\Pi_{nat}[t]=(-1)^{\nu+1}\frac{kT^{\nu}\nu!}{\sqrt{1-\xi^2}}\exp\left(-\xi\frac{t}{T}\right)\times$$
$$\times\sin\left[\frac{t}{T}\sqrt{1-\xi^2}+(\nu+1)\arccos\xi\right]. \tag{3.75}$$

Figure 3.6 shows the form of the response to a quadratic polynomial for the value $\nu = 2$ and $0 < \xi < 1$.

For a vehicle transfer function characterized by the value $\xi = 0$, the transform and original of the natural motion will be

$$\Pi_{\text{nat}}(s)=\frac{k(-1)^{\nu+1}\nu!}{\Omega^{\nu}}\operatorname{Im}\left\{\frac{\exp\left[j(\nu+1)\frac{\pi}{2}\right]}{s-j\Omega}\right\}, \tag{3.76}$$

$$\Pi_{\text{nat}}[t]=\frac{k(-1)^{\nu+1}\nu!}{\Omega^{\nu}}\cos\left(\Omega t+\nu\frac{\pi}{2}\right). \tag{3.77}$$

This response, added to the components of the forced motion (3.37) for $\nu = 2$ and $\xi = 0$, is also shown as a separate curve on Fig. 3.6.

Response to harmonically varying moment /98

If $0<\xi\leq 1$ in the equation of the vehicle, its natural motion is determined by formula (3.61), in which it is necessary to calculate the coefficient $X(\beta)$ for an input having the transform $X(s)=\frac{\omega}{s^2+\omega^2}$. We obtain after elementary substitution

$$X(\beta)=\frac{\omega}{\left(-\frac{\xi}{T}+j\frac{\sqrt{1-\xi^2}}{T}\right)^2+\omega^2}=$$

$$=\frac{\omega T^2\exp(j\psi)}{\sqrt{1+2(2\xi^2-1)\omega^2T^2+\omega^4T^4}},$$

where

$$\psi=\arctan\frac{2\xi\sqrt{1-\xi^2}}{\omega^2T^2+2\xi^2-1}.$$

Now the transform of the natural motion can be presented in the form

$$\Gamma_{\text{nat}}(s)=\frac{k\omega T}{\sqrt{[1+2(2\xi^2-1)\omega^2T^2+\omega^4T^4](1-\xi^2)}}\times$$

$$\times\operatorname{Im}\frac{\exp j\psi}{s-\beta}, \tag{3.78}$$

from which the following original is found:

$$\gamma_{\text{nat}}[t]=\frac{k\omega T\exp\left(-\xi\frac{t}{T}\right)}{\sqrt{[1+2(2\xi^2-1)\omega^2T^2+\omega^4T^4](1-\xi^2)}}\times$$

$$\times\sin\left(\frac{t}{T}\sqrt{1-\xi^2}+\arctan\frac{2\xi\sqrt{1-\xi^2}}{\omega^2T^2+2\xi^2-1}\right). \tag{3.79}$$

The transform of the forced motion in the case of a harmonic

input is still given by (3.42) and (3.43), and its original has the form

$$\gamma_{for}[t]=\frac{k}{\sqrt{(1-\omega^2T^2)^2+4\xi^2T^2\omega^2}}\sin\left(\omega t-\arctan\frac{2\xi T\omega}{1-\omega^2T^2}\right). \qquad (3.80)$$

Figure 3.3 shows the gain-frequency characteristics of the vehicle for $\xi \leq 1$.

If $\xi = 0$ in the equation for the vehicle, the transform (3.78) in the natural motion assumes the form

$$\Gamma_{nat}(s)=\frac{k\Omega\omega}{\Omega^2-\omega^2}\operatorname{Im}\frac{1}{s-j\Omega}, \qquad (3.81)$$

and the original is now determined not by (3.79), but by

$$\gamma_{nat}[t]=\frac{k\Omega\omega}{\Omega^2-\omega^2}\sin\Omega t. \qquad (3.82)$$

In the forced motion, the response has instead of (3.80) the form

$$\gamma_{for}[t]=-\frac{k\Omega^2}{\Omega^2-\omega^2}\sin\omega t. \qquad (3.83)$$

The responses to the harmonic input are written out in Table IV.1 on p. 195.

The last line examines the case in which the frequencies of the forced and natural oscillations coincide – a special case for purely imaginary poles of the transfer function (column 3).

In this case, the general transform of the response becomes

$$\Gamma(s)=W(s)X(s)=\frac{k\Omega^3}{(s^2+\Omega^2)^2}. \qquad (3.84)$$

Putting $\alpha = j\Omega$ and $\gamma = j2\Omega$, we can use for the transform with multiple complex poles ($\nu + 1 = 2$) the expansion formula (3.57), in which the product $U_\nu(\alpha)W(\alpha)$ should be replaced by

$$U_1(\alpha)W(\alpha)=k\Omega^2;$$

we then obtain

$$\Gamma(s)=2k\Omega^3\operatorname{Im}\left\{\left[\left(\frac{\partial}{\partial\alpha}+\frac{\partial}{\partial\gamma}\right)\frac{1}{(s-\alpha)\gamma^2}\right]_{\substack{\alpha=j\Omega\\ \gamma=j2\Omega}}\right\} \qquad (3.85)$$

In the time region, we obtain the original

$$r[t]=2k\Omega^3 \operatorname{Im}\left\{\left[\exp(j\Omega t)\left(t+\frac{\partial}{\partial\gamma}\right)\frac{j}{\gamma^2}\right]_{\gamma=j\Omega}\right\}$$

or



$$r[t]=\frac{k}{2}(\sin\Omega t-t\Omega\cos\Omega t). \tag{3.86}$$

The amplitude of the second term on the right in (3.86), i.e.,

$$A(t)=\frac{k\Omega}{2}t, \tag{3.87}$$

increases continuously, reflecting a state of ideal resonance, at a rate

$$\frac{dA}{dt}=\frac{k\Omega}{2}. \tag{3.88}$$

The first term in (3.86) represents nondamping oscillations. It affects the form of the initial segment of the response, but beginning at a time

$$t_0=\frac{20}{\Omega} \tag{3.89}$$

its contribution to the over-all response becomes smaller than 5%.

If the natural-oscillation frequencies differ from the disturbance frequency (see Table IV.1, p. 195), the amplitudes of the natural and forced oscillations present in the response will stand in a constant ratio

$$\frac{A_{\text{nat}}}{A_{\text{for}}}=\frac{\omega}{\Omega}, \tag{3.90}$$

which does not depend on time.

In the presence of damping in the motion of the vehicle, the forced-oscillation amplitude determined from the gain-frequency characteristic (see Fig. 3.3) and appearing in (3.80) will not depend on time, while the amplitude of the natural motion in (3.79) has a time-dependent, exponentially damping cofactor. Therefore, after a time interval

$$t_{5\%}=\frac{3T}{\xi} \tag{3.91}$$

the amplitude ratio of the natural and forced oscillations will be 5% of the initial (at t = 0) ratio of the same amplitudes.

Response to oscillating moment pulse

/1(

We take the input transform in the form of (3.49); then the coefficient X(β) needed to calculate natural motion from (3.61) will be

$$X(\beta)=|X(\beta)|\exp[j\psi(\beta)], \tag{3.92}$$

where

$$|X(\beta)|=\frac{\omega T^{\nu+1}\left|U\left(-\frac{\xi}{T}+j\frac{\sqrt{1-\xi^2}}{T}\right)\right|}{\{[(\sigma^2+\omega^2)T^2+2\xi(\xi-\sigma T)-1]^2+4(\sigma T-\xi)^2(1-\xi)^2\}^{\frac{\nu+1}{2}}}; \tag{3.93}$$

$$\psi(\beta)=\arctan\frac{\operatorname{Im}U(\beta)}{\operatorname{Re}U(\beta)}-$$

$$-(\nu+1)\arctan\frac{2(\sigma T-\xi)\sqrt{1-\xi^2}}{(\sigma^2+\omega^2)T^2+2\xi(\xi-\sigma T)-1}. \tag{3.94}$$

The natural motion in transform notation will therefore be

$$Q_{\text{nat}}(s)=\frac{k|X(\beta)|}{T\sqrt{1-\xi^2}}\operatorname{Im}\frac{\exp[j\psi(\beta)]}{s-\beta}, \tag{3.95}$$

which has the original

$$q_{\text{nat}}[t]=\frac{k|X(\beta)|}{T\sqrt{1-\xi^2}}\exp\left(-\xi\frac{t}{T}\right)\sin\left[\frac{t}{T}\sqrt{1-\xi^2}+\psi(\beta)\right]. \tag{3.96}$$

The forced motion can be determined from (3.58), which is universal because the transfer function W(α) that appears in it is given in general form. Let us therefore rewrite this formula using a specific transfer function. This gives

$$q_{\text{for}}[t]=\frac{2k\omega\exp(-\sigma t)}{\nu!}\times$$

$$\times\operatorname{Im}\left\{\exp(j\omega t)\left[\left(t+\frac{\partial}{\partial\alpha}+\frac{\partial}{\partial\gamma}\right)^{\nu}\frac{jU(\alpha)W(\alpha)}{\gamma^{\nu+1}}\right]_{\substack{\alpha=-\sigma+j\omega\\ \gamma=-j2\omega}}\right\}. \tag{3.97}$$

For a vehicle with a transfer function having no damping, i.e., for ξ = 0, the expressions for the natural and forced motions assume the forms /10

$$q_{\text{nat}}[t]=h\Omega|X(j\Omega)|\sin\left[\Omega t+\arctan\frac{\operatorname{Im}X(j\Omega)}{\operatorname{Re}X(j\Omega)}\right]; \qquad (3.98)$$

$$q_{\text{for}}[t]=\frac{2k\omega\exp(-\sigma t)}{\nu!}\times$$

$$\times\operatorname{Im}\left\{\exp(j\omega t)\left[\left(t+\frac{\partial}{\partial\alpha}+\frac{\partial}{\partial\gamma}\right)^{\nu}\frac{jU(\alpha)\Omega^2}{\gamma^{\nu+1}(\alpha^2+\Omega^2)}\right]_{\substack{\alpha=-\sigma+j\omega\\ \gamma=j2\omega}}\right\}. \qquad (3.99)$$

3.1.C. General Formula For Determination of the Response from Its Transform

Multiplication of the input transform by the transfer function of the vehicle yields a complicated response transform Y(s) in the form of a rational-fraction function with multiple real and complex roots:

$$Y(s)=\frac{U(s)}{\prod_{(l)}(s-\eta_l)^{r_l+1}\cdot\prod_{(k)}[(s-\bar{\alpha}_k)(s-\bar{\alpha}_k^*)]^{\varrho_k+1}}. \qquad (3.100)$$

If, in addition to the previously introduced notation

$$\overline{\overline{Y}}^{l}(s)=Y(s)(s-\eta_l)^{r_l+1} \qquad (3.101)$$

we use

$$\overline{\overline{Y}}^{k}(s)=Y(s)[(s-\bar{\alpha}_k)(s-\bar{\alpha}_k^*)]^{\varrho_k+1}, \qquad (3.102)$$

where the pair of multiple binomials corresponding to the ε-th pole and its conjugate have been struck from the denominator of the fraction in (3.100), the formula for the expansion of that fraction by terms becomes

$$Y(s)=\sum_{(l)}\left[\frac{1}{r!}\frac{\partial^r}{\partial\eta^r}\frac{\overline{\overline{Y}}^{l}(\eta)}{s-\eta}\right]_{\substack{r=r_l\\ \eta=\eta_l}}+$$

$$+\sum_{(k)}\left\{\frac{2}{\varrho!}\operatorname{Im}\left[\left(\frac{\partial}{\partial\alpha}-\frac{\partial}{\partial\gamma}\right)^{\varrho}\frac{\overline{\overline{jY}}^{k}(\alpha)}{\gamma^{\varrho+1}(s-\alpha)}\right]_{\substack{\varrho=\varrho_k\\ \alpha=\alpha_k=\eta_k+j\Omega_k\\ \gamma=j2\Omega_k}}\right\}. \qquad (3.103)$$

Hence follows the formula for the original: /103

$$Y[t]=\sum_{(l)}\left\{\left[\frac{1}{r!}e^{\eta t}\left(t+\frac{\partial}{\partial\eta}\right)^{r}\overline{\overline{Y}}^{l}(\eta)\right)\right]_{\substack{r=r_l\\ \eta=\eta_l}}\Bigg\}+$$

$$+\sum_{(k)}\left\{\frac{2}{\varrho_k!}\exp(\eta_k t)\operatorname{Im}\left\{\exp(j\Omega_k t)\times\right.\right.$$

$$\times\left[\left(t+\frac{\partial}{\partial\alpha}-\frac{\partial}{\partial\gamma}\right)^{q}\frac{j^{q}\overline{\overline{Y}}^{k}(\alpha)}{\gamma^{q+1}}\right]_{\substack{\alpha=\eta_k+j\Omega_k\\ \gamma=j\Omega_k}}^{\alpha=0_k}\Bigg\}. \tag{3.104}$$

The same formula also contains terms pertaining to simple (nonmultiple) poles, for which $\rho_k = 0$ and $r_i = 0$. We represent these terms in the separate formula

$$y_{\text{nonmult}}[t]=\sum_{(i)}\overline{\overline{Y}}^{i}(\eta_i)\exp(\eta_i t)+$$

$$+\sum_{(k)}\operatorname{Im}\left[\frac{\overline{\overline{Y}}^{k}(\eta_k+j\Omega_k)}{\Omega_k}\exp(\eta_k+j\Omega_k)t\right]. \tag{3.105}$$

## 3.2. RESPONSE OF UNGUIDED AEROSPACE VEHICLE TO QUANTIZED MOMENT INPUTS

### 3.2.A. Transforms of Quantized Input Disturbances

Level-quantized disturbances vary not continuously, but stepwise from one strength level to another. Time-quantized disturbances remain at a constant level only for the duration of a predetermined quantizing period $T_0$, so that the plot of the function representing a time- and level-quantized input is stepped, with a step width $T_0$. The height of each step is determined first of all by the shape of the envelope (modulating function). The ordinates of the quantized function are equal to the envelope ordinates, which are reckoned in whole numbers of level-quantizing steps with an excess on descending segments of the envelope and a deficiency on its rising segments.

Figure 3.7a shows a function of the form /10

$$x(t)=e^{\eta t},\ (\eta<0). \tag{3.106}$$

that has been quantized by level with a step $\Delta x$ and in time with a step $T_0$.

In Fig. 3.7b, the level-quantizing step has been reduced so greatly ($\Delta x\to 0$), that the ordinates of the envelope and the quantized function practically coincide at the times of time quantization $t=nT_0$ ($n=0, 1, 2\ldots\infty$).

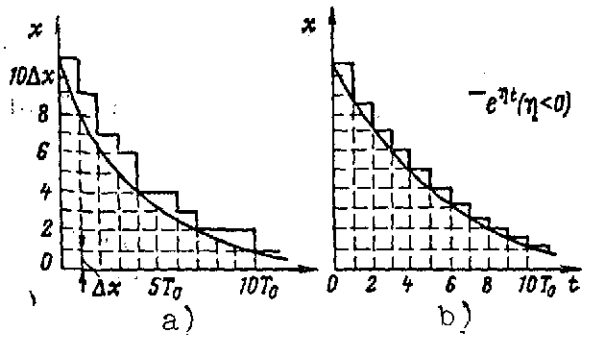


Figure 3.7. Plots of Quantized Disturbances. a) Disturbance quantized in level and time; b) disturbance quantized in time.

We shall call this function the time-quantized form of the original function and introduce for it the quantization symbol $\_|^-$, which will be placed in front of the functional notation for the envelope. For Fig. 3.7b we have

$$\_|^- x(t) = \_|^- e^{\eta t}. \quad (3.107a)$$

As is shown, for example, in [26], the Laplace transform of this quantized form is

$$L(\_|^- e^{\eta t}) = \frac{1 - e^{-T_0 s}}{[1 - e^{T_0(\eta - s)}]\, s}. \quad (3.107b)$$

Three cofactors, each of which has a specific role, must be distinghished in this formula.

The **first cofactor**

$$\frac{1}{1 - e^{T_0(\eta - s)}} = \sum_{k=0}^{\infty} e^{kT_0(\eta - s)} \quad (3.108)$$

reflects a sequence of pulses written in the form of the sum of terms of a decreasing geometrical progression. /105

The **second cofactor**

$$1 - e^{-T_0 s} \div \delta[t] - \delta[t - T_0] \quad (3.109)$$

for the transform of the pulse sequence of (3.108) serves as a transfer function containing two operations: a one-time-step shift and subtraction of the shifted (delayed) sequence from the basic sequence. Then one pulse of sequence (3.108) (each pulse) yields a pair of pulses of equal amplitude $\exp(kT_0\eta)$ and unlike signs with a one-step time shift.

The **third cofactor**

$$\frac{1}{s} \div \int_0^t \ldots dt \quad (3.110)$$

signifies the integration operation in which the pulses are con-

verted into step functions.

The signal represented by (3.100), which is more complex than (3.106), can also be converted to quantized form. If there are no multiple poles in the transform of the signal, it follows from (3.103) that

$$X(s)=\sum_{(l)}\frac{\overline{-l-}\,\overline{X}(\eta_l)}{s-\eta_l}+\sum_{(k)}\operatorname{Im}\frac{\overline{=k=}\,\overline{X}(\eta_k+j\omega_k)}{\omega_k(s-\eta_k-j\omega_k)}. \qquad (3.111)$$

After quantization to Fig. 3.7b, each elementary function

$\frac{1}{s-\eta_l}\div\exp\eta_l t$ or $\frac{1}{s-\eta_k-j\Omega_k}\div\exp[(\eta_k+j\Omega_k)t]$ acquires the transform (3.107b), so that after time quantization, the composite disturbance (3.111) will be Laplace-transformed as a composite of transforms (3.107b), i.e.,

$$L\{\overline{-|-}\,x(t)\}=\left\{\sum_{(l)}\frac{\overline{-l-}\,\overline{X}(\eta_l)}{1-\exp[T_0(\eta_l-s)]}+\right.$$

/10

$$\left.+\sum_{(k)}\operatorname{Im}\frac{\overline{=k=}\,\overline{X}(\eta_k+j\omega_k)}{\omega_k[1-\exp T_0(\eta_k+j\omega_k-s)]}\right\}\frac{1-\exp(-T_0s)}{s}. \qquad (3.112)$$

The appearance of multiple roots in the input transform does not change the structure of (3.112), but the operations of differentiation with respect to $\alpha$, $\eta$, and $\gamma$ are added under the summation sign according to (3.103).

Since the time-quantized step functions are constant on the intervals $\Delta t = T_0$, it is sufficient to have information on them at the points $t=0, T_0, 2T_0, 3T_0, \ldots$. For this purpose, we leave only the first cofactor(3.108) in expression (3.107b) and substitute in it

$$\exp T_0 s=e^{T_0 s}=z; \qquad (3.113)$$

we then obtain

$$E[z]=\frac{z}{z-\exp T_0\eta}. \qquad (3.114)$$

In exactly the same way, we obtain from (3.112) after the equivalent substitution

$$X[z]=\sum_{(l)}\frac{\overline{-l-}\,z\overline{X}(\eta_l)}{z-\exp T_0\eta_l}+$$

$$+\sum_{(k)} \operatorname{Im} \frac{z^{-k} X(\eta_k + j\omega_k)}{\omega_k [z - \exp T_0 (\eta_k + j\omega_k)]}. \qquad (3.115)$$

The functions (3.14) and (3.115) are known as z-transforms. The change from the transform of the continuous functions X(s) to the z-transform x[z] [26] is written in one of the following forms:

$$X[z] = \mathfrak{z}\{X(s)\} = \lambda_s^z \{X(s)\}. \qquad (3.116)$$

It is easy to convert the z-transform in fraction form to a power series in z by continuous division of the numerator of the fraction by its denominator. Thus, we obtain from (3.114)

/107

$$z : (z-a) = 1 + az^{-1} + a^2 z^{-2} + a^3 z^{-3} + \ldots + a^k z^{-k} + \ldots \qquad (3.117)$$

Investigating the (k + 1)-th term of the series and equating the coefficient of $z^{-k}$ to the value of the exponential function

$$a^k = e^{kT_0 \eta},$$

where

$$\eta = \frac{1}{T_0} \ln a,$$

we see that the series (3.117) characterizes the ordinates of an exponential envelope with exponent $\eta$ at the points $kT_0$.

Information on the position of each point in time is inherent directly in the transform of the shifted pulse

$$z^{-k} \doteq \delta[t - kT_0]. \qquad (3.118)$$

Information on the envelope ordinates is to a certain degree formalized, since it is given in the form of the pulse height. However, this formalization, which is inherent to the z-transform method, is an intermediate methodological device, since after the integration of 1/s, which is mandatory both in the particular formula (3.107b) and in the general formula (3.112), the height (area) of the pulse is converted to a step-function ordinate and, with consideration of the difference shift, to the ordinate of the next fixed segment of the quantized form.

The difference-shift operation expressed by (3.109) is written in the z-form as

$$1 - z^{-1} = \frac{z-1}{z}. \qquad (3.119)$$

From the original pulse sequence

$$X[z]=\sum_{k=0}^{\infty}x(nT_0)z^{-n} \tag{3.120a}$$

it enables us to obtain the difference between the two shifted sequences

$$X_{\lfloor\_\rfloor}[z]=\sum_{k=0}^{\infty}\{x(kT_0)-x[(k-1)T_0]\}z^{-k}=$$
$$=X[z](1-z^{-1}). \tag{3.120b}$$

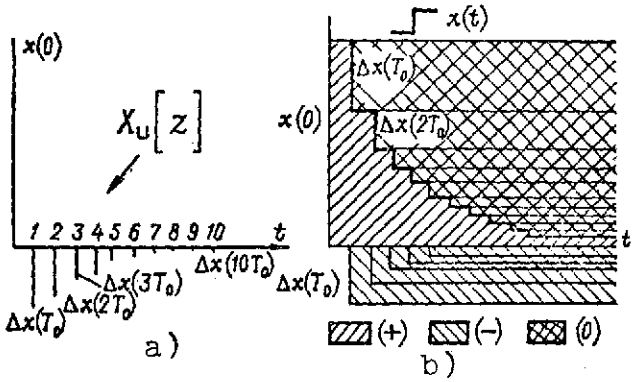


Figure 3.8. Intermediate Forms of Representation of Time-Quantized Input. a) Difference between shifted pulse sequences; b) result of integration of the difference between shifted pulse sequences.

The function (3.120b), denoted by $X_{\sqcup}[z]$, also represents the pulse sequence. If its envelope is represented by the lowercase letter with the same subscript as in (3.120), i.e., $x_{\sqcup}(t)$, then that formula becomes

$$X_{\lfloor\_\rfloor}[z]=\sum_{k=0}^{\infty}x_{\lfloor\_\rfloor}(kT_0)z^{-k}=$$
$$=x(0)z^0+\sum_{k=1}^{\infty}x_{\lfloor\_\rfloor}(kT_0)z^{-k}. \tag{3.120c}$$

Figure 3.8 shows the shifted-sequence difference for the exponential envelope considered earlier in Fig. 3.7. The first pulse in the sequence has, according to (3.120c), a height equal to the initial value of the function x(0), and the pulses that follow conform in magnitude and sign to the increments of

the function. The increments are negative for the type of decreasing function considered here.

If the shifted-sequence difference is integrated, each pulse is transformed into a shifted step function as shown in Fig. 3.8b, where the first positive step $x(0)1(t)$ is shaded in one direction and the negative steps $\Delta x(kT_0)1(t-kT_0)$ are shaded in the other direction and transposed to the top of the figure so that subtraction will be more convenient. Superposition of shading cancels the corresponding area, and it is easily seen that the part of the area with positive shading that remains in Fig. 3.8 coincides exactly with the function $\_|^{-}e^{\alpha t}$ shown in Fig. 3.7. /109

An analytical expression for the resulting function is easily derived from (3.120c) by integration:

$$\int_0^t x_{\_|}(t)\,dt = \_|^{-}x(t) = x(0)\,1[t] + \sum_{k=1}^{\infty} \Delta x(kT_0)\,1[t-kT_0]. \tag{3.121}$$

For quantized (stepped) inputs, therefore, it is necessary to convert from functional description of the envelope to description of the disturbance in sequence form; calculation of the response is then quite simple, as will be shown below.

3.2.B. Strongly Damped Motion with Quantized Disturbances

Here we consider the case in which the transfer function of the vehicle is given by (2.83). Since the quantized input must be assigned in the form $X_{\_}[z]$, the function of form (2.83) must be combined with the integrating-element transfer function (3.110); then

$$W_0(s) = \frac{k/T^2}{s(s-\beta_1)(s-\beta_2)} \tag{3.122}$$

will contain the three poles $\beta_1$, $\beta_2$, $\beta_3(\beta_3=0)$.

It is separated into three terms

$$W_0(s) = \sum_{k=1}^{3} \frac{\overline{\frac{k}{W_0(\beta_k)}}}{s-\beta_k} = \frac{k}{T^2}\left[\frac{1}{\beta_1(\beta_1-\beta_2)(s-\beta_1)} + \frac{1}{\beta_2(\beta_2-\beta_1)(s-\beta_2)} + \frac{1}{\beta_1\beta_2 s}\right]. \tag{3.123}$$ /110

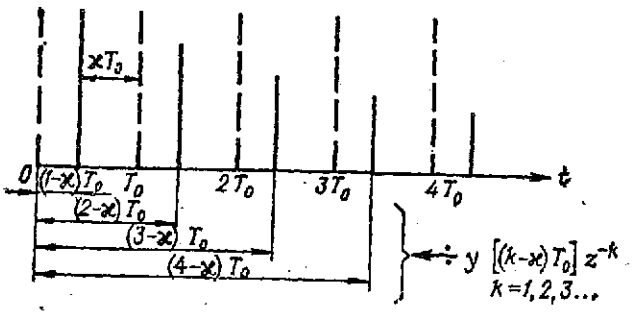


Figure 3.9. Pulse Sequence. -----) Reference Pulses at Times of input quantization; ————) vehicle response interrogation pulses with shift $1-\kappa$.

In the z-transform method [26] with consideration of quantized disturbances, the system response y is also to be studied in the form of a sequence of pulses with envelope-height modulation y(t), and it is therefore necessary to convert from the transfer function (3.123) to the Z-form. For systems with inertial elements (with memory), however, impression of a quantized input triggers a response that has a more complex form than steps in the intervals between quantization times. Thus, along with information on the output quantity at the times of input-signal quantization, it is necessary to have data on the response at intermediate times.

For this purpose, we introduce a new system of pulses that also follow one another at a repetition interval $T_0$ but are shifted by $\kappa T_0$ from the signal-quantization points.

The system of pulses introduced here involves no physical changes in the conditions of disturbance transformation at the times $(k-\varkappa)T_0$ $(k=1, 2\ldots\infty)$, but is merely part of the procedure for acquisition of data on the response at these times; it is therefore known as the interrogation-pulse system.

Figure 3.9 shows the positions of the interrogation pulses relative to the pulses produced by quantization of the input signal. As we see from the figure, the shift $\kappa T_0$ is reckoned /1
from the end of the particular quantization interval in the direction toward its beginning.

Let us examine of the terms in (3.123):

$$W_{ck}(s)=\frac{\overline{W_0(\beta_k)}^{k}}{s-\beta_k}\div\overline{W_0(\beta_k)}^{k}\exp\beta_k t \qquad (3.124)$$

and apply the z-transformation to it, using the interrogation-pulse system as the base for the transformation. We then obtain

$$\exp(1-\varkappa)T_0\beta_k\sum_{n=1}^{\infty}\exp nT_0(\beta_k-s)=$$

$$=\frac{z\exp(1-\varkappa)T_0\beta_k}{1-e^{T_0(\beta_k-s)}}. \qquad (3.125)$$

The series under the summation sign is preserved in the left member of (3.125), while the right part of the same formula gives the sum of the series, which differs from the result presented in (3.109) only in the scale and in the positions of the reading times (the shift by $\kappa T_0$). It is therefore easy to convert from (3.125) to a z-transform that depends on the argument z and the parameter $\kappa$ and is known as the modified z-transform:

$$W_{0k}[z, \kappa] = \overline{W}_0(\beta_k)\frac{z\exp(1-\kappa)T_0\beta_k}{z-\exp T_0\beta_k}, \qquad (3.126)$$

$$W_{0k}[z, m] = \overline{W}_0(\beta_k)\frac{z\exp mT_0\beta_k}{z-\exp T_0\beta_k}. \qquad (3.127)$$

Formulas (3.136) and (3.127) indicate two ways in which the interrogation-pulse shift can be reckoned: from the end of the time step, as indicated in Fig. 3.9, or from the beginning of the step, for which the new symbol $m = 1 - \kappa$, which has been used by various authors [11], [24], and others, is introduced.

The modified combined transfer function is written as follows in the z-form with consideration of (3.127):

$$W_0[z, \kappa] = \sum_{k=1}^{3}\frac{\overline{W}(\beta_k)\exp[(1-\kappa)T_0\beta_k]z}{z-\exp T_0\beta_k} \qquad (3.128)$$

or symbolically /112

$$W_0[z, \kappa] = \lambda_s^{*\kappa}[W_0(s)] = \delta^{*}[W_0(s)]. \qquad (3.129)$$

After determination of the modified combined transfer function in the z-form, the conditions of input transfer reduce to multiplication of the corresponding z-transforms:

$$Y[z, \kappa] = W_0[z, \kappa]X_{1-}[z] = W_0[z, \kappa]X[z]\frac{z-1}{z}, \qquad (3.130)$$

where $Y[z, \kappa]$ is the modified response z-transform, $W_0[z, \kappa]$ is the modified combined transfer function of the vehicle in the z-form, and $X_{1-}[z] = X[z]\frac{z-1}{z}$ is the sequence difference that corresponds to the quantized input.

The result Y[z, $\kappa$] takes the form of a rational fraction in which the coefficients of the polynomial in z that appear in the numerator are functions of the lead $\kappa$.

Fixing $\kappa$ at the successive values 1, 0.9, 0.8, ..., 0.1, we can obtain the ordinary z-transforms for each of these values, so that conversion to the original reduces to the continuous

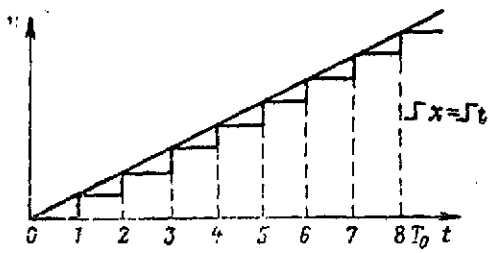


Figure 3.10. Time Quantization of Disturbance with Envelope in the Form of a Linear Function.

division indicated in (3.117).

Let us carry through the calculation of the response for a specific vehicle transfer function (3.122), which corresponds to the transfer function (3.123) with the pole values of (2.82).

In this case, the coefficients of the expansion are

$$\overset{-1-}{W}_0(\beta_1)=\frac{k}{2(\xi^2-1-\xi\sqrt{\xi^2-1})};$$

$$\overset{-2-}{W}_0(\beta_2)=-\frac{k}{2(\xi^2-1-\xi\sqrt{\xi^2-1})};\quad \overset{-3-}{W}_0(\beta_3)=W(0)=k.$$

Substituting them into (3.128), we obtain

$$W_0[z,\varkappa]=k\left\{\frac{\exp\left[-(1-\varkappa)\xi\frac{T_0}{T}\right]}{2(\xi^2-1-\xi\sqrt{\xi^2-1})}\times\right.$$

$$\times\left\{\frac{z\exp\frac{T_0}{T}(1-\varkappa)\sqrt{\xi^2-1}}{z-\exp\frac{T_0}{T}(-\xi+\sqrt{\xi^2-1})}-\right.$$

$$\left.\left.-\frac{z\exp\left[\frac{T_0}{T}(\varkappa-1)\sqrt{\xi^2-1}\right.}{z-\exp\frac{T_0}{T}(-\xi-\sqrt{\xi^2-1})}\right\}+\frac{z}{z-1}\right\}. \qquad (3.131)$$

Let us consider an input assigned in the form shown in Fig. 3.10, where the envelope of the steps is a linear function

$$x(t)=t, \qquad (3.132a)$$

and its Laplace transform is

$$X(s)=\frac{1}{s^2}=\left[\frac{\partial}{\partial\eta}\frac{1}{s-\eta}\right]_{\eta=0}=\lambda_e^X\left[\frac{1}{s-\eta}\right]. \qquad (3.132b)$$

The transform on the right in (3.132b) was obtained by the λ-transform method, which permits a similar conversion to the z-transform:

$$X[z]=\left[\frac{\partial}{\partial\eta}\frac{z}{z-\exp\eta T_0}\right]_{\eta=0}=\frac{T_0 z}{(z-1)^2} \qquad (3.133)$$

Let us now use (3.120b) to determine the z-transform of the dif-

ference between the shifted sequences /114

$$X_{1-1}[z]=\frac{T_0}{z-1} \qquad (3.134)$$

and multiply it by the modified combined transfer function (3.131); this gives

$$Y[z,\varkappa]=\frac{zkT_0}{2(z-1)(\xi^2-1-\xi\sqrt{\xi^2-1})}\times$$
$$\times\left[\frac{A(\varkappa)}{z-\exp\frac{T_0}{T}(-\xi+\sqrt{\xi^2-1})}-\right.$$
$$\left.-\frac{B(\varkappa)}{z-\exp\frac{T_0}{T}(-\xi-\sqrt{\xi^2-1}}\right]+\frac{kzT_0}{(z-1)^2}, \qquad (3.135a)$$

where

$$A(\varkappa)=\exp\left[(1-\varkappa)\frac{T_0}{T}(-\xi+\sqrt{\xi^2-1})\right], \qquad (3.135b)$$

$$B(\varkappa)=\exp\left[(1-\varkappa)\frac{T_0}{T}(-\xi-\sqrt{\xi^2-1})\right], \qquad (3.135c)$$

The last term in (3.135a) is proportional to the input disturbance (3.133):

$$\frac{kT_0z}{(z-1)^2}=kX[z], \qquad (3.136)$$

i.e., the vehicle response has a component that repeats the shape of the quantized (with linearly increasing envelope) input on a scale determined by the coefficient k. The remaining terms in (3.135a) reflect the dynamic response lag with respect to the disturbance that caused the response.

It is convenient to separate the first terms in the right-hand side of (3.135a) into forced (steady) and natural (transient, damping) components.

The forced component will contain only the poles of the input disturbance z = 1 and is now separated by the algebraic methods used previously, e.g., in (3.4) – methods that are naturally valid both for the region of the argument s and for z on conversion to the proper fraction $Y_p[z]$ with subsequent consideration of the initial poles $y(0)z^0$. Let us write the forced component separately:

$$\frac{\overline{-1-}}{\frac{Y_p[1,\varkappa]}{z-1}}=\frac{kT_0}{z-1}\times\left\{\frac{A(\varkappa)}{2(\xi^2-1-\xi\sqrt{\xi^2-1})\left[1-\exp\frac{T_0}{T}(-\xi-1\sqrt{\xi^2-1})\right]}-\right. \qquad /115$$
$$\left.-\frac{B(\varkappa)}{2(\xi^2-1-\xi\sqrt{\xi^2-1})\left[1-\exp\frac{T_0}{T}(-\xi-1\sqrt{\xi^2-1})\right]}\right\}.$$

The operators (z-functions) in the left and right members of (3.137) represent a sequence of interrogation pulses that is constant in all time steps for a fixed κ, since

$$\frac{1}{z-1}=\sum_{n=1}^{\infty}z^{-n}\doteq\sum_{n=1}^{\infty}\exp(-nT_0 s). \tag{3.138}$$

The function $\overset{-1-}{Y}[1, \varkappa]$, which is determined from A(κ) and B(κ), characterizes the change in pulse height within a quantization interval. It is sufficient to calculate $\overset{-1-}{Y}[1, \varkappa]$ once for application to each time step.

The natural component is separated from (3.135a) in the form

$$\frac{\overset{-2-}{Y_p}[z_2, \varkappa]}{z-z_2}+\frac{\overset{-3-}{Y_p}[z_3, \varkappa]}{z-z_3}=Y_{\text{nat}}[z, \varkappa]=$$

$$=\frac{kT_0A(\varkappa)}{2\left[\exp\frac{T_0}{T}(-\xi+\sqrt{\xi^2-1})-1\right]\left[z-\exp\frac{T_0}{T}(-\xi+\sqrt{\xi^2-1}\right]}-$$

$$-\frac{kT_0B(\varkappa)}{2\left[\exp\frac{T_0}{T}(-\xi-\sqrt{\xi^2-1})-1\right]\left[z-\exp\frac{T_0}{T}(-\xi-\sqrt{\xi^2-1})\right]}. \tag{3.139}$$

The functions A(κ) and B(κ), which determine the relative form of the response within the quantization interval for each time step, can be calculated for each value of κ. However, the scale will be different for each time step, and will be determined both by the constant cofactors in (3.137) and by the type of damping of the exponential components represented by the operator part of formula (3.139).

Thus, we obtain for the m-th time step /11

$$y_{\text{nat}}(nT_0, \varkappa)=\frac{kT_0\exp\frac{nT_0}{T}(-\xi+\sqrt{\xi^2-1})A(\varkappa)}{2\left[\exp\frac{T_0}{T}(-\xi+\sqrt{\xi^2-1})-1\right]}-$$

$$-\frac{kT_0\exp\frac{nT_0}{T}(-\xi-\sqrt{\xi^2-1})}{2\left[\exp\frac{T_0}{T}(-\xi-\sqrt{\xi^2-1})-1\right]}. \tag{3.140}$$

Instead of calculating the individual components in the response,

we can, as was explained above, combine all terms of (3.135) into a common fraction of the form

$$Y[z, \varkappa] = \frac{b_4(\varkappa) z^4 + b_3(\varkappa) z^3 + b_2(\varkappa) z^2 + b_1(\varkappa) z + b_0(\varkappa)}{(z-1)^2 \left[ z - \exp \frac{T_0}{T} \left( -\xi - \sqrt{\xi^2 - 1} \right) \right] \times \left[ z - \exp \frac{T_0}{T} \left( -\xi - \sqrt{\xi^2 - 1} \right) \right]} =$$

$$= \frac{b_4(\varkappa) z^4 + \ldots + b_1(\varkappa) z + b_0(\varkappa)}{z^4 + a_3 z^3 + a_2 z^2 + a_1 z + a_0} \qquad (3.141)$$

and carry out continuous division of the numerator by the denominator for fixed values of $\kappa$, when all coefficients are assigned as numbers; then the coefficients of $z^{-\kappa}$ will be complete values of the entire response in the particular time step $t = kT_0$ and at the fixed value $\kappa = \kappa_1$.

The cases considered above have been cases of real negative vehicle transfer function poles. The appearance of a positive pole will not affect the procedure of calculating the response to a quantized input, but it will not be admissible to neglect the natural-motion component in this case, the more so since it will come to dominate the over-all response with the passage of time.

### 3.2.C. Weakly Damped Motion with Quantized Inputs /117

As we noted in Sec. 3.1.B, weakly damped oscillatory motions arise when the vehicle transfer function has complex poles.

Taking transfer function (2.81) with the poles (2.82) as a base and taking account of the integrating part in the representation (3.107b) of the quantized input, we arrive at a combined transfer function of the form

$$W_0(s) = \frac{kT^{-2}}{s(s-\beta)(s-\beta^*)} = \frac{kT^{-2}}{s|s-\beta|^2}. \qquad (3.142)$$

It can be separated into components for the poles $\beta_1 = 0$, $\beta_2 = \beta$, $\beta_3 = \beta^*$, and we do so with (3.122); we determine the coefficients of the expansion

$$\overline{W_0(\beta_1)} = \frac{kT^{-2}}{\beta\beta^*} = \frac{k}{T^2|\beta|^2} = W(0) = k;$$

$$\overline{W_0(\beta_2)} = \frac{k}{T^2\beta}$$

and write the corresponding terms

$$W_0(s)=\frac{k}{T^2}\left[\frac{1}{|\beta|^2 s}+\frac{1}{\omega}\operatorname{Im}\frac{1}{\beta(s-\beta)}\right]. \qquad (3.143)$$

Substitution of the values of the poles ($\beta = \sigma + j\omega$) gives

$$W_0(s)=k\left[\frac{1}{s}+\frac{1}{\sqrt{1-\xi^2}}\operatorname{Im}\left(\frac{\dfrac{1}{-\xi+j\sqrt{1-\xi^2}}}{s+\dfrac{\xi-j\sqrt{1-\xi^2}}{T}}\right)\right]. \qquad (3.144)$$

We make the transition to the modified z-form using formula (3.128) in the form

$$W_0[z,\varkappa]=k\left\{\frac{z}{z-1}+\frac{z}{\sqrt{1-\xi^2}}\times\right.$$
$$\left.\times\operatorname{Im}\left\{\frac{(-\xi-j\sqrt{1-\xi^2})\exp\left[(1-\varkappa)\dfrac{T_0}{T}(-\xi+j\sqrt{1-\xi^2})\right]}{z-\exp\dfrac{T_0}{T}(-\xi+j\sqrt{1-\xi^2})}\right\}\right\}. \qquad (3.145)$$

We separate the imaginary part of the fraction in (3.145) by eliminating the complexity from the denominator; this yields /11

$$W_0[z,\varkappa]=kz\left[\frac{1}{z-1}+\frac{b_1(\varkappa)z+b_0(\varkappa)}{z^2+a_1z+a_0}\right], \qquad (3.146)$$

where

$$a_0=\exp\left(-\frac{2T}{T_0}\xi\right); \qquad (3.147a)$$

$$a_1=-2\exp\left(-\frac{T}{T_0}\xi\right)\cos\frac{T_0}{T}\sqrt{1-\xi^2}, \qquad (3.147b)$$

$$b_0(\varkappa)=-\frac{\exp\left[(\varkappa-2)\dfrac{T_0}{T}\xi\right]}{\sqrt{1-\xi^2}}\times$$
$$\times\sin\left[\frac{\varkappa T_0}{T}\sqrt{1-\xi^2}+\arccos\xi\right]; \qquad (3.147c)$$

$$b_1(\varkappa)=\frac{\exp\left[(\varkappa-1)\dfrac{T_0}{T}\xi\right]}{\sqrt{1-\xi^2}}\times$$
$$\times\sin\left[\frac{(\varkappa-1)T_0\sqrt{1-\xi^2}}{T}-\arccos\xi\right]. \qquad (3.147d)$$

After reducing the two fractions in (3.145) to a common denominator, we have

$$W_0[z,\varkappa]=kz\frac{[1+b_1(\varkappa)]z^2+[b_0(\varkappa)-b_1(\varkappa)+a_1]z+a_0-b_0(\varkappa)}{(z-1)(z^2+a_1z+a_0)}. \qquad (3.148)$$

For the known z-transform of the quantized input X[z], the response of the vehicle will be determined as follows in modified form according to (3.130):

$$Y[z, \varkappa]=k(z-1)X[z]\times$$

$$\times\frac{[1+b_1(\varkappa)]z^2+[b_0(\varkappa)-b_1(\varkappa)+a_1]z+a_0-b_0(\varkappa)}{z^2+a_1z+a_0}. \qquad (3.149)$$

Since the transform X[z] is assumed to be given in the form of a rational fraction, the entire product in the right member of (3.149) will reduce to a rational (more complex) fraction.

Continuous division of the numerator of this fraction by its denominator yields a representation of the over-all response at the times of interrogation $t=(n-\varkappa)T_0$. /119

Preliminary determination of the forced part of the motion, whose z-transform contains the poles of the input disturbance, permits more rapid investigation of precisely this part of the reaction if it is sufficient to have an inference only as to the rapid damping of the natural motion.

Table IV.1 gives general expressions for the quantized-input response. The notation used in the solutions is that of the z-transform. To convert to the time region, it is sufficient, after substitution of numerical values of all the coefficients for a fixed $\kappa$, to carry out continuous division of the numerator of the fraction by its denominator to obtain the power series

$$\sum_{k=1}^{\infty}y(kT_0, \varkappa)z^{-k}\div\sum_{k=1}^{\infty}y(kT_0, \varkappa)\delta[t-T_0k], \qquad (3.150)$$

whose coefficients indicate the response in sampled form.

## 3.3. STRUCTURE OF THE VEHICLE'S ANGULAR-MOTION LOOP. CONSIDERATION OF CONTROL COUPLINGS

### 3.3.A. Structure of Unguided Aerospace Vehicle

The structural diagram of the vehicle gives a graphical representation of its transfer properties and makes it easier, by comparison with the analytical description in the form of the transfer functions discussed in Secs. 3.1 and 3.2, to follow the dependence of the dynamic characteristics on the existing couplings in the uncontrolled vehicle and supplementary couplings that are introduced via the controls and autopilot.

We shall take Eq. (2.78) as a basis for the angular-motion structural diagram of the unguided vehicle, rewriting it in the

form

$$a_2 s^2 \psi(s) + a_1 s \psi(s) + a_0 \psi(s) = M_1^{\psi}(s). \qquad (3.151)^*$$

We present this equation in the conditionally solved form

$$\psi(s) = \frac{1}{a_2 s^2} [M(s) - a_0 \psi(s) - a_1 s \psi(s)]. \qquad (3.152)$$

The structural diagram of Fig. 3.11 is obtained from the conditional solution.

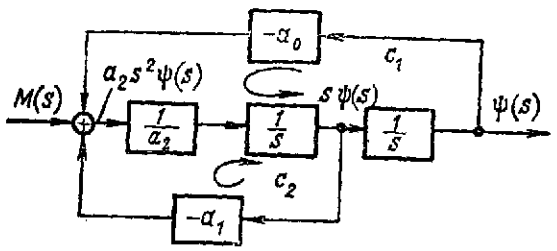


Figure 3.11. Structural Diagram of Vehicle's Angular-Motion Loop.

The first term in the brackets in (3.152) arrives at the adder via the forward loop, while the other two terms come in on the feedback lines. We can therefore simplify the adder equation

$$a_2 s^2 \psi(s) = M(s) - a_0 \psi(s) - a_1 s \psi(s), \qquad (3.153)$$

which is fully equivalent to the original equations (3.151) and (3.152).

The transfer function between the input M(s) and the output $\psi(s)$ can be calculated directly from the structural diagram:

$$W(s) = \frac{\Pi(s)}{1 + c_1(s) + c_2(s) + \ldots}, \qquad (3.154)$$

where $\Pi(s)$ is the product of all transfer functions of blocks in the forward loop and $c_1(s), c_2(s)\ldots$ are the products of the transfer functions of all blocks in the negative feedback loops. In this case, we obtain

$$W(s) = \frac{\frac{1}{a_2 s^2}}{1 + \frac{a_0}{a_2 s^2} + \frac{a_1}{a_2 s}} = \frac{1}{a_2 s^2 + a_1 s + a_0}. \qquad (3.155)$$

---

*The coefficients $a_0$, $a_1$, $a_3$ are determined from the second equation of system (2.50), where $a_2 = 1.0$, $a_1 = n_\psi$, $a_0 = n_\beta$, and M is the entire right side.

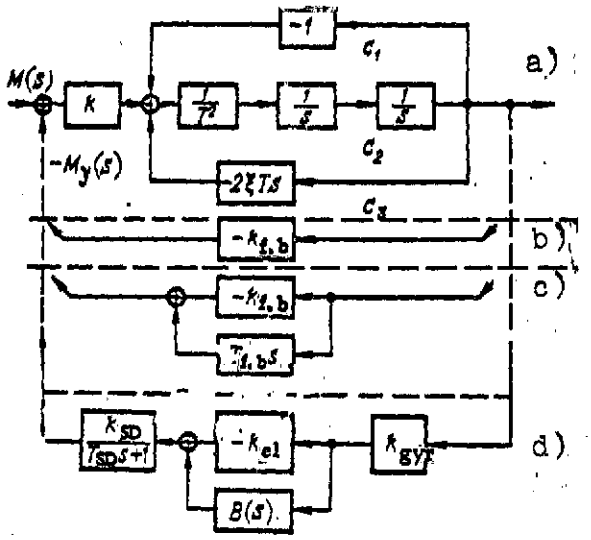


Figure 3.12. Structural Diagrams of Angular Motion After Introduction of Feedbacks Through Automatic Pilot. a) Structural diagram of unguided vehicle; b) direct negative feedback through automatic pilot; c) idealized automatic pilot in the form of a forcing element; d) real autopilot.

If the vehicle has weakly developed tailplanes and $a_1 = 0$, /121 the $c_2(s)$ loop is opened and the new transfer function assumes the form

$$W(s)=\frac{\Pi(s)}{1+c_1(s)}=\frac{\frac{1}{a_2s^2}}{1+\frac{a_0}{a_2s^2}}=\frac{1}{a_2s^2+a_0}=\frac{\frac{1}{a_2}}{s^2+\Omega^2}. \qquad (3.156)$$

If, in addition, there is no aerodynamic moment proportional to the lateral angle of slip, feedback loop $c_1(s)$ of the structural diagram is also broken, and the transfer function is even further simplified:

$$W(s)=\Pi(s)=\frac{1}{a_2s^2}. \qquad (3.157)$$

The structural diagram for the transfer function written in the standard form (2.81) is given in Fig. 3.12. The inclusion of element 1/S in loop $c_2$ in addition to those in Fig. 3.11 is compensated by the inverse element s in the feedback block, so that the properties of the loop remain unchanged. /122

### 3.3.B. Consideration of Coupling Through Analog Autopilot

Structurally, the automatic pilot is represented by a block in the negative feedback loop between the output $\psi(s)$ and the input M(s) of the vehicle's dynamic diagram. This coupling is indicated on Fig. 3.12b, where, in a first approximation, we have considered only the gain of the autopilot.

To determine the new closed-system transfer function, denoted by $\Phi_1(s)$, we can use the general formula (3.154), adding a third loop $c_3 = k_{f.b}k/T^2s^2$, which gives

$$\Phi_1(s)=\frac{\frac{k}{T^2s^2}}{1+\frac{1}{T^2s^2}+\frac{2\xi}{Ts}+\frac{kk_{f.b}}{T^2s^2}}=\frac{k}{T^2s^2+2\xi Ts+1+kk_{f.b}}. \tag{3.158}$$

We bring this transfer function to the standard form

$$\Phi_1(s)=\frac{\frac{k}{1+kk_{f.b}}}{\frac{T^2}{1+kk_{f.b}}s^2+\frac{2\xi T}{1+kk_{f.b}}s+1}=$$

$$=\frac{k_1}{T_3^2s^2+2\xi_3T_3s+1}. \tag{3.159}$$

We note first of all that application of the coupling $-k_{f.b}$ resulted in a favorable change in the static ratio between the disturbing moment and the deviation in angle of yaw:

$$k_1=\frac{\Delta\psi_{sdy}}{\Delta M}=\frac{k}{1+kk_{f.b}}. \tag{3.160}$$

When $kk_{f.b} >> 1$, we have for all practical purposes $k_1 \cong 1/k_{f.b}$, i.e., this static ratio is the reciprocal in magnitude and dimensions of the automatic-pilot gain. /1

We also see from (3.159) that the relative time constant

$$T_3=\frac{T}{\sqrt{1+kk_{f.b}}} \tag{3.161}$$

and the relative damping factor

$$\xi_3=\frac{\xi}{\sqrt{1+kk_{f.b}}} \tag{3.162}$$

have changed.

However, the absolute damping factor $\sigma = \xi/T = \xi_3/T_3$ has remained unchanged.

The new natural frequency of the oscillations is

$$\Omega_1=\frac{1}{T_1}\sqrt{1-\xi_1^2}=\frac{1}{T}\sqrt{1-\xi^2+kk_{f.b}}=$$
$$=\Omega\sqrt{1+\frac{kk_{f.b}}{1-\xi^2}}, \qquad (3.163)$$

i.e., the frequency increases with increasing $k_{f.b}$. We can provide a physical explanation for this effect by reference to the structural diagram. Thus, if we consider not the loop $c_3$ (see Fig. 3.12b), but the analogous loop in Fig. 3.11, we see that the two direct negative feedbacks $-a_0$ and $-k_{f.b}$ will be applied at the same points of the diagram, which is equivalent to a single common direct feedback

$$a_0'=a_0+k_{f.b}. \qquad (3.164)$$

The coefficient $a_0$ can be increased by changing the aerodynamic configuration of the vehicle, i.e., by developing, for example, the tailplanes. The same coefficient $a_0'$ in the presence of the automatic pilot can be increased according to (3.164) by providing only an increase in the feedback coefficient $a_{f.b}$. The designer should always consider the two possibilities. In many cases, the automatic pilot compensates for static aerodynamic instability ($a_0 < 0$) of the vehicle.

Additional couplings in the automatic pilot function similarly in determination of the vehicle's degree of damping. Figure 3.12c shows the improved coupling through the autopilot when, in addition to the coefficient $k_{f.b}$, it incorporates a concurrent-parallel branch with signal differentiation: $T_{f.b}s$, which is known as a forcing element. If loop $c_2$ of Fig. 3.11 is expanded, it is found that the feedback $a_1s$ is applied at the same points of the vehicle structural diagram as the forcing element in the automatic pilot in Fig. 3.12c. We may therefore add the transfer constants for the two couplings $a_1s$ and $T_{f.b}s$, and the new coefficient $a'_0$, which determines the degree of damping, will be

/124

$$a_1'=a_1+T_{f.b}. \qquad (3.165)$$

Consequently, the degree of damping can be increased either by

design modification of the vehicle's aerodynamic properties or by introducing a forcing loop into the autopilot.

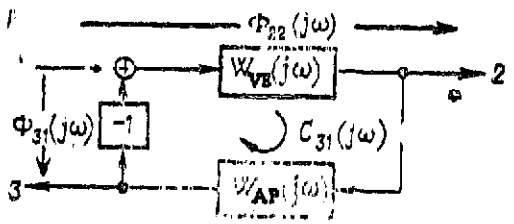


Figure 3.13. Structural Diagram of Vehicle Loop Closed by Automatic Pilot with Notation for Complex Transfer Functions Used in Application of Closing Nomogram.

When the true properties are considered, however, the automatic-pilot forcing circuit takes a somewhat more complex form than that in the idealized example considered above because of dynamic errors in the elements of the automatic pilot.

The frequency characteristics correspond to those shown in Figs. 3.2 and 3.3 for certain types of vehicles. Introduction of an automatic pilot distorts the frequency characteristics, but the system's new frequency characteristics can be determined from those of the vehicle with the aid of a standard "closing nomogram" constructed on the basis of the formula

$$\Phi(j\omega)=\frac{C(j\omega)}{1+C(j\omega)}. \qquad (3.166)$$

For application of the closing nomogram, the structural diagram of the guided vehicle must be brought to the form shown in Fig. 3.13, where $W_{VE}(j\omega)$ is the known gain-phase frequency characteristic (GPC) of the vehicle and $W_{AP}(j\omega)$ is the GPC of the automatic pilot.

The structural diagram must first be used to find the GPC of the entire closed loop:

$$C_{31}(j\omega)=W_{AP}(j\omega)W_{VE}(j\omega). \qquad (3.167)$$

Here the negative-feedback symbol is isolated in a separate block /12 as shown in Fig. 3.13, and is not included in $C_{31}(j\omega)$. Multiplication of the frequency characteristics becomes an elementary operation after conversion to the logarithmic gain and phase frequency characteristics — the LGC and LPC — and reduces to addition of the gain in decibels and the phase angle in degrees.

The closing nomogram is then used to find the closed-system GPC $\Phi_{31}(j\omega)$ from the characteristic $C_{31}(j\omega)$. Between points 1 and 2 (see Fig. 3.13), the sought GPC is determined from the characteristic obtained from the nomogram by simple conversion:

/126

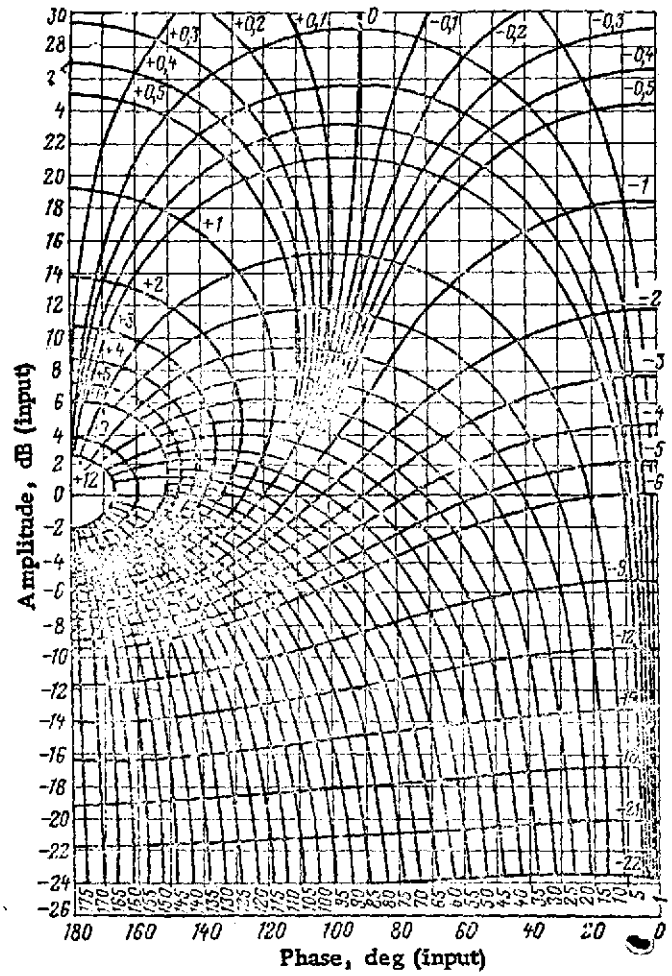


Figure 3.14. Closing Nomogram.

$$\Phi_{21}(j\omega)=\frac{\Phi_{31}(j\omega)}{W_{AP}(j\omega)}, \qquad (3.168)$$

which reduces to subtraction of the gains and phases in logarithmic coordinates.

Figure 3.14 shows the closing nomogram: its input coordinates are $\arg[C_{31}(j\omega)]$ (phase) and $20\lg|C_{31}(j\omega)|$ (amplitude), which form a uniform rectilinear coordinate grid. The output values $\arg[\Phi_{31}(j\omega)]$ and $20\lg|\Phi_{31}(j\omega)|$ are taken from the curvilinear grid of isolines. Interpolation is carried out when the input points fall into the spaces between isolines.

If $|C_{31}(j\omega)|\ll 1$, the feedback via loop $C_{31}$ is weak. This region is represented by the lower half of the nomogram, where negative values of the gain $|C_{31}|\partial\delta$ are plotted. We see from the figure that the amplitude and phase lines of the rectilinear input grid approach the output-coordinate isolines of the corresponding numeration at the bottom of the nomogram. As a result, the closed-system frequency characteristics approach the characteristics of the complete open loop. With weak coupling through the automatic-pilot loop, conversion of the characteristics becomes elementary: /12

$$\Phi_{21}(j\omega)=\frac{\Phi_{31}(j\omega)}{W_{AP}(j\omega)}\cong\frac{C_{31}(j\omega)}{W_{AP}(j\omega)}=W_{\overline{VE}}(j\omega). \qquad (3.169)$$

If $|C_{31}(j\omega|\gg 1$, the feedback in loop $C_{31}$ is strong and, according to (3.167), the transfer function $\Phi_{31}(s)$ approaches unity as a limit, i.e.,

$$\left.\begin{aligned}&\Phi_{31}(j\omega)=1;\\&20\lg|\Phi_{31}(j\omega)|=0;\end{aligned}\right\} \qquad (3.170)$$

$$\arg[\Phi_{31}(j\omega)]=0. \qquad (3.171)$$

In fact, at an open-loop gain of 30 dB at the top of the nomogram, the closed-system amplitude varies near zero in the range $\pm 0.3$ dB, and only within these limits does it depend on the input phase. The closed-system phase angle does not exceed 1°, i.e., it is also near zero for practical purposes.

In this case it follows from (3.169)-(3.171) that

$$\Phi_{21}(j\omega)\cong\frac{1}{W_{AP}(j\omega)}, \qquad (3.172)$$

i.e., the properties of the vehicle change substantially in the presence of strong feedback in the automatic-pilot loop, and the frequency characteristic of the entire closed system between points 1 and 2 becomes similar to the inverted frequency characteristic of the automatic pilot itself.

### 3.3.C. Consideration of Coupling Through Digital Automatic Pilot

Figure 3.15 shows the angular-control structural diagram of a vehicle when a digital computer is used in the automatic-pilot loop. The feedback includes, in addition to the computer, the same analog elements as before: the gyroscope, which measures $\psi$, and the control-actuator servo, which develops $M_{con}$. Since it /128 is now possible to solve complex control problems in such a system, the same figure indicates, in addition to the disturbing input $M_{dist}(s)$, the programmed input $\psi_{pr}(s)$, which might be a predetermined maneuver, etc. Each input goes to its own adder (1, 2). The output signal of adder 2 (after the gyroscope and programmer) contains an estimate of the angular imbalance $E_{M\psi}(s)$ due to the two inputs and given in analog form. Converter $\vec{AC}$ then converts the imbalance from analog to discrete form (digital code) for input into the computer with a time-quantizing interval $T_0$ long enough so that by the time of arrival of the next number characterizing the ordinate $E_{M\psi}$ the computer will already have processed the information of the preceding time step in accordance with its algorithm. After conversion to discrete form (digital code) by the computer, the signal is converted by converter $\vec{CA}$ to the analog stepped form, in which it is used to control the actuator drive that generates the controlling moment.

To avoid the introduction of additional notation for the digital code, it can be assumed as a convention that the computer algorithm transforms the input pulse sequence E[z] into the output pulse sequence F[z]. Then it is sufficient to convert from the analog form E(s) to the z-form E[z] to reflect the input into the computer of only one imbalance value during the entire interval $T_0$ (namely, the value of E at the beginning of the interval), and to obtain the step function from the z-function F[z] it is sufficient to separate the shifted-sequence difference $f_u[z]$ and then to integrate it.

If the computer algorithm is linear, the relation between the z-forms E[z] and F[z] is given by the simple formula

$$F[z]=W_{\text{ALG}}[z]E[z]. \qquad (3.173)$$

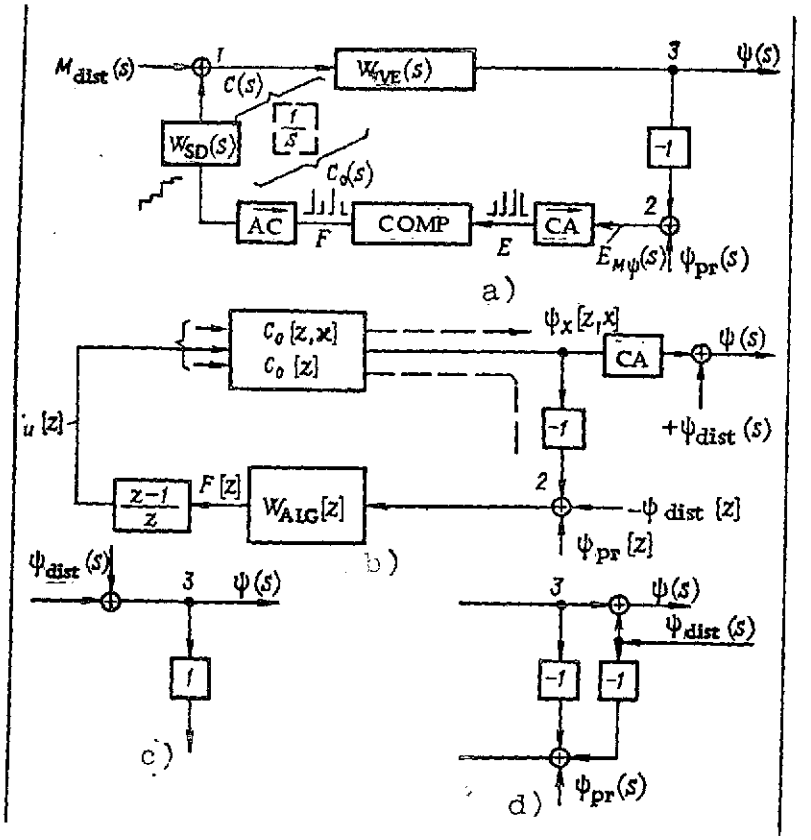


Figure 3.15. Structural Diagram of Vehicle with Digital Automatic Pilot. a) Analog-Digital Structure; b) z-structure; c) structural transformation of disturbing moment to disturbance in angle of yaw; d) duplication of disturbance in yaw angle when adder is moved across branch point on signal path.

The signal-transmision conditions are illustrated in this form in Fig. 3.15b, i.e., by the z-structure of the system. We note that the computer algorithm includes:

– the basic formula of the linear transformation that results in a rational-fraction function of z;

– a one-time-step delay (z – 1) necesitated by the computer's discrete output of the solutions;

– the scale coefficients necessary to match the transfer properties of all blocks of the structure.

In the z-structure, input disturbances must also be specified in the z-form. Since the programmed input $\psi_{pr}$ is applied to adder 2, after which only the information at the time-quantization points is used in the signals, this input is translated directly into the z-form

$$\psi_{pr}[z]=\lambda_s^z[\psi_{pr}(s)]. \qquad (3.174)$$

To convert the input $M_{dist}(s)$ similarly, it is first necessary to transfer it to adder 2. For this transfer, according to the structural rules, the input transform must be multiplied by the transfer functions of all elements between adders 1 and 2 in Fig. 3.15a, which gives

$$\psi_{dist}(s)=M_{dist}(s)W_{VE}(s). \qquad (3.175)$$

The dimensions of the disturbance will then agree with those of the second term on the adder, so that after transfer of the disturbing moment onto the angle line it will be identified as an angle disturbance $\psi_{dist}$ equivalent to the moment disturbance as indicated in Fig. 3.15, c and d.

On transfer of the disturbance $\psi_{dist}$ across junction 3, two disturbances are formed in accordance with the transfer-equivalence rules; one outside the loop and another within the loop.

For the disturbance within the loop, $-\psi_{dist}(s)$, which is equivalent to $M_{dist}$, we can convert to the z-form:

$$\psi_{dist}[z]=\lambda_s^z[M_{dist}(s)W_{VE}(s)]. \qquad (3.176)$$

We then obtain the total disturbance applied to adder 2 in the form

$$X[z]=\psi_{VE}[z]-\psi_{dist}[z]. \qquad (3.177)$$

For the disturbance $+\psi_{dist}(s)$ outside the loop, the response is analyzed separately after determination of the closed-loop operating conditions.

Continuing to trace the closed loop on Fig. 3.15b, we go from the computer function to the corresponding difference between the shifted pulse sequences in the form

$$F_{\downarrow 1}[z]=\frac{z-1}{z}F[z]. \qquad (3.178)$$ /130

This shifted pulse sequence difference excites all analog ele-

ments of the diagram that are combined with the integrating element 1/S, which participates in the shaping of the stepped signal.

To obtain $F_{-}(s)$, it is necessary to take account not only of the total input X[z], but also of the closing conditions. In this case, the loop is closed by analog elements with the overall transfer function

$$C_0(s)=\frac{1}{s}W_{SD}(s)W_{VE}(s). \tag{3.179}$$

Their response has a complex analog form, but when information is taken for the computer at discrete points, the data on the properties of the combined analog part are needed only in the form of the ordinary z-transform:

$$C_0[z]=\lambda_s^z\left[\frac{1}{s}W_{\overline{SD}}(s)W_{SD}(s)\right]. \tag{3.180}$$

It is now eacy to obtain $F_{-}[z]$ from X[z], since the z-structure contracts in the same way as the ordinary structural diagram, giving

$$F_{-1}[z]=\frac{W_{\overline{ALG}}[z]\frac{z-1}{z}}{1+C_0[z]W_{ALG}[z]\frac{z-1}{z}}. \tag{3.181}$$

After determination of the pulse sequence at the input of the analog elements in the closed system, it becomes possible to obtain the response at the output of these elements as the modified z-transform. For this purpose, we find the modified combined transfer function in the z-form for the combined analog part:

$$C_0[z,x]=\lambda_s^{zx}\left[\frac{1}{s}W_{SD}(s)W_{VE}(s)\right]. \tag{3.182}$$

Then the response $\psi_x$ caused by input x is determined from

$$\psi_x[z,x]=\frac{c_0[z,x]W_{ALG}[z](z-1)X[z]}{z+c_0[z]W_{ALG}[z](z-1)}. \tag{3.183}$$

/131

To obtain the over-all response in angle of yaw, it is necessary, as indicated in the right side of Fig. 3.15b, to add the components: $\psi_x$ given in the z-form and $\psi_{dist}$ given in the form of the Laplace transform.

The first method of obtaining the sum consists in applica-

tion of the inverse transformations according to the formula

$$\psi[(k-\varkappa)T_0] = L^{-1}\{\psi_{\overline{\text{dist}}}(s)\}_{t=(k-\varkappa)T_0} + \mathfrak{z}^{-1}\{\psi_{\varkappa}[z, \varkappa]\}, \qquad (3.184)$$

where $L^{-1}$ is the inverse Laplace transform and $\mathfrak{z}^{-1}$ is the inverse z-transform.

To reconcile the two terms in (3.184), only the values sampled at the points $t=(k-\varkappa)T_0$ are used in the continuous function obtained after the inverse Laplace transformation.

Here the sampling interval can be reduced by varying $\kappa$ in small increments.

The second method of obtaining the sum consists in conversion to the modified z-transforms for both terms:

$$\psi[z, \varkappa] = \psi_{\varkappa}[z, \varkappa] + \psi_{\text{dist}}[z, \varkappa]. \qquad (3.185)$$

In this case, in addition to the previously obtained z-transform $\psi_x[z, \kappa]$, it is necessary to find the modified z-transform $\psi_{\text{dist}}[z, \kappa]$, of the disturbance. Then, after adding in accordance with (3.185), we obtain the modified z-transform $\psi[z, \kappa]$ in the form of a common fraction, to which the inverse z-transformation (continuous division) must be applied.

Let us now consider separately the response $\psi_M$ due solely to the moment disturbance, writing it in the modified z-form

$$\psi_{\text{M}}[z, \varkappa] = \lambda_s^{z\varkappa}[W_{\text{VE}}(s) M_{\text{dist}}(s)] - \frac{c_0[z, \varkappa] W_{\text{ALG}}[z](z-1)}{z + c_0[z] W_{\text{ALG}}[z](z-1)} \psi_{\text{dist}}[z]. \qquad (3.186)$$

The first term in (3.186) represents the response of the unguided vehicle to a disturbance in moment, and the second term represents the compensation of the deviation by the control loop.

We shall retain the modified z-form (3.186) for calculations of the process at all points, but we shall also write the ordinary z-transform of the response in the form /132

$$\psi_{\text{M}}[z] = \left\{1 - \frac{c_0[z] W_{\overline{\text{ALG}}}[z](z-1)}{z + c_0[z] W_{\text{ALG}}[z](z-1)}\right\} \lambda_s^z[W_{\text{VE}}(s) M_{\text{dist}}(s)],$$

or

$$\psi_{\text{M}}[z] = \frac{z\psi_{\text{dist}}[z]}{z + c_0[z] W_{\text{ALG}}[z](z-1)} = \Phi_{\text{s}}[z] \psi_{\overline{\text{dist}}}[z], \qquad (3.187)$$

where $\Phi_\varepsilon[z]$ is the transfer function of the closed-system error in the z-form.

It is easily seen that the disturbance is compensated by an increase in the gain of the elements forming $C_0[z]$, or, for the most part by an increase in the efficiency of the controls.

Let a strong feedback $-a_1 \to -\infty$ exist in the vehicle dynamic structure shown in Fig. 3.11; then the transfer function of the part of the diagram covered by this feedback can be replaced by the gain

$$k_1 = \frac{1}{a_1}. \tag{3.188}$$

Assume also that the second feedback is very weak, $a_0 \to 0$; then the over-all transfer function of the vehicle will be

$$W_{VE} = \frac{k_1}{s}. \tag{3.189}$$

Let us use this transfer function in the structure of Fig. 3.15a, assuming as an approximation that the control actuator drive is inertialess and only changes the gain $k_1$ to the value k; then the over-all transfer function of the combined analog part of the diagram will be defined as

$$C_0(s) = \frac{k}{s^2}. \tag{3.190}$$

From this we convert to the z-form

$$C_0[z] = \frac{kT_0 z}{(z-1)^2}. \tag{3.191}$$

We shall assume a unit computer algorithm, introducing only the one-step delay of solution readout, i.e., /13

$$W_{ALG}[z] = z^{-1}. \tag{3.192}$$

We multiply all transfer functions that appear in the closed loop of the simplified digital system under consideration:

$$\frac{z-1}{z} C_0[z] W_{ALG}[z] = \frac{kT_0}{z(z-1)}, \tag{3.193}$$

and determine the closed-system transfer function

$$\Phi[z] = \frac{\frac{kT_0}{z(z-1)}}{1 + \frac{kT_0}{z(z-1)}} = \frac{kT_0}{z^2 - z + kT_0}. \tag{3.194}$$

If

$$kT_0 < \frac{1}{4}, \tag{3.195}$$

the fraction of (3.194) can be broken up into two real terms of the form

$$\Phi_1[z]=\frac{kT_0}{\left(z+\frac{1+\sqrt{1-4kT_0}}{2}\right)\left(z-\frac{1-\sqrt{1-4kT_0}}{2}\right)}=$$
$$=\frac{kT_0}{\sqrt{1-4kT_0}}\left(\frac{1}{z-\frac{1}{2}-\frac{1}{2}\sqrt{1-4kT_0}}-\right.$$
$$\left.-\frac{1}{z-\frac{1}{2}+\frac{1}{2}\sqrt{1-4kT_0}}\right) \qquad (3.196)$$

We put

$$\left.\begin{aligned} a&=\frac{1+\sqrt{1-4kT_0}}{2}=\exp\eta_1T_0;\\ b&=\frac{1-\sqrt{1-4kT_0}}{2}=\exp\eta_2T_0, \end{aligned}\right\} \qquad (3.197)$$

where

/134

$$\left.\begin{aligned} \eta_1&=\frac{1}{T_0}\ln\frac{1+\sqrt{1-4kT_0}}{2}=\\ &=-\frac{1}{T_0}\ln\frac{2}{1+\sqrt{1-4kT_0}}=-\sigma_1,\\ \eta_2&=-\frac{1}{T_0}\ln\frac{2}{1-\sqrt{1-4kT_0}}=-\sigma_2. \end{aligned}\right\} \qquad (3.198)$$

We then obtain

$$\Phi_1[z]=\frac{kT_0z^{-1}}{\sqrt{1-kT_0}}\left[\frac{z}{z-\exp(-\sigma_1T_0)}-\right.$$
$$\left.-\frac{z}{z-\exp(-\sigma_2T_0)}\right], \qquad (3.199)$$

i.e., according to (3.199), the weighting function of this closed system at the times of time quantization ($t=kT_0$; $k=1, 2, 3\ldots$) passes through the same points as the sum of the two exponentials, which are one time increment apart:

$$w[t]=\frac{kT_0}{\sqrt{1-kT_0}}\{\exp[-\sigma_1(t-T_0)]-$$
$$-\exp[-\sigma_2(t-T_0)]\}. \qquad (3.200)$$

If

$$\frac{1}{4}<kT<1, \qquad (3.201)$$

then the function (3.194) has complex poles whose absolute values are smaller than unity, and it can be presented in the form

$$\Phi_2[z]=$$

$$=\frac{kT_0}{\left(z-\frac{1}{2}-j\frac{1}{2}\sqrt{4kT_0-1}\right)\left(z-\frac{1}{2}+j\frac{1}{2}\sqrt{4kT_0-1}\right)}=$$

$$=\frac{2kT_0}{\sqrt{4kT_0-1}}\operatorname{Im}\frac{1}{z-\frac{1}{2}(1+j\sqrt{4kT_0-1})}. \qquad (3.202a)$$

We set

$$\frac{1}{2}(1+j\sqrt{4kT_0-1})=$$

$$=\sqrt{kT_0}\left(\frac{1}{2\sqrt{kT_0}}+j\sqrt{1-\frac{1}{4kT_0}}\right)=\exp(-\eta+j\Omega)T_0, \qquad (3.202b)$$

where $-\eta=\frac{1}{2T_0}\ln kT_0$ and

$$\Omega=\frac{1}{T_0}\arctan\sqrt{4kT_0-1}=\frac{\varphi}{T_0}. \qquad (3.202c)$$

Then

$$\Phi_2[z]=\frac{2kT_0}{\sqrt{4kT_0-1}}\operatorname{Im}\frac{1}{z-\exp(-\eta+j\Omega)T_0}. \qquad (3.202d)$$

We see from (3.202d) that the weighting function of the digital closed system with condition (3.201) passes through the same points at the times of time quantization as do the damping harmonic oscillations represented by the formula

$$w_1(t)=\frac{2kT_0}{\sqrt{4kT_0-1}}\exp[-\eta(t-T_0)]\sin[\Omega(t-T_0)]. \qquad (3.202e)$$

If

$$kT_0\gg 1, \qquad (3.203a)$$

we obtain by analogy with the case of (3.201)

$$w_2[t]=\frac{2kT_0}{\sqrt{4kT_0-1}}\exp\eta(t-T_0)\sin[\Omega(t-T_0)], \qquad (3.203b)$$

i.e., the weighting function contains diverging harmonic oscillations. Above we drew attention to the fact that the actual weighting functions agree with the calculated functions $w_1$, $w_2$, $w_3$ only at the points of time quantization.

However, it is evident even from the reference points obtained that closing of the negative feedback with the digital elements and a supercritical gain $k > \frac{1}{T_0}$ makes the closed system inoperative even for the simplified vehicle diagram that has been reduced to a single integrating element. It is proven in the general theory of digital control systems [11] that if poles of the closed-system transfer function have absolute values larger than unity, the resulting closed system is unstable.

We should also take note of a difference in the frequency spectra of the analog signal and the signal that has been quantized in time and amplitude. Thus, the relation between the spectra of the analog and pulsed forms will be as follows for the pulse sequence F[z] shown in Fig. 3.15a after the digital computer when the envelope F(s) is transformed: /137

$$F[j\omega]=\frac{1}{T_0}\sum_{k=-\infty}^{\infty} F\left(j\omega-j\frac{2\pi k}{T_0}\right)\cong$$

$$\cong\frac{1}{T_0}\left[F(j\omega)+F\left(j\omega-j\frac{2\pi}{T_0}\right)+F\left(j\omega+j\frac{2\pi}{T_0}\right)\right]. \qquad (3.204)$$

After conversion to the level-quantized signal $\_|\overline{F}$, which requires separation of the first difference and integration, the spectrum becomes

$$\_|\overline{F}(j\omega)=\frac{\exp j\omega T_0-1}{j\omega T_0\exp j\omega T_0}\sum_{k=-\infty}^{\infty} F\left(j\omega-j\frac{2\pi k}{T_0}\right)\cong$$

$$\cong\frac{\exp j\omega T_0-1}{j\omega T_0\exp j\omega T_0}\left[F(j\omega)+F\left(j\omega-j\frac{2\pi}{T_0}\right)+\right.$$

$$\left.+F\left(j\omega+j\frac{2\pi}{T_0}\right)\right]. \qquad (3.205)$$

The notation in the right sides of (3.204) and (3.205) permits an approximate conversion to the spectrum of the level-quantized signal from the first term, which is the spectrum of the analog signal.

## 3.4. MATRIX AND STRUCTURAL-MATRIX DESCRIPTION OF THE CHARACTERISTICS OF THE VEHICLE'S ANGLE-CONTROL LOOP

The matrix method can be used to solve the same problems directly in the time region and permits consideration of nonzero initial conditions in highly lucid form.

To illuminate the properties of the method, we write Eq. (2.78) in the time region in the modified Cauchy form:

/138

$$\left.\begin{aligned}\dot{\psi}_1(t)&=0+\psi_2(t)+\psi_1(0-)\delta[t];\\ \dot{\psi}_2(t)&=-\frac{a_0}{a_2}\psi_1(t)-\frac{a_1}{a_2}\psi_2(t)+\psi_2(0-)\delta[t]+\\ &\quad+\frac{1}{a_2}M(t)1[t].\end{aligned}\right\}\qquad(3.206)$$

The modification of the equations reduces to introduction of the pulsed components $\psi_1(0-)\delta[t]$ and $\psi_2(0-)\delta[t]$ into their right sides. On solving the differential equations after integration of the pulses introduced into the right members, we obtain the initial values of the response:

$$\psi_1(0+)=\psi_1(0-),\quad \psi_2(0+)=\psi_2(0-),$$

which are equal to the assigned initial conditions. Subsequent determination of the responses for $t>0+$ requires full solution of the differential equation system (3.206) with assigned pulse inputs and the addition to it, on the basis of the superposition principle, of the solution of the same system for the initial disturbance $\frac{1}{a_2}M(t)1[t]$.

The type (3.206) equations can be given in more general form:

$$\left.\begin{aligned}\dot{\psi}_1&=b_{11}\psi_1+b_{12}\psi_2+M_1;\\ \dot{\psi}_2&=b_{21}\psi_1+b_{22}\psi_2+M_2\end{aligned}\right\}\qquad(3.207)$$

with the complete coefficient matrix, which will be indicated here and below by straight lines:

$$|\text{Б}|=\begin{vmatrix}b_{11} & b_{12}\\ b_{21} & b_{22}\end{vmatrix}=\begin{vmatrix}0 & 1\\ -\frac{a_0}{a_2} & -\frac{a_1}{a_2}\end{vmatrix}.\qquad(3.208)$$

The coefficient matrix corresponding to the initial equation of vehicle angular motion (3.206) appears on the right in (3.206).

If the response is also written in matrix form

$$|\Psi| = \begin{vmatrix} \psi_{11} & \psi_{12} \\ \psi_{21} & \psi_{22} \end{vmatrix}, \tag{3.209}$$

with subsequent conversion from the particular responses $\psi_{ik}$ at a given output (i) to a disturbance at one of the inputs (k) to the general components $\psi_i$ of the response vector

$$|\psi| = \begin{vmatrix} \psi_1 \\ \psi_2 \end{vmatrix} = \begin{vmatrix} \psi_{11} + \psi_{12} \\ \psi_{21} + \psi_{22} \end{vmatrix}, \tag{3.210}$$

/139

then all equations of (3.207) can be written in matrix nomenclature

$$|\dot{\psi}| = |B||\psi| + |M|. \tag{3.211}$$

This equation can be solved for any input matrix |M| as a first-order matrix differential equation. Let us consider the basic steps and examples of solutions.

Derivation of normalized weighting function matrix

If the input is given in the right members of the general equations (3.206) or (3.207) in the form of unit pulses, the input matrix will be written

$$|M| = |M_\delta| = \begin{vmatrix} \delta[t] & 0 \\ 0 & \delta[t] \end{vmatrix}. \tag{3.212}$$

In this case, the response will be represented by the matrix of the normalized weighting functions

$$|\psi_\delta| = |g| = \begin{vmatrix} g_{11} & g_{12} \\ g_{21} & g_{22} \end{vmatrix}, \tag{3.213}$$

which are determined from (3.211), which assumes, for the particular input under consideration, the form

$$|\dot{g}| = |B||g| + |M_\delta|. \tag{3.1214a}$$

The formal solution of the first-order matrix equation of type (3.214a) takes the form

$$|g| = e^{|B|t} = \exp|B|t \tag{3.214b}$$

and is called the matrix exponential.

The matrix exponential is expanded in power series:

$$|g| = |E| + |B|t + |B|^2 \frac{t^2}{2!} + |B|^3 \frac{t^3}{3!} + \ldots, \tag{3.215}$$

where the matrices on the right-hand side play the role of the coefficients of the series in powers of t for the concrete angular-motion problem under consideration and have the values /140

$$|E| = \begin{vmatrix} 1 & 0 \\ 0 & 1 \end{vmatrix} \quad \text{(unit matrix):} \tag{3.216a}$$

$$|B| = \begin{vmatrix} 0 & 1 \\ -\alpha_0 & -\alpha_1 \end{vmatrix}; \tag{3.216b}$$

$$|B|^2 = \begin{vmatrix} 0 & 1 \\ -\alpha_0 & -\alpha_1 \end{vmatrix} \begin{vmatrix} 0 & 1 \\ -\alpha_0 & -\alpha_1 \end{vmatrix} = \begin{vmatrix} -\alpha_0 & -\alpha_1 \\ \alpha_0\alpha_1 & \alpha_1^2 - \alpha_0 \end{vmatrix}; \tag{3.216c}$$

$$|B|^3 = \begin{vmatrix} \alpha_0\alpha_1 & \alpha_1^2 - \alpha_0 \\ \alpha_0^2 - \alpha_0\alpha_1^2 & 2\alpha_0\alpha_1 - \alpha_1^3 \end{vmatrix}. \tag{3.216d}$$

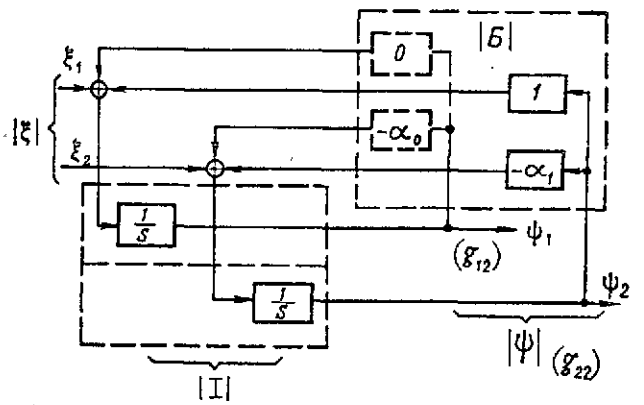


Figure 3.16. Structural-Matrix Diagram for Vehicle-Angular-Motion Channel.

The sum of the terms of series (3.215) is formed from the components (3.216a-d...) in the form

$$|g| = \begin{vmatrix} A \\ B \end{vmatrix}, \tag{3.217}$$

where

$$A = 1 - \frac{\alpha_0 t^2}{2!} + \frac{\alpha_0\alpha_1 t^3}{3!} + \ldots t - \frac{\alpha_1 t^2}{2!} + \frac{(\alpha_1^2 - \alpha_0) t^3}{3!} + \ldots;$$

$$B=-\alpha_0 t+\frac{\alpha_0\alpha_1 t^2}{2!}+\frac{\alpha_0(\alpha_0-\alpha_1^2)t^3}{3!}+\ldots$$

$$\ldots+1-\alpha_1 t+\frac{(\alpha_1^2-\alpha_0)t^2}{2!}+\ldots.$$

The multidimensional (matrix) representation of the normalized weighting function can be illustrated graphically by the structural-matrix diagram shown in Fig. 3.16, which was compiled from formulas (3.206) after normalization of the coefficients and their replacement by the more compact notation indicated in the right-hand side of (3.216b).

To clarify the principle by which one element of the response is formed, e.g., $g_{12}$, some of the lines in Fig. 3.16 have been made heavier. Examining the loop formed by these lines, /141 we note that after the first integration (1/s), the pulse has been converted to a unit function, and will have the value of the function $g_{22}(0+)=1$ at time t = 0+, which corresponds to the first term in the notation for this function in the matrix (3.217). The function $g_{12}(t)$ is determined after the second integration, so that we have $g_{12}(0+)=0$ at t = 0+, which also follows from the notation for this function in matrix (3.217) if we put t = 0 in it.

Nor is it difficult, using the expressions obtained earlier, to write the complete solutions in matrix (3.217). Thus, in the notation given in the right member of (3.216b), the weighting function (3.11) is reduced to the form

$$g_{12}(t)=\frac{1}{\sqrt{\alpha_0-\alpha_1^2}}e^{\frac{-\alpha_1 t}{2}}\sin\left(t\sqrt{\alpha_0-\alpha_1^2}\right), \qquad (3.218)$$

and the product of the series for the function $e^{\frac{-\alpha_1 t}{2}}$ and $\sin\left(t\sqrt{\alpha_0-\alpha_1^2}\right)$ gives at once the series written into matrix (3.217).

The solution obtained in matrix form is quite easily produced on a digital computer by the standard subroutine for the matrix /142 exponential that was described in [9].

In the case of higher-order equations, the structural-matrix diagram will contain the same elements that appear in Fig. 3.16, namely:

– the coefficient matrix $|E|$;

– the integrating matrix, written

$$|I|=\begin{vmatrix} \frac{1}{s} & 0 & \dots & 0 \\ 0 & \frac{1}{s} & \dots & 0 \\ \dots & \dots & \dots & \dots \\ 0 & 0 & \dots & \frac{1}{s} \end{vmatrix}; \qquad (3.219a)$$

– the input vector $\bar{M}$ or the input matrix

$$|M|=|E|M=\begin{vmatrix} M_1 & 0 & \dots & 0 \\ 0 & M_2 & \dots & 0 \\ \dots & \dots & \dots & \dots \\ 0 & 0 & \dots & M_n \end{vmatrix}; \qquad (3.219b)$$

– the response matrix $|\Psi|$;

– adders, branch points, and connecting lines.

Derivation of aftereffect vector

We shall use the term "aftereffect vector" for the process in which the dynamic system eliminates assigned nonzero initial conditions $\psi_1(0-)$ and $\psi_2(0-)$ – a process that is multidimensional in the general case but two-dimensional for the present equation system (3.206). Denoting the aftereffect vector by $\Pi$, we obtain its components $\Pi_1$ and $\Pi_2$ as linear forms of the particular normalized weighting functions $g_{ik}$ in the notation

$$\Pi=\Pi_1+\Pi_2=\begin{vmatrix} \psi_1(0-)g_{11}+\psi_2(0-)g_{12} \\ \psi_1(0-)g_{21}+\psi_2(0-)g_{22} \end{vmatrix}. \qquad (3.220)$$

Derivation of weighting function for vehicle angular motion on application of moment /143

As $\Delta t \to 0$, brief unit moment pulses

$$M_3=M_0\Delta t=1$$

give rise to a response in the form of a change in the angular position of the vehicle; this response is called the dynamic-system weighting function and is denoted by

$$w_{12}(t)=\frac{1}{a_2}g_{12}(t). \qquad (3.221a)^*$$

*In this formula and below the first subscript identifies the angle, and the second one the moment.

In the present case, we use a single concrete normalized weighting function $g_{12}$ (angle-moment).

If the pulse is not a unit pulse, but the short-duration requirement is observed ($\Delta t \to 0$), then the response takes the form of (3.221a) with its scale changed in proportion to pulse height, i.e.,

$$\psi_{12} = M_0 \Delta t w_{12}[t] = \frac{M_0 \Delta t}{a_2} g_{12}(t). \tag{3.221b}$$

If the interval $\Delta t$ is comparable with the time constant of the dynamic system, an input that is constant on this interval and vanishes outside of it is written as the difference between the shifted step functions:

$$M[t] = M_0 1[t] - M_0 1[t - \Delta t]. \tag{3.222a}$$

The response is accordingly obtained as the difference between the shifted transient responses:

$$\psi_{12}[t] = M_0 \{h_{12}[t] - h_{12}(t - \Delta t)\}. \tag{3.222b}$$

Substituting the integrals of the weighting functions for the transient responses, we obtain

$$\left.\begin{aligned} &\psi_{12}[t] = M_0 \int_0^t g_{12}(\tau) d\tau, \quad (0 \leqslant t < \Delta t); \\ &\psi_{12}[t] = M_0 \int_0^t g_{12}(\tau) d\tau - M_0 \int_{\Delta t}^t g(\tau - \Delta t) d\tau \\ &\qquad (\Delta t \leqslant t \leqslant \infty). \end{aligned}\right\} \tag{3.222c}$$

An exact evaluation of the conditions for conversion from the transient difference to the weighting function in accordance with $\Delta t$ is given in [25]. /14

Derivation of vehicle's standard-input response matrix

The standard input disturbances to the vehicle that were examined in Sec. 3.1 can be assigned in matrix form if they are regarded as solutions of the modified Cauchy equation system in the form (3.207) but are written with new coefficients and initial conditions. Writing the system for formation of the inputs simultaneously with system (3.207), we obtain the unified equation system

$$\left.\begin{aligned} \dot{\psi}_1 &= b_{11}\psi_1 + b_{12}\psi_2 + 0 + 0 + \psi_1(0-)\delta[t] \\ \dot{\psi}_2 &= b_{21}\psi_1 + b_{22}\psi_2 + b_{23}\psi_3 + 0 + \psi_2(0-)\delta[t] \\ \dot{M}_1 = \dot{\psi}_3 &= 0 + 0 + b_{33}\psi_3 + b_{34}\psi_4 + \psi_3(0+)\delta[t] \\ \dot{M}_2 = \dot{\psi}_4 &= 0 + 0 + b_{43}\psi_3 + b_{44}\psi_4 + \psi_4(0+)\delta[t] \end{aligned}\right\} \tag{3.223a}$$

In the second of these equations, the coefficient $b_{23} = 1/a_2$ introduces the function

$$\psi_3 b_{23} = \frac{1}{a_2} M(t), \tag{3.223b}$$

which is obtained as the solution of the system formed by the last two equations. These equations can be solved independently of the first two, but our objective in this article is not to solve these equations, but to write the equations for the given solution (3.223b) by selecting the coefficients $b_{ik}$ and the desired initial values $\psi_i(0+)$ (i = 3, 4); k = 3, 4).

To simplify the selection, Table IV.2 gives coefficient matrices $\begin{bmatrix} b_{33} & b_{34} \\ b_{43} & b_{44} \end{bmatrix}$ corresponding to the standard responses. Thus, the fifth line of the table gives for a harmonic input

$$b_{33} = b_{44} = 0; \quad b_{34} = 1, \quad b_{43} = -\Omega^2.$$

For the harmonic oscillations to have a phase $\phi$ and an amplitude A, it is necessary to select initial values that satisfy the conditions given in columns 3 and 4 of the table: $\psi(0+) = A \sin \varphi$, $\dot{\psi}(0+) = A\Omega \cos \varphi$. /145

After determination of all coefficients, the matrix of the combined equation system is written

$$|B| = \begin{vmatrix} b_{11} & b_{12} & 0 & 0 \\ b_{21} & b_{22} & b_{23} & 0 \\ 0 & 0 & b_{33} & b_{34} \\ 0 & 0 & b_{43} & b_{44} \end{vmatrix}, \tag{3.224a}$$

or

$$|B| = \left| \begin{array}{l|l} \text{coefficient matrix of vehicle equation system} & \begin{array}{l} 0 \; 0 \; . \; . \; . \; . \; . \; . \; 0 \\ . \; . \; . \; . \; . \; . \; . \; . \; . \; . \\ b_{23} \; 0 \; . \; . \; . \; . \; . \; . \; 0 \end{array} \\ \hline 0 \; . \; . \; . \; . \; . \; . \; . \; 0 \quad . \; . \; . \; . \; . \; . \; . \; . \; . \; . \quad 0 & \text{coefficient matrix of system of equations forming input disturbance} \end{array} \right| \tag{3.224b}$$

The rank of matrix (3.224a) is determined by the second-order vehicle dynamic equation that was chosen for the investigation and by the complexity of the input, which is also a solution of an equation system that has been reduced to the second

order. The form (3.224b) generalizes the more complex cases of arbitrary order of the equations: the coefficients of the vehicle equation system will always be placed in the upper left corner of the matrix, occupying an $n \times n$ square(where n is the order of the vehicle equation system), and the coefficients of the equation system forming the input disturbance will be placed in the lower right corner of the matrix, occupying an $m \times m$ square (where m is the order of this system of equations).

The two equation systems are related through the coefficient $b_{n,n+1}$, which appears in (3.223b). Irrespective of the rank of the matrix, the equation for determination of the partial normalized weighting functions remains in the form (3.214a), and its solution in the form of the matrix exponential (3.214b). This solution is expanded in the series form (3.215), and the digital-computer algorithm can be written in the same type of procedure regardless of the rank of the matrix. /146

Below we shall follow through the procedure for obtaining the solution only for the specific coefficient matrix (3.22-a). Inspecting the conditions for raising the coefficient matrix to various powers in the examples of formulas (3.216 a-d), we note at once that the zero elements in the lower left corner of the matrix remain vacant, and the solution in the form of the normalized weighting function matrix assumes the form

$$|g_M| = \begin{vmatrix} g_{11} & g_{12} & g_{13} & g_{14} \\ g_{21} & g_{22} & g_{23} & g_{24} \\ 0 & 0 & g_{33} & g_{34} \\ 0 & 0 & g_{43} & g_{44} \end{vmatrix}. \qquad (3.225)$$

It is easy to convert from the normalized weighting function matrix to the response to the given input and simultaneously to take account of the aftereffect regime brought about by the presence of the nonzero initial conditions. The general expression is written in the form of the vector

$$\begin{vmatrix} \psi_1 \\ \psi_2 \\ \psi_3 \\ \psi_4 \end{vmatrix} = \begin{vmatrix} \psi_1(0-)g_{11} + \psi_2(0-)g_{12} + \psi_3(0+)g_{13} + \psi_4(0+)g_{14} \\ \psi_1(0-)g_{21} + \psi_2(0-)g_{22} + \psi_3(0+)g_{23} + \psi_4(0+)g_{24} \\ \psi_3(0+)g_{33} + \psi_4(0+)g_{34} \\ \psi_3(0+)g_{43} + \psi_4(0+)g_{44} \end{vmatrix} \qquad (3.226)$$

The first component $\psi_1$ of the response vector is the basic component, and the entire procedure set forth above was, strictly speaking, elaborated for it. The terms $\psi_1(0-)g_{11}$ and $\psi_2(0-)g_{12}$ reflect the aftereffect regime, while $\psi_3(0+)g_{13}$ and $\psi_4(0+)g_{14}$ re-

flect the forced response. In the digital-computer solution, the starting functions are the $g_{11}$, $g_{12}$, $g_{13}$, and $g_{14}$ obtained in the course of the solution, and the unknown sum $\psi_1$ is formed from them with the weighting coefficients $\psi_1(0-)$, $\psi_2(0-)$, $\psi_3(0+)$, and $\psi_4(0+)$. It is unnecessary to extract the second response-vector component $\psi_2$, since it is a computer printout auxiliary. The third component $\psi_3$ represents the input disturbance, and it is helpful to print it out as a check. The fourth component $\psi_4$ /1 gives an indirect characterization of the input disturbance and need not be printed out.

Simpler formulas, e.g., a formula for the forced motion alone, follow from (3.226) when some of the weighting functions have zero values.

The second-order angular-motion equation used as a basis for the present chapter has made it possible to obtain a number of clear-cut relationships between characteristics of the vehicle that can be used for comparatively fast identification of the primary parameters of the vehicle on the basis of test data. The same method can also be extended to more complex cases.

Such simplification of the more general equation system (2.50) is typically encountered in wind-tunnel tests of models and on certain unperturbed segments of trajectories.

# CHAPTER IV

/148

# CHARACTERISTICS OF THE AEROSPACE VEHICLE AS A STATIONARY LINEAR OBJECT OF CONTROL WITH CONSIDERATION OF ADDITIONAL DEGREES OF FREEDOM

## 4.1. ADDITIONAL DEGREE OF FREEDOM INTRODUCED INTO ANGULAR-MOTION LOOP BY DISPLACEMENT OF THE CENTER OF MASS

### 4.1.A. Change in Transfer Functions

The final values of the vehicle's transfer functions, which take account of both the motion of the center of the mass and the motion about the center of mass, are given in Appendix III (see column headed "Short-Period Motion"). In the present section, we shall examine reciprocal effects between the loops describing the angular motion and the motion of the center of mass and the conditions under which their characteristics are deformed.

If we return to equation system (2.36) and confine the second equation to the steady-state relation between the elevator deflection angle $\delta_e$ and the angle of attack $\alpha$, i.e.,

$$\alpha = -\frac{M_z^{\delta_d}}{M_z^{\alpha}}\delta_d, \tag{4.1}$$

it is sufficient to use only the first equation to determine the increment in the slope angle (motion of center of mass). With this approach, the second equation of system (2.36) reflects, instead of direct coupling (4.1), an additional degree of freedom that governs the coupling between $\alpha$ and $\delta_e$ via a second-order differential equation.

If the angle of attack is expressed in terms of the angle of pitch and the trajectory slope angle in the second equation of system (2.36), and then the moments from the change in $\theta$ are combined with the elevator moment /149

$$M_{\Sigma} = M_z^{\delta_d}\delta_d - M_z^{\alpha}\Delta\theta - M_z^{\dot{\alpha}}\Delta\dot{\theta} \tag{4.2}$$

and the sum is considered to be given by program, it is sufficient to investigate the second-order equation, as was done in Chapter III, for the angular motion. In this case, the first equation of system (2.36) introduces an additional degree of freedom into the actual formation of the moment.

The change in the stationary characteristics under the additional conditions is conveniently studied on standard elements;

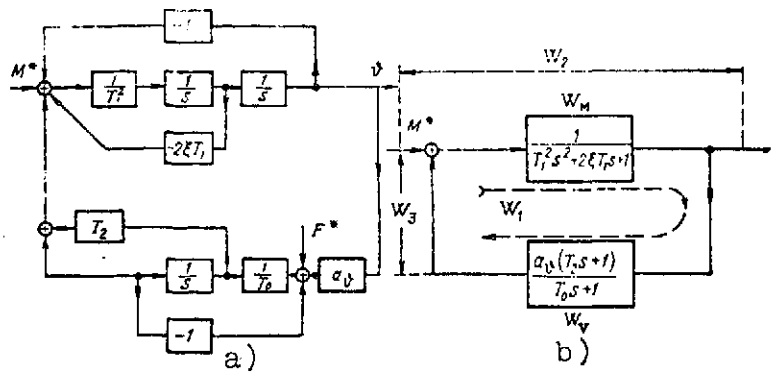


Figure 4.1. Expanded Structural Diagrams of Vehicle Longitudinal Motion. a) With disturbance in the form of a moment and a force; b) with force disturbance excluded.

for this reason, we shall rewrite Eq. (2.36) in operator form with standard coefficients, eliminating the variable $\Delta\alpha$ and the increment symbol:

$$\left.\begin{aligned}(T_0 s+1)\theta(s)&=a_\vartheta\vartheta(s)+F^*(s);\\(T_1^2s^2+2\xi T_1 s+1)\vartheta(s)&=(T_2 s+1)\theta(s)+M^*(s),\end{aligned}\right\} \qquad (4.3)$$

where

$$T_0=\frac{mV}{F_y^\alpha-F_y^\vartheta};\quad a_\vartheta=\frac{F_y^\alpha}{F_y^\alpha-F_y^\vartheta};\quad F^*=\frac{F}{F_y^\alpha-F_y^\vartheta}. \qquad (4.4)$$

These equations were used to compile the structural diagram of Fig. 4.1a, the top of which represents the vehicle's equation /15
of moments in the form of an oscillatory-element structure, while the bottom represents the equation of forces in the form of an aperiodic-element structure. We shall refer to the coupling between these elements as the major loop.

We then obtain the transfer function with respect to the input M*, and omit the force increment F*.

For an open major loop, the transfer function of the entire circuit will be

$$W_1(s)=\frac{a_\vartheta(T_2 s+1)}{(T_0 s+1)(T_1^2s^2+2\xi T_1 s+1)}. \qquad (4.5)$$

For the closed loop, with consideration of the positive sign of the feedback, we obtain a function of the form

$$W_2(s)=\frac{T_0 s+1}{T_0T_1^2s^3+\left(T_1^2+2\xi T_0T_1\right)s^2+\left(T_0+2\xi T_1-a_\phi T_2\right)s+1-a_\phi}. \qquad (4.6)$$

The dynamics of the angular motion are not affected by the equation of forces when the coefficients $a_\phi$ and $T_0$ are small.

When the relation

$$(T_1+2\xi T_0)(T_0+2\xi T_1-a_\phi T_2)\leqslant T_0T_1(1-a_\phi), \qquad (4.7)$$

which proceeds from the Hurwitz stability criterion, is satisfied, the oscillatory component in the vehicle's motion becomes non-damping, i.e., the original characteristics of the vehicle are strongly deformed. In exactly the same way, a substantial change in the characteristics and the appearance of unstable components of the motion result from a change in sign of the polynomial coefficients in the denominator of transfer function (4.6), i.e., when

$$a_\phi>1 \quad \text{or} \quad a_\phi T_2>T_0+2\xi T_1. \qquad (4.8)$$

4.1.B. Change in Frequency Characteristics

Relation (4.6) yields the gain-phase characteristic

$$W_2(j\omega)=\frac{j\omega T_0+1}{T_0T_1(j\omega)^3+\left(T_1^2+2\xi T_0T_1\right)(j\omega)^2+\left(T_0+2\xi T_1-a_\phi T_2\right)(j\omega)+1-a_\phi}. \qquad (4.9)$$

/151

From Expression (4.9), we can determine the gain-frequency characteristic

$$|W_2(j\omega)|=\sqrt{\frac{(\omega T_0)^2+1}{\left[1-a_\phi-\left(T_1+2\xi T_0\right)T_1\omega^2\right]^2+\left[\left(T_0+2\xi T_1-a_\phi T_2\right)\omega-T_0T_1\omega^3\right]^2}}. \qquad (4.10)$$

and the phase-frequency characteristic

$$\varphi_2(\omega)=\arctan\omega T_0-\arctan\frac{\left(T_0+2\xi T_1-a_\phi T_2\right)\omega-T_0T_1\omega^3}{1-a_\phi-\left(T_1^2+2\xi T_0T_1\right)\omega^2}. \qquad (4.11)$$

Instead of calculating the characteristics analytically, use may be made of the plots of the logarithmic characteristics for blocks $W_M$ and $W_C$ in Fig. 4.1b.

Let us present the closing formula (4.6) in the form

$$W_3 = \frac{1}{-W_C}\,\frac{W_M(-W_C)}{1+W_M(-W_C)} = \frac{1}{-W_C}\,\frac{-W_1}{1+(-W_1)} = \frac{1}{-W_C}\,W_3; \qquad (4.12)$$

it will then be sufficient to find the frequency characteristics of the $-W_1$ loop from the sum of the logarithmic frequency characteristics $W_M$ and $-W_C$ (the minus sign causes a 180° phase shift), use the closing nomogram (Fig. 3.14), and obtain the logarithmic frequency characteristics of the closed $W_3$ loop. To convert them to the unknown characteristics of loop $W_2$, it is necessary to subtract, in logarithmic units, the amplitude $W_C$ from $W_3$ and to add the phase $W_3$ to the phase $-1/W_C$ in accordance with (4.12).

The influence of the characteristics of the loop corresponding to the equation of forces on the frequency characteristics of the angular-motion loop (equation of moments) can be seen directly from the inverse frequency characteristic of the closed loop, which equals /15

$$\frac{1}{W_2} = \frac{1}{W_M} - W_C. \qquad (4.13)$$

If the additional term $-W_C$ yields a positive increment to the amplitude and phase of the inverse characteristic $1/W_2$, the increments of the unknown characteristic $W_2$ will have the opposite signs.

4.1.C. Root-Locus Charts

Figure 4.2a shows the structural diagram investigated previously, but without the inputs F* and M* and with an isolated coefficient $a_0$.

We introduce into the open-loop transfer function without the coefficient $a_0$ the symbol "n," which signifies normalization ($a_0 = 1$), i.e.,

$$W_{1n}(s) = \frac{T_2 s + 1}{(T_0 s + 1)\left(T_1^2 s^2 + 2\xi T_1 s + 1\right)}. \qquad (4.14)$$

The poles of this transfer function are indicated by the

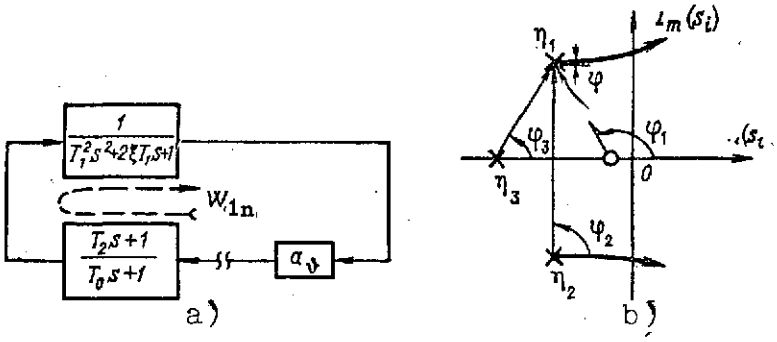


Figure 4.2. Allowance for Effect of Closing "Large Loop" (Through Equation of Forces) on Poles of Angular-Motion Transfer Function of Vehicle. a) Modified Structure (see Fig. 4.1b); b) root-locus charts plotted against coupling coefficient.

crosses in Fig. 4.2b. The two conjugate poles $\eta_1$ and $\eta_2$ coincide with the poles of $W_M$ before closing, while the third, real pole $\eta_3 = -1/T_0$ is introduced by the function $W_C$. /153

The circle in the same figure indicates the position of the zero of the operator transfer function $W_1$, i.e., $\lambda_1 = -1/T_2$.

On closing of the loop when $a_\vartheta = 0$, the poles $s_i$ of transfer function $W_3$ coincide with the poles indicated by the crosses on the figure, and then when $a_\vartheta > 0$, the poles begin to migrate, following the path known as the root locus.

We determine the angle at which the root locus emerges from point $\eta_1$ from the formula

$$\lim_{s_1 \to \eta_1} \arg(s - \eta_1) = 2\pi k - \sum_{j=1}^{m} \arg(s_1 - \lambda_j) + \sum_{i=2}^{n} \arg(s_1 - \eta_i). \qquad (4.15)$$

In the present case, the number of terms in (4.15) is determined by the orders m = 1 of the numerator and n = 3 of the denominator of transfer function $W_{1n}$. The value of the first term on the right side of the formula is governed by the positive sign of the feedback.

Connecting all poles and zeroes to the first pole with straight lines, we obtain the difference vectors that appear in the sums of formula (4.15), whose arguments are denoted by the $\phi_i$ (i = 1, 2, 3) in Fig. 4.2b.

We then obtain instead of (4.15)

$$\varphi = 0 - \varphi_1 + \varphi_2 + \varphi_3. \tag{4.16}$$

The positions of the zeroes and poles in Fig. 4.2b have been adjusted arbitrarily in such a way that the angle of emergence of the root locus (4.16) equals zero (vector $\eta_1 - \eta_2$ crosses vector $\lambda_1 - \eta_3$ at its center). The root locus beginning at point $\eta_2$ will have the same angle of emergence in virtue of symmetry.

Let us now determine the asymptote of the root locus. It has a slope that can be determined from the formula for positive feedback

$$\varphi_a = \frac{2\pi l}{n - m}, \tag{4.17}$$

i.e., we have in this case for $l$ = 2, n = 3, m = 1 /15

$$\varphi_a = \frac{4\pi}{2} = 2\pi. \tag{4.18}$$

Thus, the root loci are initially directed toward the imaginary axis. This implies that coupling via the coefficient $a_\phi$ in the equation of forces results in a decrease in the absolute value of the real parts of the transfer-function poles, i.e., the relative damping factor begins to assert itself in the characteristic of the vehicle as determined without this coupling.

Each point of the root locus corresponds to a specific value of $a_\phi$, which is determined from the positive-feedback formula:

$$a_\phi = \frac{1}{W_{\text{in}}(s_l)} = \frac{(T_0 s_l + 1)\left(T_0 s_l^2 + 2\xi T_1 s_l + 1\right)}{T_2 s_l + 1}. \tag{4.19}$$

If the root locus has already been plotted, it is sufficient to substitute the difference vectors from the particular point $s_k$ to the initial values of the poles and zeroes and apply the formula

$$a_{\phi_c} = \frac{a_n \prod_{(l)} (s_k - \eta_l)}{b_m \prod_{(j)} (s_k - \lambda_j)} \tag{4.20}$$

to key the points on the locus with values of $a_\phi$.

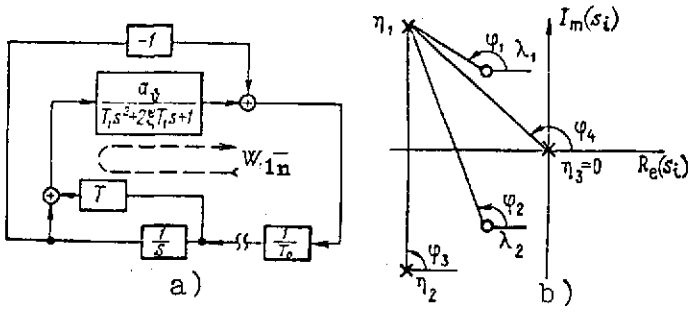


Figure 4.3. Consideration of the Influence of the Coupling Coefficient $1/T_0$ on the Poles of the Vehicle's Transfer Function. a) Structural diagram; b) root loci.

In the present case, we have in application to (4.19)

$$a_{\vartheta_k}=\frac{T_0 T_1 (s_k-\eta_1)(s_k-\eta_2)(s_k-\eta_3)}{T_2 (s_k-\lambda_1)}. \qquad (4.21)$$

Let us now investigate the dependence of the root loci on the coefficient $1/T_0$ in the equation of forces. For this purpose, we open the loop in Fig. 4.1a at the output of this coefficient and transfer the unit feedback around this coefficient to the output of the upper block as shown in Fig. 4.3a.

We determine the normalized open-loop transfer function for this structure:

$$W_{1n}(s)=\frac{\left(\frac{1}{s}+T_2\right)a_\vartheta}{T_1^2 s^2+2\xi T_1 s+1}-\frac{1}{s}= \qquad /155$$

$$=\frac{a_\vartheta(T_2 s+1)-\left(T_1^2 s^2+2\xi T_1 s+1\right)}{s\left(T_1^2 s^2+2\xi T_1 s+1\right)}. \qquad (4.22)$$

Reducing similar terms in the numerator, we have

$$W_{1n}(s)=-\frac{T_1^2 s^2+(2\xi T_1-a_\vartheta T_2)s+1-a_\vartheta}{s(T_1 s^2+2\xi T_1 s+1)}. \qquad (4.23)$$

Let us assume that the numerator of this fraction has complex roots $\lambda_1$, $\lambda_2$; then the positions of the zeroes and poles of the transfer function can be represented as seen in Fig. 4.3b.

For negative feedback, formula (4.23) has another constant term on its right-hand side, i.e.,

$$\lim_{s_1 \to \eta_1} \arg(s_1 - \eta_1) = \pi(2k-1) - \sum_{j=1}^{m} \arg(s_1 - \lambda_j) + \sum_{i=2}^{n} \arg(s_1 - \eta_i). \quad (4.24)$$

After marking out the difference vectors in Fig. 4.3b, we can calculate the angle of emergence of the root locus from point $\eta_1$ (for $1/T_0 = 0$) from the formula

$$\varphi = \pi - \varphi_1 - \varphi_2 + \varphi_3 + \varphi_4. \quad (4.25)$$

The root loci can then be graduated with values of the coefficient $1/T_0$ determined from a formula analogous to (4.19) but applying for negative feedback: /1

$$\left(\frac{1}{T_0}\right)_k = -\frac{s_k(s_k - \eta_1)(s_k - \eta_2)}{(s_k - \lambda_1)(s_k - \lambda_2)}. \quad (4.26)$$

## 4.2. ANGULAR MOTION WITH ADDITIONAL DEGREE OF FREEDOM INTRODUCED BY FIRST-HARMONIC ELASTIC OSCILLATIONS OF THE BODY

Let us present certain data on the mathematical model of an elastic element. In a complex system, all material points of a vehicle with elastic structure describe an angular and translational motion that can be represented as a combination of various harmonics. It is a rather common practice to replace a complex elastic system by a sum of linear elements with a transfer function of the form

$$W_a(s) = \frac{k_e}{s^2 + \Omega^2}, \quad (4.27)$$

where $k_e$ is the matching transfer constant and $\Omega$ is the harmonic frequency of the bending vibrations.

Vibrations in an elastic element are excited in the form of additional terms on the appearance (impression upon the input) of moment or angle increments, and the response of the elastic elements appears in the equations of moments and forces and in the angles of rotation of the vehicle's axial line. A matching transfer constant $k_e$ is chosen in accordance with the steady input and output.

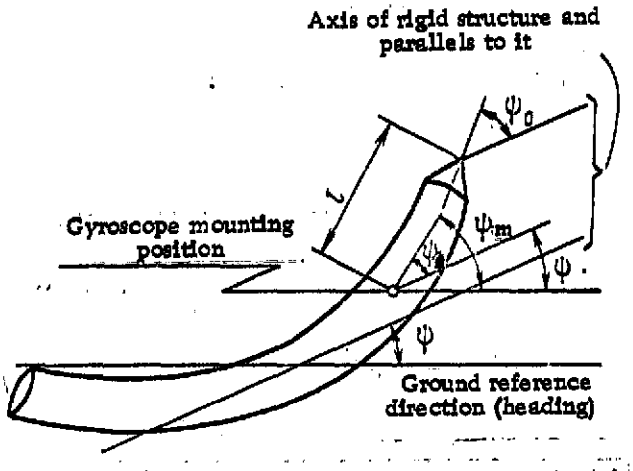


Figure 4.4. Schematic Representation of Form of First-Harmonic Elastic Vibrations in an Idealized Cylindrical Vehicle. $\psi$ is the angle of rotation of the rigid structure, $\psi_0$ is the angle of rotation of the elastic line relative to the axis of the rigid structure, measured at the nose of the vehicle; $\psi_e$ is the same angle, but measured at the position of the gyroscope; $\psi_1$ is the total angle of rotation of the elastic line, which can be measured with the automatic-stabilization system gyroscope.

Below we shall discuss only evaluation of the additional axial-line rotation-angle increment introduced by bending of the body, bearing in mind that the remaining problems are examined in the book [15]. We shall also confine ourselves to the first harmonic. We see from Fig. 4.4 that a gyroscope in the nose section measures

$$\psi_m = \psi + \psi_e. \tag{4.28}$$

When the gyroscope is mounted in the tail section, it is easy to establish that

$$\psi_m = \psi - \psi_e. \tag{4.29}$$

/157

If the part of the elastic-element transfer function (4.27) that reflects the course taken by the angular vibrations in time is written for the point corresponding to the nose of the vehicle, then it is necessary for the remaining points of the body, which have distances $l$ from the nose, to assign the function

$$\varkappa(l)=\frac{\psi_{le}}{\psi_0}, \tag{4.30}$$

which determines the sign and magnitude of the ratio of the bending angles at the arbitrary and end points.

For a selected mounting position of the angle-measuring device (gyroscope) $l$, the magnitude and sign of $\kappa(l)$ are defined, and the transfer function of the elastic element is understood to be the ratio of the transform of the response [the angle of rotation $\psi_e(s)$ of the elastic line] to the input disturbance [to the moment M(s)]:

$$W_e(s)=\frac{\psi_e(s)}{M(s)}. \tag{4.31}$$

/1

Let us now take as our base the structural diagram of the vehicle's angular motion in Fig. 3.12b and supplement it with an elastic element having the operator transfer function (4.27) for the input and output indicated in the form of (4.31). We then obtain a new structural diagram (Fig. 4.5a), on which the additional adder realizes formula (4.28) and the total angle $\phi_m$ is measured by a gyroscope in the automatic-pilot feedback $-k_{f.b}$.

Operation of the automatic pilot culminates with the development of a controlling moment at the controls that is opposite in sign and corresponds in magnitude to the disturbing moment.

Figure 4.5b repeats the preceding structural diagram (diagram "a"), except that, firstly, we have removed the adder for input of the disturbing moment, since it is not required for an investigation of the natural motion only with emphasis on stability and, secondly, we have separated an elastic-element loop with an automatic stabilizer characterized by the transfer coefficient $-k_{f.b}$, to which the element characterizing the rigid vehicle is connected in the form of a feedback. /1

It is easy to convert from diagram "b" to diagram "c" of the same figure by assigning all elements except the elastic

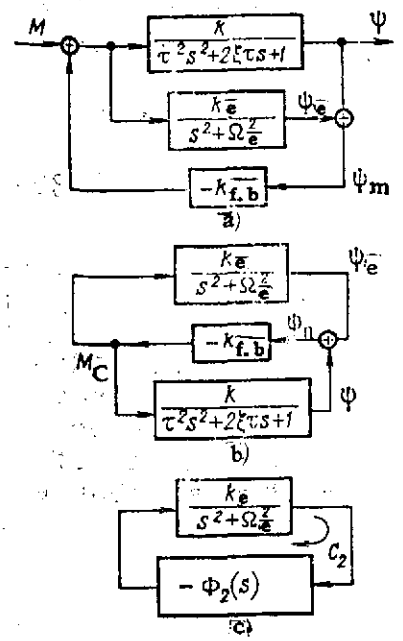


Figure 4.5. Structure of Angle-Control Loop of Vehicle With Elastic Element. a) Initial structure with elementary automatic pilot; b,c) modified structures.

element a common transfer function of the form

$$\Phi_2(s)=\frac{-k_{\overline{f.b}}}{1+\dfrac{kk_{\overline{f.b}}}{T^2s^2+2\xi Ts+1}}=$$

$$=-\frac{k_{\overline{f.b}}}{1+kk_{\overline{f.b}}}\,\frac{T^2s^2+2\xi Ts+1}{T_3s^2+2\xi_1T_3s+1}. \qquad (4.32)$$

The transfer function of the rigid vehicle closed by negative feedback across an autopilot has already been presented [see formula (3.159) for the function $\Phi_1(s)$]. Since the closing conditions remain as before in (4.32), the characteristic polynomials (denominators) in (4.32) and (3.159) are the same, so that the coefficients $T_3$ and $\xi_3$ are determined by the respective formulas (3.161) and (3.162). But since $\Phi_2(s)$ characterizes the ratio of the new transforms

$$\Phi_2(s)=\frac{M_e(s)}{\psi_e(s)}, \qquad (4.33)$$

its numerator is not the same as that of $\Phi_1(s)$ and it has a different transfer constant

$$k_2=\frac{k_{\overline{f.b}}}{1+kk_{\overline{f.b}}}. \qquad (4.34)$$

Let us carry out a stability analysis of the guided vehicle with the elastic element. For this purpose, we shall first use the Nyquist frequency criterion, in which the rotation angle of the N-vector is estimated [25].

According to this criterion, we investigate the gain-phase frequency characteristic of the entire open loop $C_2(j\omega)$ shown in Fig. 4.5c, which equals /160

$$C_2(j\omega)=\left[\Phi_2(s)\frac{k_{\overline{e}}}{s^2+\Omega_{\overline{e}}^2}\right]_{s=j\omega}=\Phi_2(j\omega)\frac{k_{\overline{e}}}{\Omega_{\overline{e}}^2-\omega^2}. \qquad (4.35)$$

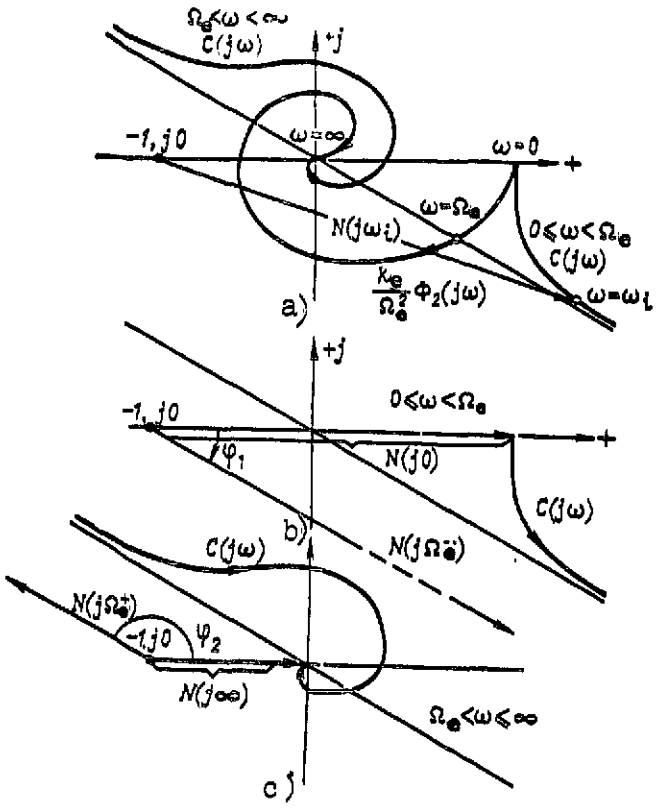


Figure 4.6. Gain-Phase Characteristics of Vehicle's Angle-Control Loop Opened at Elastic Element. a) Characteristics of Guided vehicle $\Phi_2$ and loop C with elastic element according to structure of Fig. 4.5c; b) excerpted segment of loop frequency characteristic for calculation of vector rotation angle as far as point of discontinuity; c) same, beyond point of discontinuity (when the frequencies of the elastic vibrations are on the segment of the GPC in the lower half of the complex plane).

The formulation of the closed-system frequency criterion of stability depends on the nature of the poles of its open-loop transfer function.

Let us assume that the function $\Phi_2(s)$ that appears in the loop formula (4.35) has all poles situated in the left half of the complex plane. The second cofactor in this same formula (4.33) is written in expanded form and has two poles $s_{1,2} = \pm j\Omega_e$ situated on the imaginary axis, i.e., two so-called

neutral poles.

Stability requires the argument increment

$$\left.\begin{aligned}\Delta \arg N(j\omega) = \Delta\varphi_N = 2\frac{\pi}{2} = \pi.\\ 0 \leqslant \omega \leqslant \infty\end{aligned}\right\} \qquad (4.36)$$

Figure 4.6a is a plot of the gain-phase characteristic C(jω). The construction was carried out in two steps:

– construction of the hodograph of the function $\frac{k_e}{\Omega_e^2}\Phi_2(j\omega)$ in a form that is arbitrary for general validity of the conclusions;

– multiplication of each vector of this hodograph by the scalar $W_{e.n}(\omega) = \frac{\Omega_e^2}{\Omega_e^2 - \omega^2}$ in accordance with formula (4.35).

At point ω = 0, we have $W_{e.n}(0) = 1$, and the hodograph of C(jω) coincides with that of $\frac{k_e}{\Omega_e^2}\Phi_2(j\omega)$. At point ω → ∞, we shall have $W_{e.n}(\omega) \to -C$; here the amplitude decrease is inversely proportional to the square of the frequency, so that the terminal segment of the hodograph of C(jω) is opposite in sign to the initial segment of the GPC $\frac{k_e}{\Omega_e^2}\Phi_2(j\omega)$ and approaches zero more rapidly. At the point $\omega = \Omega_e$, the hodograph of C(jω) has a discontinuity, so that it is necessary to examine the segments of the hodograph before and after the point of discontinuity. We denote

$$\Omega_{e-} = \lim_{\Delta\omega \to 0}(\Omega_e - \Delta\omega) \qquad (4.37)$$

and /162

$$\Omega_{e+} = \lim_{\Delta\omega \to 0}(\Omega_e + \Delta\omega), \qquad (4.38)$$

then

$$C(j\Omega_{e-}) = +\infty\frac{k_e}{\Omega_e^2}\Phi_2(j\Omega_e), \qquad (4.39)$$

i.e., the asymptote for this point of the hodograph is a semi-infinite straight line drawn from the origin through the point $\frac{k_e}{\Omega_e^2}\Omega_2(j\Omega_e)$. Figure 4.6b shows the entire segment of the C(jω)

hodograph for variation of the frequency in the range $0 \leqslant \omega < \Omega_e$.

The hodograph for frequencies in the range $\Omega_e < \omega \leqslant \infty$ appears in Fig. 4.6c, where the value of the vector at the point of discontinuity is

$$C(j\Omega_e+) = -\frac{k_e}{\Omega_e^2}\Omega_2(j\Omega_e). \tag{4.40}$$

The asymptote for this vector is a semiinfinite line drawn from the same point $\frac{k_e}{\Omega_e^2}\Phi_2(j\omega)$ through the origin.

The point $-1$, $j0$ on the left half of the real axis is the origin of the vector $N(j\omega)$, which ends on the $C(j\omega)$ hodograph. Figure 4.6a shows the vector for the frequency $\omega = \omega_1$, i.e., $N(j\omega_1)$. To find the increment of the argument of the N-vector and compare it with (4.36) for the discontinuous GPC, it is necessary to make separate measurements for the increments of the argument $\phi_1$ before the discontinuity and the argument $\phi_2$ after the discontinuity and add them [25].

We have from Fig. 4.6b

$$\varphi_1 = \arg N(j\Omega_e-) - \arg N(j0), \tag{4.41}$$

and it follows from Fig. 4.6c that

$$\varphi_2 = \arg N(j\infty) - \arg N(j\Omega_e+) = -\pi - \varphi_1, \tag{4.42}$$

from which we obtain the sum

$$\Delta \arg N(j\omega) = \varphi_1 + \varphi_2 = -\pi = -2\frac{\pi}{2}.$$

For this particular form of the hodograph and for the case in which the point $\omega = \Omega_e$ lies in the lower half of the complex plane, the N-vector has rotated through minus two quadrants, since both of the terms $\phi_1$ and $\phi_2$ are negative. Consequently, condition (4.36) is not satisfied and the system is unstable, i.e., the elastic oscillations sensed by the autopilot's measuring gyroscope are then converted to moment increments at the controls that increase them instead of stabilizing them.

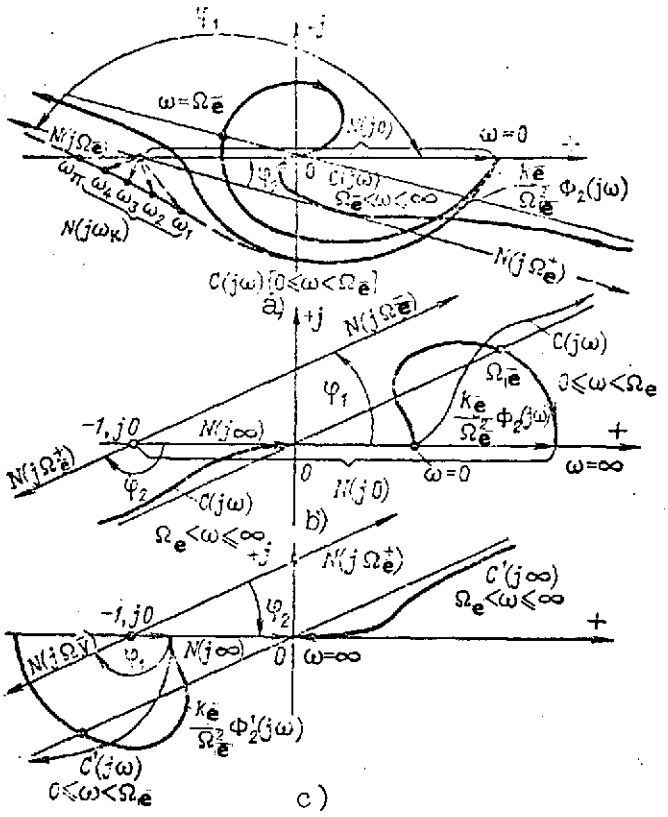


Figure 4.7. Gain-Phase Frequency Characteristics of Open Loop with Elastic Element and the Following Features: a) Frequency of elastic oscillations on segment of GPC in upper half of complex plane; b) same, but GPC $\Phi_2$ entirely within the first quadrant; c) GPC $\Phi_2$ entirely within the third quadrant due to change in position of gyroscope in the vehicle.

Let us now consider the case in which the point $\omega = \Omega_e$ on the hodograph of $\Phi_2(j\omega)$ lies in the upper half of the complex plane (Fig. 4.7a). Drawing an infinite straight line through this point and the origin, we obtain an asymptote to which the following vectors are parallel: $N(j\Omega_e-)$ in the upper half-plane and $N(j\Omega_e+)$ in the lower half-plane. Calculating the increment of the argument of the N-vector (Fig. 4.7a), we obtain

– for the zone $0 \leqslant \omega < \Omega_e$:

$$\varphi_1 = \arg N(j\Omega_y -) - \arg N(j0) > 0; \tag{4.43}$$

– for the zone $\Omega_e < \omega \leqslant \infty$:

$$\varphi_2 = \arg N(j\infty) - \arg N(j\Omega +) = +\pi - \varphi_1. \tag{4.44}$$

The sum of the angles is

$$\Delta \arg N(j\omega) = \varphi_1 + \varphi_2 = +\pi = +2\,\frac{\pi}{2} \tag{4.45}$$

and satisfies condition (4.36).

Thus, for a system that is stable without the elastic element, the transfer function $\Phi_2(s)$ has all poles in the left half-plane. Closing of its loop by a negative feedback across the elastic element does not disturb the stability conditions if the frequency of the elastic oscillations on the hodograph of $\Phi_2(j\omega)$ lies on the segment occupying the upper half-plane. This condition can be written analytically in the form

$$\begin{aligned} &\operatorname{Im} \Phi_2(j\Omega_y) > 0, \text{ or} \\ &0 < \arg \Phi_2(j\Omega_e) < \pi. \end{aligned} \tag{4.46}$$

This is a necessary but insufficient stability condition for the present system with an elastic element. In fact, if the $C(j\omega)$ hodograph crosses the negative real semiaxis to the left of the point $-1$, j0 (see dashed lines on Fig. 4.7a), i.e., if the modulus of the N-vector is greater than unity at the frequency of intersection of the real axis denoted by $\omega_\pi$, then the new increment to the argument on segment $0 \leqslant \omega < \Omega_e$ will be

$$\varphi_1' = -2\pi + \varphi_1, \tag{4.47}$$

and the sum of the increments

$$\Delta \arg N'(j\omega) = \varphi_1' + \varphi_2 = -\pi \tag{4.48}$$

will not satisfy condition (4.36). /165

Changes in the magnitude and sign of $\phi_1'$ result from the new conditions of motion of the N-vector along the $C(j\omega)$ hodograph. We see from the vectors $N(j\omega_k)$ $(k = 1, 2, 3, 4 \ldots)$ indicated on the figure around the point $-1$, j0 that the N-vector rotates in the negative direction.

Thus, the necessary and sufficient stability conditions are

the phase condition (4.46) and the amplitude condition

$$|C(j\omega_\pi)|<1, \tag{4.49}$$

which is formulated as failure of the C(jω) hodograph to bracket the point −1, j0. If $\Phi_2(s)$ is considered not in general form, but in its specific form (4.32), then the hodograph of $\frac{k_e}{\Omega_e^2}\Phi_2(j\omega)$ will assume the form shown in Fig. 4.7b. The terminal segments of the hodograph are determined by limit transitions in (4.32), i.e.,

$$\frac{k_e}{\Omega_e^2}\Phi_2(j0)=\frac{k_e}{\Omega_e^2}\lim_{\omega\to 0}\Phi_2(j\omega)=\frac{k_e k_{1.b}}{(1+k_e k_{1.y})\Omega_e^2}, \tag{4.50}$$

$$\frac{k_e}{\Omega_e^2}\Phi(j\infty)=\frac{k_e k_{1.b}}{\Omega_e^2}; \tag{4.51}$$

The GPC lies entirely in the first quadrant. In this case, as before, we mark the point on the hodograph with the frequency $\omega = \Omega_e$, draw the asymptote and construct the segments of the C(jω) hodograph for the frequency ranges before and after $\Omega_e$. Such constructions are indicated on the same figure and permit calculation of the increment to the N-vector argument:

$$\varphi_1=\arg N(j\Omega_e-)-\arg N(j0)>0, \tag{4.52}$$

$$\varphi_2=\arg N(j\infty)-\arg N(j\Omega_e+)=+\pi-\varphi_1. \tag{4.53}$$

This is followed by determination of the sum

$$\Delta\arg N(j\omega)=\varphi_1+\varphi_2=+\pi=2\frac{\pi}{2}. \tag{4.54}$$

The sum satisfies condition (4.36), and the vehicle's angular-control loop with negative feedback across the elastic element is always stable. However, in accordance with Fig. 4.4 and formula (4.30), the sign of the negative feedback through the elastic element depends on the position of the measuring gyroscope along the elastic axis of the structure. The gyroscope becomes most sensitive at the nodal points; when it is transferred from one node to another, the sign of $k_e$ changes and the loop shown in Fig. 4.5b becomes a positive rather than a negative feedback loop as a result of the two sign reversals in $\Phi_2(s)$ and $k_e$. /166

Since the entire preceding stability analysis and the formulation of the frequency stability criterion were oriented to the case of negative feedback in the loop, the simplest approach is to reduce the positive feedback loop to the same case. For this it is sufficient to consider, instead of the element

$\Phi_2(s)$, another element $\Phi_2'(s)$ with the opposite sign, i.e.,

$$\Phi_2'(s) = -\Phi_2(s). \tag{4.55}$$

Then element $\Phi_2'(s)$ is covered by the negative feedback through the elastic element.

In Fig. 4.7c, we have constructed a hodograph of $\frac{k_{\bar{e}}}{\Omega_{\bar{e}}^2}\Phi_2'(j\omega)$ simply by changing the signs of all vectors of the $\frac{k_{\bar{e}}}{\Omega_{\bar{e}}^2}\Phi_2(j\omega)$ hodograph of Fig. 4.7b. Since the $\frac{k_{\bar{e}}}{\Omega_{\bar{e}}^2}\Phi_2'(j\omega)$ hodograph was entirely within the third quadrant (lower half of the complex plane), the necessary condition (4.46) is not satisfied and the system is always unstable. This also seen from Fig. 4.7c, where the increments to the N-vector argument are both negative and their sum is

$$\varphi_1 + \varphi_2 = -\pi. \tag{4.56}$$

We note that the more general hodograph of $\Phi_2(j\omega)$ in Fig. 4.6a will, after the sign change, have segments in both the lower and upper half-planes. Thus elastic oscillation frequencies at which the system as a whole is stable exist for it even when the sign of $k_e$ changes. /16

In many of the cases examined above, therefore, the vehicle has the potential capability of retaining stability even when secondary bending vibrations of the body make their appearance. In these cases, the stabilization is due to a favorable phase relation in the loop, which results in a response of the controls such that moments that tend to cancel the bending oscillations are applied to the body.

Cases in which condition (4.49) is not satisfied call for a change in the amplitude relations that reduces to a decrease in the gain of the loop containing the elastic element.

Let us consider one more potentially possible way of stabilizing elastic oscillations that is offered by the controlled aerospace vehicle. Let the vehicle have no aerodynamic damping ($\xi = 0$), and let the role of this damping be taken by a transient feedback in the autopilot (see Fig. 3.11c). Then

$$k_{f.b}(s) = k_{f.b} + T_{f.b}s \tag{4.57}$$

must be substituted for $k_{f.b}$ in (4.32), and the vehicle's W(s) must be replaced by the new transfer function

$$W(s)=\frac{k}{\tau^2 s^2+1}, \tag{4.58}$$

which gives

$$-\Phi_2(s)=\frac{k\overline{k_{f.b}}+T_{f.b}s}{1+\dfrac{kk\overline{k_{f.b}}+kT\overline{k_{f.b}}s}{\tau^2 s^2+1}}=\frac{(k\overline{k_{f.b}}+T_{f.b}s)(\tau^2 s^2+1)}{\tau^2 s^2+kT\overline{k_{f.b}}s+1+kk_{f.b}}=$$
$$=\frac{k\overline{k_{f.b}}}{1+kk_{f.b}}\cdot\frac{(1+Ts)(1+\tau^2 s^2)}{T_3^2 s^2+2\xi_3 T_3 s+1}. \tag{4.59}$$

here

$$\left.\begin{aligned} T'&=\frac{T_{f.b}}{k_{f.b}},\\ T_3&=\frac{\tau}{\sqrt{1+kk\overline{k_{f.b}}}},\\ \xi_3&=\frac{kT_{f.b}}{2T'\sqrt{1+kk_{f.b}}}. \end{aligned}\right\} \tag{4.60}$$

We now determine the transfer function of the entire open loop shown in Fig. 4.5c: /168

$$C(s)=\frac{k_e k_{f.b}}{1+kk_{f.b}}\cdot\frac{(1+Ts)(1+\tau^2 s^2)}{(T_3^2 s^2+2\xi_3 T_3 s+1)(s^2+\Omega_e^2)}. \tag{4.61}$$

We denote

$$k_*=\frac{k_e k_{f.b}}{(1+kk_{f.b})\Omega_{ie}^2} \tag{4.62}$$

and

$$\Omega_n=\frac{1}{\tau}. \tag{4.63}$$

Then relation (4.61) becomes

$$C(s)=\frac{k_*(1+Ts)(s^2+\Omega_n^2)\Omega_{ie}^2}{\Omega_n^2(T_3^2 s^2+2\xi_3 T_3 s+1)(s^2+\Omega_e^2)}=\frac{U(s)}{V(s)}. \tag{4.64}$$

Here $\Omega_n$ is the frequency of the vehicle's natural undamped vibrations as an ideal rigid body.

Let us investigate analytically the stability of the loop closed by negative feedback with the transfer function of the entire open loop (4.64). For this purpose, it is sufficient to write the characteristic polynomial

$$U(s)+V(s)=\Omega_n^2\left\{T_{s1}^2s^4+\left[2\xi_sT_s+\left(\frac{\Omega_e}{\Omega_n}\right)^2k_vT\right]s^3+\right.$$
$$\left.+\left[T_{s1}^2\Omega_e^2+1+\left(\frac{\Omega_e}{\Omega_n}\right)^2k_v\right]s^2+(2\xi_sT_s+k_vT)\Omega_e^2s+(1+k_v)\Omega_e^2\right\}. \quad (4.65)$$

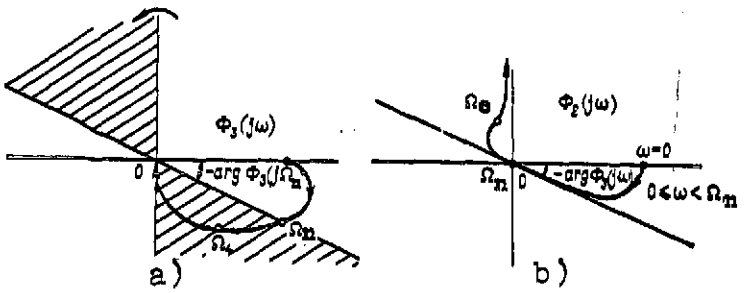


Figure 4.8. GPC's of Undamped Vehicle in Loop Closed by Forcing Autopilot. a) First stage in construction of GPC marked with natural and elastic vibration frequencies; b) second stage in construction of GPC from complete formula.

For simplicity in the notation, we cancel the terms containing T and use this polynomial to write the next-to-last Hurwitz determinant [26]:

$$\Delta_3=4\xi_s^2T_s^2\begin{vmatrix}1 & T_s^2 & 0\\ \Omega_e^2 & 1+T_s^2\Omega_e^2+\left(\frac{\Omega_e}{\Omega_c}\right)^2k_v & 1\\ 0 & (1+k_c)\Omega_e^2 & \Omega_y^2\end{vmatrix}=$$
$$=4\xi_s^2T_s^2\Omega_e^2k_v\left[\left(\frac{\Omega_e}{\Omega_n}\right)^2-1\right]. \quad (4.66)$$

According to the Hurwitz criterion, it is sufficient to satisfy the condition /16

$$\Omega_n<\Omega_e \quad (4.67)$$

for the determinant of (4.66) to be positive, i.e., the frequency of the rigid-vehicle natural vibrations must be smaller than the frequency of the elastic vibrations, which is usually the case.

The fact that the elastic vibrations can potentially be stabilized in this way is easily explained with reference to the frequency characteristics. Figure 4.8 is a plot of the GPC of the function

$$\Phi_3(s)=\frac{1+Ts}{T_3^2s^2+2\xi_3T_3s+1}, \qquad (4.68)$$

which differs from the function $\Phi_2(s)$ by the cofactor $1+\tau^2s^2=\frac{\Omega_n^2+s^2}{\Omega_n^2}$ in the numerator of the fraction in (4.59). Since the denominator of function (4.68) is of order one higher than its numerator, the entire hodograph is situated, as a rule, in the fourth quadrant. The points $\omega = \Omega_n$ and $\omega = \Omega_e$ are marked on the hodograph.

It is easy to convert from the hodograph of $\Phi_3(j\omega)$ to that of $\Phi_2(j\omega)$. Indeed, the cofactor

$$\left[\frac{\Omega_n^2+s^2}{\Omega_n^2}\right]_{s=j\omega}=\frac{\Omega_n^2-\omega^2}{\Omega_n^2} \qquad (4.69)$$

causes the entire function to vanish at the frequency $\omega = \Omega_n$: /170
$\Phi_2(j\Omega_n) = 0$, where the tangent to the hodograph at the coordinate origin has the slope

$$\arg \Phi_3(j\Omega_n).$$

It is indicated in Fig. 4.8b that the segment of the hodograph for the frequency range $0 \leq \omega < \Omega_n$ is oriented along the tangent whose direction has been transferred from Fig. 4.8a near $\Omega_n$, where the characteristic passes through zero.

For the segment of the hodograph in the frequency range $\Omega_n < \omega \leq \infty$, because the numerator of (4.59) has a higher order than the denominator, the absolute value of the fraction increases without limit, and the sign change of the cofactor of (4.69) for $\omega > \Omega_n$ transfers this entire segment of the hodograph from the lower shaded sector in Fig. 4.8a into the upper sector.

It now becomes clear that when condition (4.67) is satisfied, the point with frequency $\omega = \Omega_e$ falls on the segment of the hodograph in the upper half of the complex plane – a necessary stability condition, as follows from the constructions given in Fig. 4.7. The same condition (4.67) is sufficient for this type of hodograph, since its intersection with the real axis occurs at zero absolute magnitude, and the amplitude limitation (4.49) is unconditionally satisfied.

## 4.3. CONSIDERATION OF EFFECTS OF SEVERAL ELASTIC-VIBRATION HARMONICS ON STABILIZATION CONDITIONS

We shall use a formula analogous to (4.27) to take account of additional elastic-vibration harmonics:

$$W_{e\,i}(s)=\frac{k_i}{s^2+\Omega_i^2}=\frac{\psi_i(s)}{M(s)}. \qquad (4.70)$$

Here i is the number of the harmonic, $\Omega_i$ is the bending-vibration frequency of the harmonic under investigation, $\psi_i$ is the additional angle introduced by the vibrations of this harmonic in the gyroscope readings, and $k_i$ is a coupling coefficient whose magnitude and sign are determined by the conditions of harmonic analysis of the elastic vibrations at the mounting position of the gyroscope.

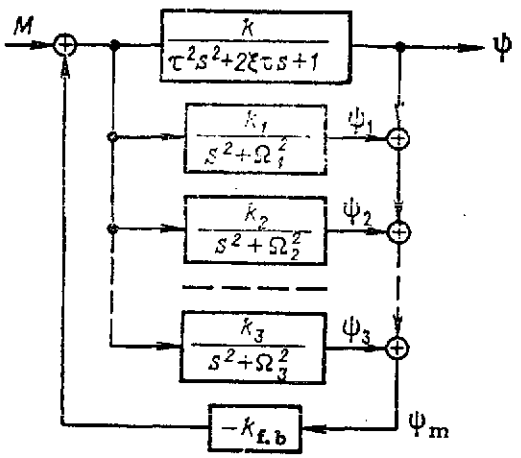


Figure 4.9. Structural Diagram of Guided Aerospace Vehicle with Elastic Elements of Several Harmonics.

The angle measured by the gyroscope in the presence of several harmonics is /17

$$\psi_m=\psi+\sum_{i=1}^{n}\psi_i. \qquad (4.71)$$

The angular-stabilization structure of the vehicle has been constructed in Fig. 4.9 in accordance with (4.70) and (4.71); it is a development of Fig. 4.5a.

It is convenient for the analysis to replace the concurrent-parallel elastic elements by a single composite elastic element whose transfer function is determined from the formula

$$W_e(s)=\sum_{i=1}^{n}\frac{k_i}{s^2+\Omega_i^2}=\frac{U(s^2)}{V(s^2)}=\frac{k_1(s^2+\Omega_2^2)\dots(s^2+\Omega_n^2)+k_2(s^2+\Omega_1^2)(s^2+\Omega_3^2)\dots}{(s^2+\Omega_1^2)(s^2+\Omega_2^2)\dots}$$

$$\frac{\dots(s^2+\Omega_n^2)+\dots+k_n(s^2+\Omega_1^2)\dots(s^2+\Omega_{n-1}^2)}{\dots(s^2+\Omega_n^2)} \qquad (4.72)$$

We then substitute $s^2 = p$ in the numerator polynomial $U(s^2)$ and reduce the polynomial to the form /1

$$\left.\begin{aligned} U(p)&=A_{n-1}p^{n-1}+A_{n-2}p^{n-2}+\ldots+A_1p+A_0,\\ A_{n-1}&=\sum_{i=1}^{n}k_i\\ &\cdots\cdots\cdots\\ A_0&=\sum_{i=1}^{n}\Omega_1\Omega_2\ldots\Omega_{i-1}k_i\Omega_{i+1}\ldots\Omega_{n-1}\Omega_n. \end{aligned}\right\} \quad (4.73)$$

where

From the condition

$$U(p_l)=0 \quad (4.74)$$

we find the roots of this polynomial:

$$p_1, p_2, \ldots, p_{n-1},$$

and we can then write instead of (4.72)

$$W_{\text{e}}(s)=\frac{k_l\prod_{l=1}^{n-1}(s^2-p_l)}{\prod_{m=1}^{n}(s^2+\Omega_m^2)}. \quad (4.75)$$

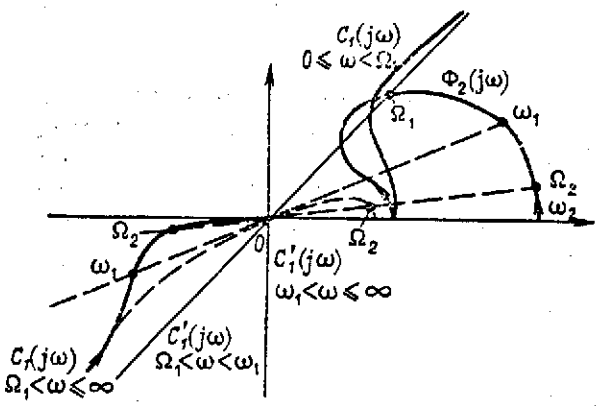


Figure 4.10. Construction of GPC of Guided Vehicle with Several Elastic-Vibration Harmonics.

If the roots $p_l$ are real and negative, we can make the substitution

$$-p_l=\omega_l^2. \quad (4.76)$$

Then (4.75) is brought to the form

$$W_{\text{e}}(s)=k_l\frac{\prod_{l=1}^{n-1}(s^2+\omega_l^2)}{\prod_{m=1}^{n}(s^2+\Omega_m^2)}. \quad (4.77)$$

This element is closed by the feedback loop with $\Phi_2(s)$, whose GPC is shown in Fig. 4.7b and repeated in Fig. 4.10.

We mark the points with frequencies $\Omega_1$, $\omega_1, \Omega_2, \omega_2, \ldots$ on this hodograph. Figure 4.10 examines the case in which these frequencies alternate, i.e.,

$$\Omega_1 < \omega_1 < \Omega_2 < \omega_2 < \Omega_3 \ldots$$ /173

We shall convert to the hodograph corresponding to the complete open-loop transfer function

$$C(s) = \Phi_2(s)\, k_l \frac{\prod_{l=1}^{n-1} (s^2 + \omega_l^2)}{\prod_{m=1}^{n} (s^2 + \Omega_m^2)}, \qquad (4.78)$$

and, finally, estimate stability by steps.

As the first step, we construct the hodograph with only one of the cofactors in (4.78), i.e.,

$$C_1(s) = \Phi_2(s) \frac{k_1}{s^2 + \Omega_1^2}. \qquad (4.79)$$

This construction has been carried out in Fig. 4.10 and was discussed previously with the aid of division into the frequency zones before and after $\Omega_1$. We then mark the points with frequencies $\omega_1$, $\Omega_2$, ... on the second segment of the hodograph.

On the basis of the criteria considered above, the elastic vibrations are stabilized in the $C_1(s)$ loop. We now go over to the loop

$$C_2(s) = C_1(s) \frac{k_2}{s^2 + \Omega_2^2}. \qquad (4.80)$$

On the hodograph of $C_1(j\omega)$, the point with frequency $\Omega_2$ lies in /174 the lower half of the complex plane; therefore a system with two elastic-vibration harmonics, having a transfer function of the form (4.80), is unstable.

But before drawing this conclusion, let us consider a $C_1'(s)$ complicated by one of the cofactors in the numerator of the fraction in (4.78), namely:

$$C_1'(s) = C_1(s)(s^2 + \omega_1^2). \qquad (4.81)$$

The additional cofactor moves the hodograph to the coordinate origin, and the segment for frequencies $\omega_1 < \omega \leq \infty$ falls in the first quadrant, i.e., in the upper half-plane.

Now for the loop with the function

$$C_2'(s) = C_1'(s) \frac{k_2}{s^2 + \Omega_2^2}. \qquad (4.82)$$

we have prepared the segment of the hodograph indicated in Fig. 4.10 by the dashed line; the point with frequency $\omega = \Omega_2$ lies on this segment, and since it is in the upper half-plane, the second-harmonic vibrations are stabilized.

Thus, the fortunately placed zeroes in the transfer function of the combined elastic element (4.77), which alternate with poles of the same function, can preserve the stability of the controlled vehicle in the presence of elastic structural vibrations of several harmonics.

The condition for alternation of the zeroes and poles

$$\Omega_1 < \omega_1 < \Omega_2 < \omega_2 < \Omega_3 \ldots, \tag{4.83}$$

which is necessary to ensure stability, conforms rigorously to the theoretical premises of the gain-phase criterion. Indeed, each pair of neutral poles in the open-loop transfer function it is necessary for a stable system that the vector turn through a positive angle $\pi$ [see formula (4.36)], while an increment n times larger in the N-vector argument is required for a formula of the type (4.78), i.e.,

$$\Delta \arg N(j\omega) = n\pi. \tag{4.84}$$

These increments of the N-vector argument, which are necessary for stability, are, so to speak, generated automatically by the discontinuity conditions of the GPC as the N-vector slides along the hodograph from the direction of the positive real semiaxis to the direction $\arg\Phi_2(j\Omega_1)$ and from the direction $-\arg\Phi_2(j\Omega_1)$ to the direction of the positive real semiaxis with observance of the amplitude conditions of stabilization (4.49) and when the segment of the hodograph with frequency $\Omega_1$ lies in the upper half of the complex plane. And this comes about each time the hodograph passes through a point with frequency $\omega_1$, where the GPC contracts to zero and changes sign. /175

## 4.4. CHARACTERISTICS OF LIQUID-LOAD OSCILLATIONS

To take account of oscillations of the liquids in the tanks, a single generalized input coordinate is introduced for the oscillatory system; it is denoted in Fig. 4.11 and in the formulas that follow by $r_1$, where i is the number of the tank in which the oscillations are being investigated.

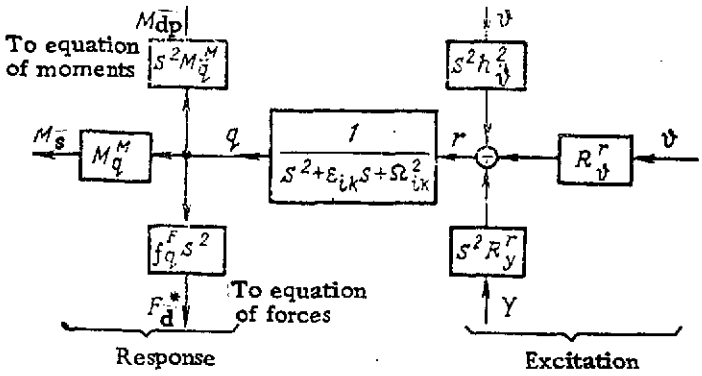


Figure 4.11. Block Diagram Taking Account of Liquid Oscillations in the Vehicle's Tanks. $M_{\dot{q}}^{M}$ is the dynamic moment coefficient; $M_{q}^{M}$ is the static moment coefficient, $f_{q}^{F}$ is the dynamic force coefficient, $R_{\dot{\vartheta}}^{r}$ is the coefficient for a dynamic input proportional to the angular acceleration in pitch $(\ddot{\vartheta})$; $R_{\vartheta}^{r}$ is the coefficient for a static input proportional to $\vartheta$; $R_{\dot{y}}^{r}$ is the coefficient for a dynamic input proportional to the linear acceleration in the vertical plane.

The following coefficients must be assigned for this coordinate: /1

$$\varepsilon_{\nu},\ \Omega_{\nu},\ k_{\nu},\ R_{\nu\dot{y}},\ R_{\nu\ddot{\vartheta}},\ R_{\nu\dot{\vartheta}},\ R_{\nu z},\ R_{\nu},\ R_{\nu\dot{r}}.$$

As was indicated in Sec. 2.3, the generalized output coordinate $g_{ik}$ (k is the number of the liquid-oscillation harmonic) satisfies an equation of the form

$$\ddot{q}+\varepsilon\dot{q}+\Omega^{2}q=R_{\dot{\vartheta}}^{r}\ddot{\vartheta}+R_{\vartheta}^{r}\vartheta+R_{\dot{y}}^{r}\ddot{y}. \qquad (4.85)$$

The discussion that follows, which treats certain problems of the influence of liquid tank loads on the dynamics of the vehicle, will be based in this chapter on the assigned equation of the liquid oscillatory system (4.85) and the corresponding structural diagram, which appears in Fig. 4.11. The center of this diagram is occupied by the transfer function of the liquid oscillatory system, which is defined as the ratio of the transforms of the generalized response q(s) and the generalized input r(s), i.e.,

$$W_{\text{liq}}(s)=\frac{q(s)}{r(s)}=\frac{1}{s^2+\varepsilon s+\Omega^2}. \qquad (4.86)$$

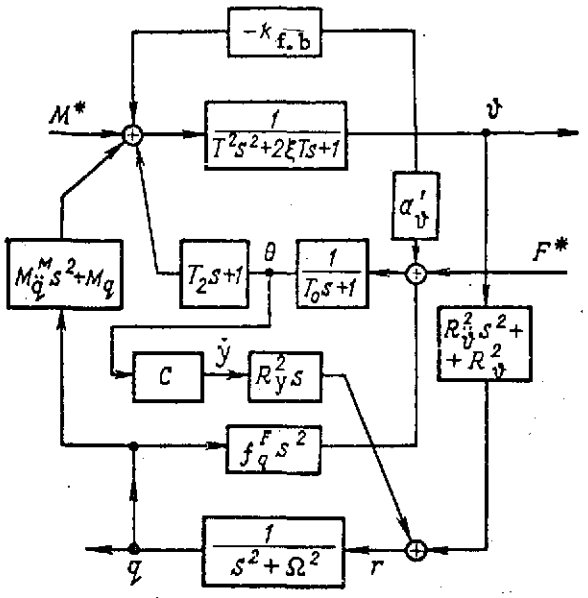


Figure 4.12. Expanded Longitudinal-Motion Structural Diagram of Guided Vehicle with Consideration of One Harmonic of Liquid-Load Oscillations.

The coefficient ε at the first power of s in the denominator of (4.85) ensures damping of the oscillations and is governed by the mutual friction between liquid particles, but principally by the provision of additional baffles with small perforations in the tanks. Since this increases weight, damping of liquid oscillations is often made the function of an automatic stabilizing device. Then the equation of the object itself, if ε = 0 is simplified to

$$W_{\text{liq}}(s)=\frac{1}{s^2+\Omega^2_{ik}}, \qquad (4.87)$$

where $\Omega_{ik}$ is the k-th harmonic frequency of the liquid-load oscillations in the i-th tank.

In Fig. 4.12, this element has been made part of the over-all structural diagram of the vehicle. This diagram was based on Eqs. (4.3), in which the angle θ was replaced by the coordinate ẏ, which is related to it by $\dot y=V(t)\sin\theta$. For small increments, we have from Δθ and ΔV

$$\Delta\dot y=V(t)\cos\theta(t)\,\Delta\theta+\Delta V(t)\sin\theta(t)=c(t)\,\Delta\theta+\nu(t). \qquad (4.88)$$

For the program-assigned values of V(t) and θ(t) about which the controlled process takes place and given values of ΔV(t), the product Vcosθ can be included in the common coefficient c(t), and $\Delta V(t)\sin\theta(t)$ can be replaced by the function ν(t) as indicated in the right member of (4.88). Thereafter, c(t) is regarded as an assigned time function, and this function is "frozen" at specific seconds in the analysis of the liquid-load oscillations, which are rapid by comparison with c(t). As an added assigned input, the function ν(t) will henceforth be omitted in the stability analysis. The coefficients in the basic equations are fixed in similar fashion, and after conversion to the increments the equations can be

/177

rewritten in operator form:

$$\left.\begin{aligned}
&(T_1^2 s^2 + 2\xi T_1 s + 1)\,\vartheta(s) = (T_2 s + 1)\,\theta(s) + \\
&\quad + (M_q^{M'} s^2 + M_q^{M'})\,q(s) + M^*; \\
&(T_0 s + 1)\,\theta(s) = a_0^{\vartheta}\,\vartheta(s) + f_q^F s^2 q(s) + F^*; \\
&(s^2 + \Omega^2)\,q(s) = (R_\theta^r s^2 + R_0^r)\,\theta(s) + R_y^r s^2 y(s) = \\
&\quad = R_y^r c s\theta(s) + (R_\theta^r s^2 + R_0^r)\,\vartheta(s); \\
&s y(s) = c\theta(s).
\end{aligned}\right\} \qquad (4.89)$$

The last equation of system (4.89), which agrees with (4.88) after elimination of the increment symbol and the disturbance $\vartheta$, can be taken into account if interest attaches to a separate investigation of the behavior of the y-coordinate and can be omitted if, as was done in the right member of the third equation of (4.89), a conversion is made to the direct dependence of the input on $\theta$.

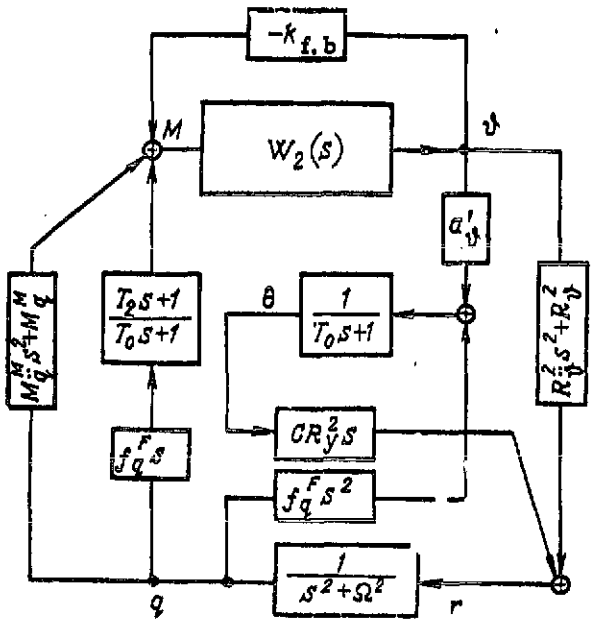


Figure 4.13. First Step in Transformation of Structure of Fig. 4.12.

Figure 4.12 repeats the dynamic structural diagram for the vehicle's motion in the vertical plane as it appeared in Fig. 4.11, except that the transfer function $W_C(s)$ has been divided into two elements corresponding to the denominator and numerator of the fraction $W_C(s)$. For this reason, $\theta$ is indicated in the diagram after the function $1/(T_0 s + 1)$, and the signal $\dot\vartheta$ is shaped after multiplication by the coefficient c. The coordinates y and $\vartheta$ are the input disturbances for the liquid oscillatory element, and this makes it easy to introduce this element into the structure under consideration and to apply its response q via the appropriate coefficients to the adders in the partial structures based on the equations of moments and forces.

In Fig. 4.13, we have eliminated the force and moment input disturbances, since we propose to consider only problems of stability, for which the inputs are omitted in a linear analysis.

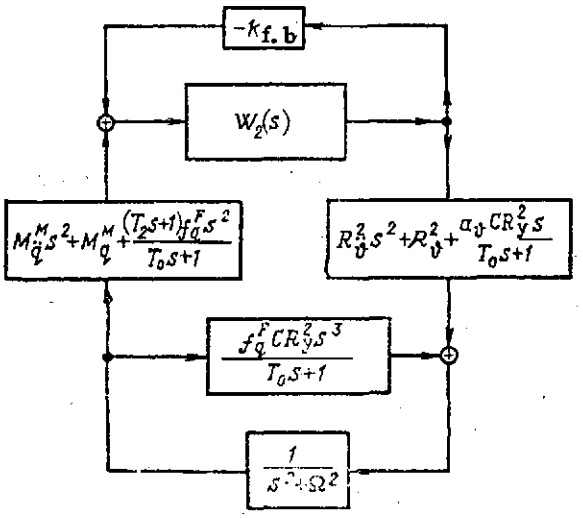


Figure 4.14. Second Step in Transformation of Structure of Fig. 4.12.

Figure 4.13 is further simplified by elimination of the cross couplings present in the structure. For this purpose, each term participating in formation of the quantity θ is also brought to the generalized input adder r, i.e. the element $\frac{cR_e^rs}{T_0s+1}$ is duplicated. Here the signal $\vartheta$ will encounter the element $\frac{a_\vartheta cR_y^rs}{T_0s+1}$ on its path to the adder r. This transfer function is combined in Fig. 4.14 with the already existing coupling between the same points of the diagram via the element $R_{\ddot{\vartheta}}^rs^2+R_\vartheta^r$.

The transfer functions $M_{\ddot{q}}^Ms^2+M_q^M$ and $\frac{(T_2s+1)f_q^Fs^2}{T_0s+1}$ have been combined similarly in the left-hand side of Fig. 4.14 for diagram segment q-M.

After removal of the cross coupling on the q-r segment of the structure, we are left with the elements $\frac{f_q^FcR_y^rs^3}{T_0s+1}$, which are indicated on Fig. 4.14.

After the completed transformations, the liquid oscillatory element in Fig. 4.14 is found to be bracketed by a feedback loop which, while complex, has standard element circuit diagrams. We may therefore plot methods for stability analysis of such a system. For this purpose, the frequency characteristic $W_2(j\omega)$ is converted according to the rules set forth in Sec. 3.3.B into the GPC of a diagram with negative feedback thorugh $k_{f.b}$, i.e., $\frac{W_2(j\omega)}{1+k_{f.b}W_2(j\omega)}$. This GPC is multiplied by the GPC of the series-connected elements $-M_q^M-M_{\ddot{q}}^M\omega^2-\frac{(1+j\omega T_2)f_q^F\omega^2}{1+j\omega T_0}$ and $R_\vartheta^r-R_{\ddot{\vartheta}}^r\omega^2+j\frac{a_\vartheta cR_y^r\omega}{1+j\omega T_0}$ and added to the GPC of the element connected in parallel, i.e.,

$$-j\frac{f_q^F cR_y^r\omega^3}{1+j\omega T_0}.$$

A complex-plane hodograph is plotted from the general GPC obtained in this way. Just as in the case of elastic oscillations, the oscillations in the liquid oscillatory element are damped if the point with frequency $\Omega$ lies on the segment of the hodograph in the lower half of the complex plane (the case of positive feedback) when that element is closed by this feedback. /18

The stability analysis can also be carried out by analytical methods, since we have the complete system of initial equations (4.89), to which we should either add the autopilot equation

$$M_{con} = -k_{f.b}\vartheta \tag{4.90}$$

or simply rewrite an equivalent equation system from the structural diagram of Fig. 4.12, as the equations of its adders.

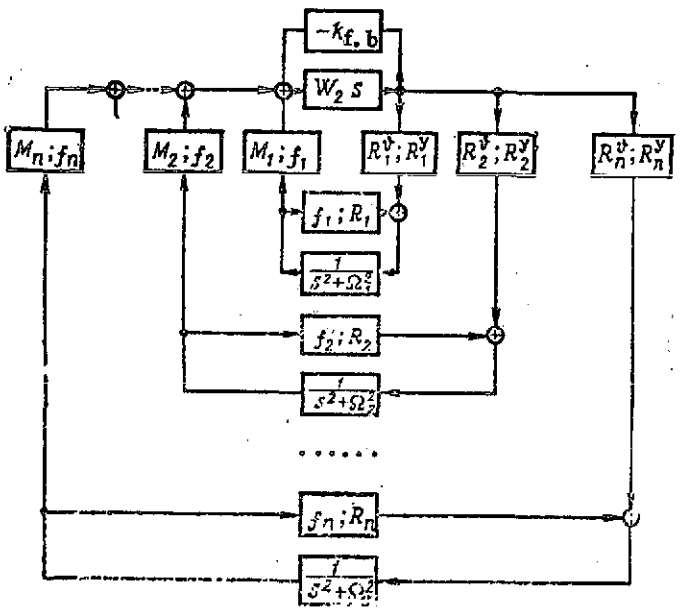


Figure 4.15. Expanded Longitudinal-Motion Structural Diagram of Guided Vehicle with Consideration of Several Liquid-Load Oscillation Harmonics.

To consider not only the first harmonic of the the liquid-load oscillations, but also higher harmonics, it is necessary to introduce the appropriate additional oscillatory elements into the structural diagram of Fig. 4.14, each with its own frequency $\Omega_i$ and new coupling coefficients $R_i$ and $M_i$. Building up the structural diagram to take account of several liquid-oscillation harmonics is a somewhat more complicated task than that of building up the structural diagram for elastic vibrations as indicated in Fig. 4.11, since it is necessary to add a total of 7 elements and coefficient blocks to the structure according to Fig. 4.11 for each new harmonic. If the already transformed structure in Fig. 4.14 is used as a base, each new harmonic requires the introduction of four elements.

Figure 4.15 shows the development of the structural diagram for several harmonics.

The structural diagram is built out in exactly the same way in the presence of several liquid-filled tanks on the vehicle. The coupling coefficients obtained are quite different in magnitude and sign when the effects of tanks in the nose and tail sections of the vehicle on stabilization dynamics are considered.

Thus, while a position of the GPC in one half of the complex plane is found to be favorable for stability in the case of nose-section tanks, it may be necessary to have the GPC in the other half for tail-section tanks.

In reality, it is necessary to consider three types of oscillations simultaneously in the complete dynamic stabilization system for a heavy vehicle: /182

1) oscillations of a vehicle with ideally rigid structure and "solidified" liquid in the tanks;

2) elastic vibrations of the body in all harmonics that influence the readings of a gyroscopic instrument;

3) oscillations of the liquid load in all tanks and in a number of harmonics in each of the tanks.

Despite the complexity of this general case, the methods of analysis that we have examined above with reference to simpler examples remain quite effective.

In some case, it is necessary to consider the effects of the elasticity of the controls and the points of attachment of the control engines in the vehicle transfer functions in addition to the factors examined above.

## 4.5. POSSIBILITIES FOR USE OF EXPANDED STRUCTURAL DIAGRAM OF VEHICLE AND ANALOG AUTOPILOT FOR DEVIATION AND DISTURBANCE CONTROL /183

We shall examine this problem with reference to the vehicle lateral motion given by Eqs. (2.50). We convert from these equations to the operator form with standard coefficients:

$$(T_0 s+1)\Psi(s)=a_\psi\psi(s)+F^*; \tag{4.91a}$$

$$(T_1^2 s^2+2\xi T_1 s+1)\psi(s)=(T_2 s+1)\Psi(s)+M^*, \tag{4.91b}$$

where

$$T_0=\frac{1}{z_\beta},\ a_\psi=1,$$
$$T_1^2=\frac{1}{n_\beta};\quad 2\xi T_1=\frac{n_{\dot\psi}}{n_\beta};\quad T_2=\frac{n_{\dot\beta}}{n_\beta}.\qquad (4.92)$$

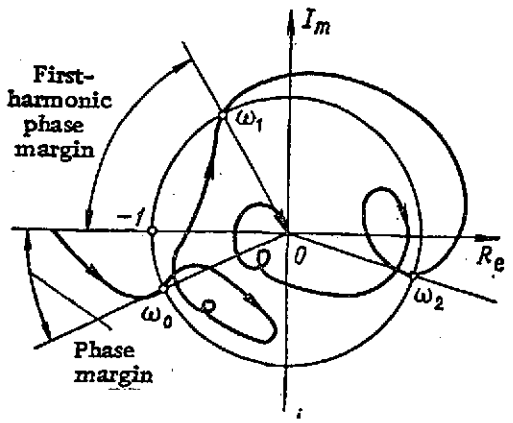


Figure 4.16. Control-Loop GPC of American "Saturn" Rocket Booster with Many Degrees of Freedom.

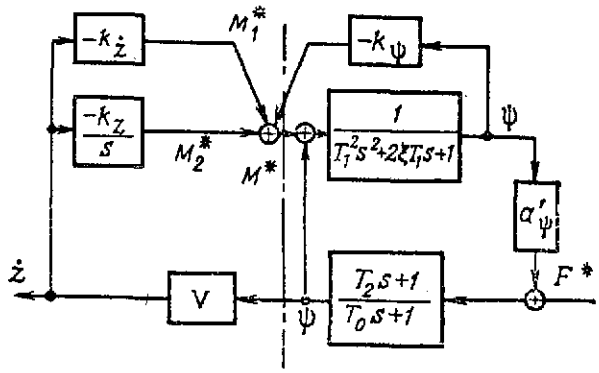


Figure 4.17. Expanded Structural Diagram of Lateral-Motion Loop of Vehicle with Automatic Pilot Working on the Principle of Deviation Control in Angular and Linear Coordinates.

The right-hand side of the structural diagram is drawn in accordance with formulas (4.91a) and (4.91b).

Let us consider the case in which there is no disturbing moment from external factors and M* is developed only by the automatic pilot. We shall use $k_\psi$ to denote the coefficient of feedback through the automatic pilot in the yaw loop. It is expressed in terms of the autopilot coefficient, which relates the deflection of the gyroscope to the deflection of the control surfaces

$$\dot k_{\mathrm{AP}}=\frac{\Delta\delta_{\mathrm{r}}}{\Delta\dot\psi},\qquad (4.93)$$

and the coefficients of the equation as follows:

$$k_\psi=\frac{k_{\delta_{\mathrm{r}}}\dot k_{\mathrm{AP}}}{n_\beta}.\qquad (4.94)$$

This coefficient has been introduced into the structural diagram of Fig. 4.17a.

The control deflection also gives rise to a force that is evaluated by the second term on the right in Eq. (2.44). After normalization of the coefficients, which has been done in

(4.91a), the coupling coefficient between the equations of forces and moments is replaced by the new coefficient

$$a_{\psi}^{\prime}=1-\frac{k_{\psi}z_{a_T}}{z_{\beta}n_{a_T}}=1-\frac{k_{AP}z_{a_T}}{z_{\beta}n_{\beta}} \qquad (4.95)$$

with consideration of the static behavior of the automatic pilot. /184
We shall ignore the dynamics of the automatic pilot in the present analysis. The moment M* of Fig. 4.17 also includes additional components, which are formulated on the left side of the structural diagram. Let us analyze these components with the principle of deviation control as our example.

Let the vehicle be acted upon by a (normalized) force F* that causes a deviation that can be converted into a lateral velocity by the formula

$$\dot{z}=V\Psi. \qquad (4.96)$$

The lateral acceleration can be measured by accelerometers mounted on a gyroscopic platform stabilized in the z-direction, converted to autopilot signals, integrated, and used to generate (normalized) moments that compensate the deviation and are proportional to the velocity ($M_1^*$), the coordinate ($M_2^*$), etc. For these moments we introduce the transfer functions

$$M_1^*(s)=-k_1^*[sZ(s)], \qquad (4.97)$$

$$M_2^*(s)=-k_2^*\frac{1}{s}[sZ(s)] \qquad (4.98)$$

and indicate the conditions of their generation on the left side of Fig. 4.17. According to deviation control principle, negative feedbacks are created after measurement of the deviation: static feedbacks without integrating elements and floating feedbacks that contain integrating elements. The number of integrating elements determines the order of astatism and the possibility of compensating the constant component of the disturbance and its varying part. /185

In the present case, the deviation can be understood as the lateral velocity

$$\dot{z}(t)\doteq sZ(s), \qquad (4.99)$$

so that an integrating element is present for it in the moment feedback.

If the disturbance is constant, $F^*=F_0^*=\text{const}$, its transform is $F_0^*/s$, and we can obtain the steady-state value of the system

response z to this disturbance from the formula

$$\dot{z}_{\text{ady}} = \lim_{s \to 0} F^*_0 W_{\dot{z}F}(s), \tag{4.100}$$

where $W_{\dot{z}F}$ is the operator transfer constant from the disturbance to the response $\dot{z}$.

This function is determined from the structural diagram in the form /18

$$W_{\dot{z}F}(s) = \frac{sV(T_2 s+1)\left(T_1^2 s^2 + 2\xi T_1 s + \right.}{s\left[\left(T_1^2 s^2 + 2\xi T_1 s + 1 + k_\psi\right)(T_0 s+1) - a'(T_2 s+1)\right] + \left. +1+k_\psi\right)} \\ + V\left(k_{\dot{z}} s + k_z\right)(T_2 s+1)\, a'_\psi \tag{4.101}$$

the order of astatism is equal to the exponent ν of the lowest-order term in the numerator of the transfer function. In this case, ν = 1,

$$\lim_{s \to 0} W_{\dot{z}F}(s) = 0, \tag{4.102}$$

and a constant disturbance is fully compensated in the steady state (t → ∞). If the disturbance varies at a constant rate $F^*(s) = V_0/s^2$, its compensation requires second-order astatism, i.e., two integrating elements. With increasing order of the polynomial describing the disturbance, the necessary order of astatism, i.e., the necessary number of integrating elements, increases accordingly.

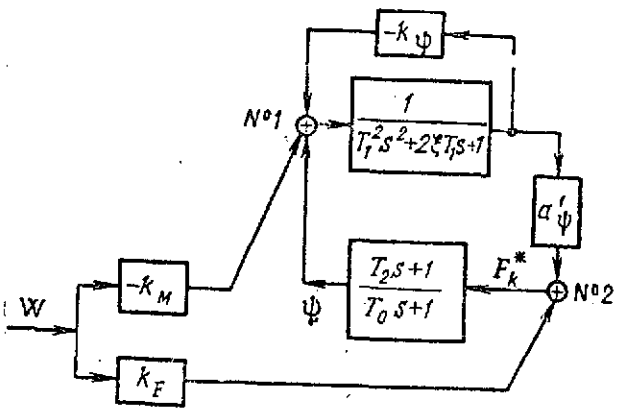


Figure 4.18. Expanded Structural Diagram of Vehicle with Minor-Loop Control and Compensation of Wind Action on the Basis of the Disturbance-Control Principle.

The transition to the steady state involves long time in-

tervals (theoretically, $t \to \infty$). Treatment of the guided aerospace vehicle as a stationary system becomes highly approximate in this case, so that only the tendency toward compensation of a disturbance can be estimated, while exact calculation naturally requires consideration of nonstationary behavior.

Similar estimates can be made for the other disturbances operating on the vehicle and in the autcmatic-pilot loop. If it brackets the point of application of the disturbance, the negative feedback is the compensating factor for all disturbances in the case of deviation control, but the degree of compensation and even the order of astatism of a given system may be different for different disturbances.

Let us now consider the possibility of compensation based on another principle, which is known as the principle of disturbance control. Let a vehicle in the atmosphere be acted upon by a wind whose velocity is $W_w$. If the center of pressure does not coincide with the center of mass but is aft of it, it becomes possible to compensate the wind drift by adjusting the characteristics of the vehicle and the automatic pilot. /187

Let the normalized force and moment from the wind be

$$F_{\bar{e}}^{*} = k_F W_{\bar{e}}, \tag{4.103}$$

$$M_{\bar{e}}^{*} = -k_M W_{\bar{e}}. \tag{4.104}$$

We represent the wind action on the structural diagram of Fig. 4.18, on which we isolate the segment pertaining directly to the vehicle, eliminating all inputs and introducing only the disturbances (4.103) and (4.104).

The conditions for full compensation of the lateral-drift wind effect reduce to balancing of the forces summed on adder 2. If the total force $F_k^*$ equals zero, the steady-state response will also be equal to zero, i.e., the line from $F_k^*$ to $\Psi$ on the structural diagram can be broken.

The notation for the force-balance equation is extremely simple:

$$k_F W_{\bar{e}} = k_M W_{\bar{e}} \frac{a_\psi'}{T_1^2 s^2 + 2\xi T_1 s + 1 + k_\psi}. \tag{4.105}$$ /188

A content corresponding to the right-hand side of the above equation must be invested in the coefficient $k_F$ to obtain compensation at any time. For the steady state ($t \to \infty$, $s = 0$) the balance reduces to the algebraic relation

$$k_F = k_M \frac{a_\psi'}{1 + k_\psi}. \tag{4.106}$$

If the vehicle is unguided, i.e., there is no feedback through the autopilot and $k_\psi = 0$, the balance of forces will take an even simpler form:

$$k_F = k_M a'_\psi. \tag{4.107}$$

The physical sense of this relation is that the moment from the wind turns the body of the vehicle in such a way that the projection of the thrust P, which appears in the coefficient, and the lateral aerodynamic force, which is proportional at small deviations to the angle of attack, compensate the disturbing force of the wind.

Compensation is possible only when the center of pressure is aft of the center of mass; then the nose of the vehicle will be turned in the direction opposite to the direction of the wind force, as indicated by the minus sign in (4.104). But when the disturbing and compensating forces are of opposite signs, Eq. (4.107) can be satisfied in the presence of variable parameters at some single point on the trajectory. The situation is different when the vehicle is automatic-pilot controlled. It is then necessary to revert to formula (4.106), from which we obtain

$$k_\psi = \frac{k_M a'_\psi}{k_F} - 1. \tag{4.108}$$

The coefficient of the feedback through the autopilot is shaped by elements of the autopilot system whose gains are easily adjusted. Then, by varying $k_\psi$ in accordance with (4.108), it is possible to arrive at a condition such that the forces are compensated at any point on the flight path.

/189

# CHAPTER V

## CHARACTERISTICS OF THE VEHICLE AS A NONSTATIONARY LINEAR OBJECT OF CONTROL

### 5.1. COEFFICIENT MATRIX FOR DESCRIPTION OF THE LONGITUDINAL MOTION OF THE UNGUIDED VEHICLE

The aerospace vehicle must be regarded as a nonstationary object of control in analyses of the complete dynamic system with all degrees of freedom, including the loop for the motion of its center of mass, and in obtaining estimates for large time intervals, when freezing of the coefficients at their average levels results in unacceptably large errors.

Let us consider the equations for the longitudinal motion of a rigid vehicle (2.36). Formally, the conversion to the standard form of the coefficients (4.4) is made in the same way as for relation (4.3), but the coefficients for the nonstationary object of control must be regarded as functions of time, so that conversion to the Laplace transform becomes difficult and the result is written in the form of differential equations:

$$T_0(t)\dot{\vartheta}(t)+\vartheta(t)=a_\delta(t)\delta(t)+F^*(t); \tag{5.1}$$

$$T_1^2(t)\ddot{\vartheta}(t)+2\xi_0 T_1(t)\dot{\vartheta}(t)+\vartheta(t)= =T_2(t)\dot{\vartheta}(t)+\vartheta(t)+M^*(t). \tag{5.2}$$

These equations were used to construct the nonstationary diagram in Fig. 5.1, which is identical in form with Fig. 4.1a but reflects couplings only in the time region. The nonstationary structure can be used to arrive at an analog model with variable coefficients, but it is not possible to obtain the operator transfer function directly. Thus, conversion to the nonstationary structure and introduction of the coefficient system (4.4) add little to our information on the characteristics of the vehicle as compared to assignment of the initial equations (2.36). /190

Conversion to the coefficient system (matrix) corresponding to the equations in the normal Cauchy form is more informative in this sense.

To convert to this form, $\alpha$ must be eliminated from Eqs. (2.36), and notation for the coordinates and their derivatives must be introduduced in the form of the unified system

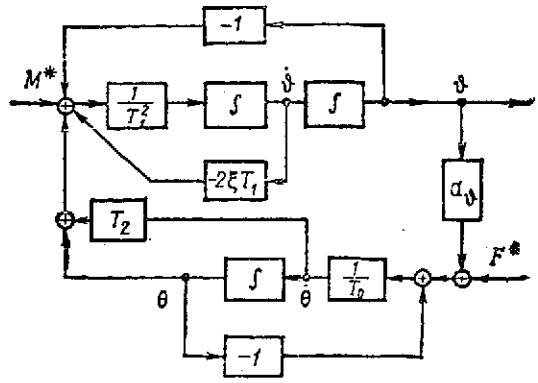


Figure 5.1. Nonstationary Structure of Major Loop in Longitudinal Control of Unguided Vehicle.

$$\theta=\theta_1;\quad \vartheta=\theta_2;\quad \dot{\vartheta}=\theta_3. \tag{5.3}$$

We then obtain

$$\left.\begin{aligned}\dot{\theta}_1&=v_{11}\theta_1+b_{12}\theta_2+0+0(t_0-)\delta[t-t_0]+f^*_{\text{dist}};\\ \dot{\theta}_2&=0+0+\theta_3+\vartheta(t_0-)\delta[t-t_0];\\ \dot{\theta}_3&=b_{31}\theta_1+b_{32}\theta_2+b_{33}\theta_3+\dot{\vartheta}(t_0-)\delta[t-t_0],\end{aligned}\right\} \tag{5.4}$$

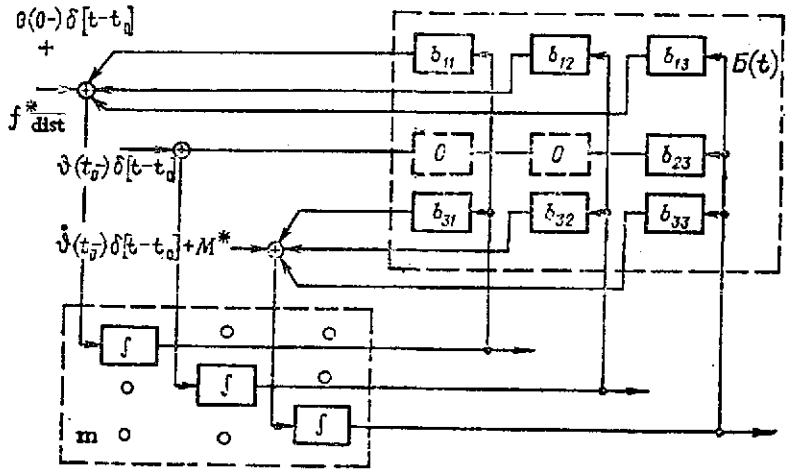


Figure 5.2. Detailed Nonstationary Matrix Structure of the Vehicle's Longitudinal-Motion Loop.

where

$$\left.\begin{aligned}b_{11}&=a_\theta=\frac{g}{V}\sin\theta_0-\frac{c_x^a SQV}{2m};\\ b_{12}&=a_\vartheta=\frac{c_C^a SQV}{2m};\quad b_{13}=0;\quad b_{23}=1;\\ b_{31}&=-\frac{bSQV}{2J_z}(m_z^a V+m_z^{\bar{a}}ba_\theta);\\ b_{32}&=\frac{bSQV}{2J_z}(m_z^a V-a_\vartheta m_z^{\bar{a}}b);\\ b_{33}&=\frac{b^2SQV}{2J_z}(m_z^{\bar{a}}+m^{\bar{\omega}z}).\end{aligned}\right\} \tag{5.5}$$

Equation system (5.4) was used in Fig. 5.2 to obtain a nonstationary matrix structure that is similar in many structural respects to Fig. 3.16, but has a more complex, time-dependent coefficient matrix:

$$|B(t)|=\begin{vmatrix} b_{11}(t) & b_{12}(t) & 0 \\ 0 & 0 & 1 \\ b_{31}(t) & b_{32}(t) & b_{33}(t) \end{vmatrix} \qquad (5.6)$$

/192

We write the matrix equation for the normalized weighting functions in the form

$$|\dot{0}|=|\dot{g}|=|B||g|+|\delta[t-t_0]|. \qquad (5.7)$$

Its solution in the form of the matrixant [9] will be

$$||g|=E+\int_{t_0}^{t}|B(t)|dt+\int_{t_0}^{t}|B(t)|dt\int_{t_0}^{t}|B(t)|dt+\ldots. \qquad (5.8)$$

It is convenient to count the time $\tau$ from the time of application of the pulse that excites the weighting function, i.e.,

$$\tau=t-t_0. \qquad (5.9)$$

Then the coefficients of matrix (5.6) can be expanded in Taylor series around the point $t_0$ in the form

$$b_{ik}(t)=b_{ik}(t_0+\tau)=b_{ik}(t_0)+\dot{b}_{ik}(t_0)\tau+\ddot{b}_{ik}(t_0)\frac{\tau^2}{2!}+\ldots, \qquad (5.10)$$

and the matrix itself is written

$$B(\tau)=\begin{vmatrix} b_{11}+\dot{b}_{11}\tau+\ldots & b_{12}+\dot{b}_{12}\tau+\ldots & b_{13}+\dot{b}_{13}\tau+\ldots \\ 0 & 0 & 1 \\ b_{31}+\dot{b}_{31}\tau+\ldots & b_{32}+\dot{b}_{32}\tau+\ldots & b_{33}+\dot{b}_{33}\tau+\ldots \end{vmatrix} \qquad (5.11)$$

The notation of the solution (5.8) changes accordingly, assuming the form

$$|g|=E+\int_0^{\tau}B(\tau)\,d\tau+\int_0^{\tau}B(\tau)\left[\int_0^{\tau}B(\tau)\,d\tau\right]d\tau+$$
$$+\int_0^{\tau}B(\tau)\left\{\int_0^{\tau}B(\tau)\left[\int_0^{\tau}B(\tau)\,d\tau\right]\right\}d\tau+\ldots=\sum_{i=1}^{\infty}I_i. \qquad (5.12)$$

The terms of the series (5.12) are determined by the following rules:

/193

$$I_1=E=\begin{vmatrix} 1 & 0 & 0 \\ 0 & 1 & 0 \\ 0 & 0 & 1 \end{vmatrix}; \qquad (5.13)$$

$$I_2=\int_0^{\tau} B(\tau)\,d\tau=$$

$$=\begin{vmatrix} b_{11}\tau+\dot{b}_{11}\frac{\tau^2}{2!}+\dots & b_{12}\tau+\dot{b}_{12}\frac{\tau^2}{2!}+\dots & b_{31}\tau+\dot{b}_{31}\frac{\tau^2}{2!}+\dots \\ 0 & 0 & \tau \\ b_{31}\tau+\dot{b}_{31}\frac{\tau^2}{2!}+\dots & b_{32}\tau+\dot{b}_{32}\frac{\tau^2}{2!} & b_{33}\tau+\dot{b}_{33}\frac{\tau^2}{2!} \end{vmatrix}; \qquad (5.14)$$

$$I_3'=|B|\,I_2;$$

$$I_3=\int_0^{\tau} I_3'\,d\tau=$$

$$=\begin{vmatrix} F_{11}(\tau_1 t_0) & F_{12}(\tau_1 t_0) & F_{13}(\tau_1 t_0) \\ \frac{b_{31}\tau^2}{2!}+\frac{\dot{b}_{31}\tau^3}{3!}+\dots & \frac{b_{32}\tau^2}{2!}+\frac{\dot{b}_{32}\tau^3}{3!} & \frac{b_{33}\tau^2}{2!}+\frac{\dot{b}_{33}\tau^3}{3!} \\ F_{31}(\tau_1 t_0) & F_{32}(\tau_1 t_0) & F_{33}(\tau_1 t_0) \end{vmatrix}. \qquad (5.15)$$

Only the first derivatives of the coefficients were taken into account in the expansions in (5.14) and (5.15), but it is quite simple to include the remaining terms in a machine computation by the procedure considered above.

The relatively simple functions are represented in the matrices in series form, while more complex ones are grouped under single symbols. For example,

$$F_{12}'(\tau,\ t_0)=\left[b_{11}(t_0)+\dot{b}_{11}(t_0)\tau\dots\right]\left[b_{12}(t_0)\tau+\dot{b}_{12}(t_0)\frac{\tau^2}{2!}\dots\right]+$$

$$+\left[b_{13}+b_{13}\tau\left[\left[b_{32}\tau+\dot{b}_{32}\frac{\tau^2}{2!}\dots\right]\right.\right.$$

/1

$$F_{12}(\tau,\ t_0)=(b_{11}b_{12}+b_{13}b_{32})\frac{\tau^2}{2!}+\dots.$$

The above matrix analysis of a system with variable parameters makes the closest possible approach to the method considered in Sec. 3.4 for the investigation of linear stationary systems, but it is easily seen that the solution depends in the case of nonstationary systems not only on the current argument $\tau$, but also on the time of pulse application $t_0$, something that must be reflected in the notation for the normalized weighting functions in one of the following forms:

$$g[\tau,\ t_0)=g[t-t_0,\ t_0)=g(t,\ t_0). \qquad (5.16)$$

In addition, calculation of the matrix series is more complicated for nonstationary than for stationary systems. But after this procedure is mastered, it is easy to convert from the normalized weighting functions to the response of the vehicle to any input disturbance if the disturbance is given in the form of matrices, some of which appear in Table III.2, and the matrix of the process is then combined with matrix (5.11) by the procedure set forth in Sec. 3.7.

Then the response will be computed according to a formula similar to (5.12), but with more complex matrices. Thus, the characteristics of the vehicle in composite motion with consideration of the center-of-mass motion were determined above as functions of time-variable coefficients or matrices composed of these coefficients. These matrix relations are expanded with the aid of the computer.

It is also possible to replace formula (5.12) with a multiplicative integral [9] of the form

$$|g| = |E + B(\tau_n)\Delta\tau_n| \ldots |E + B(\tau_2)\Delta\tau_2||E + B(\tau_1)\Delta\tau_1|, \quad (5.17)$$

where $B(\tau_k)$ is the coefficient matrix with the coefficient values fixed at their averages in the interval $\Delta\tau_k$.

In accordance with (5.17), the calculations reduce to multiplication of matrices with coefficient values that change stepwise as $\tau$ increases.

## 5.2. THE MATRIX OF THE BASE WEIGHTING FUNCTIONS OF THE VEHICLE /195

The nonstationary aerospace vehicle can be characterized by its standard responses. It is sufficient to determine the responses in the form of weighting functions for subsequent conversion to other response forms.

For a nonstationary system, the weighting function (5.16), i.e., the unit-pulse response, depends on two arguments: the present time and the time of application of the pulse, with the former replaced in functional notation by its increment $\tau = t - t_0$. To describe the controlled object itself and for purposes of subsequent coupling of the vehicle to the controlled system, it is sufficient in the present case to consider the following base functions:

$$|W| = \begin{vmatrix} w_{\theta M}(\tau, t) & w_{\theta F}(\tau, t) \\ w_{\theta M}(\tau, t) & w_{\theta F}(\tau, t) \end{vmatrix}. \quad (5.18)$$

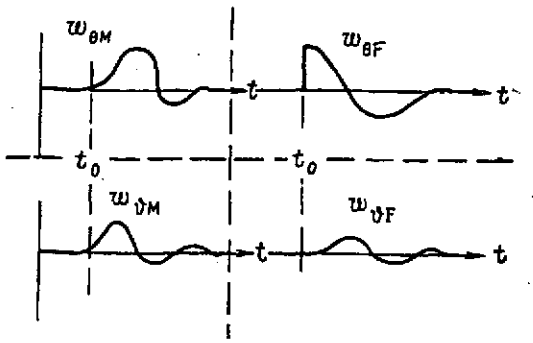


Figure 5.3. Matrix of Weighting-Function Curves for the Nonstationary Structure of Fig. 5.1.

The first indices of the weighting functions indicate the position of the response in the form of the angular rotation of the vehicle's velocity vector $\theta$ or its axis $\vartheta$. The second index indicates the point of application of the pulse disturbance in the form of a moment M or force F. For subsequent consideration of real disturbances to the assigned input functions, it will be necessary to add the equivalent inputs that were omitted in the conversion from the complete weighting-function matrix to the base functions. Transfer of the inputs from one point of the structural diagram to another involves a change in the passage of the signal through elements with variable parameters. If the transfer is forward along the signal path, the transformations inherent to the skipped elements are introduced into the input circuit. If the transfer is backward, the inverse operations are included in the input circuit. These rules and other devices used in structural transformation of nonstationary systems are discussed in detail in [25].

Figure 5.3 shows the matrix of the weighting-function curves corresponding to the aforementioned outputs and inputs for one of the times of pulse application. The shapes of the curves are adjusted in accordance with the vehicle's parameters after solution of the corresponding equations, but the initial segments of /19 the curves can be evaluated qualitatively without detailed solutions.

Thus, only the weighting function $w_{\theta F}$ will have a step change in the coordinate ($\theta$) at $\tau = 0$; the remaining weighting functions will have zero initial values for the coordinate, and the function $w_{\theta M}$ will also have one for its first derivative (the velocity) $\dot{\theta}$.

On the change in the time of pulse application, there will be a change in the form of the response in the nonstationary system. Consequently, it is necessary to have a series of /19 curves for various times in order to assign the properties of the vehicle as a controlled object. Instead of a catalog of curves, we can examine a three-dimensional plot of the weighting function as shown, for example, in Fig. 5.4. Here one of

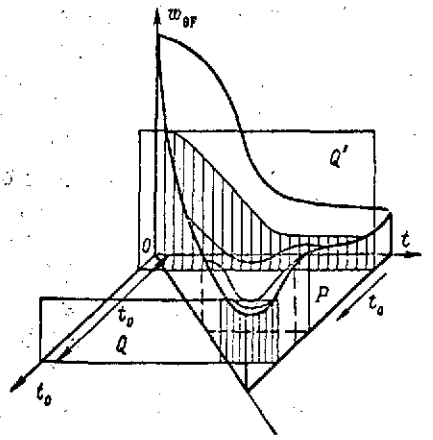


Figure 5.4. Family of Nonstationary-System Weighting-Function Curves Assigned in Relief.

the sections of the relief cut by a plane Q perpendicular to the $Ot_0$ axis at a distance $t_0$ from the origin is used for each specific time of input-pulse application. Since the response cannot occur before the input (pulse) is applied, the line $t = t_0$, i.e., the bisector of the angle between the coordinate axes Ot and $Ot_0$, serves as the boundary for the initial segments of the weighting functions. All weighting functions lie between the coordinate axis Ot and this bisector.

If we pass a plane P perpendicular to the Ot axes at a distance $t_0'$ from the origin, we can obtain a new relief section as shown on the same figure. Such sections, in which t is fixed and serves as the parameter while the second argument $t_0$ is varied, represent the parametric weighting function, whose role will be explained below. The parametric weighting function can be continued analytically into the region $t_0 < 0$; this device is used in converting to operator representations of nonstationary-system transfer properties.

## 5.3. NONSTATIONARY STRUCTURE OF THE VEHICLE WITH CONSIDERATION OF CERTAIN CONTROL COUPLINGS

Let us examine the structure of the nonstationary vehicle with autopilot feedbacks for lateral motion.

The initial equations (2.50) will then be rewritten

$$T_0(t)\dot{\Psi}+\Psi=a_\psi\psi+F^*, \tag{5.19}$$

$$T_1(t)\ddot{\psi}+2\xi(t)T_1(t)\dot{\psi}+\psi=T_2(t)\dot{\Psi}+\Psi+M^* \tag{5.20}$$

with the standard coefficients

$$\left.\begin{aligned} T_0(t)&=\frac{1}{z_\beta(t)};\ a_\psi=-1;\\ T_1^2(t)&=\frac{1}{n_\beta(t)};\ 2\xi T_1=\frac{n_{\dot\alpha}(t)}{n_\beta(t)};\ T_2=\frac{n_{\dot\beta}(t)}{n_\beta(t)}\end{aligned}\right\} \tag{5.21}$$

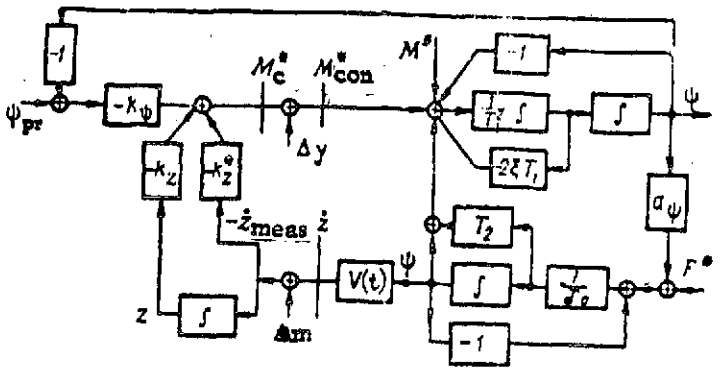


Figure 5.5. Nonstationary Structure of Guided Lateral Motion of Vehicle.

The nonstationary structure of the vehicle itself has been constructed from these equations on the right side of Fig. 5.5. For analysis of additional feedbacks in the lateral-motion control loop, we add one more kinematic equation linking the lateral velocity to the flight-path rotation angle:

$$\dot{z}=V(t)\Psi. \qquad (5.22)$$

These relationships were used to form the structural diagram (see Fig. 5.5), on which a vertical line ż appears. To introduce feedback for the purpose of eliminating lateral drift, it is necessary to have an instrument that measures the coordinate z or its derivatives. As we know, self-contained instruments (accelerometers) measure only the acceleration z̈ of the vehicle, and their designs may include a converter (integrator) for acquisition of the velocity ż. Radio devices can also be used for such measurements.

We shall omit the specific properties of the measuring instruments from consideration in a general description of the lateral-motion control loop, but on converting from the actual lateral velocity ż to the measured lateral velocity $z_{meas}$ we shall introduce the measurement-instrument error $\Delta_m$ that is inevitable in a real instrument.

This is reflected analytically by the formula

$$\dot{z}_{meas}=\dot{z}+\Delta_m, \qquad (5.23)$$

and on the structural diagram by introduction of an additional adder to introduce the error $\Delta_m$.

The linear coordinate is easily obtained by an additional (instrumental) integration with respect to velocity:

$$z_{meas}=\int_0^t \dot{z}(t)\,dt. \qquad (5.24)$$

If the control system includes a gyroscopic instrument that measures the angle or its deviation from the programmed value

$\psi_{pr}$, an instrument that measures the velocity $\dot{z}$, and an integrator to obtain the z-coordinate, it is possible to provide autopilot feedbacks in the following generalized coordinates:

– in angle, $-k_\psi \Delta\psi$;

– in lateral velocity $k_{\dot{z}}\dot{z}$;

– in the lateral coordinate, $-k_z z$.

All of these couplings are shown in Fig. 5.5. The coefficients $k_\psi$, $k_{\dot{z}}$, and $k_z$ include the conditions for conversion from the measurand to the corresponding fraction of the controlling-moment command and reconcile their dimensions, reducing them to the dimensions of the terms in Eqs. (5.2).

The controlling-moment command $M_c^*$ must be distinguished from the actual powered controlling moment $M_{con}^*$, and for this purpose two separate vertical lines appear on the structural diagram. The commands are converted to controlling moments by amplifiers and actuator devices. We omit all aspects of the conversions, introducing only a symbol for the the conversion and amplification errors, $\Delta_a$. It appears in the formula

$$M_{con}^* = M_c^* + \Delta_c, \tag{5.25}$$

and a separate adder is provided for it in accordance with the structural diagram.

In analytic form, the complication of the structural diagram reduces to replacement of the total moment in Eq. (5.20) by the difference between the disturbing and controlling moments:

/200

$$M^* = M_{dist}^* - M_{con}^* \tag{5.26}$$

and the introduction of the following relation for the controlling moment:

$$M_{con}^* = k_\psi \psi + k_{\dot{z}} V(t)\Psi(t) + k_z \int_0^t V(t)\Psi(t)\,dt. \tag{5.27}$$

## 5.4. CHARACTERISTICS OF STATE OF NONSTATIONARY VEHICLE AT A GIVEN TIME ACCORDING TO ADJOINT EQUATIONS

In analyzing the state of the vehicle on its flightpath, it is often most important to establish the values of all of its phase coordinates at characteristic fixed times. For multistage vehicles, for example, it is important to know the state

at the time of staging $t_s$; the values of the coordinates at this time are then used as initial conditions in subsequent calculation of the dynamics of the separated stage.

A certain amount of preliminary work must be done in order to determine the conditions of response accumulation as a result of earlier disturbances of complex form at a given time $t_s$. Let us first examine the procedure for determining the values of the weighting function at the same fixed time $t_s$, but with a variable current time of application of the exciting pulse. If the position of the pulse is measured in terms of the so-called "reversed argument" $\tau_*$ from the time of observation $t_s$ back to the time of pulse application, the weighting function at $t_s$ will be

$$g(t_s, \tau_*) = g_*(t_s, \tau) \tag{5.28}$$

and will be called the parametric normalized weighting function, in which the time $t_s$ serves as a parameter and only the second, reversed argument $\tau_*$ varies.

In determining the matrix of parametric normalized weighting functions $g^*_{lk}(t, \tau)$, it is now necessary to use, instead of the initial equations in the form (5.7), adjoint equations of the form

$$\left|\frac{d}{d\tau} g^*(t, \tau)\right| = |B^*(t_s - \tau)|\,|g^*[t, \tau)| + |\delta[\tau]|. \tag{5.29}$$

The first cofactor on the right in this equation is the transposed coefficient matrix with the reversed argument, i.e., a matrix of the form /20

$$B^*(t_s - \tau) = \begin{vmatrix} b_{11}(t_p - \tau) & 0 & b_{31}(t_s - \tau) \\ b_{12}(t_p - \tau) & 0 & b_{32}(t_s - \tau) \\ 0 & 1 & b_{33}(t_s - \tau) \end{vmatrix}, \tag{5.30}$$

where the rows and columns of (5.6) have changed places and the argument in the coefficients has been replaced by the difference $t_s - \tau$, which decreases with increasing $\tau$.

Let us now go over to the structure corresponding to Eq. (5.29) with the adjoint matrix $B^*$ (5.30) and the reversed coefficients, which is known as the reverse-adjoint (RA) structure [25].

Its form will depend on the sequence in which the coefficients are arranged in the matrix structural diagram, of which there are two possible versions.

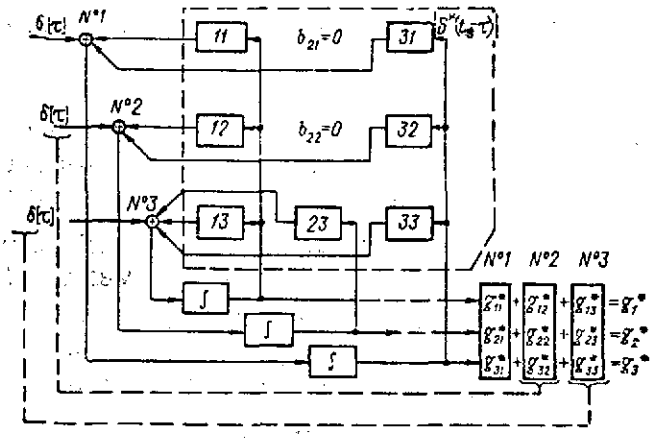


Figure 5.6. Reversed-Adjoint Structure Obtained from Transpose of Coefficient Matrix (First Version).

In the first version, the coefficient arrangement given by the transpose (5.30) must be taken as a basis. Then Eq. (5.29) can be represented graphically in structural-diagram form. On this diagram (Fig. 5.6), integration is preceded by summing paired products of row elements of the coefficient matrix and column elements of the weighting-function matrix: /202

$$\mathbf{g}^*[t,\tau]=\begin{vmatrix} g^*_{11} & g^*_{12} & g^*_{13} \\ g^*_{21} & g^*_{22} & g^*_{23} \\ g^*_{31} & g^*_{32} & g^*_{33} \end{vmatrix}. \qquad (5.31)$$

To explain the physical significance of each matrix element of (5.31), assignment of the multidimensional pulse input that appears on the right in (5.29) is indicated separately in Fig. 5.6 for the input of each integrator. With zero initial conditions, the weighting functions $g^*_{ik}$ (i is the number of the output and k the number of the input) are obtained at the integrator outputs. Actually, the responses at the outputs are summed over the second index for disturbances given at all inputs:

$$g^*_i=\sum_{(k)} g^*_{ik}. \qquad (5.32)$$

In the second version, it is necessary to retain the coefficient arrangement that corresponds to the initial matrix and Fig. 5.2; then, to obtain the same solution (5.31), the summation at the integrator inputs must be carried out with the column elements of the coefficient matrix rearranged, preferably as shown in Fig. 5.7. Here, as in Fig. 5.6, the coefficients $b_{ik(t-\tau)}$ have been replaced only by their numbers (indices), but the responses at each of the outputs are indicated as summed over all pulse inputs according to (5.32). /203

Figures 5.6 and 5.7 illustrate the procedure of obtaining reverse-adjoint structures for the specific equation system (5.4) of the vehicle with a relatively small number of couplings (n = 3 and $b_{21} = b_{22} = 0$). It is quickly observed that this method is valid for more complex cases with either higher-order equation systems or larger numbers of couplings. It is also ap-

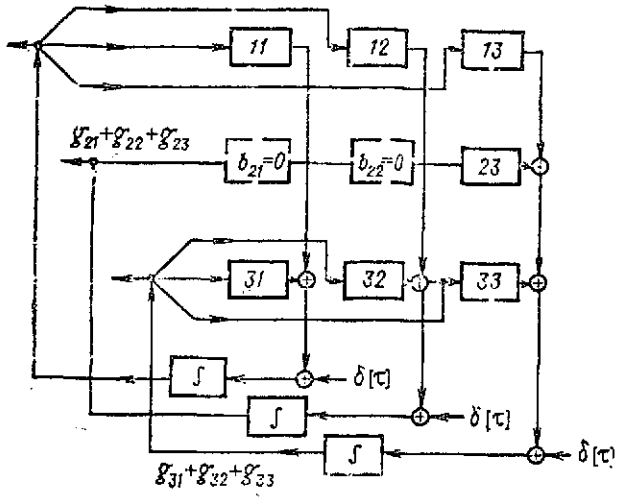


Figure 5.7. Reverse-Adjoint Structure Obtained from Original Coefficient Matrix (Second Version).

plicable to one-dimensional systems with a single input and output that are described by a common differential equation.

Let it be required to evaluate the characteristics of a vehicle with respect to one input F with M = 0 and one output θ on the basis of equation system (5.1)-(5.2). Then, instead of the equation system, it is sufficient to consider a general equation of the form

$$\dddot{\theta}+a_2(t)\ddot{\theta}+a_1(t)\dot{\theta}+a_0(t)\theta=\varphi(t). \tag{5.33}$$

In the transformed equations (5.1) and (5.2), it is necessary to assume zero initial conditions and then, after substituting and equalizing to eliminate the coefficients of the variables $\vartheta$ and $\dot{\vartheta}$, to normalize the coefficients with respect to the highest-order term.

These transformations determine the form of the disturbing function $\phi$. The procedure of contracting the system of equations with variable parameters to a single equation is made easier by the method of noncommutative determinants [25].

Introducing the symbol g for the weighting function corresponding to Eq. (5.33), we rewrite it in the Cauchy form:

$$\left.\begin{aligned}\dot{g}_1&=0+g_2+0;\\ \dot{g}_2&=0+0+g_3;\\ \dot{g}_3&=-a_0g_1-a_1g_2-a_2g_3+\delta[t-t_0].\end{aligned}\right\} \tag{5.34}$$

Now the coefficient matrix will be

/20

$$[\beta]=\begin{vmatrix}\beta_{11}&\beta_{12}&\beta_{13}\\ \beta_{21}&\beta_{22}&\beta_{23}\\ \beta_{31}&\beta_{32}&\beta_{33}\end{vmatrix}=\begin{vmatrix}0&1&0\\ 0&0&1\\ -a_0&-a_1&-a_2\end{vmatrix} \tag{5.35}$$

The structure of the nonstationary system corresponding to Eqs. (5.34) has been developed from this matrix in Fig. 5.8a. The solution matrix of equation system (5.34) will present the weighting functions

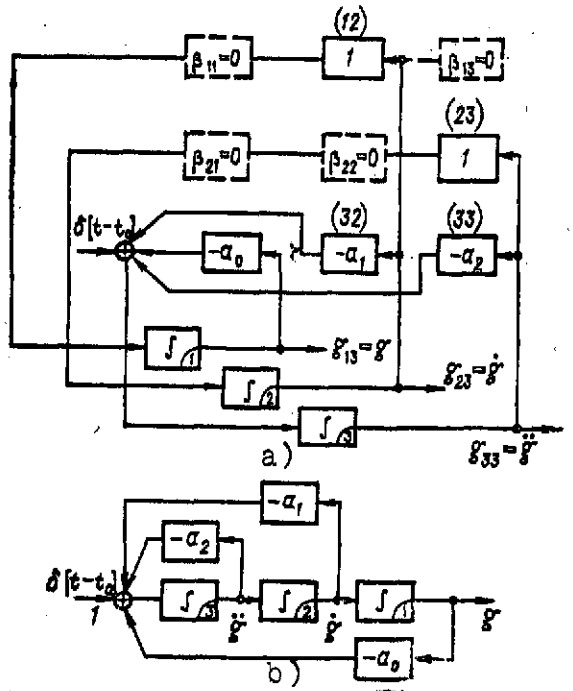


Figure 5.8. Detailed Nonstationary Matrix Structure. a) Equivalent to one-dimensional nonstationary structure; b) representing one third-order equation.

$$\begin{vmatrix} g_{11} & g_{12} & g_{13} \\ g_{21} & g_{22} & g_{23} \\ g_{31} & g_{32} & g_{33} \end{vmatrix} = \begin{vmatrix} \cdot & \cdot & \cdot & g \\ \cdot & \cdot & \cdot & \dot{g} \\ \cdot & \cdot & \cdot & \ddot{g} \end{vmatrix}, \qquad (5.36)$$

i.e., the responses at the various outputs (i = 1, 2, 3) to pulses applied at the various inputs (k = 1, 2, 3). /205

By the formulation of the problem that proceeds from the assigned equation (5.33), the only unknown is the function $g_{13} = g$. The functions $g_{23} = \dot{g}$ and $g_{33} = \ddot{g}$, which are given in the third column of matrix (5.36), may also be used to evaluate velocity and acceleration (g-force). The functions in the other columns may not be used in the final solution of the problem (unless a case of nonzero initial conditions is being investigated), but they will be needed to obtain the basic solutions ($g$, $\dot{g}$, $\ddot{g}$) in the form of the matrixant. If other methods are used in the solution, all integrators in the structural diagram can be arranged in the same line, as shown in Fig. 5.8b. /206

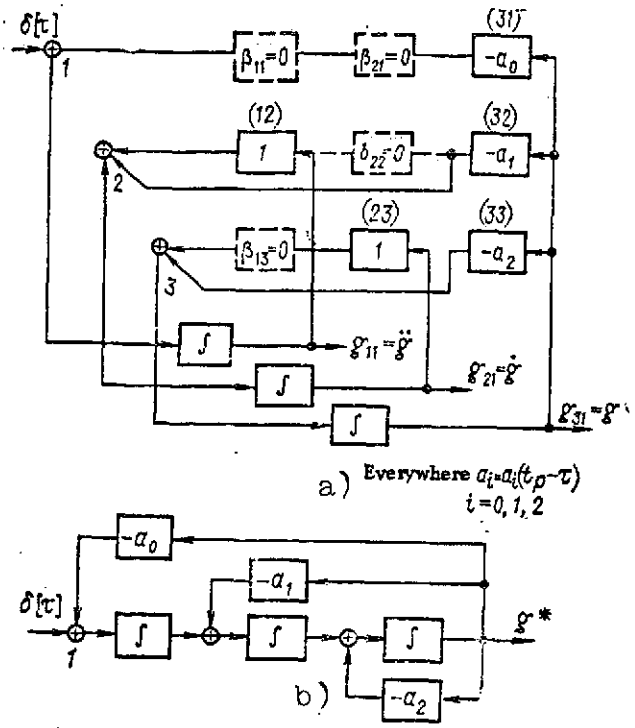


Figure 5.9. Reverse-Adjoint Structure Obtained from Transposed Coefficient Matrix (a) and its One-Dimensional Equivalent (b).

The diagrams of Figs. 5.8a and b are equivalent, as is easily seen on tracing the connections between the integrators, which are indicated by heavier lines, and from the supplementary couplings via the coefficients.

The conversion to the adjoint equations and structures from the single initial equation (5.33) will also be made in two versions.

In the first version, the coefficient matrix is transposed just as in Fig. 5.6 except that, owing to the absence of a number of couplings, the structure obtained is somewhat simpler, as shown in matrix form in Fig. 5.9a and in a form corresponding to the in-line arrangement of the integrators in Fig. 5.9b.

In the second version, the coefficients remain in the same /207
positions as in the original matrix, and the reverse-adjoint structure of Fig. 5.10a is obtained from Fig. 5.8 after removal of the absent couplings.

If the integrators are arranged in line, the result is the diagram of Fig. 5.10b. It is quite identical to that of Fig.

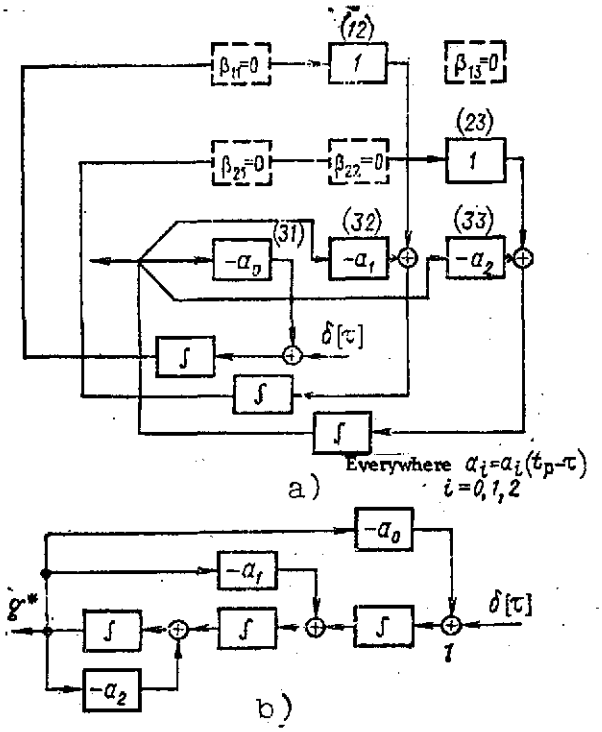


Figure 5.10. Reverse-Adjoint Structure Obtained from Original Coefficient Matrix (a) (See Fig. 5.3) and Its One-Dimensional Equivalent (b).

5.9b. Either of these diagrams readily yields the RA equation inherent to them:

$$\sum_{l=0}^{3}\frac{\partial^l}{\partial\tau^l}[a_l(t_s-\tau)\,g^*(t,\tau)]=\delta[\tau]. \tag{5.37}$$

It is obtained as the sum on the input adder after the necessary differentiation of the products in the sum, which are disconnected from the integrator inputs.

For the original vehicle equation (5.33), the corresponding reverse-adjoint equation for determination of the weighting function takes the form

$$\frac{\partial^3}{\partial\tau^3}g^*(t-\tau)+\frac{\partial^2}{\partial\tau^2}[a_2(t-\tau)\,g^*(t-\tau)]+$$

$$+\frac{\partial}{\partial\tau}[a_1(t-\tau)\,g^*(t-\tau)]+a_0(t-\tau)\,g^*(t-\tau)=\delta[\tau]. \tag{5.38}$$

The rules for obtaining the reverse-adjoint equations, as illustrated by (5.37), can be generalized to any order (n) of the original equation. The rules for deriving the reverse-ad-

joint strucutre from the initial structure are generalized in exactly the same way and reduced to the following simple structure:

– reversal of diagram input and output positions;

– substitution of branch points for adders and vice versa, with a simultaneous change in the directions of all signals;

– reversal of the argument in the coefficients by conversion to the functions $a_i(t_s - \tau)$ instead of $a_i(t)$.

Naturally, the rule for formation of the reverse-adjoint structures from the transposed coefficient matrix can also be generalized to any order of the equations. Here the pulse must be applied at the input of the k-th integrator of the diagram to obtain the parametric weighting function between the k-th input and the i-th output, in order to satisfy the "starting" conditions of the diagram:

$$g^*_{kk}(t, 0) = 1. \qquad (5.39)$$ /20

After the parametric weighting function g* has been obtained, the response of the nonstationary system to an input disturbance x(t) is determined from the convolution formula

$$y(t, \tau_{max}) = \int_0^\infty g^*(t, \tau) x(\tau_{max} - \tau) d\tau, \qquad (5.40)$$

where $\tau_{max}$ is the interval from the start of impression of the input disturbance to the time $t_s$ of observation of the accumulated response. When $\tau$ reaches the value $\tau_{max}$, further integration stops, since the function x is thereafter equal to zero.

For a concrete equation, e.g., (5.33), the parametric weighting function $g^*_{\theta\phi}(t, \tau)$ must be substituted into (5.40). If the assigned equation contains derivatives or variable coefficients in its right member, the parametric weighting function is denoted by $w^*(t, \tau)$ and determined by the procedure set forth in [25], and Eq. (5.40) is witten in the more general form

$$y(t_1\tau_{max}) = \int_0^\infty w^*(t,\tau) x(\tau_m - \tau) d\tau. \qquad (5.41)$$

## 5.5. OPERATOR FORM OF ASSIGNMENT OF THE VEHICLE'S NONSTATIONARY CHARACTERISTICS

The convolution equation (5.41) can be Laplace-transformed:

SUMMARY OF VARIOUS METHODS OF ASSIGNING AND USING CHARACTERISTICS OF NONSTATIONARY FLIGHT VEHICLE

| Flight vehicle characteristics | Characteristics of input | Intermediate solution | Response |
|---|---|---|---|
| I. Coefficient matrix of equations in normal Cauchy form | Standard-input matrix according to Table IV.2 | Combined coefficient matrix | In form suitable for computer input – matrixant (5.8) or multiplicative integral (5.17) |
| II. Parametric base weighting functions: – in form of table for various $\lambda$ or as relief of the function (Fig. 5.4) | Analytic form of assignment with consideration of time shift | Convolution formula (5.41) | Tabulated results of integration by convolution formula for various t |
| III. Transpose of coefficient matrix with argument reversed | Diagonal unit-pulse matrix | Adjoint structure | Parametric normalized detailed weighting functions assigned for II |
| IV. Parametric transfer functions | Laplace transform without consideration of time shift | Parametric transform of response; formula (5.42) | Inverse Laplace (5.45) or Fourier transformation by methods set forth in Chap. III |

$$Y^*(t,s)=W^*(t,s)X^*(s), \tag{5.42}$$

where

$$W^*(t,s)=\int_0^\infty w^*(t,\tau)e^{-\tau s}d\tau, \tag{5.43}$$

$$X^*(s)=\int_0^\infty x(\tau_m)e^{-\tau_m s}d\tau_m. \tag{5.44}$$

In (5.43), the Laplace transformations are carried out with respect to the second argument with the parameter $t = t_s$, and the transform (5.43) is known as the parametric operator transfer function. /20

The result (5.42) is called the parametric transform of the response Y at time $t = t_s$ to an input disturbance of specified shape x and arbitrary time shift. The inverse Laplace transform of the parametric response transform, i.e., the original at point $t_s$

$$L^{-1}[Y^*(t,s)]=y^*(t,\tau_m), \tag{5.45}$$

covers all possible intervals ($\tau_m$ = var) of action of a disturbance of the specified form on the system.

Thus, the conditions for transfer of the disturbance from the input to the output of the nonstationary system are described by the simple formula (5.42), in which the parametric transfer function and the transform of the unshifted disturbance are multiplied. Thus, although the answer to (5.42) is obtained for a fixed time $t = t_s$, the characteristic of the nonstationary system is given in terms of its parametric function.

Let us illustrate the derivation of the parametric transfer function with reference to transformation of Eq. (5.33) as an example. If its right-hand side $\phi(t)$ is regarded as a unit input, then according to [26] the parametric transfer function can be determined by successive approximations. The first approximation takes the form

$$G^*(t,s)=\frac{1}{s^3+(s-\partial)^2a_2(t)+(s-\partial)a_1(t)+a_0(t)}=$$
$$=\frac{1}{s^3+a_2(t)s^2+[a_1(t)-2\dot{a}_2(t)]s+a_0(t)-\dot{a}_1(t)+\ddot{a}_2(t)}, \tag{5.46}$$

where $\partial = d/dt$ is the algebraized differentiation symbol.

Since the coefficients in the parametric transfer function

become numbers when $t_s$ is fixed, the inverse Laplace transformation is carried out in the same way as for stationary systems by the methods set forth in Chap. III.

The table presents a summary of the characteristics that can be used to specify a nonstationary vehicle for subsequent analyses as an object of control.

# APPENDIXES

/211

## Appendix I

## COEFFICIENTS IN EQUATIONS OF MOTION AND TRANSFER FUNCTION OF THE F-101 AIRPLANE AS FUNCTIONS OF FLIGHT SPEED AND ALTITUDE

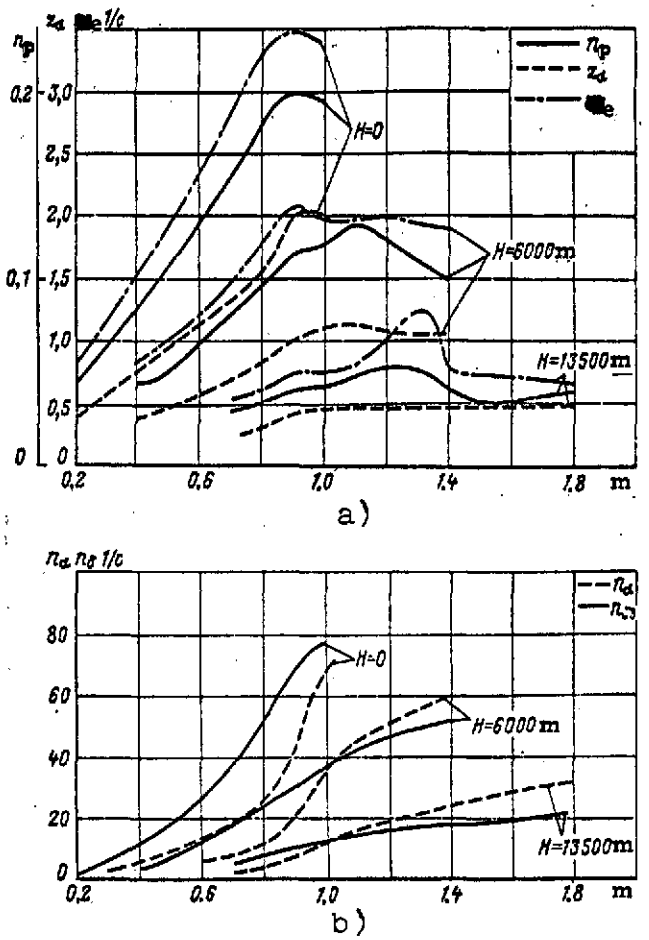


Figure I.1. Coefficients of Equations

PRECEDING PAGE BLANK NOT FILMED

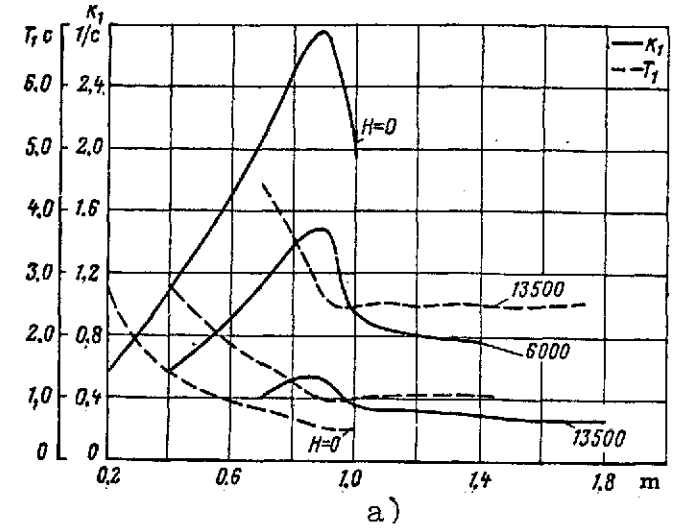


Figure I.2. Coefficients of Transfer Functions.

Appendix II

TRANSFER-FUNCTION COEFFICIENTS OF V-2 BALLISTIC MISSILE AS FUNCTIONS OF TIME OF FLIGHT

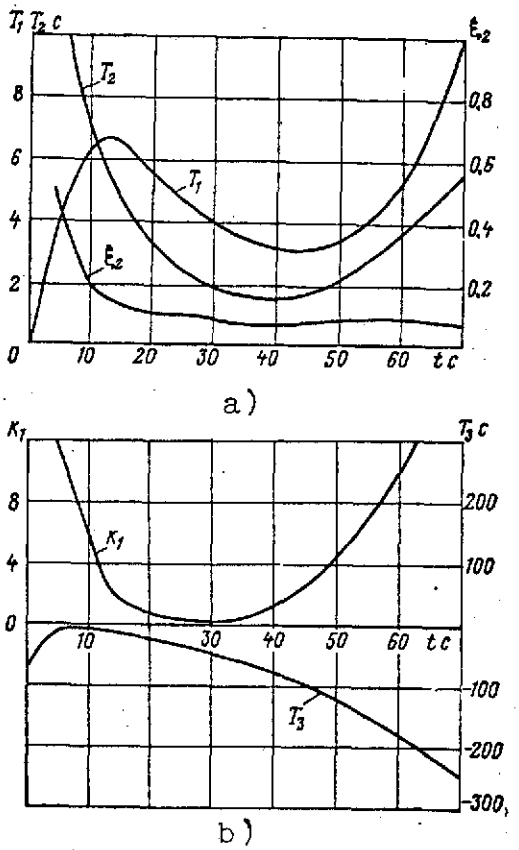


Figure II.1. Transfer-Function Coefficients of Ballistic Missile as Functions of Time of Flight

# Appendix III

## TABLES OF STANDARD AEROSPACE VEHICLE TRANSFER FUNCTIONS

Table III.1

### TRANSFER FUNCTIONS OF THE VEHICLE IN THE LONGITUDINAL PLANE

| | Transfer-function notation | Form of transfer function |
|---|---|---|
| Long period motion | $W^V_{\delta_t}(s) = \frac{V(s)}{\delta_t(s)}$ | $W^V_{\delta_t}(s) = \frac{1}{\Delta} a_{z_1}\left[s^2 - \left(c_{23} + \frac{z_{\delta_t}}{a_{z_1}} c_{13}\right)s - c_{33}\left(c^*_{24} + \frac{z_{\delta_t}}{a_{z_1}} c^*_{14}\right)\right]$ |
| | $W^\theta_{\delta_t}(s) = \frac{\theta(s)}{\delta_t(s)}$ | $W^\theta_{\delta_t}(s) = \frac{1}{\Delta}\left[z_{\delta_t} s^2 + a_{z_1}\left(c^*_{21} - \frac{z_{\delta_t}}{a_{z_1}} c^*_{11}\right)s + a_{z_1} c_{31}\left(c^*_{24} + \frac{z_{\delta_t}}{a_{z_1}} c^*_{14}\right)\right]$ |
| | $W^H_{\delta_t}(s) = \frac{H(s)}{\delta_t(s)}$ | $W^H_{\delta_t}(s) = \frac{1}{\Delta} a_{z_1}\left\{\left[c_{31} + \frac{z_{\delta_t}}{a_{z_1}} c_{33}\right]s + \left[c_{33}\left(c^*_{21} - \frac{z_{\delta_t}}{a_{z_1}} c^*_{11}\right) - c_{31}\left(c_{23} + \frac{z_{\delta_t}}{a_{z_1}} c_{13}\right)\right]\right\}$ |
| | $W^V_{\delta_e}(s) = \frac{V(s)}{\delta_e(s)}$ | $W^V_{\delta_e}(s) = \frac{1}{\Delta} a_{z_1}\left[s^2 - \left(c_{23} + \frac{z^*_{\delta_e}}{a_{z_1}} c_{13}\right)s - c_{33}\left(c^*_{24} + \frac{z^*_{\delta_e}}{a_{z_1}} c^*_{14}\right)\right]$ |
| | $W^\theta_{\delta_e}(s) = \frac{\theta(s)}{\delta_e(s)}$ | $W^\theta_{\delta_e}(s) = \frac{1}{\Delta}\left[z^*_{\delta_e} s^2 + a_{z_1}\left(c^*_{21} - \frac{z^*_{\delta_e}}{a_{z_1}} c_{11}\right)s + a_{z_1} c_{31}\left(c^*_{24} + \frac{z^*_{\delta_e}}{a_{z_1}} c^*_{14}\right)\right]$ |

| | Transfer-function notation | Form of transfer function |
|---|---|---|
| Short-period motion | Without consideration of gravity component (level flight) ($z_\vartheta = 0$)<br>$W^H_{\delta_e}(s) = \frac{H(s)}{\delta_e(s)}$ | $W^H_{\delta_e}(s) = \frac{1}{\Delta} a_{\delta_e} \left\{ \left[ c_{31} + \frac{z^*_{\delta_e}}{a_{\delta_e}} c_{33} \right] s + \left[ c_{33} \left( c^*_{21} - \frac{z_{\delta_e}}{a_{\delta_e}} c^*_{11} \right) - c_{31} \left( c_{23} + \frac{z^*_{\delta_e}}{a_{\delta_e}} c_{13} \right) \right] \right\}$,<br>where<br>$\Delta = s^3 + (c^*_{11} - c_{23}) s^2 - (c^*_{11} c_{23} + c^*_{21} c_{13} + c^*_{24} c_{33} + c^*_{14} c_{31}) s - c^*_{24} (c_{33} c^*_{11} + c_{13} c_{31}) - c^*_{14} (c^*_{21} c_{33} - c_{31} c_{23})$ |
| | With consideration of gravity component ($z_\vartheta \neq 0$)<br>$W^\alpha_{\delta_e}(s) = \frac{\alpha(s)}{\delta_e(s)}$ | $W^\alpha_{\delta_e}(s) = -\frac{1}{\Delta} \cdot [z_{\delta_e} s^2 + (n_\tau z_{\delta_e} - n_{\delta_e}) s + n_{\delta_e} z_\vartheta]$ |
| | $W^\vartheta_{\delta_e}(s) = \frac{\vartheta(s)}{\delta_e(s)}$ | $W^\vartheta_{\delta_e}(s) = \frac{1}{\Delta} \cdot [(n_{\delta_e} + z_{\delta_e} n_\alpha) s + n_{\delta_e} z_\alpha + n_\alpha z_{\delta_e}]$ |
| | $W^\theta_{\delta_e}(s) = \frac{\theta(s)}{\delta_e(s)}$ | $W^\theta_{\delta_e}(s) = \frac{1}{\Delta} [z_{\delta_e} s^2 + z_{\delta_e} (n_\alpha + n_\tau) s + n_{\delta_e} (z_\alpha + z_\vartheta) + n_\alpha z_{\delta_e}]$ |
| | $W^{n_y}_{\delta_e}(s) = \frac{n_y(s)}{\delta_e(s)}$ | $W^{n_y}_{\delta_e}(s) = k_\alpha W^\alpha_{\delta_e}(s)$; $k_\alpha = \frac{c^\alpha_y \cdot S \cdot \varrho \cdot V^2 + 2P}{2mg}$,<br>where $\Delta = s^3 + (n_\tau + z_\alpha + n_\alpha) s^2 + (z_\alpha n_\tau + n_\alpha - z_\vartheta n_\alpha) s - z_\vartheta n_\alpha$ |

TABLE III. 1, (CONT'D.)

| | Transfer-function notation | Form of transfer function |
|---|---|---|
| Short-period motion | Without consideration of gravity component (level flight) ($z_\vartheta = 0$)<br>$W^{\alpha}_{\delta_e}(s) = \frac{\alpha(s)}{\delta_e(s)}$ | $W^{\alpha}_{\delta_e}(s) = -\frac{z_{\delta_e} s + n_T z_{\delta_e} - n_{\delta_e}}{\Delta} = -\frac{k(T_1 s + 1)}{\Delta^*}$,<br>where<br>$k = \frac{n_T z_{\delta_e} - n_{\delta_e}}{z_\alpha n_T + n_\alpha}$; $T_1 = \frac{z_{\delta_e}}{n_T z_{\delta_e} - n_{\delta_e}}$. |
| | $W^{\vartheta}_{\delta_e}(s) = \frac{\vartheta(s)}{\delta_e(s)}$ | $W^{\vartheta}_{\delta_e}(s) = \frac{(n_{\delta_e} + z_{\delta_e} \cdot n_\alpha) s + n_{\delta_e} z_\alpha + n_{\dot\alpha} z_{\delta_e}}{s\Delta} = \frac{k(T_1 s + 1)}{\Delta^*}$,<br>where $k = \frac{n_{\delta_e} z_\alpha + n_{\dot\alpha} z_{\delta_e}}{z_\alpha n_T + n_\alpha}$; $T_1 = \frac{n_{\delta_e} + z_{\delta_e} \cdot n_\alpha}{n_{\delta_e} z_\alpha + n_{\dot\alpha} z_{\delta_e}}$ |
| | | |

(TABLE III. 1, (CONT'D)

| | Transfer-function notation | Form of transfer function |
|---|---|---|
| Short-period motion | $W^{\theta}_{\delta_e}(s) = \frac{\theta(s)}{\delta_e(s)}$ | $W^{\theta}_{\delta_e}(s) = \frac{z_{\delta_e} s^2 + z_{\delta_e}(n_{\dot{\alpha}} + \ldots) s + n_{\delta_e} z_\alpha + n_{\dot{\alpha}} z_{\delta_e}}{s\Delta} = k \frac{T_1^2 s^2 + 2\xi_1 T_1 s + 1}{\Delta^*}$, where $k = \frac{n_{\delta_e} z_\alpha + n_{\dot{\alpha}} z_{\delta_e}}{z_\alpha n_T + n_\alpha}$; $T_1 = \sqrt{\frac{z_{\delta_e}}{n_{\delta_e} z_\alpha + n_{\dot{\alpha}} z_{\delta_e}}}$; $\xi_1 = \frac{(n_{\dot{\alpha}} + n_T)}{2} \sqrt{\frac{z_{\delta_e}}{n_{\delta_e} z_\alpha + n_{\dot{\alpha}} z_{\delta_e}}}$ |
| | $W^{n_y}_{\delta_e}(s) = \frac{n_y(s)}{\delta_e(s)}$ | $W^{n_y}_{\delta_e}(s) = k_\alpha W^{\alpha}_{\delta_e}$, where $\Delta = s^2 + (n_T + z_\alpha + n_{\dot{\alpha}}) s + z_\alpha n_T + n_\alpha$; $\Delta^* = T_2^2 s^2 + 2\xi_2 T_2 s + 1$; $T_2 = \sqrt{\frac{1}{z_\alpha n_T + n_\alpha}}$; $\xi_2 = \frac{n_T + z_\alpha + n_{\dot{\alpha}}}{2\sqrt{z_\alpha n_T + n_\alpha}}$ |

TABLE III. 2

TRANSFER FUNCTIONS OF THE VEHICLE IN LATERAL MOTION

| | Transfer-function notation | Coefficients of polynomial $A_3s^3 + A_2s^2 + A_1s + A_0$ in numerator of transfer function |
|---|---|---|
| 1 | $W^{\beta}_{\delta_{(r)}}(s) = \frac{\beta(s)}{\delta_{(r)}(s)}$ | $A_3 = z_{\delta_{(r)}}$;<br>$A_2 = a_0 l_{\delta_{(r)}} + n_{\delta_{(r)}} + (n_r + l_p) z_{\delta_{(r)}}$;<br>$A_1 = (z_\gamma + n_{\dot{\gamma}} + a_0 n_r) l_{\delta_{(r)}} + (a_0 l_r + l_t - z_\gamma \operatorname{tg}\vartheta_0) n_{\delta_{(r)}} + (l_t n_r - n_{\dot{\gamma}} l_r) z_{\delta_{(r)}}$;<br>$A_0 = z_\gamma [(l_r - l_t \operatorname{tg}\vartheta_0) n_{\delta_{(r)}} + (n_r - n_p \operatorname{tg}\vartheta_0) l_{\delta_{(r)}}$ |
| 2 | $W^{\omega_x}_{\delta_{(r)}}(s) = \frac{\omega_x(s)}{\delta_{(r)}(s)}$ | $A_3 = l_{\delta_{(r)}}$;<br>$A_2 = z_{\delta_{(r)}}(l_\beta - l_r n_{\dot{\beta}}) + (z_\beta + n_r + n_{\dot{\beta}}) l_{\delta_{(r)}} + l_r n_{\delta_{(r)}}$;<br>$A_1 = (l_\beta n_r - n_\beta l_r) z_{\delta_{(r)}} + (n_\beta + n_r z_\beta - z_\gamma n_{\dot{\beta}} \operatorname{tg}\vartheta_0) l_{\delta_{(r)}} + (l_\beta + l_r z_\beta) n_{\delta_{(r)}}$;<br>$A_0 = -z_\gamma \cdot \operatorname{tg}\vartheta_0 (n_\beta l_{\delta_{(r)}} + l_\beta n_{\delta_{(r)}})$. |

TABLE III. 2, (CONT'D.)

| | Transfer-function notation | Coefficients of polynomial $A_3s^3 + A_2s^2 + A_1s + A_0$ in numerator of transfer function |
|---|---|---|
| 3 | $W^{\omega_y}_{\delta_{\text{в}}}(s) = \frac{\omega_y(s)}{\delta_{\text{в}}(s)}$ | $A_3 = n_{\delta_{\text{в}}} - z_{\delta_{\text{в}}} \cdot n_{\dot{\beta}}$;<br>$A_2 = n_{\delta_{\text{в}}}(z_\beta + l_t) + l_{\delta_{\text{в}}}(n_{\dot{y}} - a_0 n_{\dot{\beta}}) - z_{\delta_{\text{в}}}(n_{\dot{\beta}} l_t + n_\beta)$;<br>$A_1 = n_{\delta_{\text{в}}}(z_\beta l_t - a_0 l_\beta) + l_{\delta_{\text{в}}}(n_{\dot{y}} z_\beta - a_0 n_\beta - z_\gamma n_{\dot{\beta}}) - z_{\delta_{\text{в}}}(n_\beta l_t - n_y l_\beta)$;<br>$A_0 = -(n_{\delta_{\text{в}}} \cdot l_\beta + l_{\delta_{\text{в}}} \cdot n_\beta) z_\gamma$ |
| 4 | $W^{\gamma}_{\delta_{\text{в}}}(s) = \frac{\gamma(s)}{\delta_{\text{в}}(s)}$ | $A_2 = (l_{\delta_{\text{в}}} - z_{\delta_{\text{в}}} \cdot n_{\dot{\beta}} \operatorname{tg}\vartheta_0 - n_{\delta_{\text{в}}} \operatorname{tg}\vartheta_0)$;<br>$A_1 = l_{\delta_{\text{в}}}[z_\beta + n_r + n_{\dot{\beta}} + \operatorname{tg}\vartheta_0 (a_0 \cdot n_{\dot{\beta}} - n_{\dot{y}})] + z_{\delta_{\text{в}}}[(l_\beta - l_r \cdot n_{\dot{\beta}}) +$<br>$+ \operatorname{tg}\vartheta_0 (l_t n_{\dot{\beta}} + n_\beta)] + n_{\delta_{\text{в}}}[l_r - \operatorname{tg}\vartheta_0 (z_\beta + l_t)]$;<br>$A_0 = l_{\delta_{\text{в}}}[(z_\beta \cdot n_r + n_\beta) + \operatorname{tg}\vartheta_0 (a_0 n_\beta - n_y z_\beta)] + z_{\delta_{\text{в}}}[l_\beta n_r - l_r n_\beta -$<br>$- \operatorname{tg}\vartheta_0 (l_\beta n_{\dot{y}} + n_\beta l_t)] + n_{\delta_{\text{в}}}[z_\beta l_r + l_\beta + \operatorname{tg}\vartheta_0 (a_0 l_\beta - z_\beta l_t)]$. |

TABLE III. 2, (CONT'D.)

| | Transfer-function notation | Coefficients of polynomial $A_3s^3 + A_2s^2 + A_1s + A_0$ in numerator of transfer function |
|---|---|---|
| 5 | $W^{\beta}_{\delta_a}(s) = \frac{\beta(s)}{\delta_a(s)}$ | $A_2 = n_{\delta_a} + a_0 l_{\delta_a}$;<br>$A_1 = n_{\delta_a}(a_0 l_r + l_{\dot{z}} - z_\gamma \operatorname{tg}\vartheta_0) + l_{\delta_a}(a_0 n_r + n_{\dot{y}} + z_\gamma)$;<br>$A_0 = z_\gamma [n_{\delta_a}(l_r - l_{\dot{z}} \operatorname{tg}\vartheta_0) + l_{\delta_a}(n_r - n_{\dot{y}} \operatorname{tg}\vartheta_0)]$. |
| 6 | $W^{\omega_x}_{\delta_a}(s) = \frac{\omega_x(s)}{\delta_a(s)}$ | $A_3 = l_{\delta_a}$;<br>$A_2 = l_{\delta_a}(z_\beta + n_r + n_{\dot{\beta}}) + l_r n_{\delta_a}$;<br>$A_1 = l_{\delta_a}(n_\beta + n_r z_\beta - z_\gamma n_{\dot{\beta}} \operatorname{tg}\vartheta_0) + n_{\delta_a}(l_\beta + l_r z_\beta)$;<br>$A_0 = -z_\gamma \operatorname{tg}\vartheta_0 (n_\beta l_{\delta_a} + l_\beta n_{\delta_a})$. |
| 7 | $W^{\omega_y}_{\delta_a}(s) = \frac{\omega_y(s)}{\delta_a(s)}$ | $A_3 = n_{\delta_a}$;<br>$A_2 = n_{\delta_a}(z_\beta + l_{\dot{z}}) + l_{\delta_a}(n_{\dot{y}} - a_0 n_{\dot{\beta}})$;<br>$A_1 = n_{\delta_a}(z_\beta l_{\dot{z}} - l_\beta a_0) + l_{\delta_a}(n_{\dot{y}} z_\beta - a_0 n_\beta - z_\gamma n_{\dot{\beta}})$;<br>$A_0 = -z_\gamma (n_{\delta_a} l_\beta + l_{\delta_a} n_\beta)$. |

| | Transfer-function notation | Coefficients of polynomial $A_3s^3 + A_2s^2 + A_1s + A_0$ in numerator of transfer function |
|---|---|---|
| 8 | $W^{\gamma}_{\delta_{\mathbf{a}}}(s) = \frac{\gamma(s)}{\delta_{\mathbf{a}}(s)}$ | $A_2 = l_{\delta_{\mathbf{a}}} - n_{\delta_{\mathbf{a}}} \operatorname{tg} \vartheta_0;$<br>$A_1 = l_{\delta_{\mathbf{a}}}[z_\beta + n_r + n_{\dot{\beta}} + \operatorname{tg} \vartheta_0 (\alpha_0 n_{\dot{\beta}} - n_y)] + n_{\delta_{\mathbf{a}}}[l_r - \operatorname{tg} \vartheta_0 (z_\beta + l_t)];$<br>$A_0 = l_{\delta_{\mathbf{a}}}[(z_\beta n_r + n_\beta) + \operatorname{tg} \vartheta_0 (\alpha_0 n_\beta - n_y z_\beta)] + n_{\delta_{\mathbf{a}}}[z_\beta l_r +$<br>$+ l_\beta + \operatorname{tg} \vartheta_0 (\alpha_0 l_\beta - z_\beta l_t)]$ |
| | Coefficients of polynomial $s^4 + B_3s^3 + B_2s^2 + B_1s + B_0 = \Delta$ in denominator of transfer function | $B_3 = l_t + n_r + z_\beta + n_{\dot{\beta}};$<br>$B_2 = l_t n_r - n_y l_r + z_\beta (l_t + n_r) - \alpha_0 (l_r n_{\dot{\beta}} - l_\beta) + (l_t n_{\dot{\beta}} + n_\beta) - z_\gamma n_{\dot{\beta}} \operatorname{tg} \vartheta_0;$<br>$B_1 = z_\beta (l_t n_r - n_y l_r) + \alpha_0 (l_r n_\beta - l_\beta n_r) + (n_\beta l_t - l_\beta n_y) +$<br>$+ z_\gamma [l_r n_{\dot{\beta}} - l_\beta - \operatorname{tg} \vartheta_0 (l_t n_{\dot{\beta}} + n_\beta)];$<br>$B_0 = z_\gamma [(l_r n_\beta - l_\beta n_r + \operatorname{tg} \vartheta_0 (l_\beta n_y - n_\beta l_t)$ |

**TABLE III. 3**

SIMPLIFIED VEHICLE TRANSFER FUNCTIONS IN LATERAL MOTION

| | Transfer-function notation | Form of transfer function |
|---|---|---|
| Roll channel | $W^{\omega_x}_{\delta_a}(s) = \frac{\omega_x(s)}{\delta_a(s)}$ | $W^{\omega_x}_{\delta_a}(s) = \frac{l_{\delta_a}}{s + l_t} = k\frac{1}{T_1 s + 1}$ ; where $k = \frac{l_{\delta_a}}{l_t}$ ; $T_2 = \frac{1}{l_t}$ |
| | $W^{\gamma}_{\delta_a}(s) = \frac{\gamma(s)}{\delta_a(s)}$ | $W^{\gamma}_{\delta_a}(s) = \frac{l_{\delta_a}}{s(s + l_t)}$ |
| channel | $W^{\psi}_{\delta_r}(s) = \frac{\psi(s)}{\delta_r(s)}$ | $W^{\psi}_{\delta_r}(s) = \frac{n_{\delta_r}}{s^2 + n_r s + n_\beta} = \frac{k}{T_2^2 s^2 + 2\xi_2 T_2 s + 1}$ where $k = \frac{n_{\delta_r}}{n_\beta}$ ; $T_2 = \sqrt{\frac{1}{n_\beta}}$ ; $\xi_2 = \frac{n^2}{2\sqrt{n_\beta}}$ |

| | Transfer-function notation | Form of transfer function |
|---|---|---|
| Yaw | $W^{\Psi}_{\delta_r}(s) = \frac{\Psi(s)}{\delta_r(s)}$ | $W^{\Psi}_{\delta_r}(s) = \frac{z_{\delta_r} s^2 + z_{\delta_r} n_r s + (z_{\delta_r} n_\beta + z_\beta n_{\delta_r})}{s\left[s^2 + (z_\beta + n_r)s + (n_\beta + n_r z_\beta - z_\beta n_\beta)\right]} = \frac{k\left[T_1^2 s^2 + 2\xi_1 T_1 s + 1\right]}{s\left[T_2^2 s^2 + 2\xi_2 T_2 s + 1\right]}$, where $k = \frac{z_{\delta_r} n_\beta + z_\beta \cdot n_{\delta_r}}{n_\beta + n_r z_\beta - z_\beta n_\beta}$ |
| Roll and yaw channel (without equation of force projection onto Oz axis) | $W^{\psi}_{\delta_a}(s) = \frac{\psi(s)}{\delta_a(s)}$ | $W^{\psi}_{\delta_a}(s) = \frac{n_{\delta_a} s + n_y l_{\delta_a} + n_{\delta_a} l_t}{\Delta}$ |
| | $W^{\omega_x}_{\delta_a}(s) = \frac{\omega_x(s)}{\delta_a(s)}$ | $W^{\omega_x}_{\delta_a}(s) = \frac{l_{\delta_a} + (l_r n_{\delta_a} + n_r l_{\delta_a}) s + n_\beta l_{\delta_a} - l_p n_{\delta_a}}{\Delta}$ |
| | $W^{\psi}_{\delta_r}(s) = \frac{\psi(s)}{\delta_r(s)}$ | $W^{\psi}_{\delta_r}(s) = \frac{n_{\delta_r} s + n_{\delta_r} l_p + l_{\delta_r}}{\Delta}$ |
| | $W^{\omega_x}_{\delta_r}(s) = \frac{\omega_x(s)}{\delta_r(s)}$ | $W^{\omega_x}_{\delta_r}(s) = \frac{l_{\delta_r} s^2 + (l_r n_{\delta_r} + n_r l_{\delta_r}) s + (n_\beta l_{\delta_r} + n_{\delta_r} l_\beta)}{\Delta}$ |
| | | where $\Delta = s^3 + (n_r + l_t) s^2 + (n_\beta - l_t n_r + n_p l_r) s + l_t n_\beta - n_y l_\beta$. |

## Appendix IV

## TABLES OF BASIC CHARACTERISTICS OF VEHICLE'S ANGULAR MOTION AS A FUNCTION OF DISTURBANCE

**TABLE IV. 1**

### RESPONSE OF VEHICLE IN ANGULAR MOTION AS A FUNCTION OF THE TYPE OF DISTURBING MOMENT AND THE POLES OF THE TRANSFER FUNCTION

| Input disturbance | Nature of poles of transfer function $W(s) = \frac{k}{T^2 s^2 + 2\xi T s + 1}$ | |
|---|---|---|
| | Real | |
| $X(s) \div x(t)$ | $\beta_1 = \frac{1}{T}(-\xi + \sqrt{\xi^2 - 1})$; $\beta_2 = \frac{1}{T}(-\xi - \sqrt{\xi^2 - 1})$ $\Big\} < 0$<br>$\xi > 1$ | $\beta_1 = \frac{1}{T}(-\xi + \sqrt{\xi^2 + 1}) > 0$; $\beta_2 = \frac{1}{T}(-\xi - \sqrt{\xi^2 + 1}) < 0$;<br>$\xi > 0$; $T_1 = \frac{1}{\beta_1}$; $T_2 = \frac{1}{\lvert\beta_2\rvert}$ |
| $1 \div \delta[t]$ | $\frac{k}{T^2(s-\beta_1)(s-\beta_2)} = \frac{k}{2T\sqrt{\xi^2-1}}\left(\frac{1}{s-\beta_1} - \frac{1}{s-\beta_2}\right)$ | $\frac{k}{(T_1 s - 1)(T_2 s + 1)} = \frac{kT}{2\sqrt{\xi^2+1}}\left(\frac{T_1}{T_1 s - 1} - \frac{T_2}{T_2 s - 1}\right)$ |

| Input disturbance | Nature of poles of transfer function $W(s) = \frac{k}{T^2 s^2 + 2\xi T s + 1}$ | |
|---|---|---|
| | Real | |
| $1 \div\!\!\to \delta[t]$ | $\frac{\exp\left(-\xi + \sqrt{\xi^2-1}\right)\frac{t}{T} - \exp\left(-\xi - \sqrt{\xi^2-1}\right)\frac{t}{T}}{2T\sqrt{\xi^2-1}} k$ | $\frac{\exp\left(-\xi + \sqrt{\xi^2+1}\right)\frac{t}{T} - \exp\left(-\xi - \sqrt{\xi^2+1}\right)\frac{t}{T}}{2T\sqrt{\xi^2+1}} k$ |
| $\frac{1}{ks} \div\!\!\to \frac{1}{k} 1[t]$ | $\frac{1-\exp\left(-\xi - \sqrt{\xi^2-1}\right)\frac{t}{T}}{2\left(1-\xi^2-\xi\sqrt{\xi^2-1}\right)} + \frac{1-\exp\left(-\xi + \sqrt{\xi^2-1}\right)\frac{t}{T}}{2\left(1-\xi^2+\xi\sqrt{\xi^2-1}\right)}$ | $\frac{1-\exp\left(-\xi - \sqrt{\xi^2-1}\right)\frac{t}{T}}{2\left(1+\xi^2-\xi\sqrt{\xi^2+1}\right)} - \frac{1-\exp\left(-\xi + \sqrt{\xi^2-1}\right)\frac{t}{T}}{2\left(1+\xi^2+\xi\sqrt{\xi^2+1}\right)}$ |
| $\frac{1/k}{s-\eta} \div\!\!\to \frac{1}{k} e^{\eta t}$ | $\frac{1}{2T\sqrt{\xi^2-1}}\left(\frac{\exp\beta_1 t}{\beta_1-\eta} - \frac{\exp\beta_2 t}{\beta_2-\eta}\right) + \frac{\exp\eta t}{T^2\eta^2 + 2\xi T\eta + 1}$ | $\frac{1}{2T\sqrt{\xi^2+1}}\left(\frac{\exp\beta_1 t}{\beta_1-\eta} - \frac{\exp\beta_2 t}{\beta_2-\eta}\right) + \frac{\exp\eta t}{T^2\eta^2 + 2\xi T\eta + 1}$ |

TABLE IV. 1, (CONT'D.)

| Input disturbance | Nature of poles of transfer function $W(s) = \frac{k}{T^2 s^2 + 2\xi T s + 1}$ | |
|---|---|---|
| | Real | |
| $X(s) \div x(t)$ | $\beta_1 = \frac{1}{T}(-\xi + \sqrt{\xi^2 - 1})$; $\beta_2 = \frac{1}{T}(-\xi - \sqrt{\xi^2 - 1})$ $\left.\right\} \leqslant 0$ <br> $\xi > 1$ | $\beta_1 = \frac{1}{T}(-\xi + \sqrt{\xi^2 + 1}) > 0$; $\beta_2 = \frac{1}{T}(-\xi - \sqrt{\xi^2 + 1}) < 0$; <br> $\xi > 0$; $T_1 = \frac{1}{\beta_1}$. $T_2 = \frac{1}{\lvert\beta_2\rvert}$ |
| $\frac{\nu!}{s^{\nu+1}} \div t^\nu$ | $\frac{k\nu!}{2T\sqrt{\xi^2 - 1}}\left(\frac{\exp \beta_1 t}{\beta_1^{\nu+1}} - \frac{\exp \beta_2 t}{\beta_2^{\nu+1}}\right) + W(0)t^\nu + \nu W'(0)t^{\nu-1} + \frac{\nu(\nu-1)}{2!}W''(0)t^{\nu-2} + \ldots + W^\nu(0)$ | $\frac{k\nu!}{2T\sqrt{\xi^2 + 1}}\left(\frac{\exp \beta_1 t}{\beta_1^{\nu+1}} - \frac{\exp \beta_2 t}{\beta_2^{\nu+1}}\right) + \left[\left(\frac{\partial}{\partial s} + t\right)^\nu W(s)\right]_{s=0}$ |
| $\sum_{l=\mu}^{\nu} \frac{l!\,\varkappa_l}{s^{l+1}} \div$ <br> $\div \sum_{l=\mu}^{\nu} \varkappa_l t^l$ | $\frac{k}{2T\sqrt{\xi^2 - 1}}[X(\beta_1)\exp \beta_1 t - X(\beta_2)\exp \beta_2 t] +$ | $\frac{k}{2T\sqrt{\xi^2 + 1}}[X(\beta_1)\exp \beta_1 t - X(\beta_2)\exp \beta_2 t] +$ |
| | $+ W(0)x(t) + W'(0)\dot{x}(t) + \frac{W''(0)}{2!}\ddot{x}(t) + \cdots + \frac{W^{(l)}(0)}{l!}\dot{x}^{(l)}(t)$ | |

TABLE IV. 1, (CONT'D.)

| Input disturbance | Nature of poles of transfer function $W(s) = \frac{k}{T^2 s^2 + 2\xi T s + 1}$ | |
|---|---|---|
| | Real | |
| $\frac{\omega}{s^2+\omega^2} \div \sin \omega t$ $(\omega \neq \Omega)$ | $\frac{k\omega}{2T\sqrt{\xi^2-1}}\left(\frac{\exp \beta_1 t}{\beta_1^2+\omega^2} - \frac{\exp \beta_2 t}{\beta_2^2+\omega^2}\right) +$ | $\frac{k\omega}{2T\sqrt{\xi^2+1}}\left(\frac{\exp \beta_1 t}{\beta_1^2+\omega^2} - \frac{\exp \beta_2 t}{\beta_2^2+\omega^2}\right) +$ |
| | $+ \lvert W(j\omega)\rvert \sin\left\{\omega t + \operatorname{arc\,tg}\left[\frac{\operatorname{Im} W(j\omega)}{\operatorname{Re} W(j\omega)}\right]\right\}$ | |
| $\frac{\Omega}{s^2+\Omega^2} \div \sin \Omega t$ $(\omega = \Omega)$ | —.— | —.— |
| $(-1)^\nu \frac{\partial^\nu}{\partial \sigma^\nu} \times$ $\times \frac{\omega}{(s+\sigma)^2+\omega^2} =$ $= \frac{\omega U_\nu(s)}{[(s+\sigma)^2+\omega^2]^{\nu+1}} \div$ $\div t^\nu e^{-\sigma t} \sin \omega t$ $U_0(s) = 1;$ $U_1(s) = 2(s+\sigma)$ $U_2(s) = 2[3(s+\sigma)^2 - \omega^2]$ $U_3(s) = 24(s+\sigma)[(s+\sigma)^2 - \omega^2]$ | $\frac{k\omega}{2T\sqrt{\xi^2-1}}\left\{\frac{U(\beta_1)\exp \beta_1 t}{[(\beta_1+\sigma)^2+\omega^2]^{\nu+1}} - \frac{U(\beta_2)\exp \beta_2 t}{[(\beta_2+\sigma)^2+\omega^2)^{\nu+1}}\right\} +$ | $\frac{k\omega}{2T\sqrt{\xi^2+1}}\left\{\frac{U_1(\beta_1)\exp \beta_1 t}{[(\beta_1+\sigma)^2+\omega^2]^{\nu+1}} - \frac{U(\beta_2)\exp \beta_2 t}{[(\beta_2+\sigma)^2+\omega^2]^{\nu+1}}\right\} +$ |
| | $+ \frac{2\omega \exp(-\sigma t)}{\nu!} \operatorname{Im}\left\{\exp(j\omega t)\left[\left(t + \frac{\partial}{\partial \alpha} + \frac{\partial}{\partial \gamma}\right)^\nu \frac{jU(\alpha)W(\alpha)}{\gamma^{\nu+1}}\right]_{\substack{\alpha = -\sigma + j\omega \\ \gamma = j2\omega}}\right\}$ | |

TABLE IV. 1, (CONT'D.)

| Input disturbance | Nature of poles of transfer function $W(s)=\frac{k}{T^2s^2+2\xi Ts+1}$ | |
|---|---|---|
| | Real | |
| $X(s)\div x(t)$ | $\beta_1=\frac{1}{T}(-\xi+\sqrt{\xi^2-1});$ $\beta_2=\frac{1}{T}(-\xi-\sqrt{\xi^2-1})$ $\Big\}<0$ | $\beta_1=\frac{1}{T}(-\xi+\sqrt{\xi^2+1})>0;$ $\beta_2=\frac{1}{T}(-\xi-\sqrt{\xi^2+1})<0;$ |
| | $\xi>1$ | $\xi>0;\quad T_1=\frac{1}{\beta_1};\quad T_2=\frac{1}{\lvert\beta_2\rvert}$ |
| $\sqcup\!\sqcap x(t)$ | $X_{\sqcup\!\sqcap}[z]\,k\left\{\frac{\exp\left[-(1-\varkappa)\xi\frac{T_0}{T}\right]}{2(\xi^2\mp1-\xi\sqrt{\xi^2\mp1})}\left[\frac{z\exp(1-\varkappa)\frac{T_0}{T}\sqrt{\xi^2\mp1}}{z-\exp\frac{T_0}{T}(-\xi+\sqrt{\xi^2+1})}-\right.\right.$ $\left.\left.-\frac{z\exp(\varkappa-1)\frac{T_0}{T}\sqrt{\xi^2\mp1}}{z-\exp\frac{T_0}{T}(-\xi+\sqrt{\xi^2+1}}\right]+\frac{z}{z-1}\right\}$ | |

TABLE IV. 1, (CONT'D.)

| Input disturbance | Nature of poles of transfer function $W(s) = \frac{k}{T^2 s^2 + 2\xi T s + 1}$ | |
|---|---|---|
| | Complex | Imaginary |
| $X(s) \div x(t)$ | $\beta = \frac{1}{T}(-\xi + j\sqrt{1-\xi^2})$; $\beta^* = \frac{1}{T}(-\xi - j\sqrt{1-\xi^2})$; $0 < \xi < 1$ | $\beta = j\Omega$; $\beta^* = -j\Omega$; $\xi = 0$; $\Omega = \frac{1}{T}$ |
| $1 \div \delta(t)$ | $\frac{k}{T^2 s^2 + 2\xi T s + 1} = \frac{k}{T\sqrt{1-\xi^2}} \operatorname{Im} \frac{1}{s-\beta}$ | $\frac{k\Omega^2}{s^2+\Omega^2} = k\Omega \operatorname{Im} \frac{1}{s-j\Omega}$ |
| | $\frac{k \exp\left(-\xi \frac{t}{T}\right) \sin \frac{t}{T}\sqrt{1-\xi^2}}{T\sqrt{1-\xi^2}}$ | $\frac{k}{T} \sin \frac{t}{T} = k\Omega \sin \Omega t$ |
| $\frac{1}{ks} \div \frac{1}{k} 1(t)$ | $1 - \frac{\exp\left(-\xi \frac{t}{T}\right)}{\sqrt{1-\xi^2}} \times \sin\left(\frac{t}{T}\sqrt{1-\xi^2} + \arccos \xi\right)$ | $1 - \cos \Omega t$ |

TABLE IV. 1, (CONT'D.)

| Input disturbance | Nature of poles of transfer function $W(s) = \frac{k}{T^2 s^2 + 2\xi T s + 1}$ | |
|---|---|---|
| | Complex | Imaginary |
| $X(s) \div x(t)$ | $\beta = \frac{1}{T}(-\xi + j\sqrt{1-\xi^2})$; $\beta^* = \frac{1}{T}(-\xi - j\sqrt{1-\xi^2})$; $0 < \xi < 1$ | $\beta = j\Omega$; $\beta^* = -j\Omega$; $\xi = 0$; $\Omega = \frac{1}{T}$ |
| $\frac{1/k}{s-\eta} \div \frac{1}{k} e^{\eta t}$ | $\frac{\exp\left(-\xi\frac{t}{T}\right)}{\sqrt{(1-\xi^2)(T^2\eta^2 + 2\xi T\eta + 1)}} \sin\left(\frac{t}{T}\sqrt{1-\xi^2} + \right.$ $\left. + \arccos\frac{\xi + \eta T}{T^2\eta^2 + 2\xi T\eta + 1}\right) + \frac{\exp \eta t}{T^2\eta^2 + 2\xi T\eta + 1}$ | $\frac{\Omega^2 \exp \eta t}{\eta^2 + \Omega^2} -$ $- \frac{\Omega}{\sqrt{\Omega^2 + \eta^2}} \sin\left(\Omega t + \arccos\frac{\Omega\eta}{\eta^2 + \Omega^2}\right)$ |
| $\frac{\nu!}{S^{\nu+1}} \div t^\nu$ | $\frac{k(-1)^{\nu+1}\nu! T^\nu \exp\left(-\xi\frac{t}{T}\right)}{\sqrt{1-\xi^2}} \sin\left[\frac{t}{T}\sqrt{1-\xi^2} + \right.$ $\left. + (\nu+1)\arccos\xi\right] + \sum_{l=0}^{\nu} \frac{W^{(l)}(0)\,(t^\nu)^{(l)}}{l!}$. | $k\frac{(-1)^{\nu+1}\nu!}{\Omega^\nu} \cos\left(\Omega t + \nu\frac{\pi}{2}\right) +$ $+ \sum_{l=0}^{\nu} \frac{\nu!\, W^{(l)}(0)\, t^{\nu-l}}{l!(\nu-e)!}$ |

| Input disturbance | Nature of poles of transfer function $W(s) = \frac{k}{T^2 s^2 + 2\xi T s + 1}$ | |
|---|---|---|
| | Complex | Imaginary |
| $\sum_{l=\mu}^{\cdot} \frac{l!\,x_l}{s^{l+1}} \div \cdot$<br>$\cdot \div \sum_{l=\mu}^{\cdot} x_l t^l$ | $\frac{k\lvert\lambda\cdot\beta)\rvert \exp\left(-\xi\frac{t}{T}\right)}{T\sqrt{1-\xi^2}} \sin\left[\frac{t}{T}\sqrt{1-\xi^2} + \right.$<br>$\left. + \operatorname{arc\,tg}\frac{\operatorname{Im} X(\beta)}{\operatorname{Re} X(\beta)}\right] +$<br>$+ W(0)\,x(t) + W'(0)\dot{x}(t) + \frac{W''(0)}{2!}\ddot{x}(t) + \ldots + \frac{W^{(l)}(0)}{e!}x^{(l)}(t)$ | $k\Omega\lvert X(j\Omega)\rvert \sin\left[\Omega t - \operatorname{arctg}\frac{\omega\sum_{(m)} x_{2m-1}(-\omega)^{2m}}{\sum_{(n)} x_{2n}\omega^{2n}}\right] +$ |
| $\frac{\omega}{s^2+\omega^2} \div \sin\omega t$<br>$(\omega \neq \Omega)$ | $\frac{k\omega t \exp\left(-\xi\frac{t}{T}\right)}{\sqrt{[1+2(2\xi^2-1)\omega^2T^2+\omega^4T^4](1-\xi^2)}} \times$<br>$\times\sin\left[\frac{t}{T}\sqrt{1-\xi^2} + \operatorname{arc\,tg}\frac{2\xi\sqrt{1-\xi^2}}{\omega^2T^2+2\xi^2-1}\right] +$<br>$+ \lvert W(j\omega)\rvert \sin\left\{\omega t + \operatorname{arc\,tg}\left[\frac{\operatorname{Im} W(j\omega)}{\operatorname{Re} W(j\omega)}\right]\right\}$ | $\frac{k\Omega}{\Omega^2+\omega^2}(\omega\sin\Omega t - \Omega\sin\omega t) +$ |
| $\frac{\Omega}{s^2+\Omega^2} \div \sin\Omega t$<br>$(\omega = \Omega)$ | —,— | $\frac{k}{2}(\sin\Omega t - t\Omega\cos\Omega t)$ |

TABLE IV. 1, (CONT'D.)

| Input disturbance | Nature of poles of transfer function $W(s)=\frac{k}{T^2s^2+2\xi Ts+1}$ | |
|---|---|---|
| | Complex | Imaginary |
| $X(s) \div x(t)$ | $\beta=\frac{1}{T}(-\xi+j\sqrt{1-\xi^2})$; $\beta^*=\frac{1}{T}(-\xi-j\sqrt{1-\xi^2})$; $0<\xi<1$ | $\beta=j\Omega$; $\beta^*=-j\Omega$; $\xi=0$; $\Omega=\frac{1}{T}$ |
| $(-1)^\nu\frac{\partial^\nu}{\partial\sigma^\nu}\times$ $\times\frac{\omega}{(s+\sigma)^2+\omega^2}=$ $=\frac{\omega U_\nu(s)}{[(s+\sigma)^2+\omega^2]^{\nu+1}}\div$ $\div t^\nu e^{-\sigma t}\sin\omega t$. $U_0(s)=1$ $U_1(s)=2(s+\sigma)$ $U_2(s)=$ $=2[3(s+\sigma)^2-\omega^2]$ $U_3(s)=24(s+\sigma)\times$ $\times[(s+\sigma)^2-\omega^2]$ | $\frac{k\lvert X(\beta)\rvert}{T\sqrt{1-\xi^2}}\exp\left(-\xi\frac{t}{T}\right)\sin\left[\frac{t}{T}\sqrt{1-\xi^2}+\right.$ $\left.+\operatorname{arc\,tg}\frac{\operatorname{Im}X(\beta)}{\operatorname{Re}X(\beta)}\right]+$ | $k\Omega\lvert x(j\Omega)\rvert\sin[\Omega t+$ $+\operatorname{arc\,tg}\frac{\operatorname{Im}X(j\Omega)}{\operatorname{Re}X(j\Omega)}]+$ |
| | $+\frac{2\omega\exp(-\sigma t)}{\nu!}\operatorname{Im}\left\{\exp(j\omega t)\left[\left(t+\frac{\partial}{\partial\alpha}+\frac{\partial}{\partial\gamma}\right)^\nu\frac{jU(\alpha)W(\alpha)}{\gamma^{\nu+1}}\right]\begin{matrix}\alpha=-\sigma+j\omega\\ \gamma=j2\omega\end{matrix}\right\}$ | |

TABLE IV. 1, (CONT'D.)

| Input disturbance | Nature of poles of transfer function $W(s) = \frac{k}{T^2 s^2 + 2\xi T s + 1}$ | |
|---|---|---|
| | Complex | Imaginary |
| $\_\lceil x(t)$ | $X_{\underline{\lfloor\_\rfloor}}[z] \cdot k \left\{ \frac{\exp(\varkappa - 1)\xi \frac{T_0}{T}}{\sqrt{1-\xi^2}} \times \right.$ $\times \frac{z^2 \sin\left[(1-\varkappa)\frac{T_0}{T}\sqrt{1-\xi^2} - \arccos\xi\right] -}{z^2 - 2z\exp\left(-\frac{T_0}{T}\xi\right)\cos\frac{T_0}{T}\sqrt{1-\xi^2} +}$ $\left. \frac{-z\exp\frac{T_0}{T}\xi\sin\left(\frac{\varkappa T_0}{T}\sqrt{1-\xi^2} + \arccos\xi\right)}{+\exp\left(-\frac{2T_0}{T}\xi\right)} + \frac{z}{z-1} \right\}$ | $X_{\underline{\lfloor\_\rfloor}}[z]\, k \left\{ \frac{z}{z-1} + \right.$ $\left. + \frac{z\cos(\varkappa\Omega T_0) - z^2\cos[(1-\varkappa)\Omega T_0]}{z^2 - 2z\cos\Omega T_0 + 1} \right\}$ |

**TABLE IV. 2**

CONDITIONS OF MATRIX-FORM REPRODUCTION OF INPUTS IN THE FORM OF ASSIGNED FUNCTIONS THAT ARE SOLUTIONS OF SECOND-ORDER DIFFERENTIAL EQUATIONS

| Assigned function | Coefficient matrix | Initial values | | Normalized-weighting-function matrix |
|---|---|---|---|---|
| | $\begin{vmatrix} b_{33} & b_{34} \\ b_{43} & b_{44} \end{vmatrix}$ | $\psi_{(0+)}$ | $\dot{\psi}_{(0+)}$ | $\begin{vmatrix} g_{11} & g_{12} \\ g_{21} & g_{22} \end{vmatrix}$ |
| $Vt + C \cdot 1(t)$ | $\begin{vmatrix} 0 & 1 \\ 0 & 0 \end{vmatrix}$ | $C$ | $V$ | $\begin{vmatrix} 1(t) & t \\ 0 & 1(t) \end{vmatrix}$ |
| $Be^{\eta t} + C\,1(t)$ | $\begin{vmatrix} 0 & 1 \\ 0 & \eta \end{vmatrix}$ | $B + C$ | $\eta B$ | $\begin{vmatrix} 1(t) & e^{\eta t} - 1 \\ 0 & e^{\eta t} \end{vmatrix}$ |
| $B(1 - e^{-\alpha t}) + C1(t)$ | $\begin{vmatrix} 0 & 1 \\ 0 & -\alpha \end{vmatrix}$ | $C$ | $\alpha B$ | $\begin{vmatrix} 1(t) & \frac{1}{\alpha}(1 - e^{-\alpha t}) \\ 0 & e^{-\alpha t} \end{vmatrix}$ |

| Assigned function | Coefficient matrix $\begin{vmatrix} b_{33} & b_{34} \\ b_{43} & b_{44} \end{vmatrix}$ | Initial values $\psi_{(0+)}$ | Initial values $\dot{\psi}_{(0+)}$ | Normalized-weighting-function matrix $\begin{vmatrix} g_{11} & g_{12} \\ g_{21} & g_{22} \end{vmatrix}$ |
|---|---|---|---|---|
| $Be^{\eta t} + Ce^{\theta t}$ | $\begin{vmatrix} 0 & 1 \\ -\eta\theta & \eta+\theta \end{vmatrix}$ | $B+C$ | $\eta B+\theta C$ | $\begin{vmatrix} \eta e^{\theta t} - \theta e^{\eta t} & e^{\eta t} - e^{\theta t} \\ \eta\theta\,(e^{\theta t} - e^{\eta t}) & \eta e^{\eta t} - \theta e^{\theta t} \end{vmatrix} \frac{1}{\eta-\theta}$ |
| $A \sin(\Omega t + \varphi)$ | $\begin{vmatrix} 0 & 1 \\ -\Omega^2 & 0 \end{vmatrix}$ | $A \sin\varphi$ | $A\Omega\cos\varphi$ | $\begin{vmatrix} \cos\Omega t & \frac{1}{\Omega}\sin\Omega t \\ -\Omega\sin\Omega t & \cos\Omega t \end{vmatrix}$ |
| $Ae^{\eta t}\sin(\Omega t + \varphi)$ | $\begin{vmatrix} 0 & 1 \\ -(\eta^2+\Omega^2) & 2\eta \end{vmatrix}$ | $A \sin\varphi$ | $A\Omega\cos\varphi + A\eta\sin\varphi$ | $\begin{vmatrix} \cos\Omega t - \frac{\eta}{\Omega}\sin\Omega t & \frac{1}{\Omega}\sin\Omega t \\ -\frac{\eta^2+\Omega^2}{\Omega}\sin\Omega t & \cos\Omega t + \frac{\eta}{\Omega}\sin\Omega t \end{vmatrix} e^{\eta t}$ |

## REFERENCES




1. Abgaryan, K.A. and Rapoport, I.M. Dinamika Raket (The Dynamics of Rockets). Moscow, "Mashinostroyeniye," 1969.
2. Appazov, R.F., Lavpov, S.S. and Mishin, V.P. Ballistika Upravlyayemykh Raket Dal'nego Deystviya (The Ballistics of Guided Long-Range Missiles). Moscow, "Nauka," 1966.
3. Barkovskiy, V.V., Zakharov, V.N. and Shatalov, A.S. Metody Sinteza Sistem Upravleniya (Methods of Control-System Synthesis). Moscow, "Mashinostroeniye," 1969.
4. Blakelock, J.H. Automatic Control of Aircraft and Missiles (Russian Translation). Moscow, "Mashinostroyeniye," 1969.
5. Bodner, V.A. and Kozlov, M.S. Stabilizatsiya Letatel'nykh Apparatov i Avtopiloty (Aerospace-Vehicle Stabilization and Automatic Pilots), Moscow, "Oborongiz," 1961.
6. Bodner, V.A. Teoriya Avtomaticheskogo Upravleniya Poletom (Theory of Automatic Flight Control). Moscow, "Nauka," 1964.
7. Byushgens, G.S. and Studnev, R.V. Dinamika Prostranstvennogo Dvizheniya Samoleta (Dynamics of the Three-Dimensional Motion of the Airplane). Moscow, "Mashinostroyeniye," 1967.
8. Gantmakher, F.R. and Levin, L.M. Teoriya Poleta Neupravlyayemykh Raket (Flight Theory of Unguided Missiles). Moscow, Fizmatgiz, 1959.
9. Gantmakher, F.R. Teoriya Matrits (Matrix Theory). Moscow, "Nauka," 1967.
10. Gorbatenko, S.A. Makashov, E.M., Polushkin, Yu. F. and Sheftel', L.V. Mekhanika Poleta (The Mechanics of Flight). Moscow, "Mashinostroyeniye," 1969.
11. Jury, E. Sampled-Data Control Systems (Russian Translation). Edited by Ya. Z. Tsypkin. Moscow, "Fizmatgiz," 1963.
12. Dobrolenskiy, Yu. P. Dinamika Poleta v Nespokoynoy Atmosfere (The Dynamics of Flight in the Disturbed Atmosphere). Moscow, "Mashinostroeniye," 1969.
13. Dobronravov, O.Ye. and Kirilenko, Yu.I. Osnovy Avtomaticheskogo Regulirovaniya. Avtomaty i Sistemy Upravleniya Letatel'nykh Apparatov (Fundamentals of Automatic Control. Aerospace Vehicle Automatic Devices and Control Systems). Moscow, "Mashinostroyeniye," 1965.
14. Kazakov, I.Ye. Statisticheskiye Metody Proyektirovaniya System Upravleniya (Statistical Methods of Control-System Design). Moscow, "Mashinostroyeniye," 1969.
15. Kolesnikov, K.S. Zhidkostnaya Raketa Kak Ob"yekt Regulirovaniya (The Liquid-Propellent Rocket as an Object of Control). Moscow, "Mashinostroyeniye," 1969.
16. Lebedev, A.A. and Chernobrovkin, L.S. Dinamika Poleta Bespilotnykh Letatel'nykh Apparatov (Flight Dynamics of Pilotless Aerospace Vehicles). Moscow, Oborongiz, 1962.
17. Mikishev, G.N. and Rabinovich, B.I. Dinamika Tverdogo Tela s Polostyami, Chastichno Zapolnennymi Zhidkost'yu (Dynamics

of a Solid Body with Cavities Partly Filled with Liquid). Edited by A.Yu. Ishlinskiy. Moscow, "Mashinostroyeniye," 1968.
18. Ostoslavskiy, I.V. Dinamika Poleta Trayektorii Letatel'nykh Apparatov (Flightpath Dynamics of Aerospace Vehicles). Moscow, "Mashinostroyeniye," 1969.
19. Ostoslavskiy, I.V. Aerodinamika Samoleta (Airplane Aerodynamics). Moscow, Oborongiz, 1957.
20. Ostoslavskiy, I.V. and Kalachev, G.S. Prodol'naya Ustoychivost' i Upravlvayemost' Samoleta (Longitudinal Stability and Controllability of the Airplane). Moscow, Oborongiz, 1957.
21. Ostoslavskiy, I.V. and Strazheva, I.V. Dinamika Poleta. Ustoychivost' i Upravlyayemost' Letatl'nykh Apparatov (The Dynamics of Flight. Stability and Controllability of Aerospace Vehicles). Moscow, "Mashinostroyeniye," 1955. /237
22. Svyatodukh, V.K. Dinamika Prostranstvennogo Dvizheniya Upravlyayemykh Raket (Dynamics of the Three-Dimensional Motion of Guided Missiles). Moscow, "Mashinostroyeniye," 1959.
23. Sovremennyye Metody Proyektirovaniya Sistem Avtomaticheskogo Upravleniya. Analiz i Sintez (Modern Methods of Automatic Control System Design. Analysis and Synthesis). [General Editors: B.N. Petrov, V.V. Solodovnikov, and Yu.I. Topcheyev. Moscow, "Mashinostroyeniye," 1967.
24. Tsypkin, Ya.Z. Teoriya Lineynykh Impul'snykh Sistem (The Theory of Linear Pulsed Systems). Moscow, Fizmatgiz, 1963.
25. Shatalov, A.S. Strukturnyye Metody v Teorii Upravleniya i Elektroavtomatike (Structural Methods in the Theory of Control and Electroautomation). Moscow, Leningrad, Gosenergoizdat, 1962.
26. Shatalov, A.S. Preobrazovaniya Signalov i Izobrazhayushchikh Funktsiy Obobshchennymi Lineynymi Sistemami Automaticheskogo Upravleniya (Transformation of Signals and Functions Representing them by Generalized Linear Automatic Control Systems). Moscow-Leningrad, Gosenergoizdat, 1962.
27. Lee, S.Y. A Time-Optimal Adaptive Control System Via Adaptive Switching Hypersurface, IACC, Preprints of Technical Papers, 1967, pp. 484-491.
28. Afonin, P.A., Golubev, I.S., Kolotkov, N.I., Manucharov, V.A., Novikov, V.N., Khmelevskiy, G.V., Chernobrovkin, L.S., and Churakov, V.N. Bespilotnyye Letatel'nyye Apparaty (Pilotless Aerospace Vehicles). Moscow, "Mashinostroyeniye," 1967.
29. Barrer, M., Zhomott, A., Vebek, B.F., and Vanderkerkkhove, Raketnyye Dvigateli (Rocket Engines), Moscow, Oborongiz, 1962.
30. Shuneyko, I.I. Winged Spacecraft. In Collection Entitled: Raketostroyeniye (Rocket Building), Moscow, Institute of Scientific Information, USSR Academy of Sciences, 1966.
31. Astronautics and Aeronautics, September, 1964, Vol. 2, No. 9; December 1965, Vol. 3, No. 12; October 1966, Vol. 4, No. 10.



☆ U.S. GOVERNMENT PRINTING OFFICE: 1974—739-160/120